CRANFIELD UNIVERSITY

Muhammad Adeel Irfan

In vitro toxicity of new engineered nanoparticles through their life cycle

Cranfield Health

Supervisor: Dr Huijun Zhu
Co-Supervisor: Dr James Njuguna
November 2013

CRANFIELD UNIVERSITY

Cranfield Health

Muhammad Adeel Irfan

In vitro toxicity of new engineered nanoparticles through their life cycle

Supervisor: Dr Huijun Zhu
Co-Supervisor: Dr James Njuguna
November 2013

This thesis is submitted in partial fulfilment of the requirements for the degree of PhD

© Cranfield University 2013. All rights reserved. No part of this publication may be reproduced without the written permission of the copyright owner.

ABSTRACT

The rapid development of nanotechnology has caused concerns about nanoproducts on human health throughout their lifecycle. As part of the consortium NEPHH (nanomaterial related environmental pollution on human health through their life cycle, funded by EU-FP7), this project aimed to assess the potential effect of novel polymer-silicon composites on human health from a lifecycle perspective, focusing on *in vitro* toxicity of raw silica nanoparticles (SiNP) and dust nanoparticles (NP) released from silicon-based polymer composites. The main objectives were to characterise a group of amorphous SiNP and dust NP in water and cell culture medium; assess NP toxicity potential in *in vitro* models; and establish mode of SiNP action.

The selection of SiNP of size 7-14 nm was based on their wide use in developing polymer nanocomposites. Dust NP were generated from mechanical processing of polymer composites made of polyamide-6 (PA6), polyurethane (PU) and polypropylene (PP), each incorporated with SiNP or 3 other different silicon reinforcement materials. The dispersion and size of NP in water and in cell culture medium were characterized using dynamic light scattering, scanning electron microscopy and transmission electron microscopy. The chemical composition of NP was assessed by infra-red spectroscopy. NP were assessed *in vitro* for induction of membrane damage, intracellular reactive oxygen species (ROS), loss of cell viability, and cellular uptake by flow cytometry and confocal microscopy. In order to identify potential biomarkers for toxicity prediction, miRNA array and extracellular metabonomic assays were performed.

The size of SiNP (10-100 µg/ml) ranged from ~200-500 nm in water and ~20-500 nm in culture medium, indicating the presence of aggregates. The infra-red spectrum of SiNP dried from culture medium showed a slight difference as compared with that dried from water, indicating protein adsorption. SiNP induced acute ROS increase, cell membrane damage, and reduction in cell viability after 48 h in human lung carcinoma epithelial A549 cells, lung fibroblast MRC-5 cells and skin HaCaT keratinocytes. SiNP were up taken by all 3 cell types, and located in the cytosol. Six early (<48h) SiNP responsive miRNAs were identified in A549 cells. SiNP also induced

early changes in metabolites including glucose, lactate, ethanol, phenylalanine, histidine and tyrosine. Dust NP generated from PA6 group materials were more toxic than those from other polymer composites when assessed at 25-100 μg/ml at 72 h in A549 cells.

The results obtained from this study suggest that 1) both small and larger SiNP aggregates are taken up into the target cells; 2) conventional cytotoxicity assays combined with miRNA and metabonomic assays provide insight into the molecular mechanisms of the nanotoxicity; 3) metabonomics and miRNA assays can serve as robust tools for recognising sub-toxic dose-effect relationships; 4) the toxicity of dust NP from polymer composites depends on polymer type but not reinforcement materials. This study demonstrated the importance of lifecycle analysis as opposed to single stage analysis of novel materials. Further studies need to improve study design to enable interpretation of cytotoxicity in relation to NP size, physiochemical property and intracellular dose, and to simulate the health effect of polymer-silicon composites under more realistic scenarios.

Keywords:

Nanotoxicology, Silica, *in vitro*, physical characterisation, life cycle analysis.

ACKNOWLEDGEMENTS

All praise is to Allah for His blessing in completing this thesis.

This has been a life changing experience, where I have grown and developed into a scientist. I could not achieve this without my family. I thank my mother and my father for their support and understanding during the last 3 years, without their prayers and well wishes this was not possible. I would also like to give my gratitude to my family members; Ami, Abu, Nana khala, Mani bhai and all of my cousins and nephews and nieces. A special thanks to Firdevs Kokkokoğlu for her help, her time, her love and support.

I thank Dr Huijun Zhu for her patience, unerring help and her support, without her this project would not be possible. I thank Dr James Njuguna for his suggestions and for time to discuss matters regarding project.

Thanks also to the people who aided my work during these 3 years Dr Cauchi for his aid with statistical analysis, Dr Edmands (Imperial) for his time and efforts to analyse NMR samples and to Dr Sophia Sachse, for all of her help and contribution towards the project.

The project is financially support by the European Commission under the FP7 program (NEPHH CP-FP 228536-2).

Also would like to thank all the Cranfield Health staff and my colleagues for their support advice and time.

ABBREVIATIONS

Al_2O_3	Aluminium oxide
CNT	Carbon nano tube
C_{60}	Fullerenes
COPD	Chronic obstructive pulmonary disease
COSHH	Control of substance hazardous to health
CO_2	Carbon dioxide
DNA	Deoxyribonucleic acid
DEFRA	Department for environmental food and rural affairs
DMSO	Dimethyl sulfoxide
DLS	Dynamic light scattering
DCFH-DA	2',7'-dichlorofluorescein diacetate
DMEM	Dulbecco's modified eagle medium
EHS	Environmental health and safety
ELISA	Enzyme linked Immunosorbant assay
FBS	Foetal bovine serum
FGC	Foam glass crystal
GF	Glass fibre
h	Hour
H_2O_2	Hydrogen peroxide

IC_{50}	Inhibitory Concentration of 50% of population
IL-1	Interleukin-1
IL-6	Interleukin-6
IL-8	Interleukin-8
ISO	International standards organization
IARC	International agency for research on cancer
LD_{50}	Lethal Dose of 50% of population
LPS	Lipopolysaccharide
m	Minute
M	Molar
mM	Millimolar
mg	Milligram
μg	Microgram
μg/ml	Microgram per millilitre
MMT	Montmorillonite
MNCNT	Multi walled carbon nano tube
MTT	(3-4,5-Dimethylthiazol-2yetl)-2,5-diphenyltetrazolium bromide
NF-κB	Nuclear factor kappa-light-chain-enhancer of activated B cells
NP	Nanoparticles
nm	Nano meter
PA6	Polyamide 6

PP	Polypropylene
PU	Polyurethane
PM_{10}	Particulate matter <10μm
PBS	Phosphate buffer saline
RO	Hydroxyl radical
ROO	Peroxy radical
ROS	Reactive oxygen species
RNS	Reactive nitrogen species
RPM	Rotation per minute
SiNP	Silica nanoparticles
SiO_2	Silica
SWCNT	Single walled carbon nanotube
SEM	Scanning electron microscopy
TNF-α	Tumour necrosis factor- alpha
TEM	Transmission electron microscopy
ZNO	Zinc oxide

TABLE OF CONTENTS

LIST OF FIGURES

LIST OF TABLES

LIST OF EQUATIONS

CHAPTER ONE

1 Introduction

Nanomaterials/nanotechnologies hold great economic potential for many industries, and the European economy as a whole. As of April 2008, the Project on Emerging Nanotechnologies claimed that over 600 nanotechnology products exist, with new ones reaching the market at a pace of 3-4 per week (Woodrow Wilson International Centre for Scholars 2010). According to the estimate by the Lux Research group, the market potential of nanotechnology products could be worth up to USD 2.6 trillion (around €1.9 trillion) by 2014 (Maynard, 2006).

Despite the rapid growth in the development and application of nanomaterials over the last two decades, little is known about the environmental and health risks posted by nanomaterials. Initial research has indicated that some nanomaterials may be more toxic than their larger counterparts when interacting with living organisms. As activity shifts rapidly from research to the applications, there exists an urgent need to understand and manage the risks associated with the development of nanomaterials. In fact, the risk assessment of nanomaterials has now become the focus of much attention. To date the widely accepted view is that there are many unanswered questions on the potential environmental and health risks associated with the manufacture, use, distribution and disposal of nanomaterials.

In addressing the concerns over the potential risk of nanotechnology, the UK Government published a strategic plan for responsible development of nanotechnology (HM Government, 2010) as highlighted in figure 1.1. This is aligned well with the global interest in the development of nanotechnology that offers better quality of life without compromising environment and human health.

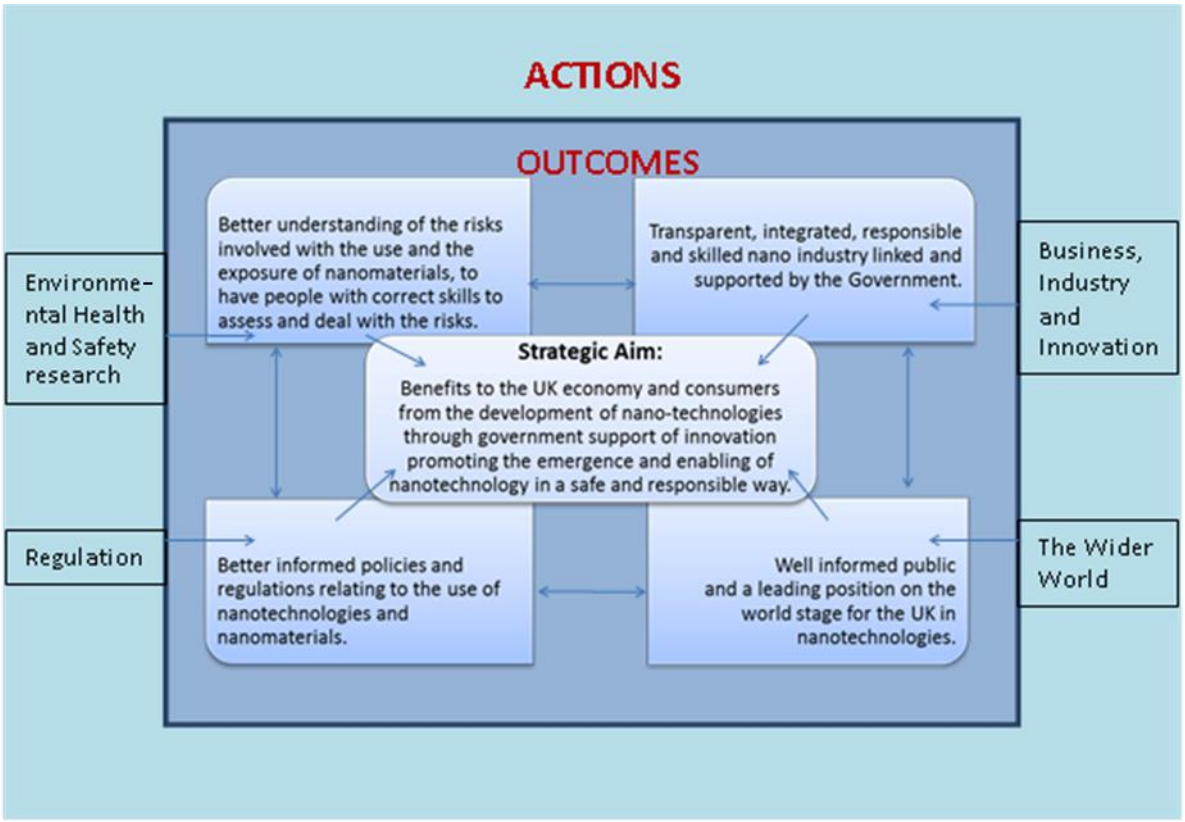

Figure 1.1 Plan of action outlined by HM Government for the control of nanotechnology.

1.1 Nanomaterials-related Environmental Pollution and Health Hazards

Nanomaterial-related Environmental Pollution and Health Hazards (NEPHH) is a project funded by the European Commission under the 7th Framework programme (CP-FP 228536-2), aiming to identify nanotechnology-related environmental pollutions and health hazards that could result from nanomaterial-reinforced products throughout their life cycle, and develop means to mitigate negative impact of nanomaterials. Through collaborations among the consortium involving 6 research institutes and 4 nanotechnology industries, the NEPHH project will address the following challenges:

1. Due to their small size, nanomaterials may have different interaction patterns from bulk material of the same composition with living organisms. Therefore the

methods for risk assessment of bulk materials are not suitable for the same materials in nano form. Regulators have attempted to address concerns about nanomaterials. However, size effects have not been addressed in the new European chemicals policy REACH (Regulation, Evaluation, Authorisation and restrictions of Chemicals), REACH aims to control the production and use of all chemicals and materials, limiting the potential hazards they may pose. The recommended limit of production of nanomaterials is quickly being reached, yet sufficient evidence of hazards posed is still required.

2. Characterization of nanomaterials has proven to be more difficult than anticipated for several reasons. First, standard protocols have not been developed. Second, an analytical infrastructure to allow characterization is not consistently available or well-located. In addition, biologists, physicists, and material scientists working in this area do not always communicate effectively.

3. Health, safety and environmental risks that may be associated with products and applications of nanoproducts need to be addressed throughout their life cycle, which requires integrated actions among the multidisciplinary teams.

For the NEPHH project, polymer-silicon based conventional composites and nanocomposites will be used as model materials to develop protocols for risk assessment through products life cycle analysis. Three engineering polymeric matrixes have been selected, including polyamides, polypropylenes and polyurethanes. Silicon reinforcement materials including nanosilica (SiO_2), layered silicates, glass fibres and foam-glass-crystal materials have been selected to produce polymer-silicon composites. The high potential of industrial scale production and therefore the likely release and disposal (intentionally or unintentionally) of raw materials and final products into the environment form the basis for choosing this group of materials. The specimens of the polymer-silicon composites will be provided by partners for assessing potential release of nanoparticles/nanomaterials under different scenarios, which include ageing and physical processing. The released nanoparticles and raw nanomaterials will be assessed for toxicity potential using different model systems. The results of the toxicity study

will inform the risk assessment of the chosen nanomaterials in comparison with conventional polymeric materials.

The NEPHH consists of a number of groups based around Europe. These groups all partake in the project by heading a work package, the groups involved were:

- Ekotek Ingenieria y Consultoría Medioambiental S.L. (EKOTEK)
- Cranfield University. (CRAN)
- Palladin Institute of Biochemistry of the National Academy of Sciences of Ukraine. (IBU)
- Cracow University of Technology. Department of Chemistry and Technology of Polymers. (CUT)
- Tomsk Polytechnic University.
- Fundación TECNALIA.
- Centre national de la recherché scientifique CNRS-ECCOREV.
- Grado Zero Espace Srl.
- Asociación para la prevención de accidentes.
- Laviosa Chimica Mineraria.

The details of the groups involved in each work package of the NEPHH project and the outcomes of the work packages are presented in table 1.1.

Table 1.1 Summary of NEPHH work packages, leaders of each work package and the target outcomes.

Work Package	Leaders	Target
1. Technological Surveillance System.	EKOTEK	Develop a systematic, continuous practice for selection of ENMs.
2. Working Nanomaterials: Supply and Preparation	CUT	Manufacture of selected ENMs.
3. Generation of Nanoscale Dust Particles from Macroscale Fibre Reinforced Nanostructures	CRAN	Generation of nanoparticles and nanodusts with a consideration of real life exposures throughout life cycle.
4. Health Implications	CRAN, IBC	Finding the effect of nanoparticles on the (i) lungs; (ii) structure of cells and expression of proteins
5. Environmental Implications	CRNS	Assessment of persistence, bioaccumulation and eco-toxicity studies.
6. Integrated Assessment	EKOTEK	Understanding the outcomes from WP 4 and WP 5, aiming to make available the understanding of safety, environmental and health implications.
7 & 8. Dissemination of the Research	EKOTEK	Communicating the reports gained from NEPHH.

Table 1.2 Summary of nanomaterials used for assessment by NEPHH. Table states the composition of each material using specific reinforcement materials

Polymers	Reinforcement Materials (5% ww)					
	Montmorillonite (MMT) Delite 43B	Montmorillonite (MMT) Delite 72T	Aerosil © 200 SiO_2 (Hydrophilic)	Aerosil © 974 SiO_2 (Hydrophobic)	Foam Glass Crystal (FGC)	Glass Fibre (GF)
Polyamide 6 (PA6)	PA-MMT		PA-SiO_2		PA-FGC	PA-GF
Polypropylene (PP)		PP-MMT		PP-SiO_2	PP-FGC	PP-GF
Polyurethane (PU)	PU-MMT		PU-SiO_2		PU-FGC	PU-GF

1.2 Definition of nanomaterials

Nanomaterials are generally considered as engineered materials with morphological features on the nanoscale i.e. one or more dimensions or characteristic aspects below 100 nm, whilst nanoparticle refers to a particle which has at least one dimension below 100 nm. Some organisations, however, such as the International Standardization Organization (ISO) (ISO, 2008) technical committee and the Scientific Committee of Emerging and Newly Identified Health Risks (SCENIHR), suggest that the term nanoparticle should only be used for materials with 3 dimensions below 100 nm. Therefore, materials such as nanofibres and nanotubes which may have a diameter of in the nanoscale (1-100 nm), but a length of several microns can no longer be considered nanoparticles. These are suggested to be nano-objects. The figure 1.2 outlines the latest version of the definition of nanomaterials, which could be subject to revision according to future requirement.

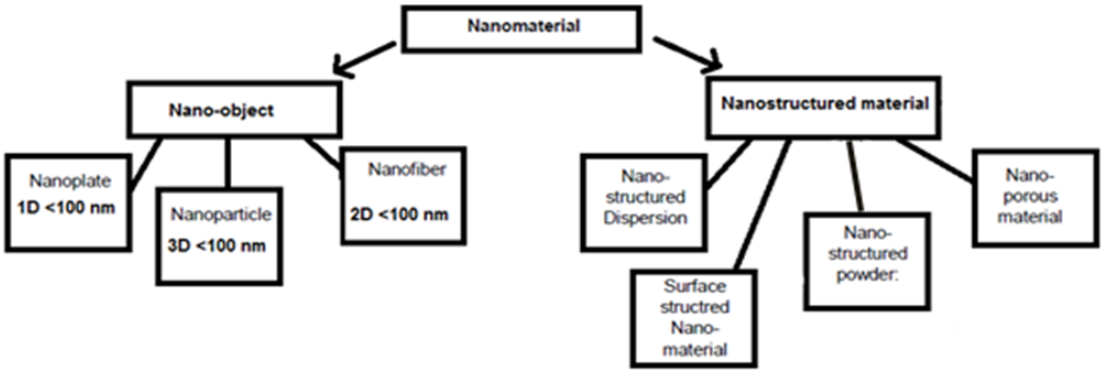

Figure 1.2 Schematic overview of nanomaterial definitions by ISO in 2008: differentiation of nanomaterials into nano-objects and nanostructured materials (ISO, 2008).

For clarity within this thesis the term nanoparticle refers to materials with all dimensions to be between 1-100 nm and nanomaterial for all other materials with at least one dimension or physical character which is at the nanoscale (ISO, 2008)

1.3 Life Cycle Analysis (LCA)

LCA is a tool that aims to compare all environmental and health effects assigned to a product to improve the processing, create policies and help make sound decisions. LCA therefore identifies all environmental and health impacts, which are associated with the product at each step of its life. LCA is also an important factor in achieving the standardisation of assessment methods for nanotechnology and nanomaterials. The urgent need and application of LCA was highlighted as an outcome of the 1992 UN meeting in Rio de Janeiro, in which the decision to take the idea of sustainability as of utmost importance was recognised. The important facet of sustainability has a reliance of having a comprehensive LCA in order to truly have a full Life Cycle Sustainability Assessment (LCSA). In the form of ISO 14040 it gives the principles and the framework to test manufactured products. Furthermore, an initiative of ISO 14044 lays the guidelines and requirements for LCA studies (ISO, 2006). LCA in itself is one of the 3 components of LCSA, with the other components being Life Cycle Costing (LCC) and Social Life Cycle Assessment (SLCA). The three pillars equate as shown:

Equation 1.1 Life Cycle Sustainability Cycle Assessment: Life Cycle Sustainability Assessment (LCSA); Life Cycle Costing (LCC); Life Cycle Analysis (LCA); Social Life Cycle Assessment (SLCA) (Kloepffer, 2008)

$$LCSA = LCC + LCA + SLCA$$

As it is also unclear exactly how nanomaterial toxicity alters during its life cycle, many groups have highlighted this as a big concern. The understanding of toxicity must encompass all stages at which nanomaterials are potentially exposed to the environment and humans (Kloepffer et al., 2008). With LCA a focus strategies are being developed to tackle the gaps in knowledge and to address the unknown risks which may be attached to nanomaterials during different points in their life (Hischier et al., 2012; Bauer et al., 2008).

According to the LCA concept, the assessment of potential human exposure to nanomaterials and associated risk is summarised in Figure 1.3. A products life is observed from the raw form through their processing and modification to the disposal or the recycling of the material. At each stage the potential of environmental and human exposures is to be assessed. The understanding of the impacts at each stage aid a better understanding of what problems may arise from the application of a product, not only at one stage and one point in time, but throughout the life of the product.

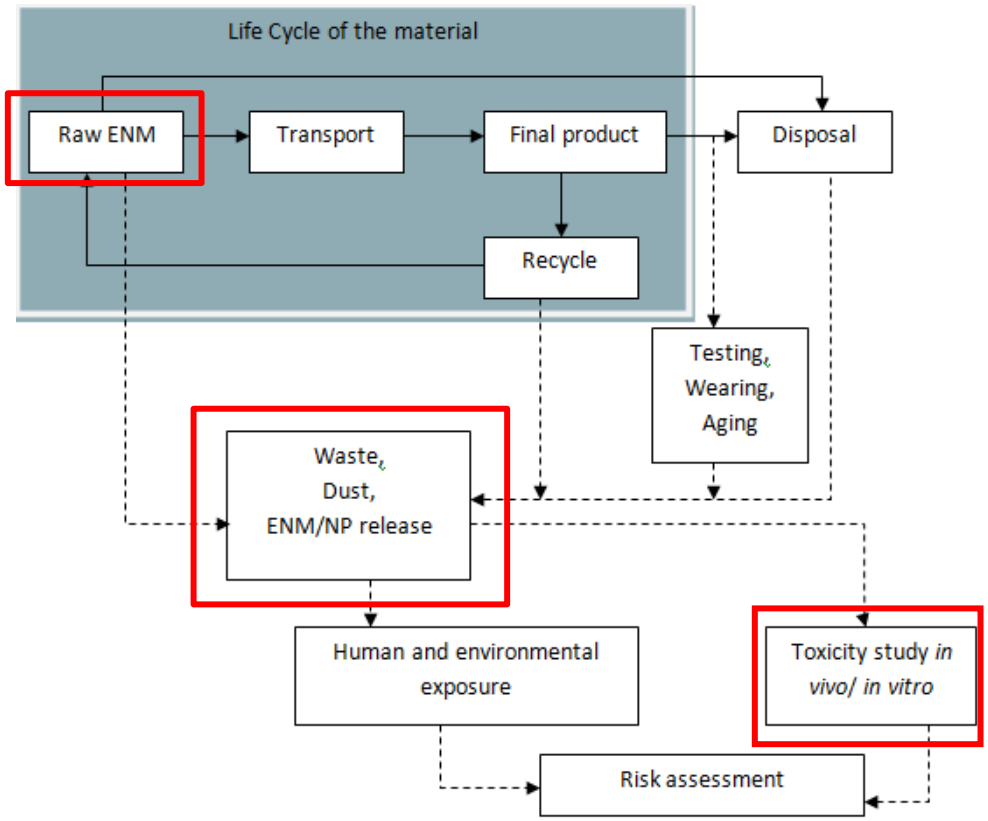

Figure 1.3 Schematic diagram of LCA: The exposure to and risk assessment of engineered nanomaterials (ENM) throughout nanoproducts life cycle. The solid lines indicate the life cycle and the dotted line indicate the points of NP release and risk assessment. This study focused on *in vitro* toxicity studies of raw ENM and waste/dust NP as highlighted by red boxes.

LCA is a very important requirement for safe production and usage of nanoparticles. It was highlighted in the studies conducted by the Woodrow Wilson International Centre for Scholars, (2010), that the majority of nanotechnology products are being used in the healthcare and fitness sector. It has been known that many creams and topical drugs contain nano sized substances, and nanocomposites have been used in a wide variety of sports equipment. Therefore LCA is a fundamental requirement for understanding of how a material will affect the surrounding environment and people.

The advantages of a complete LCA studies of a product are to be able to identify the impact of a given material before the material is exposed to the environment and therefore, potentially to avert unnecessary risks to the environment and the people in direct contact (Seager and Linkov, 2008). However, it is not easy to conduct an accurate LCA on newly engineered nanomaterials, as the products in which they will be used may still be in the testing phase and therefore the final life span of the material may not be known. This element of uncertainty is highlighted by Seager and Linkov, (2008). Not only are the mechanical properties different at nanosize range, properties which may influence the toxicity of a material are also changed, such as chemical and physical properties; usually the material on the nanoscale is more toxic than its larger counterpart bulk material (Cho et al., 2009).

Human exposure to nanomaterials can occur at many different points in the life of a material, at the processing stage of the material to the transportation and finally the final application of the material (Som et al., 2010). This would mean that not only are there variable points in the materials life that nanoparticle can be released, but also human exposure to nanoparticles can occur through different routes. Workers would be exposed during production, handling and transporting of the nanoproducts mainly through inhalation and dermal contact. However for the general public, the elderly and children, the exposure could occur through application and consumption of nano-enabled products via ingestion and dermal routes. By highlighting the possible routes of exposure it can also be predicted where the exposure will have greatest impact from which a suitable model can be derived (Christensen and Olsen, 2004).

There are few reviews of nanomaterial LCA, however they are not regarded as being comprehensive (Bauer et al., 2008). Most groups conclude that the ISO, (2008) and ISO, (2006) guidelines are sufficient to adhere to (Kloepffer, 2008). However, as understanding increases regarding NP toxicity more groups are working towards a better framework for LCA (Som et al., 2010; Irfan et al., 2012; Hischier and Walser, 2012). Specifically Hischier and Walser, (2012) produced an excellent review regarding this subject. In the review they presented all recent studies specific to NP LCA. They concluded that the studies that have been published so far lack credible data, 7 out of 17 studies used only 1 weight unit of material, this implies that an acceptable model for continuous release and exposure has not been established. They argue that this is only examining the risks associated with the production process and not the functionality of the materials.

Taking the studies and reviews conducted thus far into consideration, this study focuses on helping to fill some aspects of this gap in knowledge regarding NP LCA. Through consideration of airborne release, physical characteristics, the toxicology of the released particles and the toxicology of the unprocessed starting material, a comprehensive set of data can be produced for assisting the health risk assessment of NP.

1.4 Characteristics of nanomaterials and micromaterials used in NEPHH

It is known that the properties of a material are altered when within the nanoscale, where the laws of quantum size begin to have an increasing influence (Volokitin et al., 1996). Not only are the mechanical properties different at this size range, properties which may influence the toxicity of a material are also changed, such as chemical and physical properties; usually the material on the nanoscale is more toxic than its larger counterpart bulk material (Cho et al., 2009).

The idea that the properties of nanomaterial differ considerably from the bulk material can be traced back to as early as 1982, when Boutonnet et al., (1982) used microemulsions to generate ultrafine (UFP diameter = <100nm) monodisperse particles of Pt, Pd and Rh. Later, in 1995 this work was built upon to generate TiO_2 nanoparticles (Chhabra et al., 1995), which was confirmed by Transmission Electron Microscopy (TEM) imagery. Further work, conducted in 2000 on TiO_2 nanotubes, began to show changes in morphological, structural and chemical properties of these nanomaterials. They went on to show in fact that dependant on the size and form (nanoparticle or nanotube) the chemical structure can be altered by the alteration of electronic interaction with atoms, leading to an increase in photo catalytic decolourisation (Zhang et al., 2000). Using Fourier Transform Infra-Red (FT-IR) spectra assay, Zhang et al. (2000) also showed that the change in Ti-O-Ti bond while producing TiO_2 nanoparticles from bulk caused this change in photo catalytic property; and that it may be due to electron interaction within atoms.

These differences in chemical bonding and the effect on the properties of the materials can be advantageous in specific applications. This beneficial nature can be used to impart onto other materials and structures in the form of a composite. Studies by groups such as Wacharawichanant et al., (2008) showed that nanosized zinc oxide composites had increased mechanical properties, i.e. tensile strength and young's modulus compared with micron sized particles in a composite. It is known now that the fracture toughness of an epoxy resin can be improved by dispersing spherical nanosilica within the organic matrix. This was shown by Chen et al., (2008) who used 12 nm spherical silica particles that caused the energy to dissipate throughout the material therefore to increase the energy required to fracture the resin, which without the nanoparticles is known to be brittle.

In the NEPHH project, SiO_2 and MMT have been used to develop polymer-nanocomposites. For comparison, some microsized silicon particles were also used as filler to generate polymer silicon-composites. This section reviews currently available information on the characteristics of these filler materials, which could be important features governing their toxicological behaviour in biological systems.

1.4.1 Silicon dioxide nanoparticles (SiO_2 NP)

Naturally occurring silicon dioxide or silica is found abundantly on Earth, present predominantly as alpha-crystalline quartz (figure 1.4b). Crystalline silica has been classified by the International Agency for Cancer Research (IARC) as a probable carcinogen in 1987 and in 1997 it was reclassified as a Group 1 carcinogen, i.e. that there was sufficient evidence for carcinogenicity in experimental animals and sufficient evidence for carcinogenicity in humans (IARC, 1997). Crystalline silica is often used as a positive control in toxicology testing (Lin et al., 2006; Donaldson and Borm, 1998). Man-made silica, however, is predominantly in the form of amorphous particles (figure 1.4a), these include fumed, precipitated, colloidal, and mesoporous silicas. Fumed silica is produced as dry aggregates under high temperature flame (Pratsinis, 1998), These silica particles have been manufactured at industrial scale to meet an ever-increasing demand for a wide range of applications including construction materials, cosmetics, food, and medicine (Fruijtier-Pölloth, 2012; Kumar et al., 2010).

a b

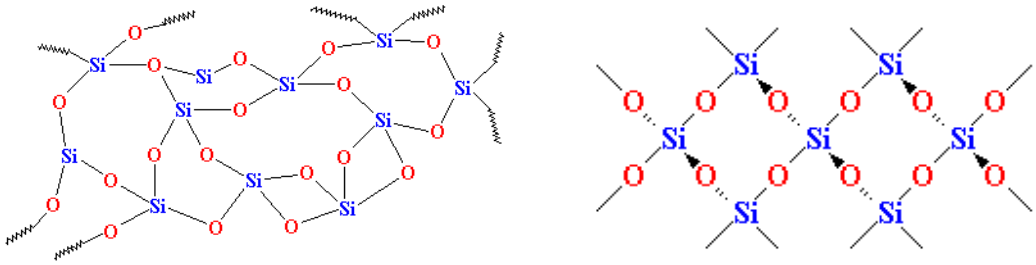

Figure 1.4 Chemical structure of silica. a. amorphous structure of silica; b. crystalline structure of silica.

Amorphous nanosilica is often used as filler to reinforce composites. Recent studies have been conducted using nanoindentation (a variety of hardness testing for

materials) to derive the elastic modulus of individual SiNP, the toughness/elastic modulus for SiNP is around 70 GPa (Tetard et al., 2008). The SiNP to be used in NEPHH are amorphous spherical particles with an average diameter of 12 nm sourced from Degussa Evonik. The SiNPs provided were, Aerosil 200 (hydrophilic) and Aerosil 974 (hydrophobic). The Aersoil 974 surface was modified by dimethyldichlorosilane treatment, rendering it hydrophobic. Another two fumed SiO_2 NP 7 nm and 14 nm were acquired from Sigma-Aldrich, both considered hydrophilic. As fumed SiNP are more likely to become airborne, therefore posing a higher risk for environmental exposure. Studies are deemed necessary to establish the toxicity potential of fumed SiNP. For these reasons fumed SiNPs were included as controls in toxicity study without surface modifications.

1.4.2 Montmorillonite (MMT)

MMT is a soft phyllosilicate group of minerals which form crystals, which in turn forms a clay. The clay is known to have 2 tetrahedral sheets on either side of a central octahedral sheet to form layer structure. The chemical formula and structure of MMT are as follows:

Equation 1.2 Montmorillonite chemical formula

$$(Na, Ca)0.33(Al, Mg)2(Si4O10)(OH)2 \cdot nH2O.$$

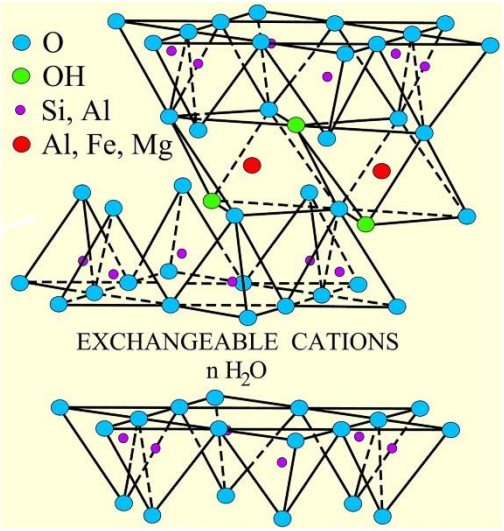

Structure of montmorillonite (MMT) adapted from Grim 1962.

Figure 1.5 Structure of MMT as adapted from Grim, (1962).

The individual layer has an up to 100 micrometre across and few nanometres in thickness. This high aspect ratio gives MMT its superb property as nanomaterials with a variety of applications. MMT has a considerably high modulus, a toughness of 170 GPa which is higher than that of titanium alloys around 105-120 GPa. The Society of Plastic Engineers (SPE) concluded as an outcome of ANTEC 2002 conference that the dispersion of nanoclays does increase the base properties of the resin used if dispersed uniformly and thoroughly (Cho et al., 2002).

The basic material properties of MMT are (Rockwood specialities, 2006):

- Modulus: 170GPa
- Shape: Platelet
- Aspect Ratio: 1 nm thick, 75-100 nm across
- Surface Area: >750 m^2/g
- Particle: robust under shear, not abrasive

1.4.3 Glass fibres (GF)

The GF has a similar structure to that of amorphous silica shown in figure 1.4. GF are also extremely light materials and have been used for a long time in the automotive industry in various applications. For example they have been used to strengthen plastics for making bumpers in vehicles. The basic material and physical properties are (MATBASE, 2009):

- Modulus: 73 GPa
- Shape: Fibre
- Aspect Ratio: 8-20 µm thick, long fibrous material
- Density: 2600 kg/m^3

GF are generally generated in micron size, combining with polymer matrix will create a strong composite.

1.4.4 Foam-glass-crystal (FGC)

The exact crystal structure of this material is not disclosed due to commercial use. Made totally from recycled glass with minimum virgin additives, FGC is preferred to be used in civil constructions and insulations due to its watertight nature. The use of this material allows structural and mechanical improvements in a given final product such as composite for making lightweight vehicles.

Made from 98% recycled material and only 2% additives (inorganic salts) (ENCO Engineering GmbH Switzerland, 2004), FGC is a model of excellence for re-cycling and green friendly environment. Due to lack of availability of published data on this new and innovative material, it is difficult to highlight the properties of this material with respect to this study.

1.5 Toxicology of Nanomaterials (both *in vivo* and *in vitro*)

The area of nanotoxiocology was first recognized in the early 2000s emphasizing the need for identification of hazardous nanomaterials. In fact some concepts of nanotoxicology were derived from studies of ultrafine particles (UFPs), which are defined as particles smaller than 100 nm (Donaldson et al., 2000). UFPs studies have led to a greater understanding of nanoparticles. Studies have shown that UFPs are more toxic than their related micron sized particles at the same dosage in both *in vitro* and *in vivo* studies.

Rat models exposed to UFPs showed increased lung injury and pathology than rats exposed to larger particles of similar material (Donaldson et al., 1998). Studies with particles less than 50 nm in diameter also showed toxicity greater than larger particles after chronic inhalation exposure *in vivo* using rat models, leading to fibrosis and lung tumours (Oberdörster, 1996). The same dose both inhaled over 12 weeks, the UFP (approximately 20 nm) TiO_2 particles, had considerably higher retention in the lungs, and bronchoalveolar inflammatory response as compared with fine particles (approximately 250 nm) in rat. Some groups have worked on ultrafine particles for over 10 years concluding that the particles with such small sizes make them increasingly difficult to remove from the contact area leading to a large deposit over time and sustained exposure, which in turn leads to prolonged contact. This prolonged contact was hypothesised to cause inflammation, with the vast surface area in contact with epithelial cells leading to possible generation of free radicals (Donaldson and Borm, 1998; Oberdörster et al., 2004; Oberdörster et al., 2005)

UFPs are produced in a broad spectrum of chemical composition and sizes, this heterogeneous nature of UFPs makes it difficult to compare the effect of the particles on human exposure to engineered nanoparticles, which may have a concise size range and shape (Donaldson et al., 2004). Once at a nanoscale not only does a material have differing physical properties to that of the bulk material but this change may cause a different biological effect, which suggests a possibility of toxicity being increased. Since the recognition of nanotoxicology, research into the toxicity and associated

mechanisms of nanomaterials has increasingly drawn attention from government, regulatory bodies, consumers and different industrial sectors including pharmaceuticals, chemical industry, and cosmetics. The studies so far have been conducted in a range of nanomaterials that have been prioritized for study in the EU and some other regions in recognition of the potential value of their applications. For critical review of nanomaterial/nanoparticle toxicity data published in peer reviewed literatures, Silica NP and MMT that are involved in NEPHH project, together with some representative nanoparticles of different forms as listed in the table 1 were selected, with an aim to understand the relationship of nanoparticle characteristics and toxicity.

There are some important measurements that used for toxicology studies, which are used to assess at which concentration a substance is harmful. These measurements allow for a better understanding of how to control toxic substances. Two of these measurements that are widely used are:

- Lethal Dose 50 (LD_{50}); calculated dose of a substance which causes the death of 50% of an entire defined experimental animal population.
- Inhibitory Concentration 50 (IC_{50}); calculated concentration of a substance which causes inhibition of growth in 50% of an entire defined population.

Yang et al., (2002) worked on determining the effective concentration of a toxin *in vivo* and *in vitro*. It was suggested that IC_{50} *in vitro* is as accurate in the prediction of toxicity as LD_{50} from rats *in vivo*. It is also argued that not all cytotoxic responses are basal responses (Clemedson et al., 1998), but they are linked to the specific function of the cell line. These studies maintain the importance of both forms of studies, but also show there is a correlation between what results may be found.

1.5.1 SiO_2 NP

It is known that crystalline silica is highly toxic, and a class 1 carcinogen (IARC, 1997). Exposure to crystalline silica could lead to severe silicosis (IARC,

1987). This information was a product of necessity due to occupational health concerns dealing with inhalation of crystalline silica (Hessel and Sluis-Cremer, 1987). Furthermore a study by Calvert et al., (2003) showed that crystalline silica is also associated with lung cancer, chronic obstructive pulmonary disease, rheumatoid arthritis and tuberculosis.

Amorphous silica on the other hand has been much less studied. Some brief work has led to the conclusion that amorphous silica has varying toxicity potentials, which may be dependent on other characteristics of the material, such as size, shape and surface chemistry (Warheit, 2001). The varying toxicity potential derived from different studies has caused concerns as to what causes differences in essentially the same substance. Is it the size, the surface chemistry, or is it more complex than that?

An *in vivo* study conducted on mice that were intratracheally administered with both amorphous and crystalline silica at 2, 10 and 50 mg/kg found that the amorphous silica nanoparticles induced a higher level of lactate dehydrogenase (LDH) increase in Bronchoalveolar Lavage (BAL) fluid and inflammation in the lungs at early stage than crystalline silica, BAL fluid collected via insertion of a tube into the bronchial pathway and fluid is squirted into the lungs then recollected for examination. LDH is an enzyme found usually inside cells, it is produced as a response to ROS; an increase of LDH suggests increase ROS. However, these effects were detected to have subsided at 1 and 4 weeks after exposure. It was therefore concluded that the SiNP induced transient but severe lung inflammation (Cho et al., 2007). LDH is an enzyme which is present in cells, it is used to catalyse the pyruvate to lactate reaction. An increase of LDH in the BAL suggests the membrane damage of cells in the lungs. Another study examined the production of LDH in BAL in rats after inhalation of crystalline (3 mg/m^3) and silica amorphous silica (50 mg/m^3) for 6 hours a day and 5 days a week for up to 13 weeks. The amorphous silica produced almost twice the production of LDH in BAL than the crystalline. However, over the recovery period the levels of MIP-2 (chemokine expressed due to oxidative DNA damage) in rats treated with amorphous silica decreased to close to controls, whereas the level of MIP-2 in rats treated with crystalline silica remained high. High concentrations of amorphous silica over a prolonged period

caused pulmonary cell damage as indicated by initial high levels of LDH in BAL (Johnston et al., 2000).

With all the work which has been conducted it is still not clear as to what is the underlying mechanism for these adverse inflammatory effects induced by silica, as presented by the studies above, although there seems some evidence that both inflammatory and oxidative stress are involved through a linked pathway i.e. oxidative stress triggering the production of inflammatory markers to initiate a response. It has been suggested that one may mediate the other i.e. oxidative stress leading to inflammation (Oberdörster et al., 1990; Oberdorster et al., 1992; Øvrevik et al., 2006; Park and Park, 2009; Huaux, 2007).

Kaewamatawong et al., (2006) found moderate to severe inflammatory responses in mice which were intratracheally instilled with 0, 0.3, 3, 10, 30 or 100 μg of ultrafine colloidal silica particles. Park and Park, (2009) investigated the response to silica NPs both *in vivo* and *in vitro*. They found that mice treated with a single dose (50mg/kg) led to increased blood level of IL-1β and TNF-α, both associated with inflammation. With higher doses (100 and 200 mg/kg) SiNP induced splenocyte viability reduction, which was associated with the overproduction of nitric oxide (NO), a signalling molecule that causes the increase of IL-1β and TNF- α concentration in blood. The increase in IL-1β and TNF-α expression was suggested to be the consequence of oxidative stress induced by ROS. These cytokines have been identified to be important mediators of inflammation caused by silica nanoparticle treatment (Park and Park, 2009; Sharma et al., 2007).

As mentioned earlier there may be other factors which affect toxicity potential further than just crystalline structure. Size is one of the factors that have been explored by some groups who looked at the effects of different sized silica nanoparticles. Using SiNP particles sized 60 and 100 nm to treat A549 cells and THP-1 macrophages, it was shown that the smaller size induced a higher LDH response than lager particles (Wottrich et al., 2004). There are many other reports on size effect of SiNP toxicity, although sometimes contradicting to some degree.

Studies have also been conducted on testing the idea that particle surface property is a key factor in determining SiNP toxicity. Using erythrocyte haemolysis as a toxicity endpoint, the effect of surface silanol group on SiNP toxicity has been studied. It was suggested that the density of surface silanol group was associated with aerosol particle toxicity (Fenoglio et al., 2000; Murashov et al., 2006). More recently studies suggested that surface area, chemical, hydrophilicity and catalytic properties should all be considered when studying toxic properties of particles (Limbach et al., 2007) (Fubini et al., 1999). By heat treating crystalline silica, Fubini et al., (1999) altered the surface chemistry making one sample hydrophilic and one hydrophobic. It was found that hydrophilic sample was considerably more toxic than the hydrophobic sample as tested on mouse monocyte macrophages J774 (Fubini et al., 1999). However, they did not offer an explanation to their findings. This study leaves an interesting question to whether the same will apply to the amorphous silica.

1.5.2 Montmorillonite (MMT)

MMT has been used in a wide range of areas including construction materials, food and medicine. Although it is conventionally considered safe for use in food and medicine, MMT property could be changed after modifications as required in some applications.

It has been shown in rats that MMT can be absorbed into the body within 2 hours without any accumulation in any specific organ or toxicity (Baek et al., 2012). The tests were conducted over 24-72 hours and at concentrations ranging from 0.5-1000 μg/ml from single exposure orally.

Very few *in vitro* tests have been conducted on unmodified MMT. Recently as the interest has grown in medical application of MMT, some groups have conducted toxicity experiments on modified MMT. Using Caco-2 cells as a model, it was suggested MMT-chitosan are biocompatible based on the observation that cell growth was enhanced in the presence of MMT-chitosan at 5 to 500 μg/ml (Salcedo et al., 2012).

A study by Styan et al., (2008) was also in favour of biomedical uses of MMT. However, with surface coating modifications they feared toxicological effects following release of coating molecules. There are some other groups suggesting that with a suitable coating, MMT is a very good candidate for biomedical application (Zhuang et al., 2007; Zheng et al., 2007).

1.5.3 Other inorganic nanomaterial toxicology

Inorganic nanoparticles have been of great interest due to their applications in medical diagnostics and treatments. They include iron oxide nanoparticles (Fe_2O_3), titanium oxide (TiO_2), quantum dots (QD), gold (Au) and silver (Ag) nanoparticles.

Oxides:

Iron oxide (Fe_2O_3/Fe_3O_4)

Iron oxide is referred to as a ferromagnetic material; this means it will respond to an external magnetic field by producing a magnetic moment along the external field lines. This is caused by the alteration of the Weiss domains (magnetic domains). However, once the magnetic field is removed these domains can remain coupled and create a residual magnetism. Iron oxide based NP have been explored to develop cost effective, sensitive and versatile assays for medical diagnosis (Mornet et al., 2004).

However, studies conducted in rat showed that exposure to 8.5 mg/kg twice a day for three days of iron oxide (Fe_2O_3) NP induces acute histopathalogical changes in liver and lung. There was no elevation in serum enzyme activities, which are often reported *in vitro* studies due to cell membrane damage (Wang et al., 2010). Studies using *in vitro* model, such as J774 cell line, suggested that iron oxide NP could interfere with cellular function causing cell membrane damage, as suggested by an increase in LDH leakage (Naqvi et al., 2010).

Titanium (TiO_2)

Titanium dioxide NPs are generally considered safe for topological application and have been used extensively in sun screen creams. A recent study, using rat liver cells (BRL 3A) as a model, showed that TiO_2 NP had no toxic effect at lower dose (<50 µg/ml) but had significant toxic effect at higher doses (>100 µg/ml), as assessed by cell viability and LDH leakage assays (Hussain et al., 2005).

Installation tests using rat models have shown somewhat contrary results to the belief that TiO_2 is an inert nanoparticle. After oral administrations over a period of 65 days through feeding with 1% and 2% TiO_2 NP, albino rats showed a significantly reduction in fertility and liver hepatic cell damage (EL- Sharkawy et al., 2010).

Cerium (CeO_2)

Eom and Choi, (2009a) worked *in vitro* with CeO_2 NP to assess their toxicity, and found that these particles induce oxidative stress in BEAS-2B (human bronchial epithelial) cells. They concluded that the induction of oxidative stress occurs through ROS generation leading to heme oxygenase (HO-1) upregulation via the p38-nrf-2 pathway. Most interestingly they showed that larger particle induced a greater level of toxicity, which was against the idea that smaller particles are more toxic due to an increased surface area to volume ratio.

In vivo studies have been conducted using rats. CeO_2 was shown to induce apoptosis in alveolar macrophages (Ma et al., 2011). It was concluded that CeO_2 NP induced inflammation, cytotoxicity and damage to airway, thus, inducing fibrosis in the lung through inflammation.

Gold

The optical features that are present in gold nanoparticles make them extremely exciting for uses in biomedical applications (Han et al., 2007). However it has been found that smaller sizes of gold NP (<4 nm) can induce cytotoxicity via entering into the nucleus of the cell (Rivera Gil et al., 2010). It was suggested that it was not the gold NP themselves which caused toxicity, rather it is caused by unwanted residue molecules from the production process. In another study, it was observed that the gold NP were taken up into K562 leukaemia cells, but the toxicity was observed in cells treated with the control residue molecules and unwashed gold NP but not in the cells treated with washed gold NP (Connor et al., 2005). Khandelia et al., (2013) developed drug loaded gold NPs which were coated with albumin to stabilise them and to increase the uptake of the NPs into cells. Doxorubicin loaded and albumin coated gold NP were taken up by HeLa cells more efficiently. Field-emission SEM showed apoptotic bodies, confirming that the doxorubicin had been released. These studies provided evidence that NP size is not necessarily the fundamental aspect determining NP toxicity potential, which may be more closely related to chemistry of the particle or indeed associated with molecules that the NP carries, such as production residues or toxic chemicals loaded as drugs for theraputics.

Quantum dots (QDs)

Quantum dots are unique nanocrystals with distinct optical and electrical features, usually consisting of a heavy metal core coated with an inert outer shell (Bruchez Jr. et al., 1998). Their fluorescence spectra make them ideal fluorophores for imaging uses *in vivo* (Chan et al., 2002).

Toxicity evaluation of quantum dots (QD) is not so easy, as difference in their production process can lead to different chemical properties which in turn can convey different toxic potentials (Hardman, 2006). In each case the surface charge, size, outer coating and oxidative/photolytic state can be different. It was found that QD with CdTe

core are toxic *in vitro* to rat PC12 cells at as little as 10 µg/ml. It was also found that an uncoated CdTe core was even more toxic, causing cytotoxicity at just 1 µg/ml (Lovrić et al., 2005a). Studies show that QD coating itself may impart toxic effects without a chemical core, and surface charge is very important to the translation of QD toxicity (Hoshino et al., 2004). Studies using different sizes of QDs with equal surface charges revealed that cytotoxicity increases as size decreases e.g., 2 nm quantum dot has greater toxicity than 5 nm quantum dot/ml (Lovrić et al., 2005b). These studies lead to a conclusion that QD toxicity is controlled potentially by three factors, the size, the surface charge and the core.

Table 1.3 (p.46) is a summary of some toxicity studies conducted on a variety of NP. Most toxicity studies suggested that physical characteristics are an important contributor to the toxicity of any NP. The surface charge and the size, have all been shown to have some effect on cell viability *in vitro* and tissue/organ damage *in vivo*, suggests that it is impossible to predict NP toxicity based on any single parameter of NP characteristics.

1.5.4 Organic nanomaterial toxicology

Organic compounds are regarded as any compounds of gaseous, liquid or solid form containing carbon. In the same way, nanomaterials containing carbon are defined as organic. These would include the family of fullerenes, which are any molecules composed entirely of carbon such as buckyballs (C_{60}/C_{70}), carbon multiwall nanotubes/singlewall nanotube (MWNT/SWNT) (Immunologie et Chimie Therapeutiques, 2004) and polymer nanoparticles e.g. polystyrene nanospheres, polymer nanocomposites and dendrimers (figure 1.6).

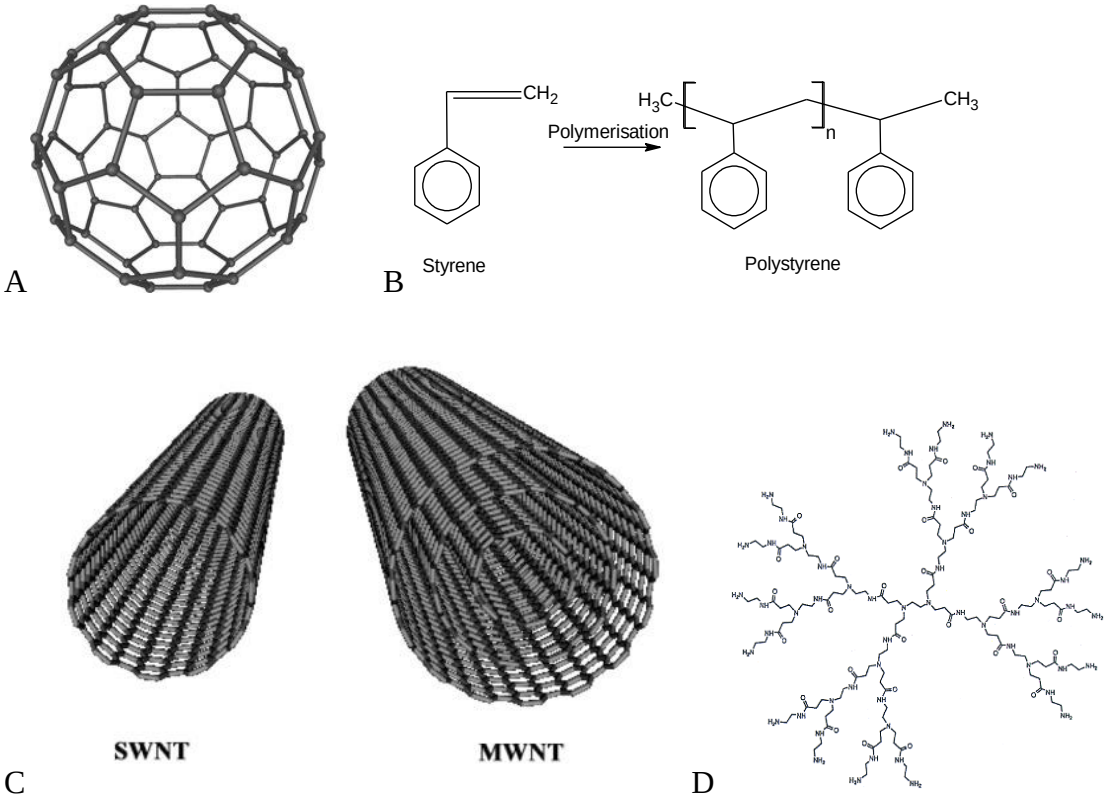

Figure 1.6 Representatives images of nanomaterials. A) Representation of C_{60} structure also known as buckyball, (Nature, 2011) B) Schematic diagram of styrene and polystyrene that may be used as a matrix in polymer nanocomposite, C) Single wall and Multiwall carbon nanotubes (SWNT/MWNT), (Immunologie et Chimie Therapeutiques, 2004), D) Polyamidoamine (PAMAM) dendrimers.

Fullerenes

There have been a number of studies conducted on fullerenes toxicity. A study by Yamawaki and Iwai. (2006) showed induction of morphological changes in HUVEC (Human Umbilical Vein Endothelial Cells) by 7.1 nm of $C_{60}(OH)_{24}$ fullerenes at 1-100 µg/ml. Vacuole formation and cell density decrease were observed in a C60(OH)24 concentration dependant manner. However, cell death was observed at the highest concentration of 100 µg/ml as assessed by Lactate Dehydrogenase (LDH) leakage assay. The chronic effects of low dose exposure to C_{60} (1 µg/ml) were also detected in endothelial cells, the cell adhesion was inhibited. A study using male rats demonstrated that treatment with water soluble C_{60} NP at 2.22 mg/m^3 for 3 hours a day for 10 days

consecutively led to the bioaccumulation of fullerene nanoparticles and atherosclerosis *in vivo*. However, the specific mechanism of toxicity was left unanswered. Baker et al., looked at bronchial alveolar (BAL) fluid after inhalation exposure to rats with 50 nm C_{60} particles. They found no statistically significant toxic effects of fullerenes (Baker et al., 2008).

Sayes et al., (2005) also worked on fullerene cytotoxicity, using LDH leakage assay they showed increase cytotoxicity in Human Dermal Fibroblasts (HDF), however the dose metric used in this study was parts per billion (ppb), making it difficult to compare with similar studies using alternative dose metrics. Thiobarbituric acid (TBA) assay was conducted to measure lipid peroxidation caused by nano-C_{60}, from this they concluded that lipid peroxidation is the mechanism of toxicity for fullerene. Studies conducted by the same group worked to identify the differences between C_{60} pristine molecules and derivative $C_{60}(OH)_{24}$, which is water soluble. The striking difference between the two molecules was the zeta potential, pristine zeta potential being ~-30 mV and the derivative being 0 mV. It was reported from this study that pristine C_{60} was seen to be 3-4 times more toxic *in vitro* then $C_{60}(OH)_{24}$. However, when assessed *in vivo* there was no difference in toxicity observed (Sayes et al., 2007).

Carbon nanotubes (CNTs) are also a member of the fullerene family. One of the most attractive features of nanotubes is the length to diameter ratio, which can be up to 132,000,000:1 (Wang et al., 2009). Single-walled nanotubes can have diameters of 1-3 nm whereas multi-walled nanotubes can have diameters of 10-100 nm. CNTs have extraordinary thermal conductivity, mechanical and electrical properties. These properties make them an exciting potential target for nanotechnology, but may also lead to increased toxicity.

Herzog et al., (2007) conducted an *in vitro* study into the toxicity of single-walled carbon nanotubes (SWNT) using three human cell lines, human lung carcinoma (A549), human skin keratinocyte (HaCaT) and bronchial epithelial cells (BEAS-2B). Their studies used clonogenic assays, which minimise substrate interaction with the nanotubes as there are no colorimetric substances added. As a comparison to SWNT they used carbon black, a by-product of incomplete combustion of petroleum used in

pigments. They found SWNT to cause significantly higher levels of cytotoxicity than carbon black. however their study did not identify the mechanism of toxicity.

Donaldson et al., (2006), highlighted in their comprehensive review the need to consider the comparisons between MWNT and SWNT, also to consider during the production process if any residual material can be incorporated into the nanotubes which may change toxicological effects, this is illustrated in figure 1.7.

Figure 1.7 illustrates the various aspects of CNTs that may influence the toxicity potential. It examines how each characteristic may influence the CNTs ADME e.g the solubility of any associated components and the size of the CNTs alone will influence which location the CNTs will be deposited. The figure then describes how the individual components have been shown to cause oxidative stresses from the induction of ROS which leads to inflammatory stress, and also to genotoxicity in the form of 8-O-dG (8-Oxo-2'-deoxyguanosine). 8-O-dG is a major product of oxidation of DNA; over presence of ROS with the cell can initiate this oxidation.

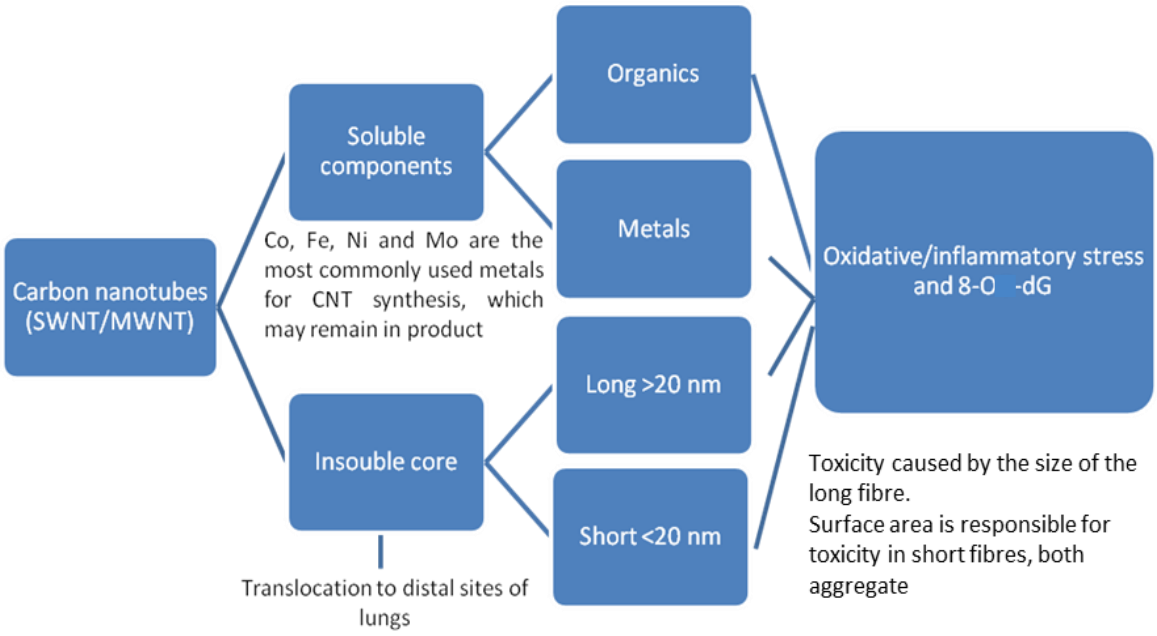

Figure 1.7 Component related CNT toxicity. Associating physical characteristics of CNT to the toxicity as derived from literature and described by Donaldson et al., (2006).

Based on the studies described above, it has been suggested that not only nanoparticle but also fibre could manifest toxicity of CNT. In a study using mice that were intratracheally instilled with 0, 0.1, or 0.5 mg of carbon nanotubes, a carbon black negative control, or a quartz positive control as a single dose, it was found on day 7 and day 90 that CNTs induced a histopathological toxicity effect in the lungs that was more severe than that induced by quartz nanoparticles and nano carbon particles, which were generally used as positive controls (Lam et al., 2004).

In vitro studies conducted on alveolar macrophages concluded that the toxicity potency of the fullerene family can be sequenced to SWNT>MWNT>quartz>C_{60}. SWNT caused considerably more cytotoxicity and inhibition of phagocytosis at low doses, whereas MWNT and quartz only induced toxic effects at high dose (Jia et al., 2005). Geys et al., (2010) detected a reduction in cell viability with increased doses of

CNTs in A549 cells. However, they highlighted that surfactants and serums interacting with CNTs may influence the results and cause disparity. For this reason they called for strict standardisation for nanotoxicity and detailed descriptions of materials for interpretation.

Polymer nanocomposites and dendrimers

Nanocomposites are multiphase materials in which one phase as dimensions below 100 nm. Polymer nanocomposites are usually made from an organic polymer matrix such as polystyrene, polyamide, polyurethane or polyamide and inorganic nanomaterials. Applications of these materials range from structural and mechanical uses to drug delivery and biological scaffolds.

Rayavarapu et al., (2010) are one group who have worked with a polymer coating on gold nanorods. Synthesised nanorods were coated with either polystyrene sulfonate (PSS) or polyethylene glycol (PEG). *In vitro* viability assays were conducted on mammary adenocarcinoma (SKBR3), human leukaemia (HL60), Chinese hamster ovary (CHO) and mouse myoblast (C2C12) cells. It was shown that PSS coatings imparted a substantial decrease in cell viability in all four cell lines as compared to little or no reduction by PEG coatings, except the mouse myoblasts in which both coats caused similar reduction of cell vaibility. However, PEG coatings made the gold nanorods more stable in solution.

Styan et al., (2008) studied the *in vitro* effects of polyether urethane matrix with montmorillonite (MMT) dispersion. The MMT was pre-treated with quaternary ammonium compounds (QAC) and amino undecanoic acid (AUA) to aid with dispersion. Using L929 mouse fibroblasts they found that organic modification was essential to achieve dispersion at nanoscale within the nanocomposite. The *in vitro* results showed an inhibition of cellular growth and cell membrane disruption in QAC modified MMT but no inhibition of growth was recorded for AUA modification.

Other inorganic nanomaterials could be stabilised by organic polymer coatings. For instance, iron oxide can have their toxicity lowered by organic coatings and association with organic materials. Iron oxides are rarely used without coating; this is due to their very poor solubility. Without coating they would accumulate under gravity leading to impedance of blood flow in circulatory system. More often than not the coatings are organic coatings such as polyvinyl alcohol, chitosan and polyethylene glycol amongst others (Gupta and Gupta, 2005). Cho et al., (2011) showed that the nanoparticle-antigen complex triggered more specific T-cell response causing delayed tumour growth, suggesting that coupling nanoparticle with antigen could lead to improved methods for cancer treatment.

Another polymer which is used in production of nanocomposites is chitosan. Chitosan is a polysaccharide composed of randomly distributed β-(1-4)-linked D-glucosamine (deacetylated unit) and N-acetyl-D-glucosamine (acetylated unit), which is often polymerised and associated with nanoparticles for biological uses. One study combined gelatine chitosan and MMT to create a possible scaffold for regenerative medicine. Their studies showed that an increased amount of MMT decreases cell viability (Zhuang et al., 2007).

It was found that chitosan polymer nanocomposite does not impart the levels of cytotoxicity expected from nanomaterials. This may be related to one of the aspects of physical character, the surface charge, as alteration of the surface charge alters the solubility and the stability of the particle in solution (Zheng et al., 2007). Results gained by other groups give weight to this theory (Chang et al., 2007), finding that the relative toxicity observed by chitosan-silica nanocomposite was significantly less than that observed for silica on its own. Chitosan has therefore been highlighted as suitable for clinical use.

Dendrimer nanocomposites are nanosized hybrid molecules of organic and inorganic elements. These hybrids may contain topological ‘guest’ atoms/molecules/nanodomains held in place by dendritic polymer. Very little is known about the toxicity of these hybrids to date. The number of repeating branching cycles during synthesis is defined as generations (Gn). Jevprasesphant et al., (2003) worked

extensively with PAMAM (Polyamidoamine) (Figure 1.6D). Their results suggested that the increase in generation of dendrimers could cause a greater toxicity in comparison to control, which is consistent with an earlier study by El-Sayed et al., (2002), who showed that later generations (G3-G4) dendrimers exhibited toxicity on Caco-2 cells, whereas G1-G2 did not.

In summary many groups have recognised potential applications of NPs in many areas. However, with these applications there are certain health concerns which are associated with application dependant exposure. The studies conducted thus far provide a rich knowledge source for a better understanding of the principles on the use of NP in a safe manner. A summary of the *in vivo* and *in vitro* studies conducted on various NPs mentioned in this section is presented in table 1.

Table 1.3 Summarisation of the variety of nanoparticle and the extent of *in vitro* and *in vivo* study conducted with summary of findings.

Nanoparticle	Size	*In vitro* cell line and concentration	*In vivo* model and concentration	Summary	Ref
$C_{60}(OH)_{24}$	<10 nm	HUVECs 1-100 µg/ml	Mice were treated over 2 weeks daily 40 mg/kg	- Cytotoxicity occurred at higher concentrations *in vitro* leading to LDH leakage and inhibition of cellular growth. - *In vivo* experiments showed that this molecule protects from γ-radiation. Stopping ionisation and possibly enhancing immune function	(Yamawaki and Iwai, 2006) (Cai et al., 2010)
C_{60}	<10 nm	HepG2 >50 ppb	Rats were instilled with single dose ranging between 0.2-3 mg/kg	- Cytotoxicity occurs at high concentrations. Detectable membrane damage, preventable by using antioxidants. - Contrary to *in vitro* studies *in vivo* studies found no difference between nano-C_{60} and $C_{60}(OH)_{24}$ as compared to control, from histopathological studies 1 day to 3 months post exposure.	(Sayes et al., 2005; Sayes et al., 2007)

SWNT	d= 1-2 nm	HaCaT; A549; BEAS-2B 1-400 µg/ml	Mice were injected with doxorubicin functionalised SWNT 5 mg/kg	- Cell growth inhibition occurs and cell viability is decreased at higher concentrations - Mice exposed to doxorubicin functionalised SWNT showed no toxicity apart from a gradual excretion of SWNT via reticuloendothelial system (RES) into faeces	(Herzog et al., 2007) (Liu et al., 2009)
MWNT	d= 20 nm	A549; T lymphocytes; Jurkat T leukaemia cell ~400 µg/ml	Mice were injected with functionalised and protein coated MWNT at 20 mg/kg	- T lymphocytes undergo apoptosis at high concentrations, oxidative and inflammatory stresses seen in lung cells - Localisation for functionalised MWNT occurred in liver, bladder and kidneys after 24 hours after injection, MWNT coated with proteins accumulated in the lungs.	(Han et al., 2010) (Bottini et al., 2006) (Jia et al., 2005) (Lacerda et al., 2008)

Dendrimers	<10 nm	Caco2; NIH3T3;U937;Rat2 ~1 µM	Mice 2.56 g/kg intraperitoneal and 1.28 g/kg intravenous	- Higher concentrations exhibited the generation of ROS, leading to oxidative and inflammatory stress. LDH leakage was also observed in later generations - *in vivo* no toxicity or chemical changes to blood levels were observed up to 2.56 g/kg of NP surface modified with PEG.	(Lesniak et al., 2005) (Naha et al., 2010) (Chen et al., 2004)
Organic nano composites e.g. PU/PP/PA, PEG or Chitosan	60-100 nm	C2C12; HL60; A549; macrophages 10-250 µg/ml	Mice were subjected to subcutaneous implantation of PEG at 10 mg/kg	- in both *in vitro* (macrophage) and *in vivo* (mice) robust pro- inflammatory responses were observed for PEG hydrogels. - Chitosan stabilised nanosized materials for integrated and lower levels of toxicity in use.	(Styan et al., 2008) (Lynn et al., 2010) (Chang et al., 2007)

Iron Oxide	10-30 nm	J774 25-500 µg/ml	Rats inhaled twice a day for three days at 8.5 mg/kg	- Serum levels of LDH were increased in *in vivo* histopathalogical analysis. Revealing severe damage to liver and lung tissue - Reduction in viability to 55% at higher concentrations increased generation of ROS.	(Wang et al., 2010) (Naqvi et al., 2010)
Titanium oxide	<10 nm	BRL 3A 10-200 µg/ml	Albino rats were fed for 65 days with 1-2 %wt	- Reduction in cell viability and increased LDH leakage observed - Rats exposed to TiO_2 in diet developed liver damage and significant reduction in fertility.	(EL- Sharkawy et al., 2010) (Hussain et al., 2005)
CeO_2	10-50 nm	ATCC; MRC-9;Beas-2B ~1 mg/ml	Rats were exposed to single intratracheal instillation of 0.15-7 mg/kg	- Reduction in cell viability observed through oxidative stress path way - *In vivo* inflammation, cytotoxicity, damage to air carrier system, enlargement of alveolar macrophages and ultimately leading to fibrosis.	(Ma et al., 2011) (Eom and Choi, 2009a)

SiO_2	12-100 nm	A549; Beas-2B; HaCaT; Lymphocytes; macrophages 10-500 µg/ml	Rats and mice have been exposed by intravenous injection and inhalation up to 10 mg/ml	- Oxidative stress and inflammatory stresses regularly occurred *in vitro* systems leading to reduction in cell viability over time - Retaining of nanoparticles in lung, liver and spleen over 30 days occurred due to uptake via endocytosis by macrophages, ultimately this leads to organ damage.	(Xie et al., 2010) (Park et al., 2010) (Johnston et al., 2000)

1.6 Mechanisms of nanotoxicity

Toxic substances can cause adverse effect at cellular and molecular levels by various mechanisms. Depending on their physiochemical properties they may cause membrane damage or may be internalised, which may lead to further interruption of cellular mechanisms. For the majority of nanoparticles, their toxicity mechanisms are still not well understood, although associations have been made with their surface area to volume ratio. For example, the large surface area of these molecules can act as a catalytic surface for reactions to occur and therefore, reactive oxygen species to be generated. This section will review evidence forming the basis of our current knowledge on the mechanisms of nanoparticle toxicity.

1.6.1 Possible uptake mechanisms of nanoparticles

It is relatively uncertain how nanoparticles enter the cells to initiate toxicity. However, it is suggested that the uptake of the nanoparticles to different locations within the cell could result in distinctive toxicity via cellular location specific mechanisms (Mühlfeld et al., 2008). If NPs are located in the nucleus this will increase the chances of DNA damage as nucleic acids become exposed more directly to NPs. Kang, el al., (2010) studied the location of gold NPs near the nucleus leading to DNA damage as a cancer targeting drug. Ultimately the location of the NPs within the cell may be driven by the uptake pathway.

A number of different pathways exist for possible particle uptake, including phagocytosis, macropinocytosis, clathrin-mediated endocytosis, clathrin- and caveolae-independent endocytosis or by caveolae-mediated endocytosis, endosomes and passive transcytotic processes (Unfried et al., 2007). These mechanisms as shown in figure 1.8 could provide access to different subcellular compartments, including nucleus, mitochondria and other parts of cytoplasm. The location may have a critical role in toxicity outcome. The nanoparticle uptake pathway could determine the model of nanoparticle toxicity. For example, if NP enter the cells via the mechanisms that may

lead to exposure to the nucleus or mitochondria, it may be possible for NP to interact with DNA, leading to DNA damage or gene mutation.

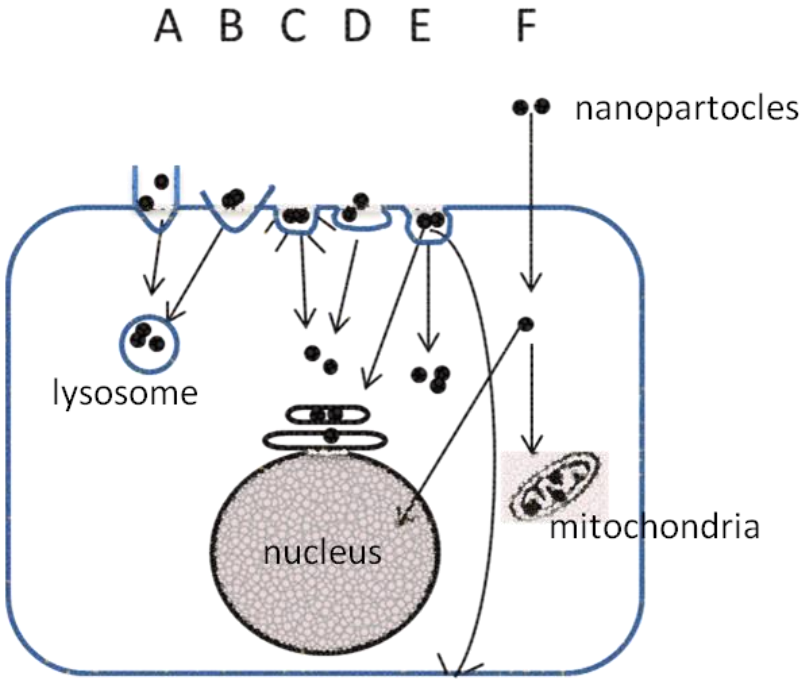

Figure 1.8 Possible mechanisms of particle uptake by cells. Particles may actively be taken up by cells via phagocytosis (A), macropinocytosis (B), clathrin-mediated endocytosis (C), clathrin- and caveolae-independent endocytosis (D) or by caveolae-mediated endocytosis (E) and finally passive uptake (F). Adapted from Unfried et al., (2007).

In most cases of active uptake, particles will be transported via vesicular structures to form phagolysosomes or endosomes (A–D) but they may also be transported to the endoplasmic reticulum, cytosol or through the cell as part of transcytotic processes (E). Apart from these mechanisms, a passive movement through the plasma membrane with subsequent access to all subcellular compartments, including nucleus and mitochondria, has been proposed (F). The significance of particular intracellular localizations and entering mechanisms for specific cellular responses awaits further study (Mühlfeld et al., 2008; Unfried et al., 2007).

Dos Santos et al., (2011) studied the uptake of various sizes (40 nm-2 μm) of fluorescently labelled polystyrene NPs. They concluded that each size NP was internalised by all cells used (A549, HeLa and RAW J774.7). However, the uptake kinetics are highly specified dependent on the cell type.

It is noted that phagocytosis is generally utilised by phagocytes such as macrophages, monocytes, neutrophils and dendritic cells for removing large particles (0.5-20 μm) (Deng et al., 2010; Erber et al., 1961). However, phagocytosis is suggested to be one of the mechanisms for NP uptake. The NP uptake pathways and size selectivity in other cell types are poorly understood and not well differentiated (Lesniak et al., 2012). Althought more recent studies such as, Mu et al., (2012), are beginning to explore the specificities of NP uptake, they suggest that an adhesive interaction between SiNPs and the lipid membranes of cells (HT29 and A549) may lead to a form of passive uptake for particles aggregating up to 500 nm in diameter.

1.6.2 Oxidative and inflammatory stress

The mode of action of NPs can be varied and dependant on a number of factors. Until now the majority of the research carried out on nanotoxicology has presented oxidative stress and inflammation in multiple testing systems (Eom and Choi, 2009b; Zhang et al., 2009; Kelly et al., 1998). These two pathways are also often suggested to be linked (Park and Park, 2009; Han et al., 2010).

Oxidative stress is caused by the accumulation of Reactive Oxygen Species (ROS), ROS are highly reactive chemical molecules containing oxygen, e.g. oxygen ions or peroxides. ROS are produced naturally as a part of homeostasis and required for normal functioning of cells in many signalling pathways. Pathways such as the Akt/mTOR pathway use ROS to induce cell proliferation as illustrated in figure 1.9. However, introduction of NPs in to cell allows for a particle with a huge surface area to volume ratio to act as a catalytic surface for unwanted ROS generation. High levels of ROS lead to activation of inflammatory stress and cell damage (Han et al., 2010).

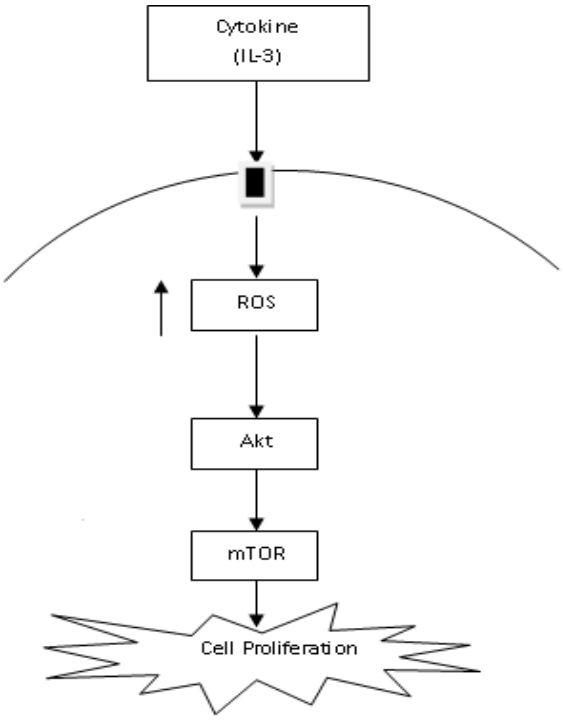

Figure 1.9 ROS regulation of cell proliferation. Akt/mTOR pathway uses ROS as signalling molecules to allow progression of cell proliferation Adapted from Pervaiz et al., (2009).

Figure 1.9 is a representation of how ROS is a natural presence within cellular systems and controls some pathways such as the Akt/mTOR pathway. Oxidative stress has been shown to play a pivotal role in the progression of disease pathogenesis and tissue damage by induction of inflammatory responses (Roberts et al., 2009). These effects are believed to be due to NPs large surface area to volume ratio, on which reactions producing ROS species can occur (Karakoti et al., 2006; Wallace et al., 2007). However the details of such NP surface reactions remain unclear.

Cells have built-in defences for neutralising oxidative stress by removing ROS by producing enzymes and using compounds like vitamins, such as vitamin C and E. Superoxide dismutase (SOD) is an enzyme that functions to counteract over production of ROS. McCord and Fridovich, (1969) discovered the enzyme which is responsible for

catalysing the reaction of superoxide radicals (O_2- + O_2- + $2H^+$ = O_2 + H_2O_2). By the presence of more reactive oxygen species the concentration of superoxide dismutase would also be raised and thus raising the concentration of the reaction products such as H_2O_2. McCord and Fridovich studied the levels of H_2O_2 within the cell to find that the presence of this molecule at high levels can trigger apoptosis through the Beclin-1 and Akt/mTOR pathway. It has been demonstrated that the oxidative stress induced by H_2O_2 and TNF-α results in upragulation of NF-κB and activator protein-1 (AP-1), which could upregulate production of IL-8, an important inflammation mediator that triggers phagocytes, such as microphages and neutrophils, to migrate to the damage sites for repairing, or further damage (Erber et al., 1961; Deng et al., 2010; Samuvel et al., 2009).

ROS generation may also cause lipid perioxidation and the oxidation of proteins, leading to the malfunction of those molecules. Lipid perioxidation and protein oxidation are two important factors of tissue damage, as suggested by many earlier works (Gutteridge et al., 1980); (Firoze Khan et al., 1997); (Zhang et al., 2009). Prolonged exposure to ROS can lead to DNA damage or initiation of apoptosis (Auten and Davis, 2009) (Bourdon et al., 2012).

Like oxidative stress, inflammatory stress is also a widely studied mechanism of toxicity. It is thought that oxidative and inflammatory stresses are very closely linked (Park and Park, 2009). However, a study has suggested there may be other pathways to induce inflammation which are unrelated to oxidative stress. Deng et al., (2011) used polymer coated gold NPs to initiate inflammatory responses by inducing unfolding of fibrinogen. This promotes interaction with integrin receptor, Mac-1, activating the Nf-κB signalling pathway. Nonetheless, majority of opinions still regard the NPs activation of inflammatory stress is based on co-mediation with oxidative stress (Oberdörster, et al., 2005; Rahman, et al., 2002). Many of the studies consider ROS mediated activation of TNF-α and NF-κB as the most likely mechanism.

Suitable biomarkers for pro-inflammatory responses are important for toxicity prediction. Studies have highlighted a number of biomarkers which are present in many cells lines. However, some markers may be more suited for use in specific cell lines.

For example, it is known that IL-8 is upregulated under oxidative and inflammatory stress (Han et al., 2010; Øvrevik et al., 2006) in A549 cells, a lung epithelial cell model that have been widely used to study the cellular and molecular mechanisms of inhalation toxicity.

It is hypothesised the oxidative stress generation by NPs lead to activation of inflammatory stress. Park and Park, (2009) compared the responses to NPs both *in vitro* and *in vivo,* they reported that a single dose treatment to mice and RAW264.7 cells with SiNPs induced ROS generation, which in turn triggers a pro inflammatory response *in vitro* and *in vivo*. It was demonstrated in another study that the installation of single dose at 0.018, 0.054 or 0.162 mg of carbon black NPs in mouse lungs led to inflammatory stress, protein malfunction, cell membrane damage and DNA damage (Bourdon et al., 2012).

After inhalation, nanoparticles may be deposited in the alveolar sacs of the lungs. Accumulation in the alveolar sacs could initiate a pro-inflammatory response, eventually leading to NP being engulfed by macrophage cells in an attempt to clear the foreign particles from the body, which may further trigger the production of factors that promote inflammation (Soto et al., 2007).

Napierska, et al. (2010) highlighted in their review on SiNPs toxicity that the limited number of *in vivo* studies conducted all suggest that there is a reversible inflammation which occurs in the lungs. They expressed that there is a need for research with standardised materials and a range of nanosilica forms to establish which physico-chemical property is responsible for toxicity. One property which has been identified is zeta potential, Cho, et al., (2012) suggest that a high positive zeta potential may cause inflammatory responses after uptake into phagolysosomes.

1.6.3 Molecular pathways of nanotoxicity

Interleukins are very important in the mediation of inflammatory responses; they are a family of pro-inflammatory cytokine thought to be involved in many acute and

chronic diseases. Kolb et al., (2001) demonstrated that transiently over expressed of IL-1β in rodent lung epithelial cells by intratracheal administration caused an increase in IL-6 and TNF-α, acute inflammation and occurrence of interstitial fibrosis in alveolar tissue. They proceeded to conclude that IL-1β should be considered as a therapeutic target for fibrosis.

Some other studies have also explored the effects of IL-1β and TNF-α on lung cell injury. These studies have led to the conclusion that these factors are important in the progression of lung fibrosis. (Sime et al., 1998) described TNF-α as an early 'alarm' type cytokine. In their study, TNF-α was upregulated as early as 3 days and peaked on day 7-14, as assessed by the ELISA (enzyme links immunosorbent assay) detection of TNF-α in the bronchoalveolar lavage (BAL) fluid. Although Sime et al. (1998) studied the effects of increased expressions of TNF-α by artificially over expressing in rat lung, this study demonstrated a causative role of NP in the secretion of TNF-α.

Miyazaki et al. (1995) also studied the effects of TNF-α on lung fibrosis. Their results corresponded with the results found by (Sime et al., 1998) that TNF-α over expression causes inflammation in the alveolar sacs leading to lung fibrosis. Miyazaki et al., (1995) have also suggested that there is a very apparent link between the inflammatory response and the oxidative stress caused by inhaled toxins. Sharma et al., (2007) also found that the signalling molecule nitric oxide plays a pivotal role in inflammation.

Many studies have identified the intermediate factors and transcription factors which regulate the inflammatory response. NF-κB, IL-6 and TNF-α are such factors. Their presence, typically at injured sites, could be a result of oxidative response, and can further trigger inflammation. In addition, as described before, ROS are important molecules in regulation of oxidative and inflammatory responses (Park and Park, 2009; Eom and Choi, 2009b; Wang et al., 2009). Figure 1.10 describes the pathways by which oxidative stress may lead to an inflammatory stress, and how this may be mediated by NPs. These pathways involve activation of Nrf2, NF-κB by NPs internalls or activation of TNF-α by ROS externally produced due to NPs, leading to inflammatory responses including cytokine production (Kim and Vaziri, 2010).

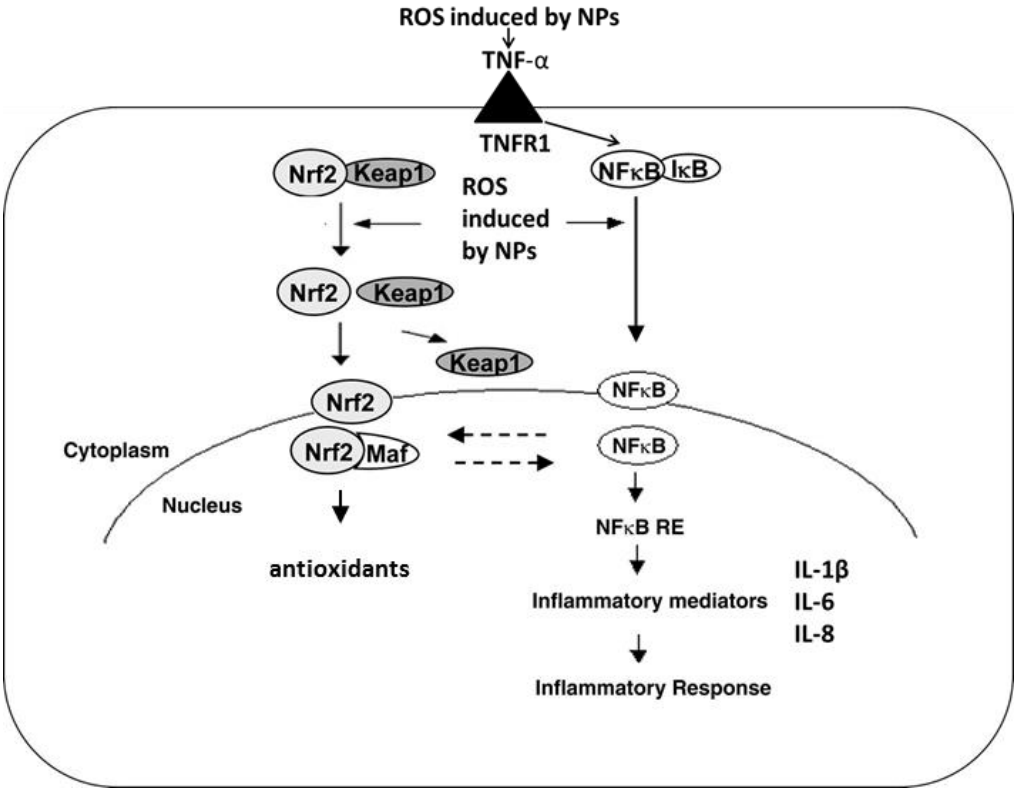

Figure 1.10 Schematic representation of Nrf2 and NF-κB activation by NP induced ROS internally and activation of TNF-α by external NP ROS production. Oxidative stress induces dissociation of Nrf2-Keap1 complex allowing translocation of Nrf2 to the nucleus and associates with transcription factor small Maf, within the nucleus producing antioxidant tanscription. Oxidative stress causes phosphorylation of IκB, which activates NF-κB leading to transcriptional of genes encoding inflammatory cytokine and chemokines. Nrf2 and NF-κB pathways inhibit one another. Adapted from Kim and Vaziri, (2010).

1.6.4 Possible involvement of microRNA in nanotoxicity

The investigation of the role of miRNA in toxicity is a fairly new and very interesting field of study. Mature miRNAs are 21–25 nucleotides in length and partially complimentary to 1 or 2 mRNAs. The main function of miRNAs is to downregulate gene expression. This may be achieved by a variety of different mechanisms including mRNA deadenylation and cleavage (Lee et al., 1993). Sequencing studies are being undertaken by a number of groups (Dar et al., 2011; Vergoulis et al., 2012; Huang et al.,

2011; Li et al., 2011b), aiming to establish a fully sequenced online database of miRNA.

The biogenesis of miRNA is illustrated in figure 1.11. It starts with transcription of primary miRNA by RNA polymerase II and III. This is followed by the cleavage of pri-miRNA by the microprocessor complex Drosha–DGCR8. This produces a precursor hairpin (pre-miRNA), which is exported from the nucleus by Exportin-5–Ran-GTP. Once in the cytoplasm, the pre-miRNA hairpin is cleaved by the RNase Dicer complex with the double-stranded RNA-binding protein TRBP, this produces the mature miRNA (Winter et al., 2009). An RNA-induced silencing complex (RISC) is a multi protein complex, which incorporates siRNA or miRNA. This can then bind to the 3' UTR region of mRNA and silence the transcription. In some cases it also induced deadenylation, this is the degradation of mRNA with in the cytoplasm.

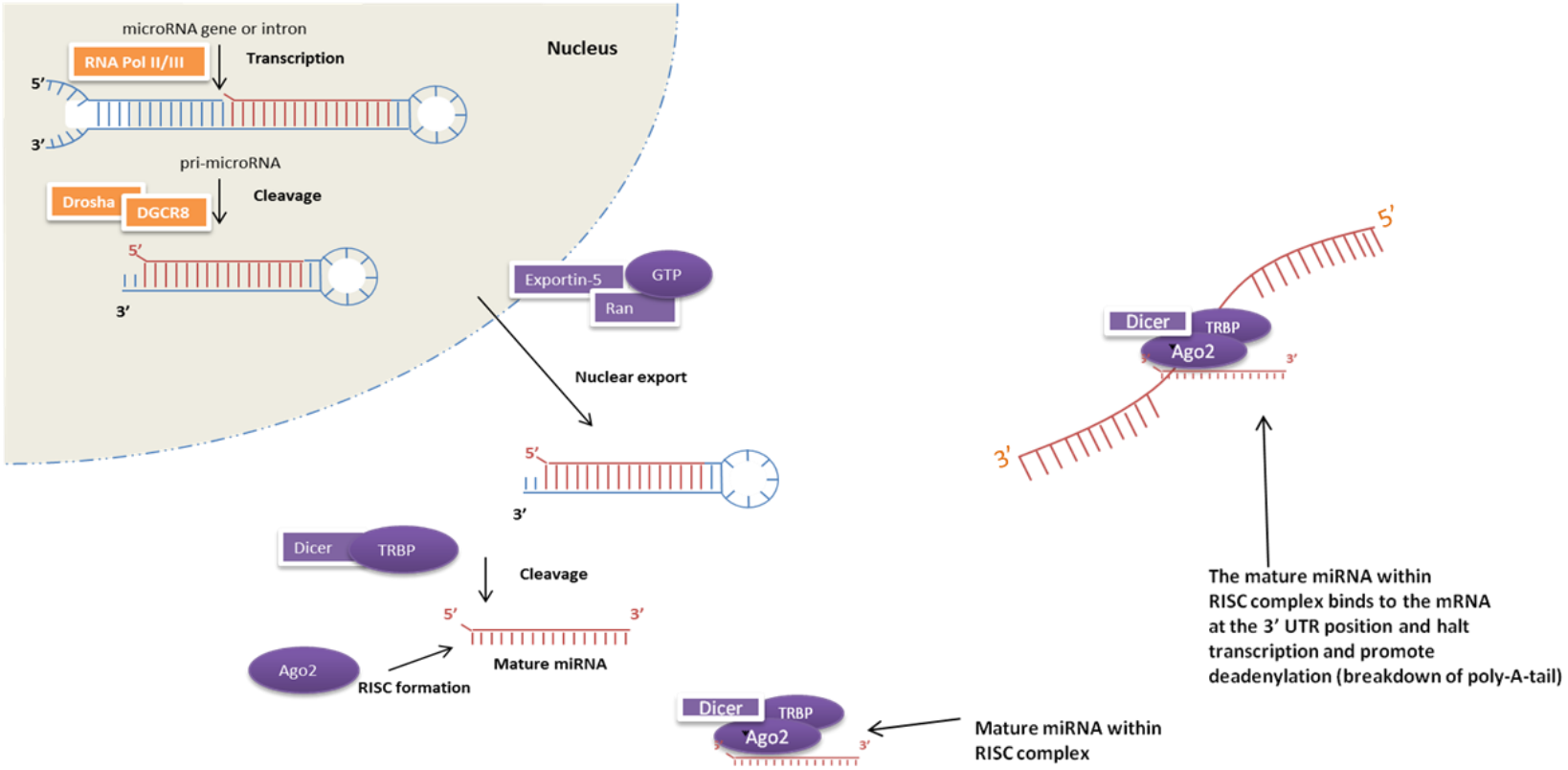

Figure 1.11 Schematic diagram of miRNA biogenesis. Pri-miRNA is produced inside the nucleus by RNA polymerase II or III, this is cleaved by Drosha complex to produce pre-miRNA hairpin in the nucleus. Hairpin pre-miRNA is exported to the cytoplasm, where is it cleaved to produce the final mature miRNA. The mature miRNA is incorporated into the RISC complex which binds to the 3' UTR of mRNA suppressing the transcription of the mRNA Adapted from Winter et al., (2009).

Early stages of research have suggested that some miRNAs could be associated to certain pathways which are involved in translation of stresses. Shah et al., (2007) used wild-type mice (n=5) to show changes in miRNA expression in response to Wy-14,643 (peroxisome proliferator-activated receptor alpha [PPARα] agonist). They concluded that the miRNA let-7C has a role in tumour suppression and is up regulated after treatment. However, this study was limited to hepatic analysis of mice, further damage may also have occurred in other organs of the mouse body.

There are few publications available regarding miRNA regulation linked to NP toxicology. One study that has been published used Fe_2O_3 NPs, CdTe QDs and MW-CNTs on NIH/3T3 cells found that the exposure to NPs led to alterations in mRNA expression (Li, et al., 2011). The present study aims to build on using a miRNA database to allow identification of specific miRNA sequences and their functions. The up and down -regulation information collected from post SiNPs treatment will give an indication to how the identified miRNA sequence regulates toxicity. This technique may prove to be a very good tool for detecting early toxicity effects *in vitro*.

1.6.5 Metabolic effect of nanotoxicity

Metabolites that are produced by cellular systems may be altered due to certain stimuli, such as NPs or chemicals. A systematic study of metabolite fingerprints of cellular processes is known as metabolomics, and the quantitative analysis of the dynamic metabolite response is known as metabonomics. Conventional study of metabolic markers of toxicity was based on changes of a few selected metabolites in response to toxicants. Application and methods of metabolomics in nanotoxicology study is a recent development allowing for a much wider selection of metabolic markers for analysis. ^{1}H-NMR -based metabonomics is one among many different methods that have being developed for metabonomic study. Duarte, (2011) suggested the potential benefits of ^{1}H-NMR as a non-invasive tool for detecting nanotoxicological and nanomedical effects. It was suggested that the changes in metabolites after chemical

treatment can be used to predict the phenotype of genetic mutation by comparing metabolic profiles of wild type and mutants (Szeto et al., 2010).

Metabonomics has also been highlighted as a tool to examine oxidative stress in cells. With the ability to probe for changes of all the metabolite pathways known to researchers, metabonomics is an ideal high throughput tool for diagnosis of disease and clinic conditions (Liu, et al., 2011), based on the few reviews which have been published that ^{1}H-NMR based metabonomics can also be a useful high throughput method for toxicity detection *in vitro*. Moreover, it may be used as a non-invasive method by utilisation of culture medium for analysis.

The knowledge base for nanomaterial toxicology is ever growing and evolving. This evolution is aided by the advancement in technology and standardisation of assessment techniques (Fadeel et al., 2007). Even with this advancement there are still large gaps in the knowledge, such as uptake specificity and toxicity mechanisms and pathways. The literature reviewed regarding SiNPs suggests a strong link between oxidative stress and pro-inflammatory environment *in vitro*, it is still not well understood how the SiNP interacts with the cell structure to induce ROS and how the production of ROS specifically governs the production of pro-inflammatory factors.

1.7 Hypothesis

Within the framework of the NEPHH project, I will participate in a work package to assess the toxicity potential and mode of action of silica NPs and nandusts generated from silicon-based polymeric composites using *in vitro* models. Based on the evidence that the characteristics including size, shape, aspect ratio and surface chemistry determines the toxicity properties of nanoparticles, the following hypothesis form the basis of my research.

- Nanoparticle toxicity is related to specific physical characteristics.

- Nanoparticles released from different nanocomposites have distinctive characteristics from ‘raw’ nanoparticles and therefore possess different toxicity potential.

- Nanoparticles with different characteristic initiate different pathways of toxicity.

- The toxicity potency is altered during the lifecycle of a material. This may be dependent on the processing and the addition of different materials/chemicals.

1.8 Aims

The aims of the project are to investigate the potential toxicity of silicon-based engineered nanomaterials and nanoparticles released from nanocomposites and their toxicity mechanisms *in vitro.* Ultimately this project, in conjunction with NEPHH partners, will present data which will allow the establishment of risk assessment protocols and allow the safe use of nanomaterials to be implemented. NEPHH aims to establish a standardised and full LCA toxicity analysis of nanoproducts, available to both public and private sectors as a guide for nanoproducts safety assessment.

To achieve the overall aims, my research will deliver the following objectives:

1. Characterisation of engineered silicon-based nanomaterials (mainly SiO_2 NP) and nanoparticles released from nanocomposites in culture medium. A range of methods will be utilised to characterise the shape, surface chemistry, dispersion pattern in culture medium.

2. Study of nanomaterial/nanoparticle toxicity potential in *in vitro* models involving lung and skin cells. Toxicity dose will be established using different testing assays for different toxicity endpoints.

3. Study of the relationship of toxicity effect and intracellular dose.

4. Study of the relationship of the nanomaterials/nanoparticle characteristics and mode of action. A number of toxicity specific molecular pathways will be tested by conventional *in vitro* cytotoxicity assays and relatively novel approaches such as miRNA array and ^{1}H-NMR-metabonomics assay to determine the mode of action of toxic nanoparticles.

CHAPTER TWO

2 Materials and methods

The materials used within the present study are summarised in table 2.1 with supplier and catalogue numbers.

Table 2.1 Materials used in this study and suppliers.

Material	Supplier	Cat no
3-Aminopropyl)triethoxysilane	Sigma Aldrich	A3648
0.5% Trypsin-EDTA (10x)	Fisher Scientific	15400054
3-(4,5-Dimethylthiazol-2-yl)-2,5-diphenyltetrazolium bromide	Invitrogen	M6494
Carboxy-H_2DCFDA	Invitrogen	C-400
Cell counting chamber slides	Invitrogen	C10312
Dimethylsulfoxide	Sigma Aldrich	D8418
Dulbecco's modified eagle medium F-12 (DMEM)	Fisher Scientific	31330038
Fluorescein isothiocyanate	Sigma Aldrich	F7250
Human foetal lung fibroblast cell line MRC-5 cells	Sigma Aldrich	84101801
Human keratinocyte HaCaT cells	Cell line service	330493
Human lung carcinoma A549 cells	Sigma Aldrich	86012804
Hydrogen peroxide	Sigma Aldrich	216763
IL8 human ELISA kit	Abcam	ab46032
Isopropanol-1-ol	Sigma Aldrich	4028932L
Lactate dehydrogenase kit	Sigma Aldrich	TOX7
miRNAeasy kit II	Sabioscience	217004
miScript II RT	Sabioscience	218161
miScript SYBR Green PCR Kit	Sabioscience	218075
Penicillin (10,000 IU/mL)/Streptomycin (10mg/mL)	Fisher Scientific	15070063
Phosphate buffer saline tablets (PBS)	Fisher Scientific	18912014
Potassium bromide	Sigma Aldrich	221864
Trypan blue stain 0.4%	Invitrogen	15250061
Virkon®	Anachem	330002

The materials used in this project were sourced from a variety of suppliers. Some were provided by project partners others purchased after careful consideration of our experiments to ensure meaningful results in context of this project and wider application of risk assessment of nanomaterials. Thus, amorphous silica nanoparticles, with sizes of 7 nm and 14 nm respectively, were purchased from Sigma-Aldrich. Two silica nanoparticles, Aerosil 200 and Aerosil 974, were sourced from Evonik Degussa Polska (Warszawa, Poland) through consortium partners. Aerosil 200 was hydrophilic and Aerosil 974 hydrophobic after treatment with dimethylchlorosilane. In addition to these 'raw' silica nanoparticles, project partners provided nanocomposites which were mechanically processed to generate nanodust. These SiNP are all spherical shaped, produced through a dry process, and share similar primary particle size (average 12 nm).

These polymer composites were produced by the partners of this project, incorporating inorganic materials of glass fibre, foam-glass-crystal, montmorillonite and SiO_2 nanomaterials into polymer matrices of polyamide, polypropylene and polyurethane. Two mechanical processes conducted to generate nanodust were designed to mimic real situations which the composite materials may undergo. These processes include crush and drilling. References (polymers without added inorganic materials) were also synthesized as controls for the release of nanoparticles. The dust generated from the mechanical test required filtering until nanosized particles are obtained and all large particles were omitted. The filtering was conducted at the School of Applied Sciences using nanofilters. Once this had been done nanoparticles were then delivered to partners for toxicity testing in different biological systems.

The nanodusts generated from mechanical tests were labelled based on the type of nanomaterial and polymer matrix. The polymer matrices were Polyamide (PA6) and Polypropylene (PP) for drilling test, and polyurethane (PU) for crushing test. The components of the polymeric composites are listed in table 2.2.

Table 2.2 Components of the specimens synthesized for physical processing test.

Composite	Inorganic Filler	Filler supplier	Filler (wt %)	Surface modification
PA6-MMT	Montmorillonite	Laviosa/Dellite	5	Tallowbenzyldimethylammon
PP-MMT	Montmorillonite	Laviosa/Dellite	5	Ditallowdimethylammonium
PU-MMT	Montmorillonite	Optibent 987,	5	-
PA6/PU-	Nanosilica	Degussa/Aerosi	5	-
PP-SiO_2	Nanosilica	Degussa/Aerosi	5	Dimethyldichlorosilane
PA6/PP/PU-	Foam glass	Tomak	5	-
PA6/PU-GF	Glass fibre	Taiwan glass	5	-
PP-GF	Glass fibre	Taiwan glass	5	-

Cell lines were bought from various sources. Human lung epithelial carcinoma (A549) cells and Foetal lung fibroblast cell line (MRC-5) were acquired from Sigma-Aldrich. Human skin keratinocyte (HaCaT) cells acquired from the cell line services (http://www.cell-lines-service.de), 3(4,5-Dimethylthiazol-2-yl)-2,5-diphenyltetrazolium bromide (MTT), carboxy-H_2DCFDA, Trypan blue stain 0.4% and the cell counting chamber slides were purchased from Invitrogen (UK). Virkon® was purchased as powder from Anachem (UK). Dulbecco's modified eagle medium F-12 (HAM) (DMEM), 0.5% Trypsin-EDTA (10x) and Penicillin (10,000 IU/mL)/Streptomycin (10mg/mL) were purchased from Fisher Scientific.

Phosphate buffer saline (PBS) tablets, lactate dehydrogenase (LDH) release kits, hydrogen peroxide (H_2O_2) and dimethylsulfoxide (DMSO) were purchased from Sigma Aldrich (Gillingham Dorset, UK). The filler materials included microsized glass fibres (TGFS 473H in PA6-composite, TGFS 202P in PP-composite, Taiwan Glass Industry Corporation), nanosilica (Aerosil 200 in PA6-composite, Aerosil 974 in PP-composite, both ~12 nm, amorphous, fumed, Evonik Degussa Polska), organically modified montmorillonite (Deillite 43B in PA6-composite, Dellite 72T in PP-composite, LAVIOSA Chimica Mineraria), and foam glass crystal (Department of Silicate Technology and Nanotechnology, Tomsk Polytechnic University, Russia).

Nanodusts were generated from crushing or drilling of the above composites, conducted by the project collaborator in the School of Applied Sciences (SAS) of Cranfield University. For drilling experiment, the specimen was mounted on a fixture (Figure 2.1) in the drilling chamber. The sampling tray was used to collect the dusts which were produced while drilling. After the particle concentration in the air returned to the background level, the sampling tray was removed from the chamber and the dusts were suspended in 150 ml of deionised water (DW). An ultrafiltration (Vivacell 250 ultrafiltration system, Sartorius Stedim Biotech GmbH, Germany) was then employed for size fractionation. Filters with a molecular weight cut-off of 5000 were used under a pressure of 3.5 bar. The concentrations of the nanoparticles in filtrates were determined by weighing 1 ml of particle solution using a balance (Precisa XR 305). The average weight of NP solution from 10 repeat measurements was compared with that derived from DW. The mass/volume concentration of NP in solution can then be derived. The NP retrieved from the dust were used for toxicity studies. Nanodusts were also obtained from crush test of the PU-composites specimens conducted by the partner in SAS.

2.1 Characterisation of nanomaterials

2.1.1 Physical characterisation

Some aspects of the characterisation were conducted by our colleagues in the School of Applied Sciences (SAS). The generation of the nanodust is one such example. Using the mobility Particle Sizer SMPS+C (Condensation Particle Counter "CPC" 5.403 With Classifier "Vienna"-DMA 5.5-U, Grimm Aerosol, Germany), which was connected to an electrostatic precipitator (ESP, Model 5.561 Grimm Aerosol, Germany) the generation of airborne NP was detected. The background level of NP was recorded for 1 h before drilling, which enabled normalisation of ‘noise’ or naturally occurring interference before measuring samples. The drilling was conducted in a self-designed chamber (Figure 2.1) using an angle drill (Makita BDA351Z 18V Angle Drill, drill bit Ø10 mm) over two measurement cycles (14 min/each) and sample collection was continued for 2.5 h after the determination of drilling. A high voltage (5000V) was

applied to the central electrode to attract the charged particles onto a sampling plate. The NP on the plate were then examined using a scanning electron microscope. After 14 min, the drill bit was removed from the chamber and the opening was sealed. The chamber was kept sealed until airborne NP concentration returned to background level.

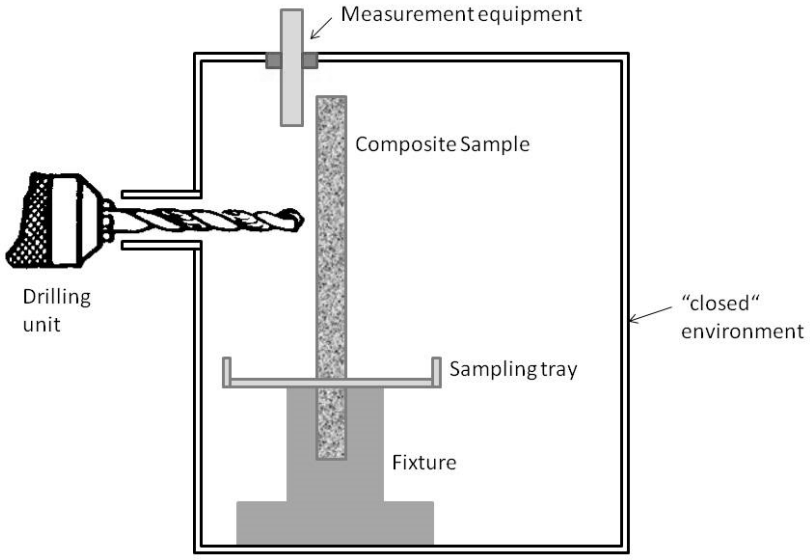

Figure 2.1 Schematic diagram of drilling chamber. Drilling chamber specifically developed for airborne particle monitoring and dust generation.

The PA- and PP-silicon composites were subject to drilling test and the airborne NP were monitored, dust NP collected. The PU-silicon composites were subject to crushing test and NPs were also collected.

2.1.2 Dynamic Light Scattering (DLS)

Dynamic light scattering (DLS) is a non-invasive technique which allows measurement of the size and size distribution of molecules and particles at the nanoscale (<100 nm) DLS typically can measure within a range of 0.2 nm to 2500 nm. DLS allows characterisation of particles and molecules, which have been dispersed or dissolved in a liquid. The particles motion, known as Brownian motion, in suspension

scatters the laser light at different angles and intensities. Using the Stokes-Einstein relationship the intensity fluctuations can be interpreted.

Nanoparticles are known to be highly unstable in solution and are known to rapidly aggregate. From the literature it was suggested that the presence of FBS or another protein would have an effect on the agglomeration of particles more specifically it may stop the agglomeration (Cedervall et al., 2007b). The DLS measurements were therefore conducted both in water and culture medium to examine the possible influence of proteins. Furthermore, different time points after suspension, nanoparticles were examined for their stability over time in different solutions.

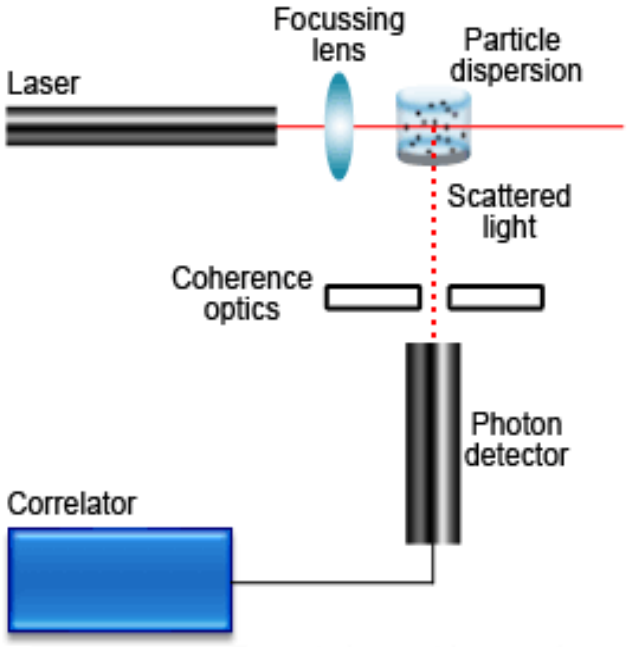

Figure 2.2 Schematic diagram of DLS measurements. A laser is focused through a liquid containing analyte, measuring the hydrodynamic diameter.

The fumed silica particles, which were supplied by Sigma-Aldrich©, were weighed and made into a stock solution of 1 mg/ml in culture media. After making this stock solution it was mixed thoroughly before analysing. From literature it was known

that a 100 µg/ml or less solution of silica is optimal to examine dispersion pattern with dynamic light scattering (Montes-Burgos et al., 2010). Therefore the particle solution was diluted at 10:1 to make a 100 µg/ml and then further diluted to make a 50, 25 and 10 µg/ml in water and in culture medium. The NPs separated from the dust samples from the crush and drilling tests were diluted in culture medium to 100 µg/ml. The NPs and dust sample dispersity and size distribution in culture medium was measured by DLS with a Malvern Nanosizer S (wavelength 633 nm and power 4 mW Malvern Instruments Ltd, Worcestershire, UK).

2.1.3 Measurement of silica NP Zeta potential

Zeta potential is the potential difference between the dispersion medium fluid and the surface of the dispersed particle. Zeta potential is a reflection of the stability of colloidal dispersions, essentially indicating the level of repulsion between adjacent particles in solution. A high zeta potential value for small molecule/particle in solutions suggests a good stability i.e. the dispersion rather than aggregation. A low value suggests that the attraction between particles is high, therefore aggregation will readily occur (Jiang et al., 2009).

2.3 Zeta potential value guidelines

Zeta potential [mV]	Stability behaviour of the colloid
from 0 to ±5,	Rapid coagulation or flocculation
from ±10 to ±30	Incipient instability
from ±30 to ±40	Moderate stability
from ±40 to ±60	Good stability
more than ±61	Excellent stability

To measure the zeta potential of our solutions the SiNPs particles were suspended in 5ml water and 5ml culture medium, respectively, at 100 µg/ml. the solutions were then injected into the Malvern Zetasizer (Malvern Instruments Ltd, Worcestershire, UK) and ran through the machine with 30 cycles of measurements, an average zeta measurement was taken for each sample.

2.1.4 Scanning Electron Microscopy (SEM) and Transmission Electron Microscopy (TEM)

SEM and TEM are electron microscopy technique, which produce images by scanning, for SEM, samples with a focused beam of electrons and transmission of electrons for TEM. The interaction of the focused electrons with the electrons on the surface of the sample produces various signals, which contains information about the sample topography.

SEM produces various signals including secondary electrons (SE), back-scattered electrons (BSE), characteristic X-rays, light (cathodoluminescence, CL), specimen current and transmitted electrons. Due to the nature of electrons the electron beams produced by SEM allow for the acquisition of high resolution images which can also represent the 3D structure of the surface.

TEM uses transmission of electrons through an ultra thin specimen, the interaction of the electrons with the specimen generates an image. This image is then magnified and focused on to an imagining device or CCD camera.

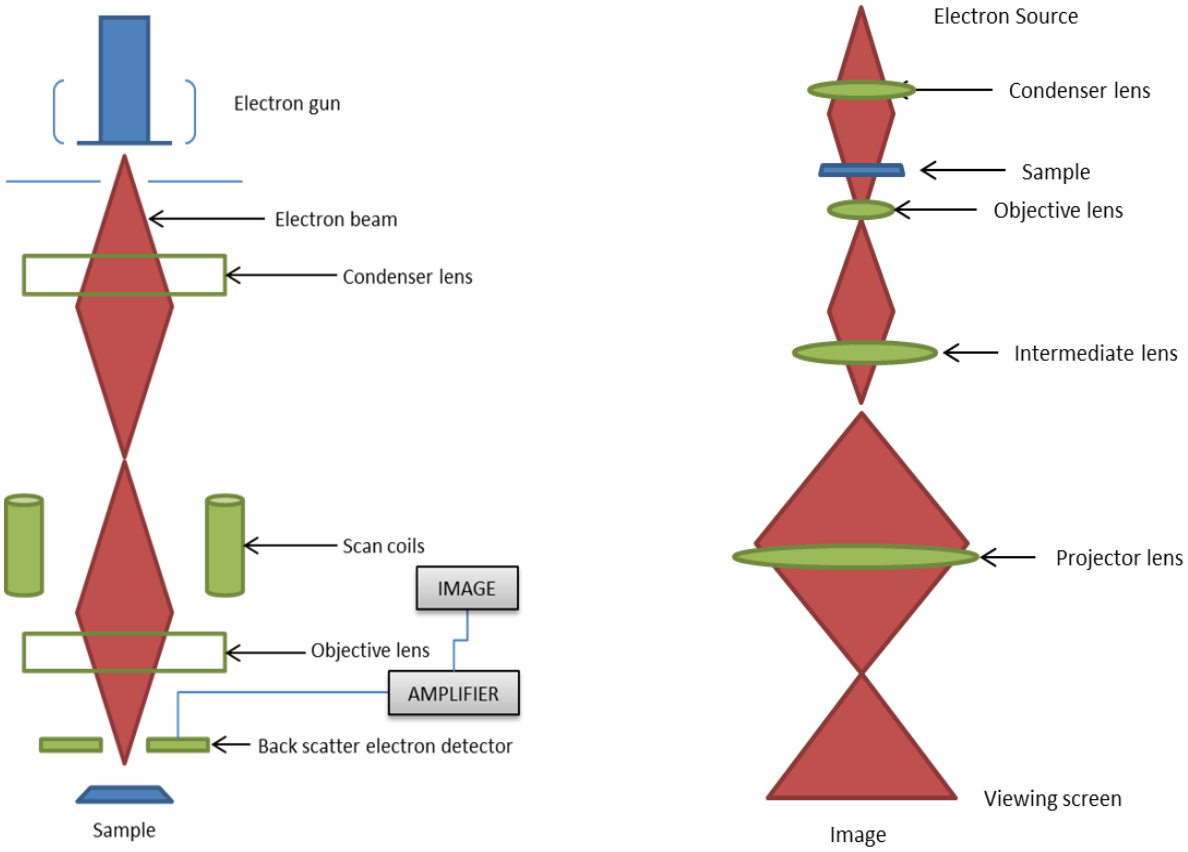

Figure 2.3 Schematic diagrams of SEM and TEM principles. For SEM electrons are emitted from the electron gun and focused onto the sample by the objective lens. The back scatter electrons are then detected. TEM utilises electrons transmitting through a sample. The electrons are then focused onto the viewing screen.

The use of electrons for SEM imaging requires a vacuum to avoid interference with atmospheric molecules. This required the sample to be dried and prepared for imagining. While drying the solution of nano particles aggregation occurred, expectedly. To minimise this aggregation a method to disperse in solution before drying on the SEM stub was used. SiNPs 7 and 14 were dispersed in culture medium at concentrations of 10 µg/ml and 100 µg/ml. Aerosil 200 and Aerosil 974 were dispersed at 100 µg/ml only, this dispersion aimed to compare surface modification effect on size and aggregation as observed by SEM. A droplet of this solution was allowed to dry on

the microscope stub overnight. These were imaged the following day with High Resolution SEM (FEI XL30 SFEG analytical SEM). The observed SEM images were used to validate the result obtained from the DLS.

The same preparation method was used to perform TEM imaging with a TEM grid used in place of SEM stub. The solution was prepared and shaken to disperse, then allowed to dry on the TEM grid overnight to be examined. The TEM used was a Philips CM20 operating at 200kV.

2.1.5 Fourier Transform Infra-Red (FT-IR)

FT-IR is based on information gathered by infra-red examination of samples. Light is generated from a source, and passed through a monochromater (this may be a salt prism). This separates the source wavelengths. The selected wavelengths are then passed through the sample, according to the chemical properties some light is absorbed and this is recorded by the detector. The collected radiation is presented in a spectrum of absorbance or transmittance (Gable, 2000).

Fourier transform infrared (FTIR) spectroscopy is used to assess the identity of molecular interactions and chemical bonds present in a sample. Infrared light is transmitted through the sample, which is mixed with a reference material, potassium bromide (KBr), and compressed into a disc. The intensity of the light is detected and a spectrum is created of either absorbance or transmittance. Each absorbance/transmittance fingerprint is related to a specific bond e.g. C=O and C-H, in a molecule, which are analysed by the Fourier transformed algorithm. This method allows the molecular composition and quantity to be determined of any given compound.

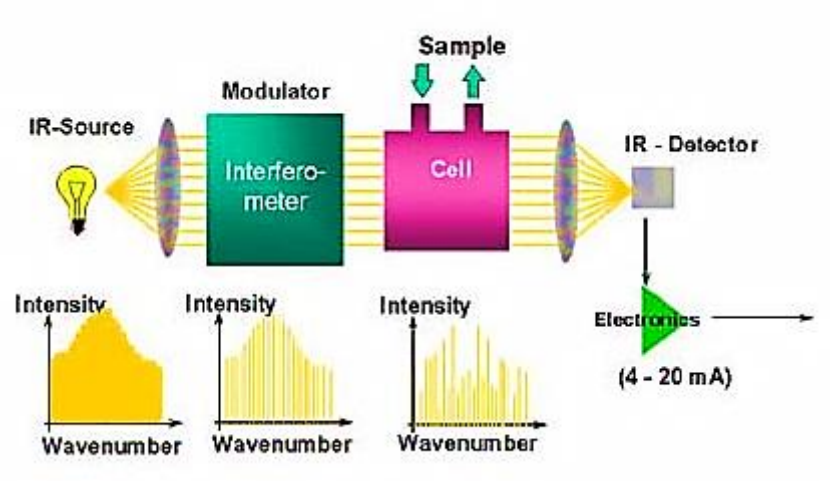

Figure 2.4 Basic principle of Fourier Transformed Infrared spectroscopy. An infrared (IR) source emits light which is modulated to specific wavelengths. The absorbance or transmission of these wavelengths through a sample is detected.

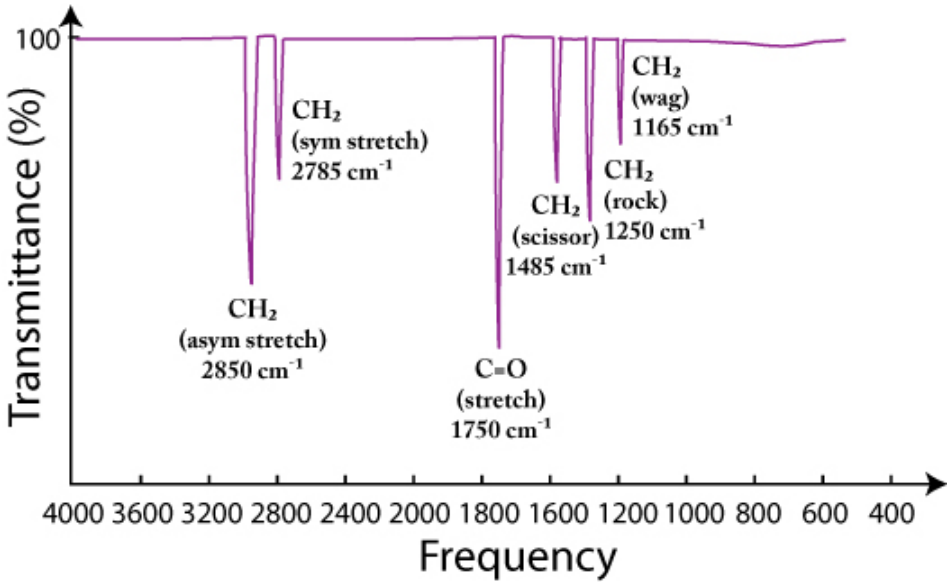

Figure 2.5 Example of FTIR absorption spectra of organic bonds. Measures % of transmission (Y-axis) across varying frequencies (X-axis). Absorption leads to a reduction in transmittance which occurs at specific frequencies for specific bonds. A C=O bond alongside CH_2 bonds of varying symmetries and conformations are presented as examples.

FTIR was used to investigate the chemical composition of SiNP. The SiNP powders were mixed with KBr powder and compressed into discs using a uniaxial press (10 tonnes). The discs were examined and compressed by IR transmission.

The SiNPs suspended in culture media at 1 mg/ml were washed with DI water and centrifuged to re-pellet the SiNPs in order to remove any excess debris from the suspension before being placed into discs applying. The pellet was dried at room temperature using the super vacuum (Eppendorf® concentrator 5301). The dried powders were pressed in a uniaxial into a disc as described above. . A transparent disc containing small amounts of the analyte was produced, which was then placed in the IR spectrometer (Thermo Nicolet Avatar 370) and transmission data was collected at a frequency range between 375 and 7800 cm^{-1}.

2.2 Analysis of cytotoxicity endpoints

2.2.1 Cell counting

Cell counting is a very important step in conducting any *in vitro* experimentation. Invitrogen Countess® is a machine specially designed to count cells and show viability of cells in a sample. It is much simpler and quicker than traditional manual counting method using haemocytometer. Similar to haemocytometer, the Countess® also uses trypan blue staining to differentiate between live and dead cells.

Cells were detached from the growth surface area with trypsin. Once detached the cells were centrifuged and resuspended in fresh media. A small volume was removed from this suspension and placed into Eppendorf tube and mixed with equal amount of trypan blue. The mixture is pipetted into a Countess Chamber slide® and analysed in the Countess®.

For NP treatment, cells were stained with trypan blue for determining number and viability using a cell counter (Countess Automated Cell Counter, Invitrogen). Cells were seeded at a density of 1 x 10^4 cells per cm^2 of growth surface area in 96 well plates

and left to attach over night at 37°C with 5% CO2. The wells containing cells were filled with 200 µl of DMEM containing 25- 100µg/ml of different dust NP or 'raw' NP samples. Cells without NP treatment were used as negative control, whilst a silica nanomaterial of 7 nm (SiNP, amorphous, fumed) and H_2O_2 were used as positive controls in dust NP studies. These were then examined at different time intervals (4-72 hours) for assessing different toxicity endpoints.

2.2.2 Cell culture

In vitro cell culture models were chosen based on their relevance to the routes of human exposure to nanoparticles and the initial and secondary contact sites of nanoparticles with the human body after exposure. These include human lung epithelial cells, foetal lung fibroblast cells and, skin keratinocytes.

Human lung adenocarcinoma A549 cells: type I lung epithelial cells acquired from Sigma-Aldrich. These cells were derived from the lung of a 58 year old Caucasian male (Health Protection Agency Culture Collections, 2011). These cells are known as being resilient and have the ability to be grown over long period of time. They are used to model in vitro responses which may be encountered in the lungs.

Foetal lung fibroblasts MRC-5: acquired from Sigma-Aldrich. These cells were established from a 14 week old male foetus (Sigma-Aldrich, 2011). These cells were used to mimic fibroblast response to toxicity exposure in vivo. Using multiple lung cell lines could help to understand the cellular mechanisms of inhalation toxicity of NP.

Human skin keratinocytes HaCaT: these cells were acquired from Health Protection Agency (HPA). This immortalised cell line was derived from a 62 year old male's skin (Cell lines services, 2011). Like A549 for lung cells, HaCaT cell line was established as a model for skin and topological exposures toxicity study.

Cells were suspended in DMEM supplemented with 10% FBS and 1% antibiotics. The cells were seeded at a density of 1 x 10^5 cells/cm^2 in flasks and

incubated at 37 °C under a humidified atmosphere with 5% CO2 and 95% air. The cells were subcultured every 3-4 days. To subculture these cells firstly they must be detached, as they are all adherent cells, with trypsin-EDTA (0.25%), followed by centrifugation at 1200 RPM in Thermo-Scientific (UK) centrifuges. The cell pellets were collected and resuspended for further culture.

2.2.3 Optimization of cell culture

It is important to optimise any assays before conducting the experiments to achieve reliable reproducible and biological relevant results. For cytotoxicity study it is important to optimise the cell growth patterns so that the treatments take effect in the growth phase of the cells, not in the lag or stationary phase.

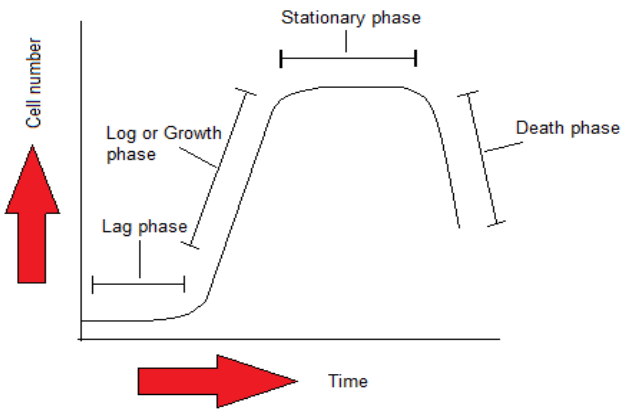

Figure 2.6 Schematic diagram of cell growth. Cell growth starts with slow growth in lag phase, followed by exponential growth in log phase, followed by stationary phase and lastly death phase.

For the optimisation of the cell growth, cell counting was used to establish cell doubling time, which is the time taken for the cell number to double. Cellular doubling times were logarithmic calculated using online calculator with multiple times point analysis (Roth, 2006). Cells were counted at seeding. For A549 and HaCaT cells, the seeding density was tested at 7000, 8000, 9000 and 10000 cells per cm^2 of growth

surface area. For MRC-5, the seeding density was tested at 10000, 20000, 30000 and 40000 cells per cm^2 of growth area. Cell growth was monitored over 72 hours of culture. At each time points, cells were counted three times and the average of the three counts was used for cell growth doubling time calculation.

2.2.4 Cell treatment with NP

The dose selected for treating cells must meet some criteria. Firstly, it must be a standardised dose metric used by majority of research groups. The mass concentration (µg/ml) is the most frequently used metric for NP toxicity study currently, this dose metric is easily compared across a selection of NPs. There are other dose metrics available but they are difficult to apply across different NP shapes and sizes, until they are standardised mass/concentration is the most accepted option. . Secondly, the dose metric must be at a range high enough to induce observable toxic effects, without causing acute cellular death. So based on a 72 hour exposure the selection for concentrations of NPs was made according to what were reported in previous literature. Dependant on cell type, SiNPs ranged from 1-200 µg/ml were used in *in vitro* toxicity studies (Park and Park, 2009; Park et al., 2009). The IC_{50} of SiNPs as reported by Wang, et al., (2009) is 80 ± 6 µg/ml for 20 nm silica and 140 ± 8 µg/ml for 50 nm silica based on 24 hour of exposure in HEK293 cells. The SiNPs used in this study are 7-14 nm in size. Based on these results, the concentration range of 10-100 µg/ml as used in the current study allows induction of cub-acute toxic effects over the period of treatment.

2.2.5 Cell viability assay (MTT assay)

MTT assay is a colorimetric test which measures the activity of enzymes (mitochondrial reductase) that reduce MTT to formazan salt, a purple crystal that is detected with photometric scanner. MTT is widely used as a tool for assessing cell

viability and cytotoxicity *in vitro*, as the conversion of MTT to formazan only occurs in viable cells with functioning mitochondria.

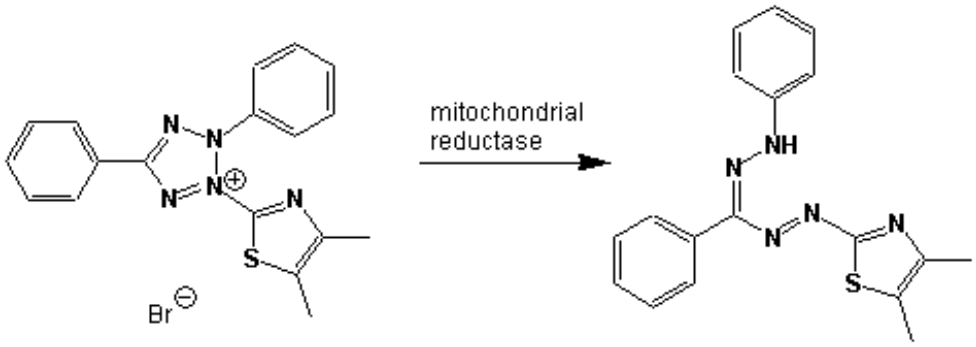

Figure 2.7 Schematic diagram of the conversion of MTT to formazan salt. Reduction utilises the enzyme mitochondrial reductase.

Cell viability was assessed at different time points of NP treatment. Cells were seeded in 96-well plates at 1x 10^4 cells/cm^2, to this 200 µl medium was added to each well. After 16 h of seeding, cells were treated with SiNP or dust NP for 24, 48 and 72 h, when 150 µl of supernatant was removed and 50 µl of MTT solution (1 mg/ml) was added. The plate was incubated for 2 h at room temperature, followed by 3x washing with phosphate buffered saline (PBS) to remove all NPs which may interfere with absorbance measurements. Then 100 µl of Dimethyl sulfoxide (DMSO) was added to solubilise the formazan salt crystals. After 20 minutes further incubation at room temperature, the plate was placed into a Thermo Scientific Varioskan plate reader and absorption was recorded at a wavelength of 570 nm.

2.2.6 Cellular membrane integrity: lactate dehydrogenase (LDH assay)

The LDH assay is a measurement of cellular membrane integrity. LDH is a stable cytoplasmic enzyme present in all cells and rapidly released into the cell culture medium upon damage of the plasma membrane. LDH activity is determined by a coupled enzymatic reaction. LDH leakage toxicity kit (TOX7-1KT) was bought from Sigma-Aldrich, whilst supernatant was taken from the same 96 multi-well plates used

for MTT assay. A mixture of LDH assay substrate solution, LDH assay cofactor preparation and LDH assay dye solution were prepared at a ratio of 1:1:1. Following this 140 µl of the LDH assay mixture solution was added to 70 µl of supernatant and left at room temperature for 30 minutess. LDH oxidizes lactate to pyruvate which then reacts with a tetrazolium dye to form coloured soluble formazan derivative, which The was detected by a Thermo Scientific Varioskan plate reader at 490 nm. A background reading was taken at 690 nm as instructed by manufacturer; the final value was obtained by subtracting the reading at 690 nm from the reading at 490 nm.

2.2.7 Intracellular ROS assay

The increase of intracellular ROS, an indication of oxidative stress, was measured using 5-(and 6)- carboxy-2',7'-dichlorodihydrofluorescein diacetate (carboxy-H_2DCFDA), which when in contact with ROS is converted to fluorescent 5-(and-6)-carboxy-2',7'-dichlorofluorescein by oxidative cleaving of one acetate group. After treatment with NP, the supernatant in the 96-well plate was removed and a fresh 50 µl of medium was added to each well. A 50 µl of carboxy-H_2DCFDA solution at 5 µM was also added to each well. The plate was left in an incubator for 30 mins before reading with a Thermo Scientific Varioskan plate reader for fluorescence intensity (excitation at 490 nm and emission at 530 nm).

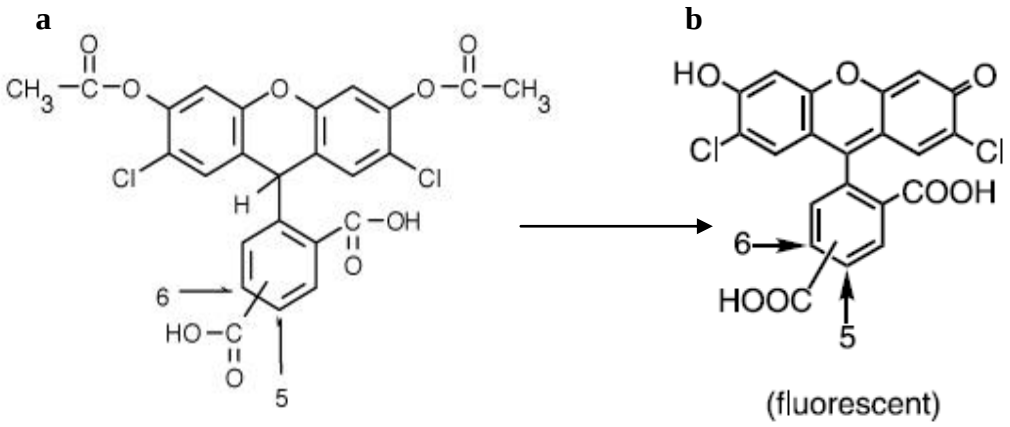

Figure 2.8 Chemical structure of ROS reagent in inactive and active forms. a) Structure of Carboxy-H_2DCFCA, a non-fluorescent form of the molecule. b) The deacetylated, oxidized product DCF, the fluorescent form of the molecule.

2.2.8 IL-8 production assay

Enzyme-linked immunosorbent assay (ELISA) was conducted using the supernatants of the cell culture to detect for IL-8 concentrations, a mediator of inflammatory stress secreted from A549 cells, after incubation with particle samples for 24 hours. The 24 hours' time point was chosen as a test time point to ensure enough time for the treatment to take action at gene and protein expression level as reported previously (Øvrevik et al., 2006; Rahman et al., 2002; Cho et al., 2007; Øvrevik et al., 2006).

For the analysis, IL-8 human ELISA kit (ab46032) was acquired from Abcam. The ELISA method was performed according to the instruction of the supplier as described in Appendix A. Each sample was conducted in duplicate as advised by the kit to obtain reliable results. Cell culture supernatant was taken after 24 h treatment with NP and added to pre-coated wells, to which biotinylated anti-IL8 was added. The samples were incubated for 1 hour and then washed thoroughly twice. Streptavidin-HRP was added, followed by 100 µl of TMB substrate solution, this solution give the ELISA protocol the visualisation by alter the sample colour dependent upon the analyte concentrations. The reaction stopped with H_2SO_4, and absorbance readings were taken at 450 nm (background reading) and 620 nm in the varioskan.

2.2.9 Labelling of SiNP with Fluorescein isothiocyanate (FITC)

In order to visualise SiNPs and image them under a fluorescent microscope, SiNPs were fluorescently tagged with FITC according to the method reported previously (Stayton et al., 2009). The SiNPs (silica 7, silica 14, Aerosil 200 and Aerosil 974) were suspended in 5% v/v APTES ((3-Aminopropyl) triethoxysilane)) in 100% EtOH (ethanol). These NPs were sonicated for 10 minutes and placed into shaker for 3 hours at 60°C. After shaking they were centrifuged and the supernatant was removed, and the pellet was washed with 100% EtOH three times. The pellet was resuspended in 1 ml of 5% glutaraldehyde, and left at 4°C for 10 hours. After centrifuging and washing with DI water, the pellet was incubated with FITC at a saturated concentration in PBS for 2-3 hours at room temperature. This was then rinsed with PBS until solution became clear. Final concentrations of the SiNP solutions were made ranging from 4 – 10 mg/ml. These were achieved by weighing the final dried powders 3 times and taking the mean of the readings and then suspended the powders in 10ml of culture media. These stock solutions were then diluted to working concentrations again in culture medium before treatment of cells.

2.2.10 Cellular uptake of NP assay

For cytotoxicity study, it is important to determine the intracellular dose of NPs. In this study, confocal microscopy and flow cytometry were employed to visualize and quantify the SiNP inside of cells.

Confocal microscopy allows visualisation of the NPs inside of cells, giving indication of intracellular location. The principle of confocal imaging overcomes one of the limitations of traditional wide-field fluorescence microscopy. Conventional microscopy floods the whole specimen with excitation light. Causing excitation of the whole sample at the same time and the resulting image therefore also contains some unfocused background. However, confocal microscope uses a focused beam and excites

only specific areas of interest in a sample through a pinhole. The focused pinhole allows higher resolution but results in a lower intensity (Sheppard and Wilson, 1981).

Cells were seeded into Ibidi© chamber slides (Ibidi, Germany) at 1 x 10^4 per well and allowed to attach overnight. Once attached the cells were treated with 10 µg/ml of SiNP-FITC and returned to the incubator. After 24 hours of treatment the cells were washed with cold PBS, followed by addition of the fluorescent nuclear DRAQ5 (1 µg/ml) and lysotracker red (75 nM) stains and incubated for 30 minutes at room temperature. After staining cold PBS was used to wash cells and 4% paraformaldehyde was used to fix cells over night at 4°C. These chambers were then ready to be observed under confocal microscopy. Figure 2.9 represents the layout of the chamber slide used, it contains 8 separate chambers which can be treated individually and in the same slide allow comparison under a microscope.

	Control	Silica 7	Silica 14	Aerosil 200
	Aerosil 974	-	-	-

Figure 2.9 Layout of Ibidi chamber slide for confocal microscopy.

2.2.11 Assessment of cellular uptake by flow cytometry

Similar to DLS, flow cytometry uses a laser scattering to measure size of cells. In addition it can be used to excite fluorescent molecules attached to cells or particles. The ability to measure both optical and fluorescent characteristics of single cells makes the flow cytometer a very attractive instrument for *in vitro* testing. In this project, the flow cytometer were used to determine and quantify cellular uptake of NP (Huang et al., 2010).

For the NP uptake study, the cells were seeded into 24 well plates at 1 x 10^4 per cm^2 (4.5 x 10^4 cell no/well) and incubated overnight at 37oC for attachment. The cells were treated with SiNP-FITC at 10, 25, 50 and 100 µg/ml for 24 hours to allow uptake

to occur before detection. The culture medium was removed and cells were washed with cold PBS to remove any excess SiNPs and debris which may interfere with the results. The cells were then trypsinated and detached from growth surface. The detached cells were transfered to Eppendorf tubes and placed on ice. The tubes were centrifuged at 1200 RPM and the trypsin was removed. The cell pellet was resuspended in PBS. The samples were placed back on ice and agitated before tested in BD Accuri C6 flow cytometer (bdbiosciences, Oxford UK).

2.2.12 Assessment of cellular response to SiNP by metabolomic assay

After conducting in depth cytotoxic assessment of the SiNP *in vitro*, it was thought that examining the sub-acute effects would reveal greater insight about the mechanisms of toxicity. Metabonomics utilises nuclear magnetic resonance (NMR) spectroscopy combined with multivariate statistics, to form a high-throughput platform. It requires small amounts of sample to gain insight into the effect of toxins on cellular functions. Moreover, intracellular metabolites are also secreted and found in significant amounts in surrounding cell culture medium or other forms of biofluid, which provide a robust and non-destructive method to recognise dose-effect relationship of toxicity in biological models. This study utilised ^{1}H-NMR to detect the protons present in a molecule, generating spectra of peaks dependant on the location of protons with respect to other protons present in the molecule. Sample was collected from culture media and cells to assess the metabolite molecules present in the culture medium and the cellular pellet using ^{1}H-NMR.

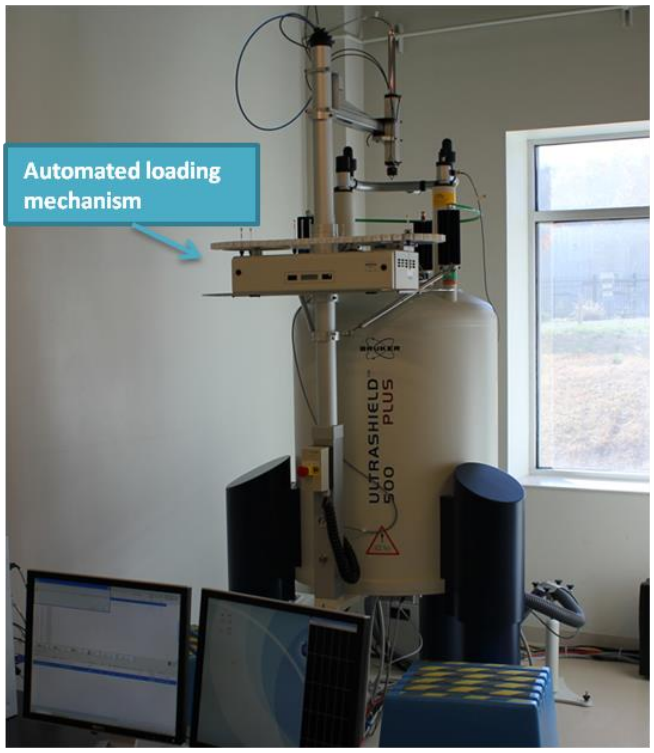

Figure 2.10 Photograph of NMR instrument.

^{1}H-NMR-metabonomcs work was conducted in collaboration with Prof Gooderham's group at Imperial College London. Post treatment cell culture media was required for analysis of extra cellular environment, for this they were seeded in 6 well plates and allowed to attach overnight. Following seeding the cells were treated with 10, 25, 50 and 100 µg/ml of SiNP. The cell culture medium was collected at 4, 12 and 24 hours respectively, and transferred into a sterile Eppendorf tubes. The culture medium was centrifuged at 4 ^{0}C, 1500 rpm, for 5 minutes. The supernatant was removed and transferred to a fresh tube and stored at -40 ^{0}C in freezer for NMR analysis. The frozen supernatants were transported on dry ice to Imperial College London for analysis. To analyse the frozen supernatant, firstly it was thawed. Once thawed 400 µl of media was mixed with 200 µl D_2O phosphate buffer containing 1 mM of 1,1,2,2-tetra-deutero-3-trimethylsilylpropionic acid (TSP) as internal standard and sodium azide (an NMR silent antimicrobial agent). ^{1}H-NMR spectra were acquired using a Bruker DRX600 spectrometer (Bruker BioSpin GmbH, Rheinstetten, Germany) operating at a frequency

of 600.13 MHz and a temperature of 300 K. Samples were analysed in a standard 5 mm probe.

A total of 75 ^{1}H-NMR spectra were acquired under automation using a Nuclear Overhauser Effect Spectroscopy (NOESY) water pre-saturation experiment. However from the total 75 samples 2 samples: 26 (4hrs, 10 µg/ml SiNP treated) and sample 73 (12hrs, 100ug/ml SiNP treated) were found to have poor water suppression and removed prior to further analyses. Full resolution (32k data points) ^{1}H-NMR spectra were automatically referenced to the internal standard TSP. Due to Fourier transformation of free induction decay the phase and baseline of NMR data require corrections. Phase and baseline were then corrected using the instrument software and data imported into Metlab for data analysis. The residual water peak (δ4.67-4.86) was also removed prior to multivariate statistical analyses. Constant receiver gain (rg: 128) was maintained throughout the automation. This was conducted to remove the need to normalise the dataset, limiting normalisation artefacts and allowing comparison and metabolite quantification across samples utilising the internal standard TSP.

2.2.13 Analysis of global MicroRNA (miRNA) expression

MiRNA may provide a new insight into the toxicity mechanisms of NP by highlighting changes occurring before cell viability is lost it may provide knowledge relating to uptake mechanism, cellular location and genotoxicty.

MiRNA expression was analysed for changes at transcriptional levels. Cells were seeded in 6 well plates over night at 1 x 10^4 cells/cm^2 growth surface area. Due to the high cost, only SiNP 7 was tested in A549 cells for its effect at low concentration and an early time point. Cells were treated with SiNP at 10 µg/ml in triplicate. Cells without treatment were used as negative control.

Total RNA was isolated and extracted using miRNAeasy kit II provided by Sabiosciences (West Sussex, UK), and purified through filtration and finally resuspened in RNA-free water to 350 ng/ml. The integrity of the extracted RNA was checked by the

Bio-Rad Experion and Picodrop. This solution was aliquoted and kept at -80°C until use. The RNAs were converted into cDNA using the miScript II kit provided by Sabiosciences. The cDNAs from cells with and without SiNP treatment were diluted in the miScript SYBR green RT-PCR array solution containing SYBR green dye (see Appendix B for detailed instruction).

These dilutions of cDNA were analysed for miRNA expression. The human miRNA array was used (MIHS-216ZA-4). This array contains a total of 1008 miRNAs in a 12 x 96-well ring format. Each ring contained 88 sequence targets with 4 internal controls. Housekeeping genes were also present within each ring to allow normalisation of the results in post processing. The PCR was performed in the Qiagen rotor gene PCR machine with a denaturation temperature of 94°C and 40 cycles of 70°C annealing and 55°C extension.

2.3 Statistics

All the experiments with cells were performed a minimum of 3 times. For MTT, LDH and ROS assays, the data were expressed as mean values of 3 replicates with standard deviation (mean ± SD). The results were represented as a percentage of the negative control (cells without treatment). One-tailed unpaired student's t-test was used for comparison of differences between each treatment with negative control and the differences were considered to be significant when $p \leq 0.05$.

For the ^{1}H-NMR data, the exploratory data analysis (EDA) using principal components analysis (PCA), an unsupervised (no target variable identified) data reduction technique, and the multidimensional data reduction projection method (Wold et al., 1987), were initially employed to detect major sources of variation and biological or analytical clustering pattern within the ^{1}H-NMR data set. Another pattern recognition technique, partial least squares discriminant analysis (PLS-DA) which is a supervised technique (identified target variable) (Barker and Rayens, 2003), was used for classification of samples for percentage of specificity and sensitivity.

Prior to classification, the data obtained from the ^{1}H-NMR metabonomics were subject to scaling treatments. These include 1) mean centring (MC): subtracting the average of every column in a given dataset from each value in the respective column; 2) auto scaling (AS): dividing MC by the standard deviation of each column in the dataset (normally referred to as unit variance scaling in metabolomics); 3) pareto scaling (PS): dividing MC by the square root of the standard deviation of each column in the dataset; 4) range scaling (RS): setting the minimum to be either 0 or -1 and the maximum to be 1 and forcing every element to be scaled between the two values; and 5) normalisation: dividing each value in a respective column by the square root of the sum of the squared values in each column (van den Berg et al., 2006). In practice, PS can be a good compromise with AS as it enhances medium intensity observations and limits incorporation of noise into the dataset.

CHAPTER THREE

3 Physical and chemical characterisation of silica nanomaterials

3.1 Introduction

As reviewed earlier in the introduction section, the characteristics of NP determine the nature of their interaction with biomolecules and cells and, therefore the toxicity potential (Warheit, 2001). In addition, NP may exhibit different characteristics in different biological systems. For examples, formation of different aggregates in the presence and absence of proteins in cell culture media. Silica nanoparticles (SiNPs) are widely used in many industrial and commercial applications, the use of SiNPs in drug delivery and therapeutics/diagnostics is a widely growing field (Mu et al., 2012; Huang et al., 2010). SiNPs are also considered to be highly adaptive dependant on production methods, for example, mesoporous SiNPs have been highlighted as perfect candidate for drug delivery, imaging and catalysis (Trewyn et al., 2008). In the NEPHH project, the commercially available silica NP Aerosil 200 and Aerosil 974 were selected by the project consortium for their suitability as fillers in new silicon-polymer composites for application in automotive industry. Another two silica NP from a different commercial source, SiNP 7 and SiNP 14, were also included for toxicity evaluation. The results will give some indications on whether SiNP from different sources will give rise to similar or different results in a toxicological study.

The main methods which are used to characterise the shape of NPs are TEM and SEM, as these methods provide the only way of visualising objects at that scale. SEM provides excellent visualisation of surface shape and structure, allowing morphology and topography to be characterised very clearly. However, sample preparation can be cumbersome and delicate, especially for organic and non-conducting samples. TEM provides another excellent solution to analyse the structure and shape of a NP. TEM however cannot analyse the surface structures of objects but can give information on the shape and size due to the manner of image collection. TEM transmits electrons go

through a sample thus collecting a shadow of the image relating to its shape and size, whereas SEM uses back scattered electrons relating to in-depth surface structures. The disadvantage of such analysis is the requirement of samples to be within a vacuum. Also the size and price of equipment is beyond the reach of some laboratories and institutes. Electron microscopy requires specialist training for high quality image collection. These two techniques were used in this project for study of NP size and aggregate states.

Apart from high resolution imaging, the technique DLS has also become the standardised method for size characterisation and distribution of NP in aqueous media. It is quick and relatively cheap. The main set back of this method is that it must assume that all particles are spherical in nature to determine a diameter. Therefore, irregularly shaped NPs will not be measured accurately. This technique was also applied in this project to characterize NP dispersion and size distribution in water and in culture medium. The results together with the information derived from SEM and TEM will provide more reliable characteristics of NP in the testing system. For chemical composition characterization, a number of techniques, including dynamic light scattering (DLS), zeta potential measurements, Fourier transform infra red, scanning electron microscopy (SEM) and transmission electron microscopy (TEM) have been used. Based on the chemical specific signal spectrum the information on chemical composition of NP can be acquired by these techniques, among which FTIR proves more advantageous. It detects chemical bonds present in the sample with a small amount of sample, simple preparation and instant measurement. For the current study, the chemical composition of NP in water and in culture medium was analysed with FTIR.

In addition, NP zeta potential was also determined as described in the materials and methods section. The information on zeta potential could indicate the stability of particles in solution according to the surface charge The combination of the selected techniques for NP characterization is highly desirable for further toxicity study, as NP of different size, shape, chemical composition, could interact with cells differently, resulting in distinct consequences.

3.2 Results

3.2.1 Size and shape as seen by SEM and TEM

SiNPs dried from water and culture media were examined by SEM imaging. As seen in figure 3.1, SiNP formed larger aggregates in water. The size of the aggregates could not be determined due to overlapping distribution of the aggregates Silica 7 and 14 nm particles were dispersed relatively well at 10 µg/ml, but formed lager aggregates at 100 µg/ml.

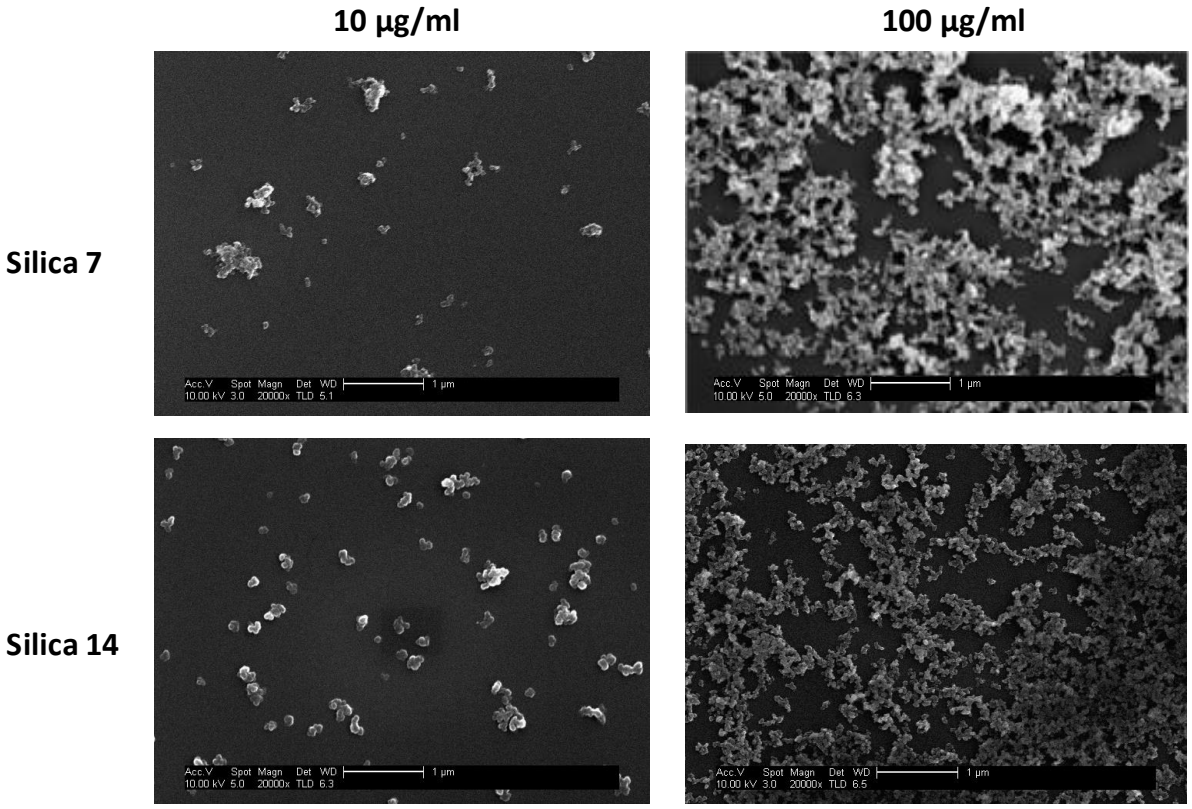

Figure 3.1 Size distribution patterns relating to concentration in water. The silica 7 and silica 14 NPs are shown to aggregate at 10 µg/ml. Presence of larger aggregates is observed at 100 µg/ml. Images taken at 30000 x magnification, scale bar = 1 µm.

Like the above two SiNP, Aerosil 200 and Aerosil 974 were also formed larger aggregates at 100 µg/ml (figure 3.2). However the density of Aerosil 974 was much lower, which is attributable to the hydrophobicity nature of the sample. Due to this nature, good dispersions are difficult to achieve as the majority of Aerosil 974 aggregates form at the surface of the solutions. On the other hand, the hydrophilic SiNP disperses rapidly into the water and forms large aggregates with higher density in the solution.

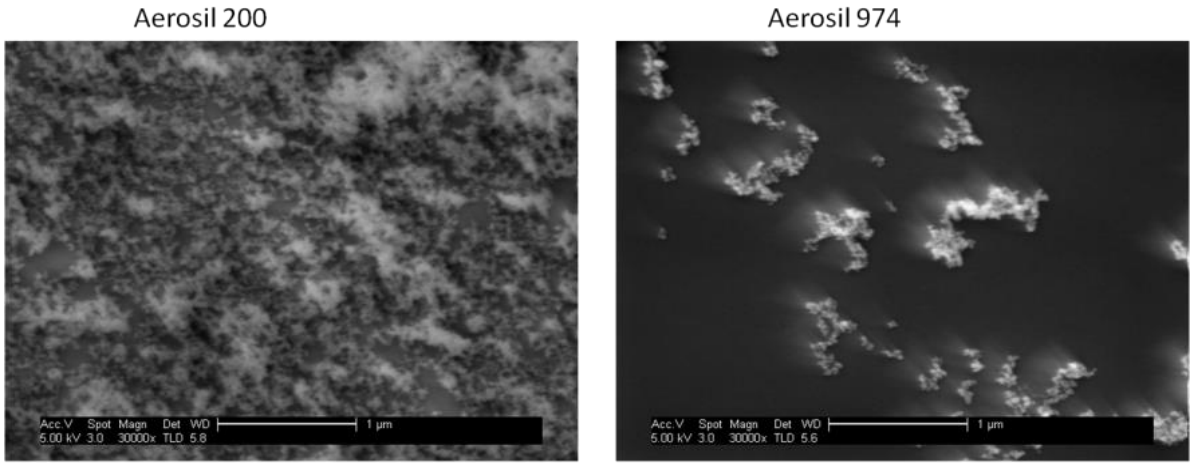

Figure 3.2 Aerosil 200 and Aerosil 974 NPs exhibit differing dispersion patterns. The particles were dried after suspension in water (100 µg/ml), and images taken at 30000 x magnification, scale bar = 1 µm.

It is known that molecules in cell culture medium could interact with NPs to form the so called "corona", which may have some effect on the NP size distribution. SEM examination of SiNP dried from cell culture medium could not produce good quality information on size and surface properties of SiNP, as illustrated in figure 3.2. It appeared that SiNP were covered by a film, which could be the result of adsorption of sugar and protein on the surface of SiNP. SEM is therefore not a suitable method for study of NP in culture medium. TEM, however, is perfect for this application as the transmission of electrons through the material will allow the visualisation of particles deep below the surface film.

The TEM images (fig 3.3 and 3.4) indicate that the concentration does not have the same profound difference in dispersions in water as observed by SEM. Figure 3.3 illustrates a high density of particles imaged from a dried 100 µg/ml water suspension, similar to the SEM images taken at the same concentration.

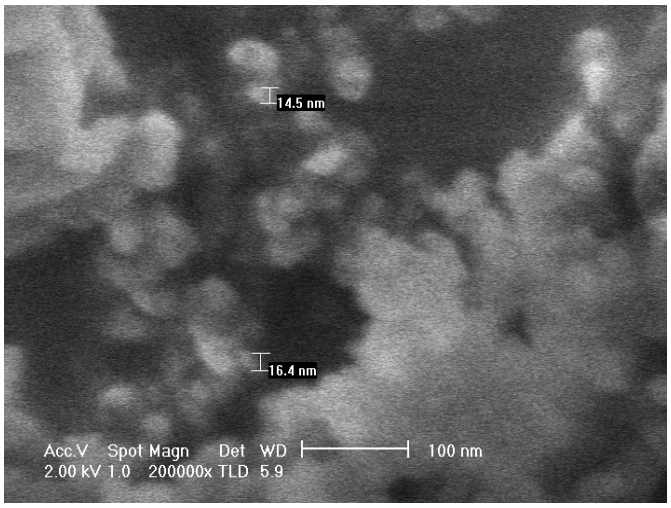

Figure 3.3 TEM image of SiNP 7 nm dried from water suspension. Particles were dispersed in water at a concentration of 100 µg/ml then dried. Image taken at 200000 x magnification.

However, in figure 3.4, the suspension in culture medium is quite different. All NPs suspended in culture media were generally of a similar size aggregate. With the exception of Aerosil 974, which form larger aggregates at low concentration. This may be a result of poor suspension, resulting in clumps of NPs. The sizes of the aggregates varied from between 10 – 200 nm. On closer inspection it was visible that the NPs were generally closely associated with adjacent NPs (examples highlighted in red circles in figure 3.4). The large dark areas in the images upon closer inspection were images of crystallised sugar formed during the drying process. The lack of difference between density between the two concentrations may be a results of the drying of culture media which may remove a larger amount of NPs to the dried film on the surface.

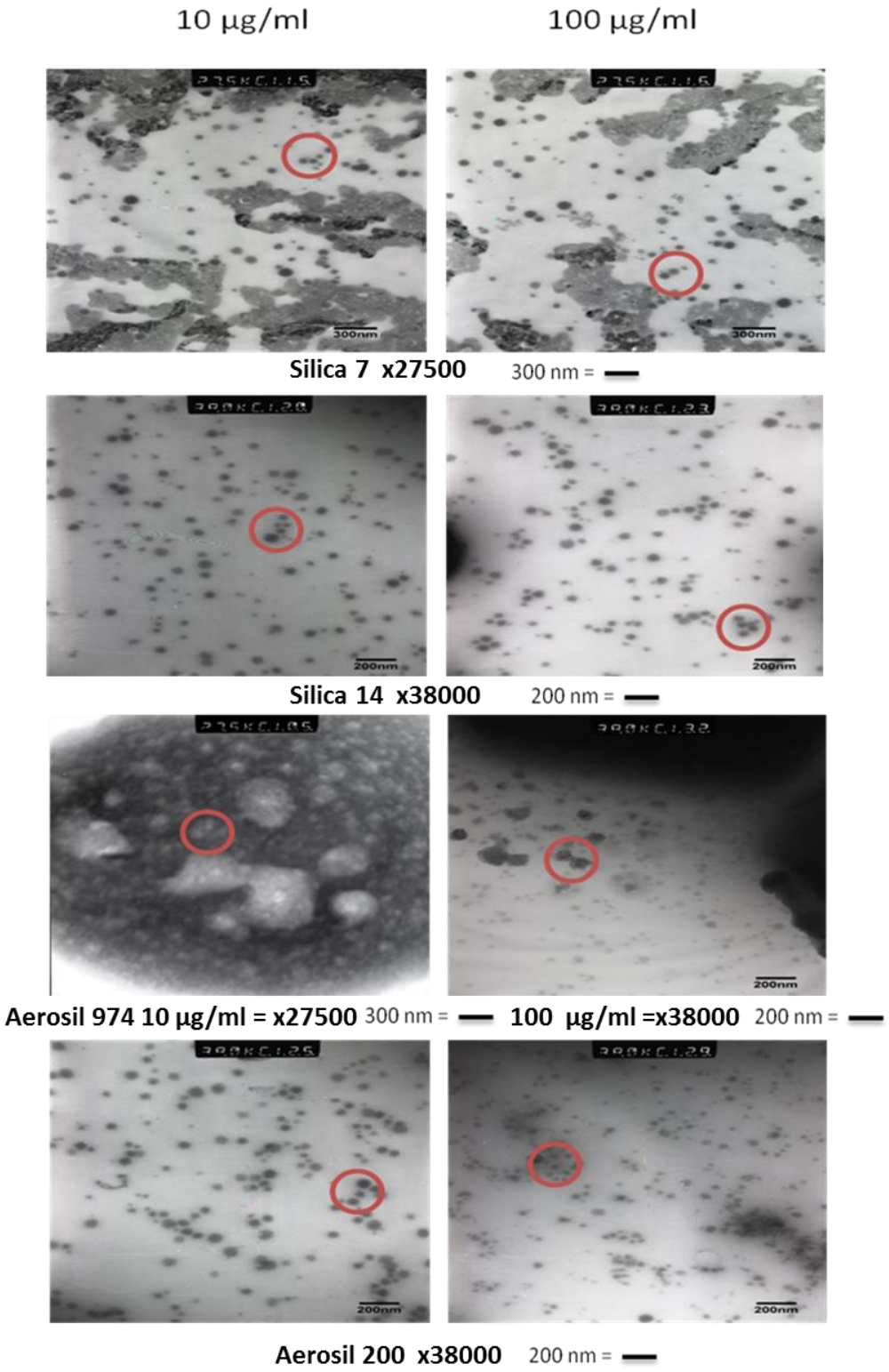

Figure 3.4 TEM image comparison of low concentration (10 µg/ml) and high concentration (100 µg/ml) solutions of SiNP in culture medium. Red circles highlight agglomeration of particles.

All NPs form regular and generally circular particles other than Aerosil 974 which forms irregular shapes as shown in figure 3.4, in which Aerosil 974 was pictured at 10 µg/ml in a largely crystallised section of the sample with the lighter areas representing irregular shaped aggregates. The interaction in culture medium suggests a protein linked interaction between the adjacent particles making the aggregates interact in a uniform manner, such as creating a chain or circular shapes.

3.2.2 Hydrodynamic size distribution in water and in culture medium of Silica nanoparticles

A monodisperse size distribution is visible in the DLS spectra of all 4 SiNPs in water (figure 3.5). The smallest silica NP (7 nm) exhibited different DLS profiles at different concentrations. At 10 and 25 µg/ml, a peak in the range of 110-130 nm appeared, whilst at 50 and 100 µg/ml, a peak in the range of of 1000 nm-1200 nm appeared. The presence of the larger peaks in the DLS profile of SiNP 7 in water may reflect that the smaller NP (7 nm) have stronger inter-particle force to form aggregates as compared with the rest of the NP (sized 12-14 nm).

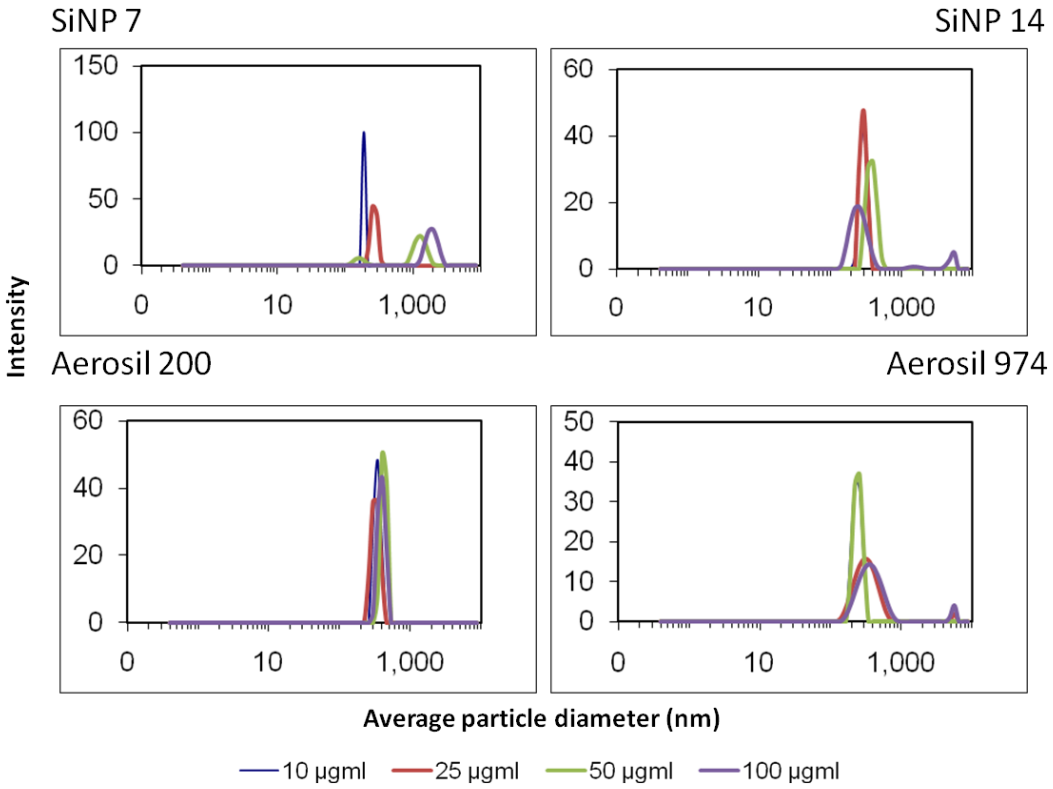

Figure 3.5 SiNPs dispersion in water at concentrations from 10 µg/ml to 100 µg/ml. Size of NPs in water shows definitive indication of large and more monodisperse particles.

There is evidence that proteins can decrease the aggregation of SiNP by interacting with NP surfaces (Cedervall et al., 2007a). As seen in figure 3.6, cell culture medium shows a 'double-hump' characteristic DLS spectrum, suggesting the presence of two main sizes of molecules sizing ~10 nm and ~50 nm, respectively. These peaks have been identified as being proteins present after the addition of 10% FBS (van Gaal, et al., (2010). In order to know whether the cell culture medium, which contains serum proteins as main components, has any effect on the SiNP dispersion pattern, the DLS profile of the SiNP in cell culture medium was also examined.

The SEM imaging analysis of SiNP suggested a link between the suspension characteristics and concentration of SiNP. Thus, concentrations which would be used to treat the cells were all studied with the DLS to gain an understanding of to what NP sizes the cells would be dealing with at given concentrations of NP. Figures 3.5 and 3.6

confirm the findings of SEM imaging of SiNP (figures 3.1 and 3.2) that an increase in concentration leads to an increase number of larger agglomerates. As high concentration of NP leads to a larger number of particles within the same volume, the concentration increase means more particles present within the same volume. This causes the proximity of particles to reduce and therefore to increase the possibility of forming large aggregates. The larger aggregation may also be translated to altered toxicity of the SiNPs. Figure 3.6 shows a 'double-hump' characteristic spectrum of culture medium, suggesting the presence of two main sizes of molecules sizing ~10 nm and ~50 nm, respectively. These peaks have been identified as being proteins present after the addition of 10% FBS (van Gaal, et al., (2010).

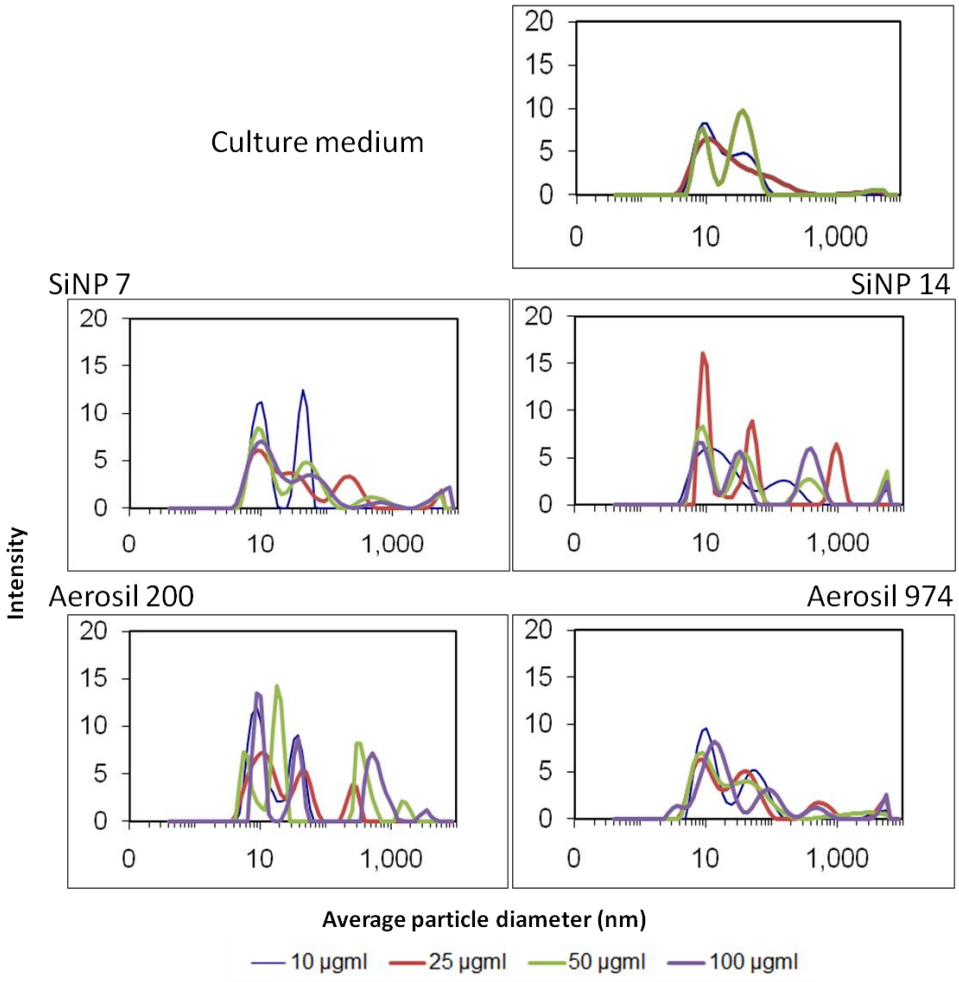

Figure 3.6 DLS assay of SiNPs dispersion in culture medium and culture medium as reference. The DLS profiles of NPs in solutions indicate= the increase of particle size in a concentration-dependent manner.

The difference in dispersion pattern of SiNP showed in water and in culture medium is an indication of the interaction of NP and proteins as suggested by Cedervall, et al., (2007). Interaction of protein and NP may be a fundamental factor in distribution of particle and aggregate size. It may also be a dictating factor in the translation of dispersion characteristics to toxicity.

Figure 3.7 presents bar graphs highlighting the percentage of SiNP aggregates with size above 300 nm formed in culture medium at different concentration. It is clear to see that this percentage is increasing with concentration in silica 7, 14 and Aerosil 200 samples. However, this is not observed in Aerosil 974 sample. The hydrophobic nature of Aerosil 974 may be an explanation to this difference. The increase in aggregate size and hydrophobic nature will drive the majority of larger particles to either sediment quickly or remain on the surface due to surface tension, making even dispersions difficult.

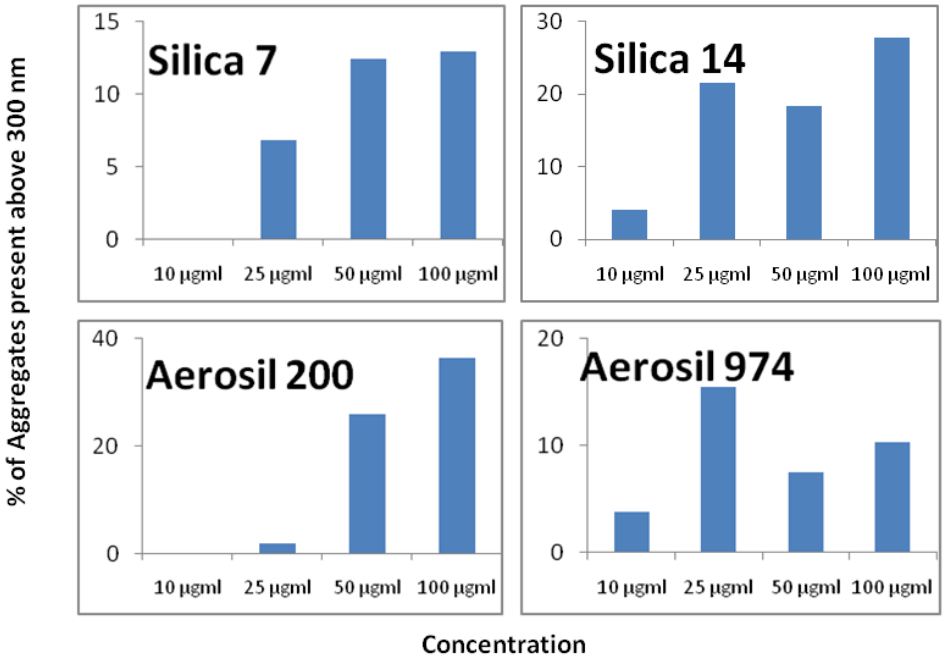

Figure 3.7 Presence of NPs with average size above 300 nm increases with concentration in culture medium. The graphs highlight an increase in the percentage of larger (>300 nm) particles proportional to the concentration of SiNPs.

3.2.3 SiNP chemistry after interaction with culture media

The DLS spectra in culture media indicated that there is possible interaction between NPs and proteins, which may lead to chemical changes to the silica. To examine whether the surface chemistry of the SiNPs was altered after dilution in culture medium the FTIR technique was used to identify the chemical bonds present on SiNP.

As shown in figure 3.8, the peaks in the FTIR spectrum of culture medium correspond to the chemical characteristics of proteins and carbohydrates. The peaks at 2925 cm-1, 1650 cm-1 and 1384 cm-1 correspond to absorption of H_2C, C=O and C-H bonds, whilst silica has signature peaks at 1100 cm-1 (Si-O stretch) and 470 cm-1 (Si-O bend), respectively. Moreover some peaks seen in culture medium were also present in the spectra of all SiNP dried from culture medium, although there were slight variations in the exact position of these peaks. This may be an indication of interactions between NP and protein molecules, resulting in changes in the proteins chemical bond or conformation, which could have significant implications for SiNP application in vivo, where proteins are main components of the serum.

The FTIR analysis suggests that SiNPs chemistry is not altered upon suspension in culture medium. However, the interaction of proteins with SiNPs may alter uptake kinetics and cellular locations of NP (Lesniak, et al., (2012), therefore it may still have some effect in the translation of NP toxicity.

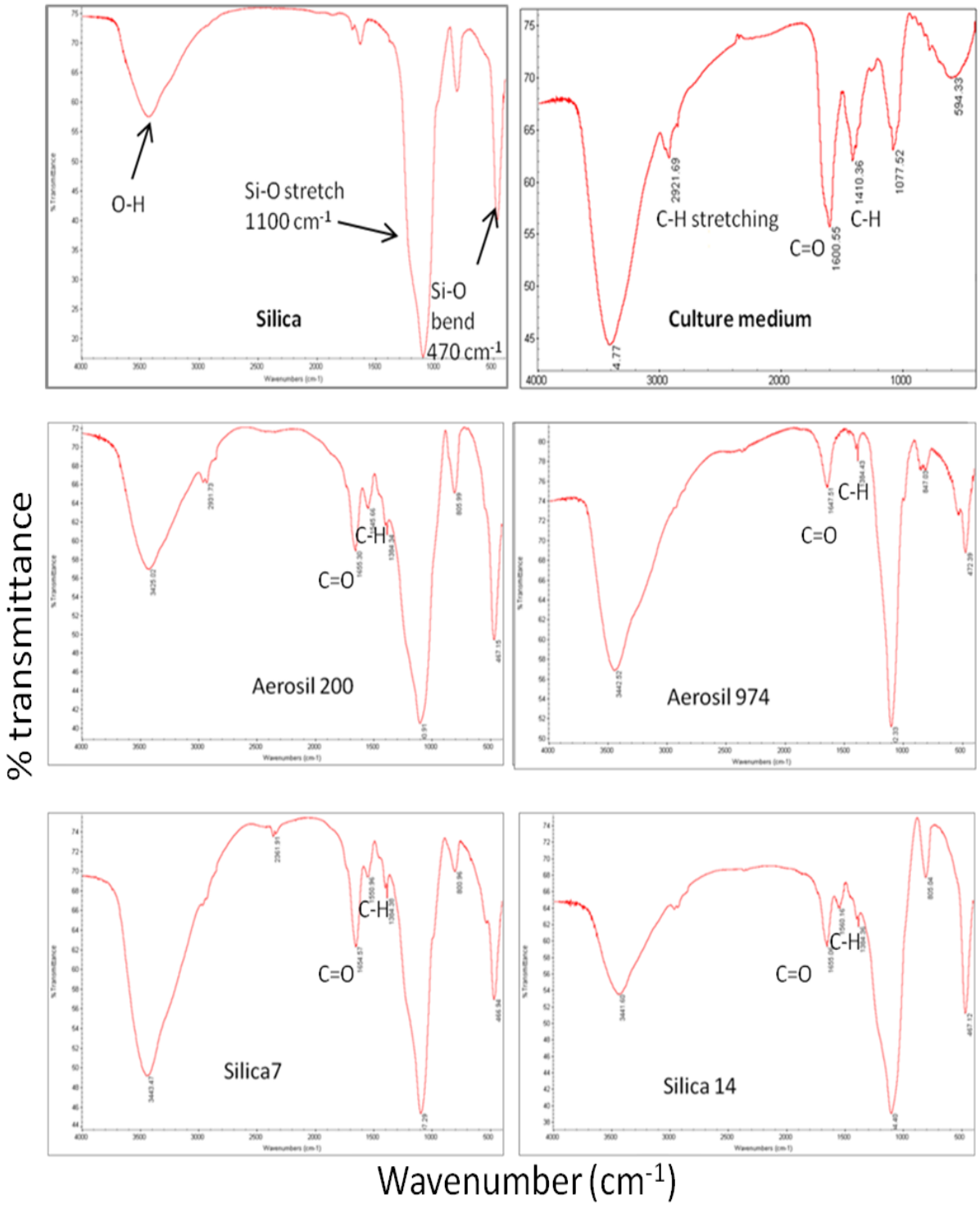

Figure 3.8 Infrared spectra of pure silica, dried culture medium and dried suspensions of SiNPs from culture medium. SiNP peaks are unaltered post culture media suspension. Culture media presence detected by C=O and C-H peaks.

3.2.4 Effect of culture media and water on the zeta potential of SiNPs

The zeta potential of SiNP was measured in both water and culture medium at a concentration of 100 µg/ml. The results are presented in table 3.1, showing a difference in zeta potential between suspensions of SiNP in water and in culture medium. When suspended in water, the zeta potential was in the range of -27~- 31 mV, as opposed to -8~-17 mV when suspended in culture medium. This suggests a destabilisation of the particles in culture medium.

Table 3.1 Zeta potential measurements of SiNP in water and in culture media.

Zeta potential							Average	
Sample	Water	(mV)		Culture	media	(mV)	Water (mV)	Culture media (mV)
Aerosil 200	-26.8	-26.4	-28.3	-10.9	-13.5	-11.4	-27.167	-11.9333
Aerosil 974	-28.4	-33.8	-31.1	-17.4	-16.9	-17	-31.1	-17.1
Silica 7 nm	-27.7	-32.2	-29.9	-10.1	-11.2	-8.1	-29.933	-9.8
Silica 14 nm	-29.2	-31.3	-29.8	-6.9	-10	-8.8	-30.1	-8.56667

NP with a high zeta potential (±) are more stable and therefore more likely to have better dispersion in the solution they are measured in than the NP with lower zeta potential. This seems to agree with the results from DLS assays, as at the same concentrations, a higher zeta potential of SiNP in water is associated with a far more well-defined monodispersed profile, and a lower zeta potential in culture medium is associated with the occurrence of a wider spread range of size distribution profile (figure 3.5 and figure 3.6). In comparison with the hydrophilic SiNP, the hydrophobic Aerosil 974 had a smaller difference in zeta potential between suspensions in water and in culture medium. This may be due to that Aerosil 974 is hydrophobic. The poor solubility of NP in water will have litte effect on the zeta potential of NP dispersed in water and in culture medium.

3.3 Discussion

Characterization of NPs has given insight into the nature of size distribution, dispersion pattern, zeta potential in suspension and chemical composition of SiNPs. It was evidenced that these characteristic of SiNPs can be altered when dispersed in the biological solution, due to their interaction with molecules present in the system. It is apparent that this interaction does not change the chemical nature of the particles, but the primary size and zeta potential of particles are altered. Both zeta potential and size have been suggested to be the fundamental factors for the toxicity NPs (Napierska et al. 2009; Cho et al., 2012).

Although all the fumed SiNP used in this project were commercially available and supplied with primary size in the range of 7-14 nm, the size distribution and dispersion pattern as measured by SEM and DLS suggest that all the SiNP formed aggregates in both water and in culture medium, which is consistent with the results reported by Montes-Burgos et al., (2010) and Fubini et al., (2010). Both groups proposed that the size of particles dictated the toxicity in the systems under investigation. The reason for formation of larger size of particle aggregates in culture medium may be linked to the formation of protein coronas, in which proteins may act as 'linker' molecules increasing the aggregate size (Cedervall et al. 2007b). Therefore, if these NPs cause toxicity in a concentration dependent manner it is less likely that the toxicity will be related simply to the primary aggregate size but rather to the size of aggregates.

Further to DLS and SEM, the TEM analysis of SiNPs in culture media proved that they were polydisperse in nature. From TEM images (figure 3.4) it was seen that NPs were associated with adjacent NPs, this is highlighted in red circles. This observation appeared to support the suggestions by Cedervall et al., (2007b), that NPs are clustered through linkers, although the identity/components of the linker molecules need to be further studied. The aggregation and polydispersity of fumed SiNP makes the interpretation of size-toxic effect relationship more complex than that of NPs with monodisperse nature in solution, such as colloid SiNP (Kaewamatawong et al., 2006).

Small alterations in peak positions of organic chemical bounds were observed in the IR spectra (figure 3.8) of blank culture medium as compared with that in SiNPs samples dried from culture medium, which may be due to conformational changes in protein structures due to SiNP and protein 'corona' formation (Cedervall et al., 2007b). This interaction raises issues of the possible competitive inhibition of proteins/enzymes by SiNP as suggested by MacCormack et al (MacCormack et al., 2012). Further to this they investigated the effect of possible interactions between nanomaterials and protein/enzymes on the conformation and activity of LDH. However, they produced no evidence to suggest that SiNPs have any effect on LDH conformation or activity. Although this project showed no conformational changes occurring in silica chemical signature, the possible change in protein structure could potentially affect the activity of some proteins/enzymes, which could lead to alteration in cell biology (Lesniak et al., 2012). It has also been suggested that the NP-protein interaction may affect the uptake and toxicity of SiNP in particular. The lack of corona could increase the interaction of NP with cell membrane interaction, leading to the increase in NP internalisation and toxicity (Lesniak et al., 2012).

SiNP showed different zeta potential in water and in culture medium, suggesting that these NP have different potential to aggregate in different solution. The higher vale for zeta potential suggests a higher instability of particles in solution, and higher the possibility to aggregate. The particles become more unstable with the presence of proteins, as suggested by the concentration dependent increase in formation of larger aggregates. Both instability and a polydisperse nature may be directly linked. As proteins alter the surface charge of NP by competitive adhesion, the interaction between SiNP is restricted. Therefore, protein binding may dictate dispersity of NP in solution.

This phenomenon may be associated with the electrochemical changes brought about by protein-nanoparticle interactions, suggested by Meiner et al., (2009), Cedervall et al., (2007a) and Cedervall et al., (2007b). As mentioned above, the zeta potential may play a pivotal role in dispersion characteristics and therefore is required to be measured.

Other studies, such as Karakoti et al., (2006) and Cho et al., (2012) have highlighted the potential impact zeta potential may have on the mechanism of toxicity. Jiang et al., (2009) also suggests that the pH of environment is the most important factor controlling the zeta potential. Doymuş, (2007) showed that pH can directly control the zeta potential of coal particles and allow control over aggregation. However, this study utilised culture medium which is mimicking the homeostatic pH for cellular growth, ensuring that the pH is not a contributing factor to cellular toxicity.

Fully characterising the NPs will be critical in interpreting the size-, chemistry- and aggregation effects on toxicity. It will also aid the understanding the mechanisms of NP toxicity *in vitro* and *in vivo*.

CHAPTER FOUR

4 Silica nanomaterial toxicity *in vitro*

4.1 Introduction

In vitro toxicology techniques are widely used to assess potential health hazards. From cosmetics to medicines the first form of testing is usually *in vitro*. For NPs it has been established that the characterisation of the particles is fundamental to assessing and understanding the toxicology of the sample. Once the characterisation is completed sufficiently the results of toxicological testing are easier to associate with a specific route and mechanism of action on the cells. The selection of *in vitro* cellular model for toxicity study is largely based on possible primary route of human exposure to NP. Considering the possibility that NPs may enter the blood stream, a wide range of cell types could be included in *in vitro* study.

To mimic inhalation exposure a cell line that best represents a bronchoalveolar model must be chosen. Human A549 lung carcinoma cells and Beas-2B bronchial epithelial cells have been widely selected for this purpose in toxicity assessment (Soto et al., 2007 Herzog et al., 2007; Eom and Choi, 2009b; Park et al., 2010). The induction of cytotoxicity by a variety of inorganic NPs over a short term treatment has been demonstrated in both cell lines. The toxicity mechanisms involved could include oxidative stress leading to the production of pro-inflammatory mediators (Soto et al., 2007). Another route of exposure which may be a result of NPs release during LCA is topological exposure. For this skin cell types such keratinocytes are widely used to model skin toxicity of NPs (Lu, et al., 2010; Samberg, et al., 2010; Park, et al., 2010; Yu, et al., 2009). Cellular Models provide a greater understanding of the mechanisms of nanoparticle toxicity at a cellular level.

Based on the exposure routes expected during the LCA of the nanomaterials concerned in the NEPHH project, this study selected A549 cells as a lung model for assessment of NP toxicity. For comparison of cellular sensitivity, lung fibroblast MRC-5 cells were also included. Finally, the skin keratinocytes (HaCaT) were also utilized to model dermal toxicity. These cell lines are the most well established cell lines to model lung

and skin exposure, respectively. The A549 cells are a carcinoma cell line, this has advantageous features that they are long lived and can be used over a longer period of time or passage number. However, there are also limitations, such as a carcinoma cell line will not behave the same way as a primary ‘normal’ cell line. For this reason MRC-5 cells are also included to serve as a variance of cell type and also a comparison between healthy primary cell reaction and a carcinoma cell line.

4.2 Results

4.2.1 Optimisation of cell growth

Before proceeding with toxicity testing the growth pattern of the cells under a given experimental condition must be investigated. As shown in figure 2.6, normal cell growth involves 4 phases: lag phase, log phase, stationary phase and death phase (figure 2.6). It is important for all *in vitro* tests to be conducted while the cellular system is under exponential growth, since other limiting factors such as senescence (cells cease to divide, normally occurring after about 50 cell divisions in vitro) and natural cell death could influence the cellular response to external stimuli.

To allow cell growth at exponential phase during toxicity test, an optimal cell seeding density needs to be determined. For easy comparison of results from different experiments using a variety of growth vessels, the seeding density is often defined as cell number/culture surface. To optimize the seeding density of cells for nanoparticle cytotoxicity assessment, cells were seeded at $7x10^3$ to $1x10^4$ cells/cm^2 in 96-well plates (0.94 cm^2/well). After overnight culture, cells were further cultured for upto 72 h and cell growth was determined by the MTT assay at 24, 48 and 72 h, and the absorbance was recorded as indicative of cell number.

For A549 cells the seeding densities examined were $7x10^3$, $8x10^3$, $9x10^3$ and $1x10^4$ cells /cm^2 in 96-well plate (growth area 0.94 cm^2). Over 72 hours the cells at density of $1x10^4$ cells/cm^2 exhibited the best growth profile as indicated by higher initial absorbance and constant increase of absorbance over the time period. The same growth pattern was also observed for HaCAT cells. These two cells lines also share very similar morphology as observed under light microscope. The MRC-5 cells, however, were a little slower in growth. The density of $3x10^4$ cells/cm^2 was determined to be optimal for 72 h culture.

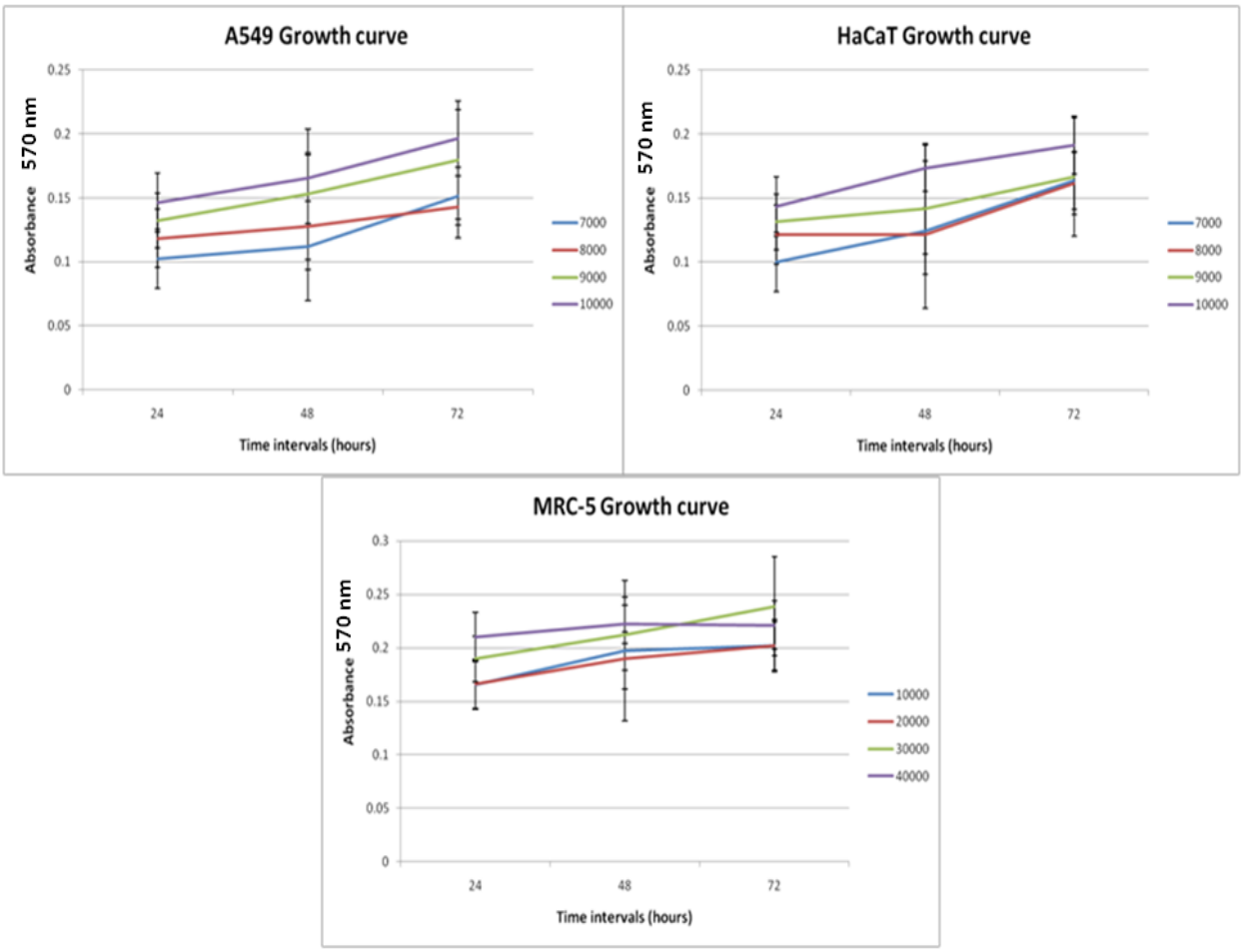

Figure 4.1 Growth of various cell densities over 72 hour period. Cells showed a consistent growth pattern over examined time period, as assessed by MTT as absorbance values. Error bars represent standard deviation of samples.

The cell numbers as determined for the optimal seeding densities at 24 h, 48 h and 72 h were then used for cell growth doubling time calculations. It was important to note that during the assay cells were initially cultured overnight before further culture for 72 h. Therefore, the actual time span in the 96-well plates could be as long as 96 hours.

The cell numbers at different time points are presented in table 4.1. These numbers were uploaded in table format to http://www.doubling-time.com/compute.php (Roth, 2006). From this cell growth rate and the doubling time were calculated. The doubling time graphs and calculations are presented in figure 4.2. The doubling times were calculated as 20.84 hours for A549 cells, 24.45 hours for HaCaT cells and 37.73 hours for MRC-5 cells. Data showed that at the chosen seeding densities, these cells were remained in exponential

growth phase for up to 72 hour. Based on these calculations the chosen seeding densities were suitable for the nanoparticle cytotoxicity study.

Table 4.1 Optimal seeding density for cell growth. Cell counts were taken at intervals of 24 hours over 72 hour period using A549, HaCaT and MRC-5 cell lines.

Time (hours)	0	24	48	72
A549 (cells/cm^2)	1x10^4	1.7x10^4	5x10^4	1x10^5
HaCaT (cells/cm^2)	1x10^4	1.5x10^4	4x10^4	7x10^4
MRC-5 (cells/cm^2)	3x10^4	3.4x10^4	4.5x10^4	10x10^4

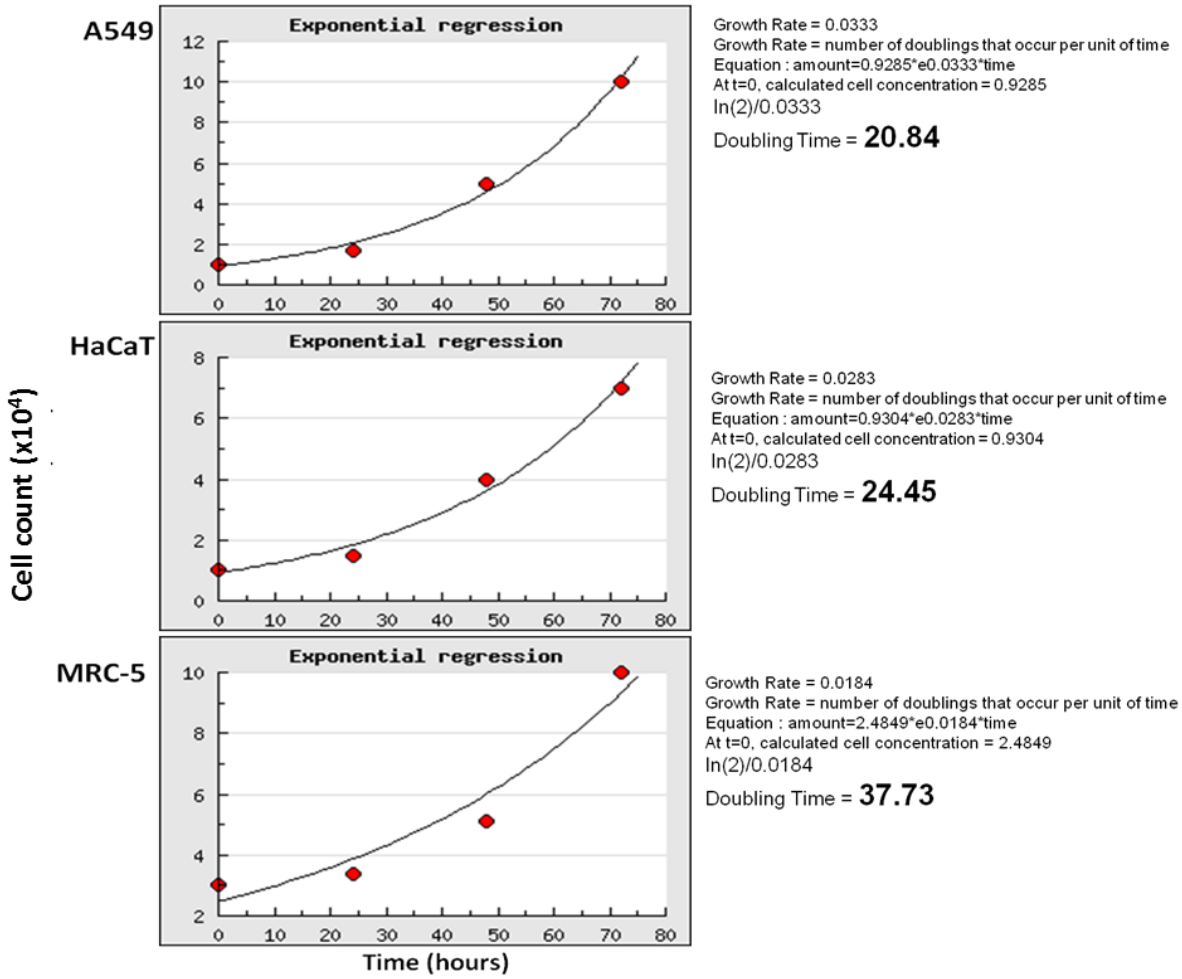

Figure 4.2 Cell growth curves and calculations for all cell lines. Using logarithmic calculations a doubling time is calculated based on growth rate of cells over.

4.2.2 Multiple cytotoxicity endpoint assays

In this study, cytotoxicity endpoints including mitochondrial function, cell membrane integrity and intercellular ROS level were analysed in 3 cell lines as described earlier. These multiple toxicity assays in combination allow elucidation the mechanisms of toxicity.

The mitochondrial function is a reflection of cell viability, which is probed by the production of formazan salts using MTT reagent. The MTT assay indicated that SiNP exhibited no effect on cell viability at 24 h, whereas the positive control (H_2O_2 of 200µM) induced a significant reduction in viability at this time point. SiNP induced a significant reduction in cell viability (< 0.05 as compared with vehicle control) after 48 h of treatment (figure 4.3). Generally a time-dependent effect was detected across all SiNP and concentrations applied. Silica 7 nm, silica 14 nm and Aerosil 200 were seemingly more toxic than Aerosil 974. The effect appeared not to be NP concentration-dependent, as a similar level of reduction in cell viability was detected across all concentrations of SiNP applied. The low toxicity of Aerosil 974 may be a reflection of poor dispersion characteristic of this NP.

The ROS assay indicated that SiNPs of 7, 14 and Aerosil 200 induced a significant increase ($p<0.05$) in intracellular ROS at 12 hours as compared to vehicle control (figure 4.3). After 24 hours, however, ROS level in NP treated cells gradually decreased. The decrease became significant at 72 h in SiNP7, SiNP14 and Aerosil 200 treated cells, which could be due to the significant loss of cell viability as detected by the MTT assay at 72 hours. A similar trend of LDH change was also detected in cells treated with the positive control (H_2O_2 of 200µM). These results suggest that the total number of viable cells needs to be considered in determining the intracellular ROS level, and that intracellular ROS level should be normalised against the number of viable cells.

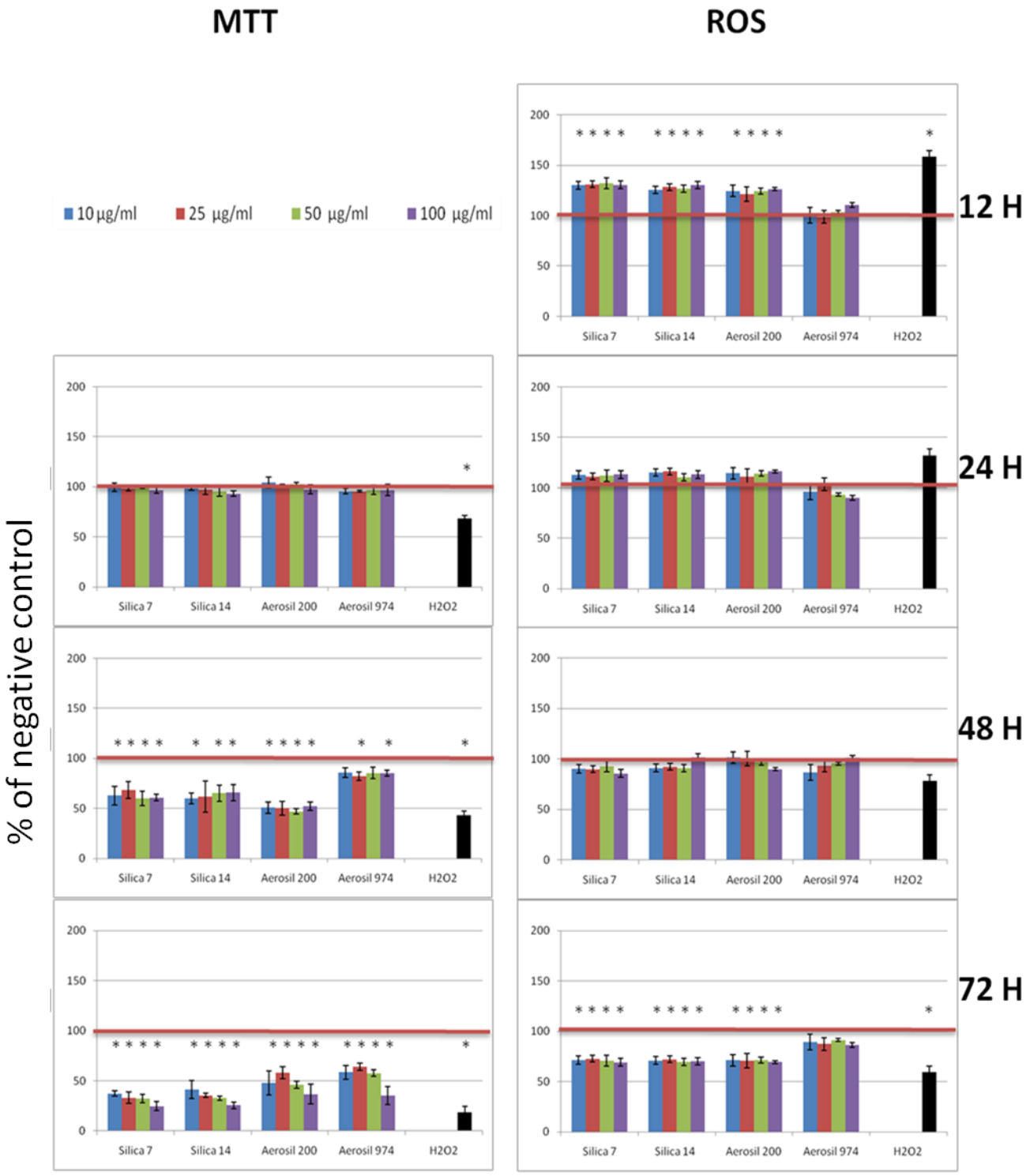

Figure 4.3 SiNP cytotoxicity assays in A459 cells. Left: MTT assay of cell viability over 72 hours. Right: Intracellular ROS assay over 72 hours of treatment. Results were presented as % of negative control. Error bars represent standard deviation. Bold line denotes 100% of negative control. (*= significance *p<0.05*).

The increase of LDH in cell culture medium, indicative of cell membrane damage, was detectable as early as 4 h after NP treatment, reached maximum at 12 h (figure 4.4) and then decreased, which was consistent with the trend of change in intracellular ROS. The effect on LDH leakage was more pronounced for cells treated with the 3 hydrophilic SiNP than those treated with the hydrophobic Aerosil 200. The detection of the SiNP effects by LDH and ROS assays suggest that these SiNPs are capable of inducing acute cytotoxicity, which, however was not detected by the MTT assay. The inability of the MTT assay to detect cytotoxicity at early time point may reflect 3 possible situations: 1) the sensitivity of the MTT assay is too poor to detect early toxicity, 2) residue SiNP may interfere with the readout of the assay when cell viability was only slightly decreased, 3) or the mitochondrion was not the initial target of SiNP acute toxicity. A similar trend of LDH change was also detected in cells treated with the positive control (H_2O_2 of 200μM).

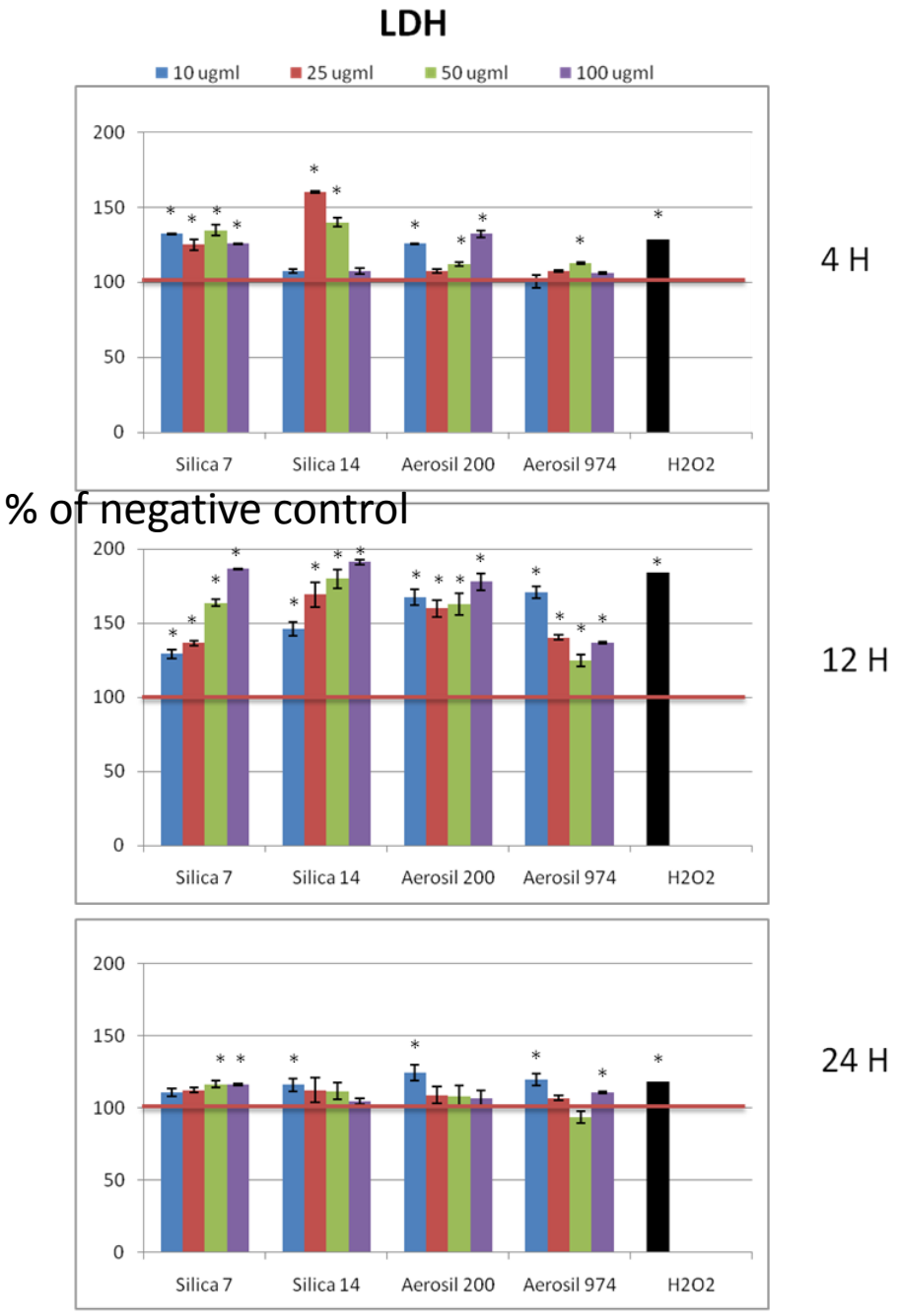

Figure 4.4 LDH leakage over 24 hours of NP treatment in A549 cells. Results were presented as % of negative control. Early LDH leakage detected in a dose dependant manner. Error bars represent standard deviation (*= significance *p<0.05*).

The limitations of the MTT assay in study of nanomaterial toxicity *in vitro* have been investigated with respect to different NPs including SWNT, MWNT and Carbon

black NPs (van Meerloo et al., 2011; Jaszczyszyn and Gasiorowski, 2008). Although silica is shown not to interfere with MTT readings, for precaution the plates are washed to remove SiNPs before proceeding with taking the readings. These studies have concluded that MTT assay is highly sensitive to NP-induced toxicity. Monteiro-Riviere et al., (2009) found that the MTT was sensitive to the toxicity induced by carbon black, SWNT and C_{60} as compared to other methods. MTT is considered as a valuable tool for study of toxicity of different NPs. In combination with other assays such as LDH leakage and intracellular ROS, it provides insight into the mechanisms of cytotoxicity.

In addition to the induction of cytotoxicity, the potential of SiNP in initiation of pro-inflammation was also studied. The induction of IL-8, a mediator of inflammation, was detected using an ELISA assay in A549 cells at 24 h after SiNP treatment at 10-100 µg/ml (Figure 4.5). The linear pattern (R^2= 0.9824) of the detection results derived from using the standard provided by the supplier suggests that the assay quality is high and reliable for IL-8 quantification. Based on the optical density readings and the standard IL8 concentration graph it was possible to calculate the IL8 production in each treated sample using the equation:

Equation 4.1 Equation for ELISA concentration conversion line of best fit

$$y = 0.0021x + 0.3806$$

$$x = \frac{y - 0.3806}{0.0021}$$

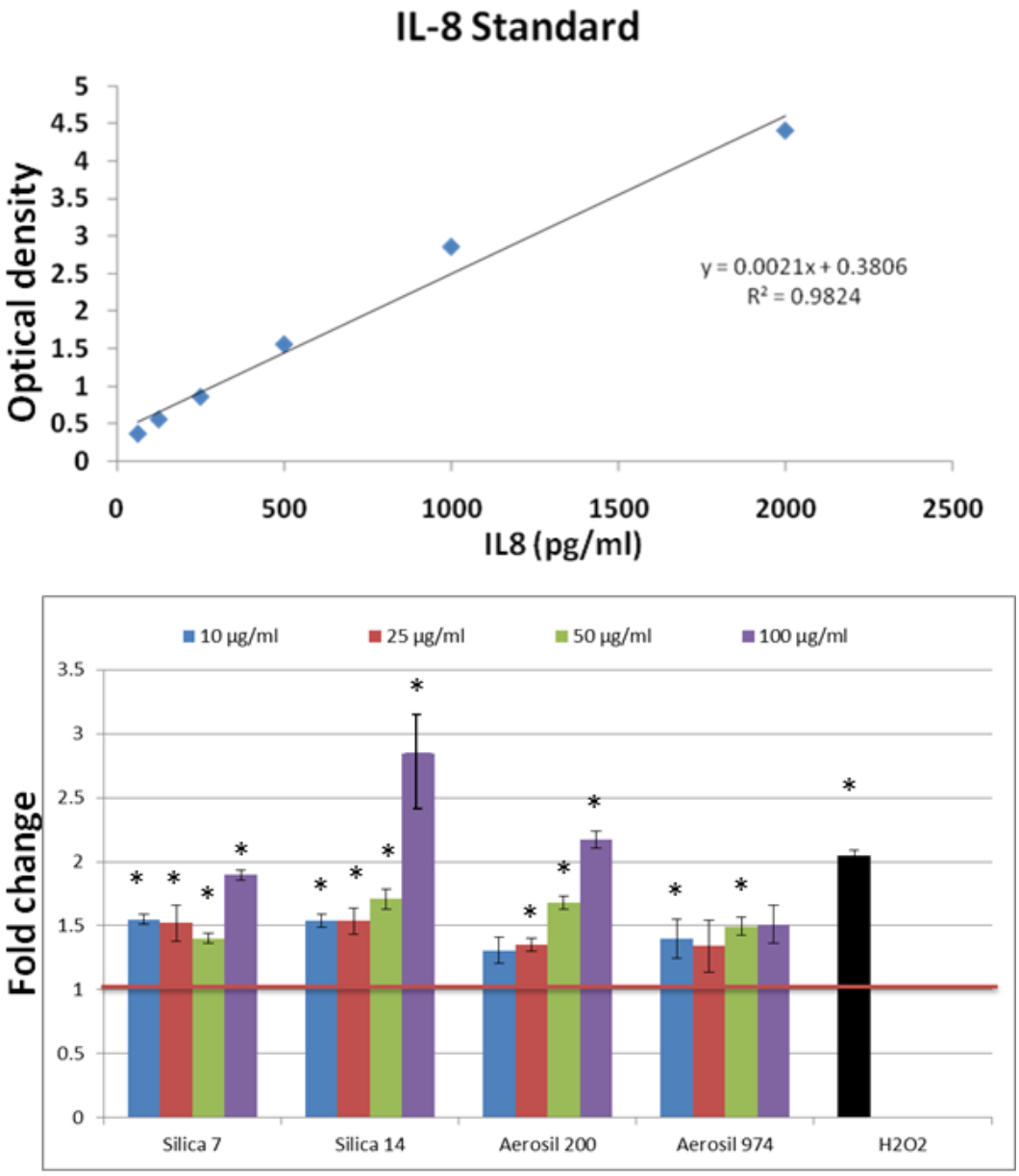

Figure 4.5 IL-8 standard curve and the production of IL-8 induced by SiNP in A549 cells. IL-8 production in sample was presented as fold change of negative control. Standard deviation shown as error bars (significance $p<0.05$*).**

The optical density readings were compared to the standard line to determine concentrations. The concentrations of IL-8 in each treatment are presented in table 4.2.

Table 4.2 IL-8 concentrations in the supernatants of cells treated with SiNP measured using line of best fit equation of IL8 standard.

Sample	Concentration (pg/ml)		
Control average	187.89		
Silica 7			
10	277.7607	426.9975	223.2406
25	267.654	509.9583	247.8749
50	222.9993	490.1608	288.9799
100	404.5838	385.0833	352.081
Silica 14			
10	199.4634	274.2813	411.9433
25	227.5459	272.4933	434.695
50	246.5679	335.574	551.5792
100	324.0746	753.9787	408.6275
Aerosil 200			
10	246.3104	188.9727	184.8642
25	236.7888	205.7127	330.765
50	287.9634	324.798	423.3083
100	341.5143	506.1887	446.7242
Aerosil 974			
10	236.7951	222.5613	250.7708
25	244.6524	200.7413	256.1175
50	289.5133	257.1647	282.9792
100	257.4431	263.0473	323.9283

This production of IL-8 in response to SiNP treatment agrees with previous studies that silica nanoparticles induced inflammatory responses, supporting a strong link between the production of IL-8 both in vitro and in vivo after NP treatment (Oberdörster et al., 2004; Øvrevik et al., 2006; Park and Park, 2009).

4.2.3 Toxicity comparison between 3 cell lines

Experiments of MTT and ROS were also performed in HaCaT and MRC-5 cell lines. The use of different cell lines gives a better indication to general toxicity for NPs. It could also be possible to identify cell type dependent mechanisms of cytotoxicity.

In order to compare the sensitivity of different cell lines to SiNP toxicity, the results from the MTT and ROS assays were converted to percentage of negative control values. As shown in figure 4.6, 4.7, 4.8 and 4.9, similar response trends were detected in A549, HaCat, and MRC-5 cells as assess by the MTT assay at 24 h, 48 h and 72 h after SiNP treatment. At 24 h all three cell lines showed little effects; the only significant difference detected at this time point was for the positive control H_2O_2, to which the three cell lines responded significantly different from each other. At 48 h and 72 h, a time-dependent reduction in cell viability was detected in all 3 cell lines. The reduction of cell viability became more apparent at 48 h and reached <60% at 72 hours.

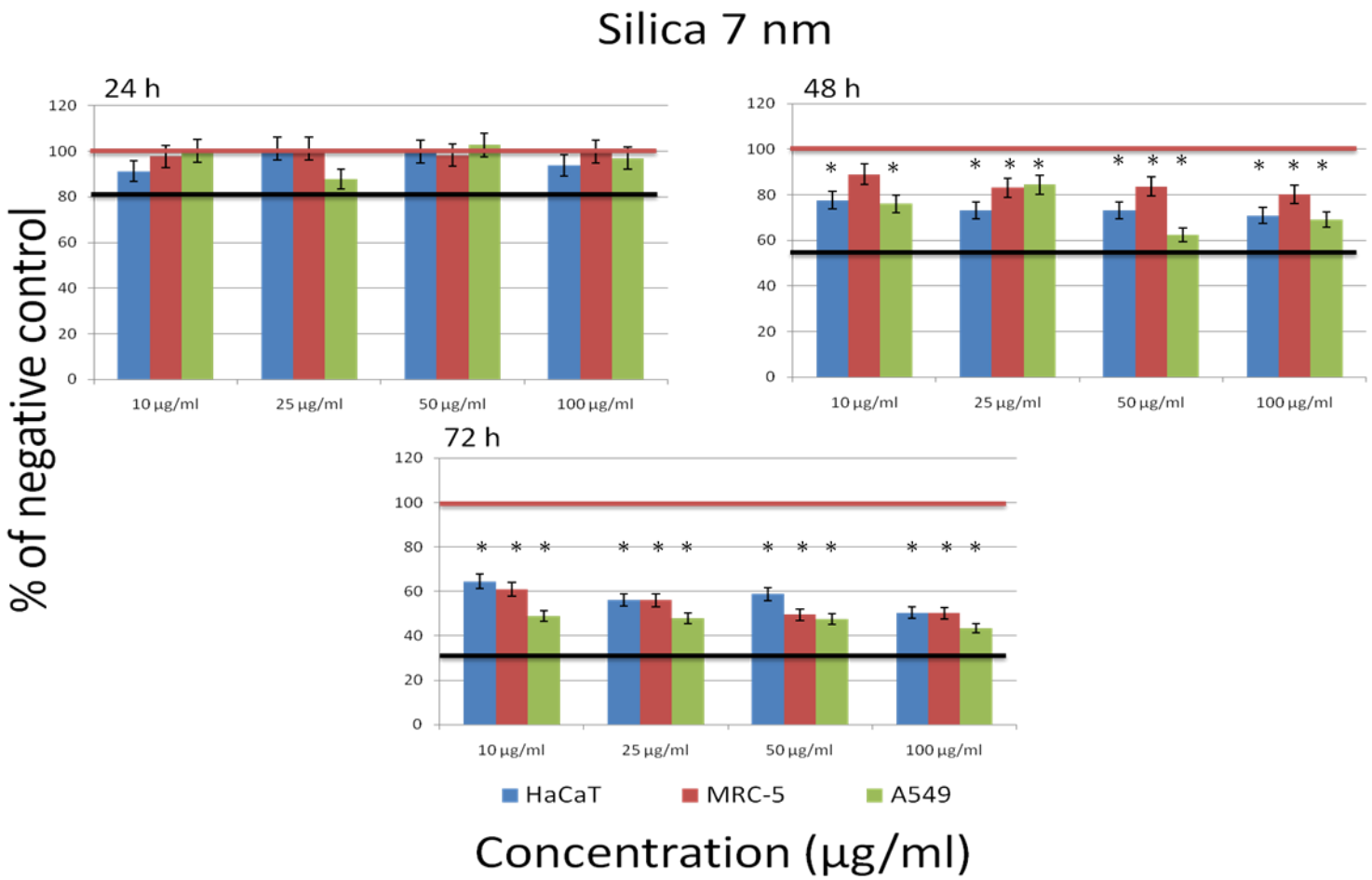

Figure 4.6 Comparison of Silica 7 nm effect on A549, HaCaT and MRC-5 cell viability over a 24 - 72 hours period by MTT assay. Results are presented as % of negative control: red line is 100% of negative control and black line indicates the average effect of H_2O_2 (200 µM) positive control treatment effect on all cell lines. Error bars are shown as standard deviation. *denotes significance ($p<0.05$).

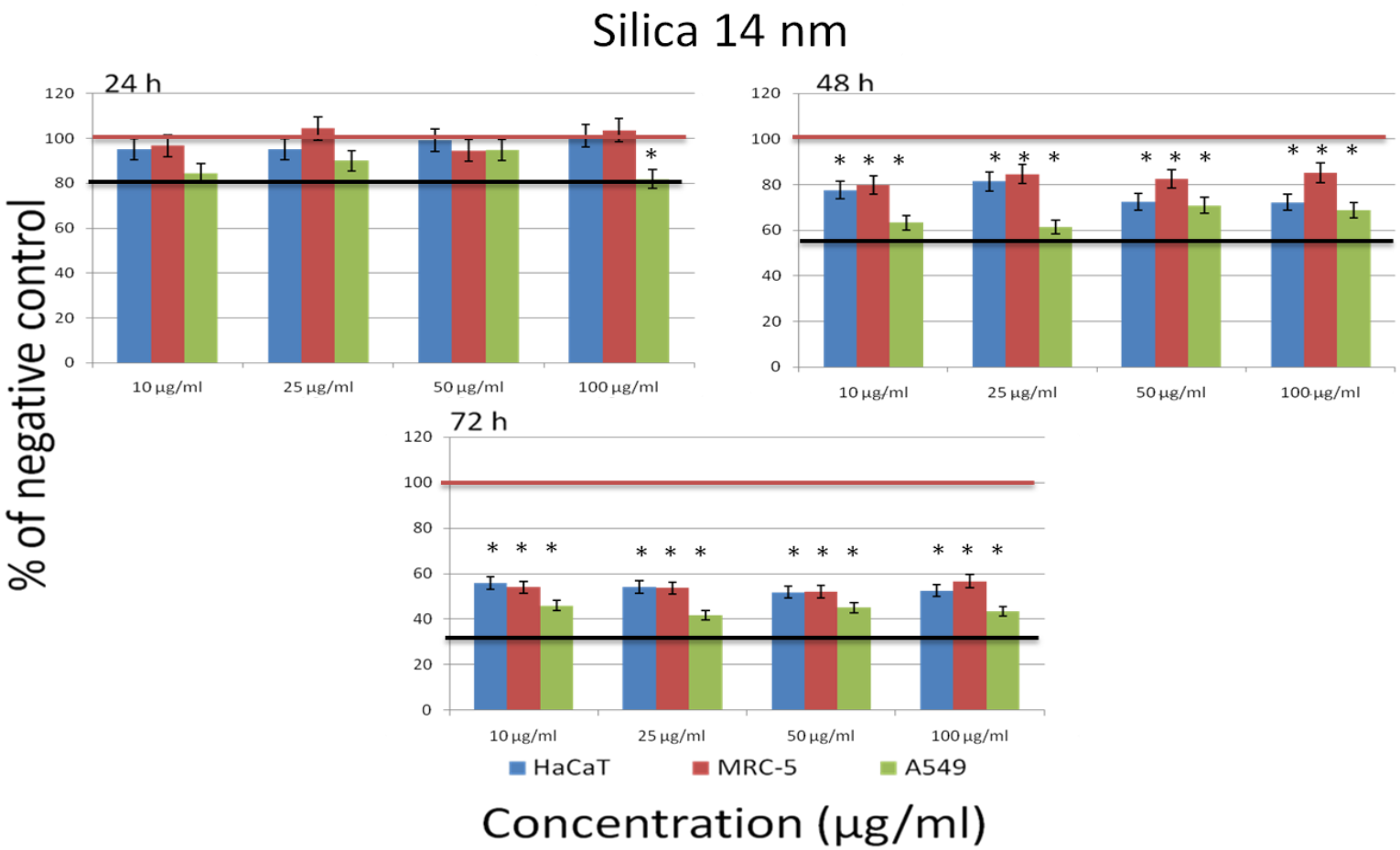

Figure 4.7 Comparison of Silica 14 nm effect on A549, HaCaT and MRC-5 cell viability over a 24 - 72 hours period by MTT assay. Results are presented as % of negative control: red line is 100% of negative control and black line indicates average effect of H_2O_2 (200 µM) positive control treatment effect on all cell lines. Error bars are shown as standard deviation. *denotes significance ($p<0.05$).

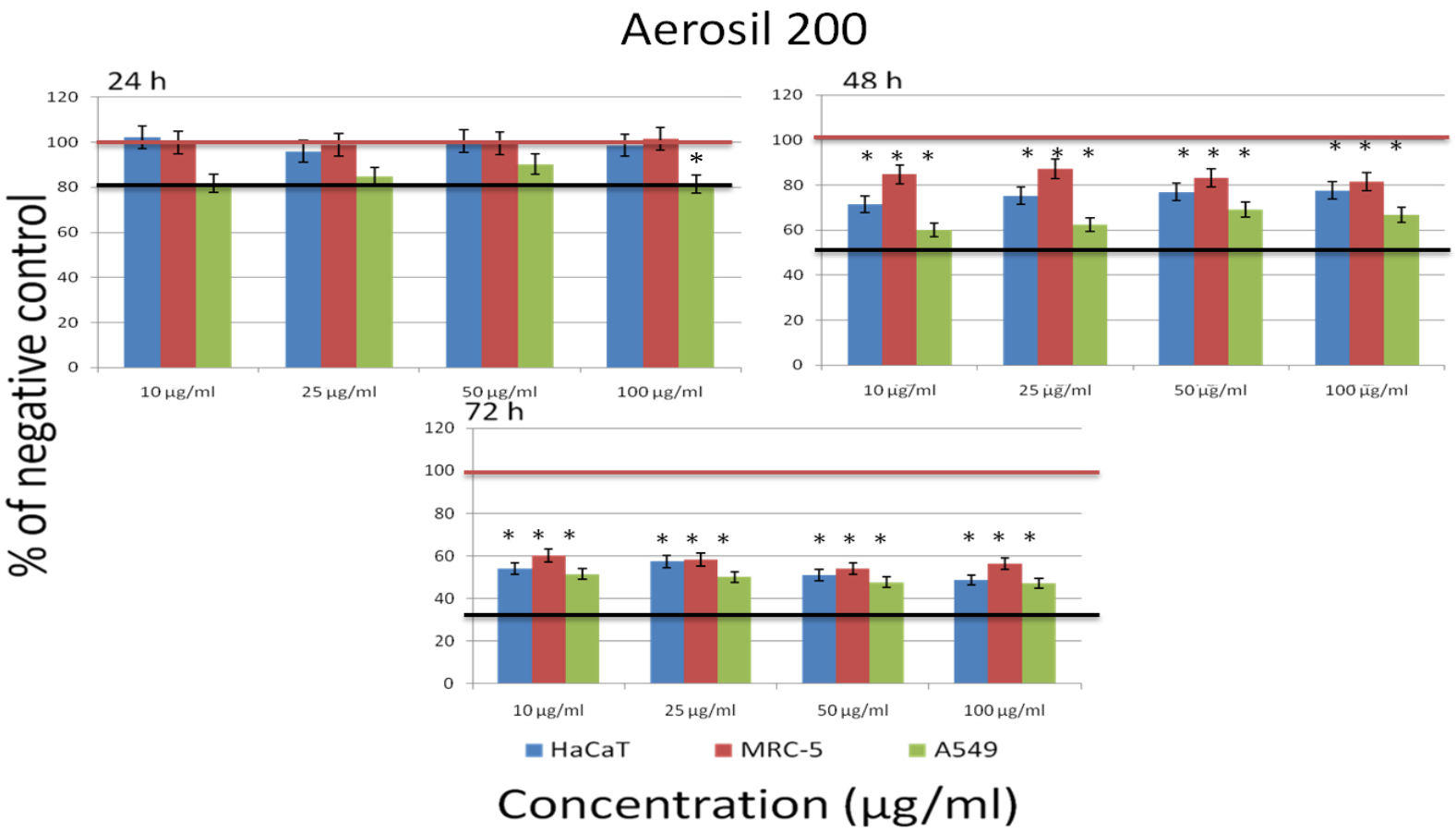

Figure 4.8 Comparison of Aerosil 200 effect on A549, HaCaT and MRC-5 cell viability over a 24 - 72 hours period by MTT assay. Results are presented as % of negative control: red line is 100% of negative control and black line indicates average effect of H_2O_2 (200 µM) positive control treatment effect on all cell lines. Error bars are shown as standard deviation. *denotes significance (*$p<0.05$*).

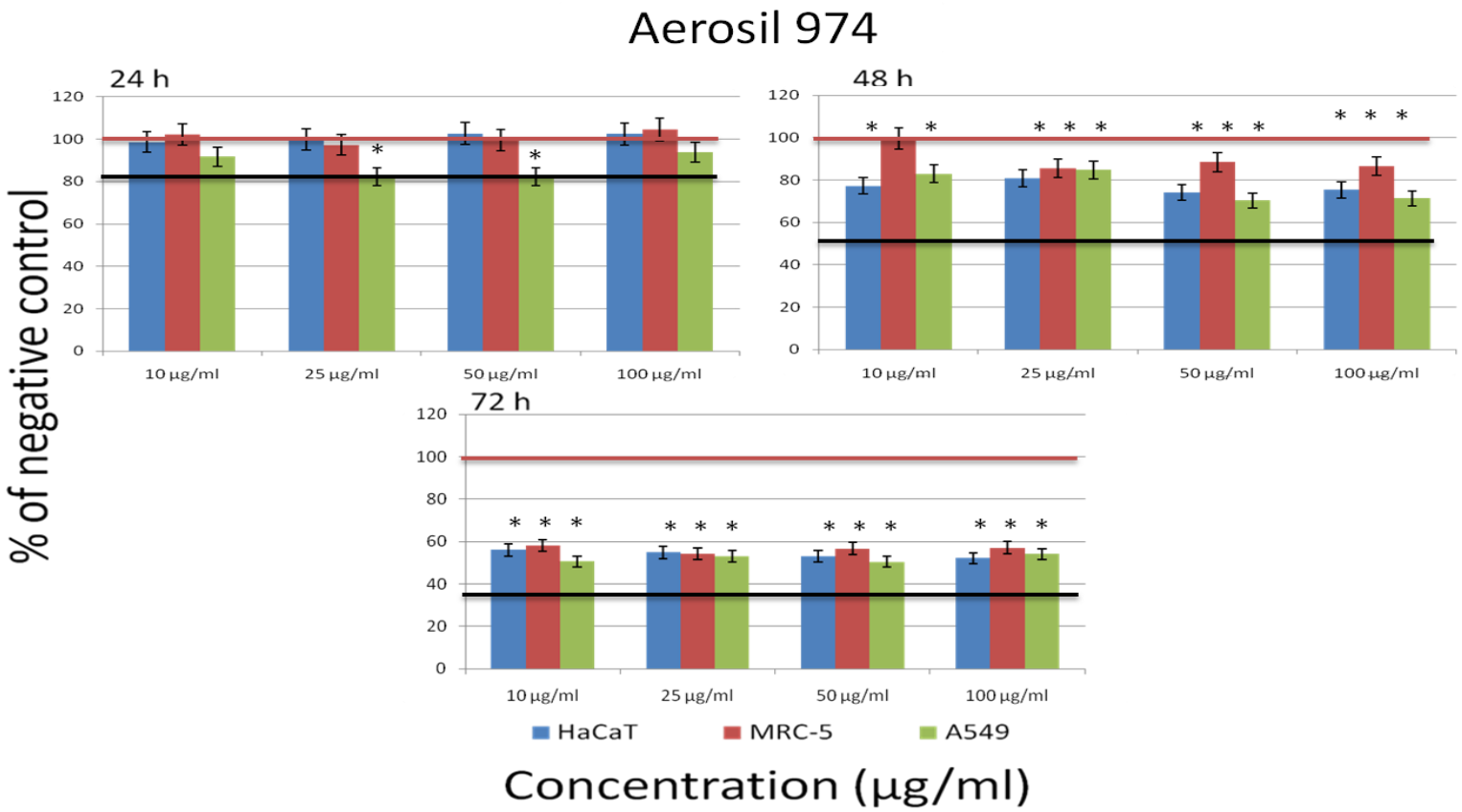

Figure 4.9 Comparison of Aerosil 974 effect on A549, HaCaT and MRC-5 cell viability over a 24 - 72 hours period by MTT assay. Results are presented as % of negative control: red line is 100% of negative control and black line indicates average effect of H_2O_2 (200 µM) positive control treatment effect on all cell lines. Error bars are shown as standard deviation. *denotes significance (*$p<0.05$*).

From figures 4.6-4.9 it appeared that A549 cells and HaCaT cells were more sensitive for SiNP induced reduction of cell viability as compared with MRC-5 cells, which was coincident with the fast growing pattern of the two cell lines as opposed to MRC-5 cells. It is also evident in all 3 cell lines that after 48 hours, cell viability was reduced to a very similar level by NP treatment at all concentrations.

The assay of intracellular ROS indicated that SiNP caused an increase in intracellular ROS in all 3 cell lines as assessed at 12 hour of NP treatment (figure 4.10), although some variations in the response to different SiNP between these cell lines. A549 cells did not produce ROS in response to Aerosil 974, but in both HaCaT and MRC-5 there is a 20% increase in ROS generation, suggesting difference in sensitivity between theses cell lines to the hydrophobic silica NP induced oxidative stress. As these cells all have a very similar level of NP uptake (figure 4.17), the difference in the production of intracellular ROS could not be associated with the intracellular dose of NP. Further study will be needed to differentiate the toxicity mechanisms of different SiNP in these cell lines.

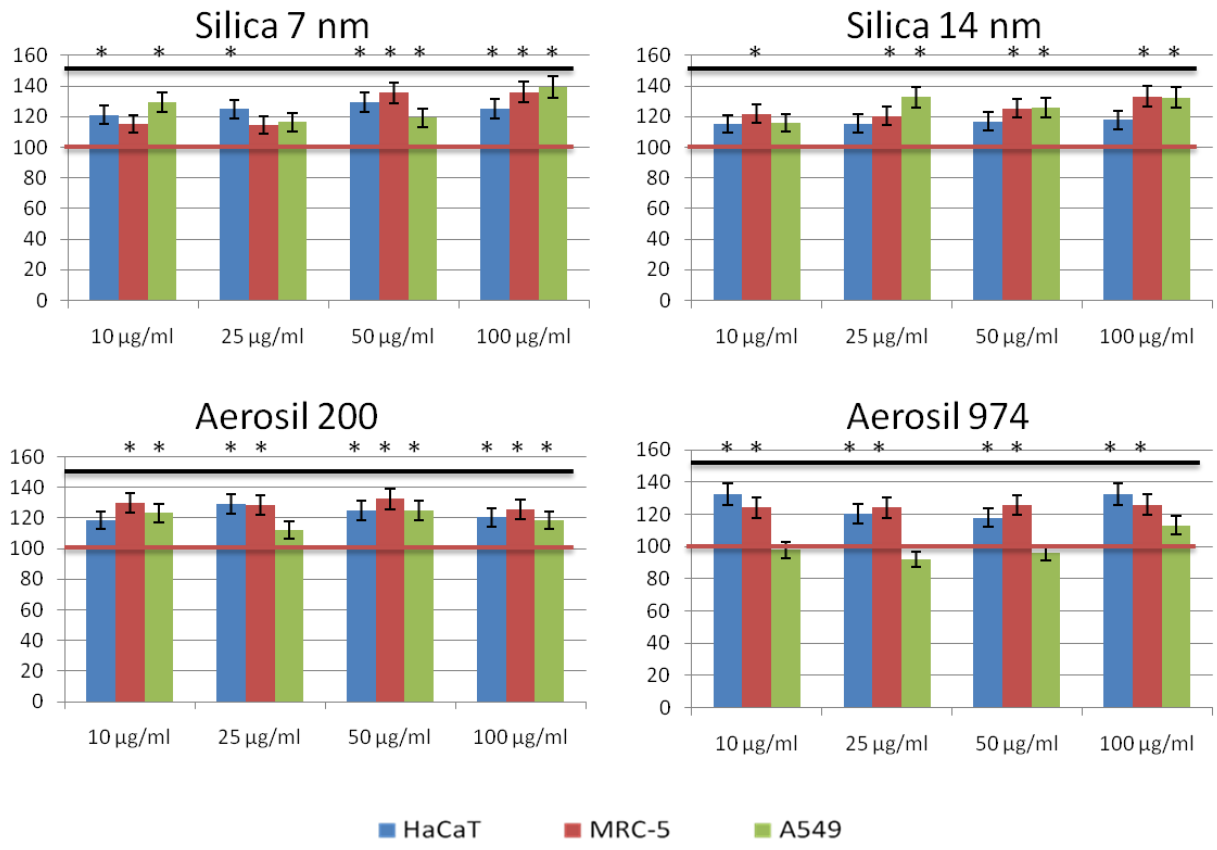

Figure 4.10 Comparison of A549, HaCaT and MRC-5 cells intracellular ROS at 12 hours of each NP treatment. Results are presented as % of negative control: red line is 100% of negative control and black line indicates average effect of H_2O_2 (200 µM) positive control treatment effect on all cell lines. Error bars are shown as standard deviation. *denotes significance (*$p<0.05$*).

4.2.4 Dose dependent uptake of SiNP in three cell lines assessed by flow cytometry

Flow cytometer offers a very reliable and effective method to test for cellular uptake of NPs. It assesses not only the size of cells or particles, it can also assess fluorescence present in a cell. This capability allows a fluorescent particle to be detected if it associated or has been taken up into the cell.

After treated with fluorescently tagged (FITC) SiNPs for 24 h, cells were analysed for uptake of NPs. Figure 4.11 presents the flow cytometry profiles of A549 cells. The control cells show lower FITC intensity than those treated with NPs. A dose-dependent

increase in fluorescence intensity was evident for cells treated with all the 4 SiNP. It appeared that the uptake was more favoured for the hydrophobic Aerosil 974 than the 3 hydrophilic NP, as indicated by the higher level of fluorescence intensity in cells treated with the lowest concentration of Aerosil 974 as compared with those treated with the same concentration of other 3 NP. The cell counts, as indicated by the peak height in the flow cytometry profiles, appeared to be reduced in NP treated samples in a concentration dependent manner, which could be due to the reduction of cell viability.

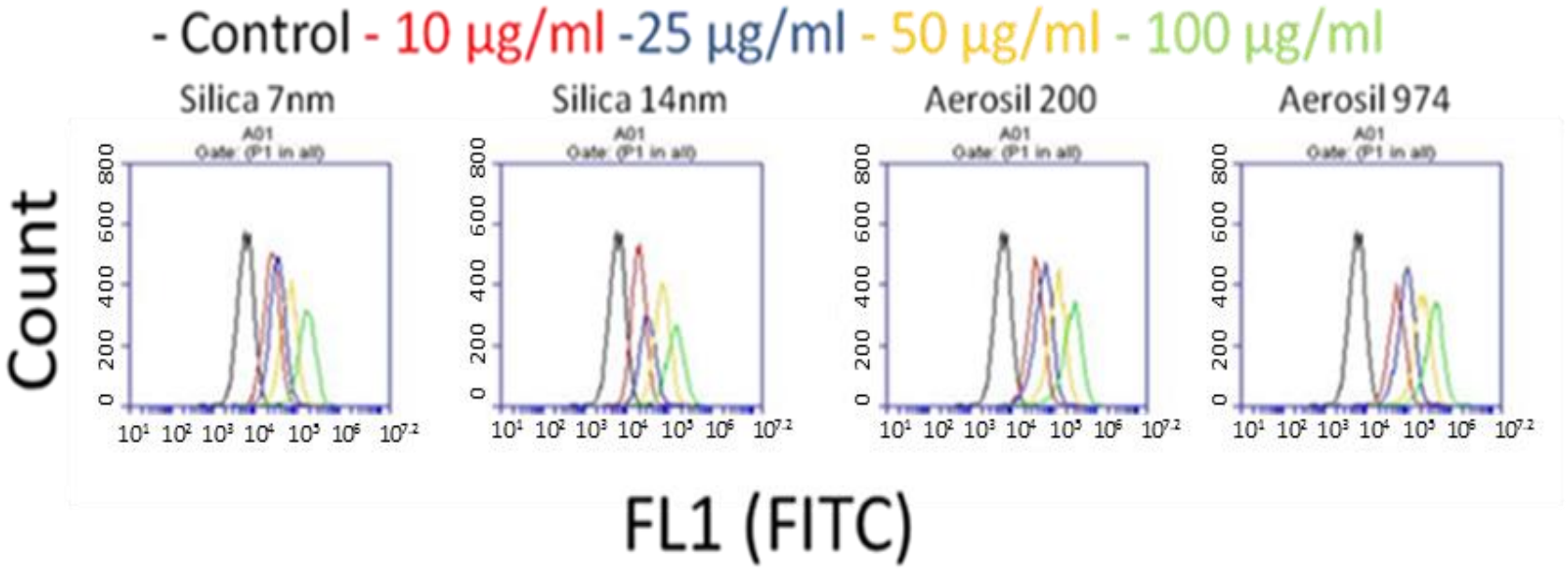

Figure 4.11 Flow cytometry NP uptake analysis in A549 cells. Results were displayed as cell count vs fluorescence intensity. FL1 represents the flourscent channel for FITC; any increase in FITC will lead to increased FL1 reading.

The flow cytometry data can also be displayed as FL1 vs. forward scatter, which gives indication of cell size changes and therefore the status of cell health. Based on the fluorescence level of control cells, a threshold level of fluorescence could be set. It can be seen in figure 4.12 that the FITC intensity is low in the negative control cells, with only 0.1% of them having intensity beyond threshold. The number of cells with higher FITC intensity increased in a NP concentration dependent manner for all 4 NP. However, it appeared that the cellular uptake of hydrophobic Aerosil 974 is higher than all 3 hydrophilic NP, as evidenced by the higher number of cells with increased FITC intensity (96.6%) at the lowest concentration than the same concentration of other 3 hydrophilic NP (37.7-88%). The uptake of SiNP in A549 cells was concentration dependent. There appeared no apparent change in cell forward scatter, suggesting that the integrity of the cells were unchanged at this time point after treatment with all 4 SiNP at the concentration range applied.

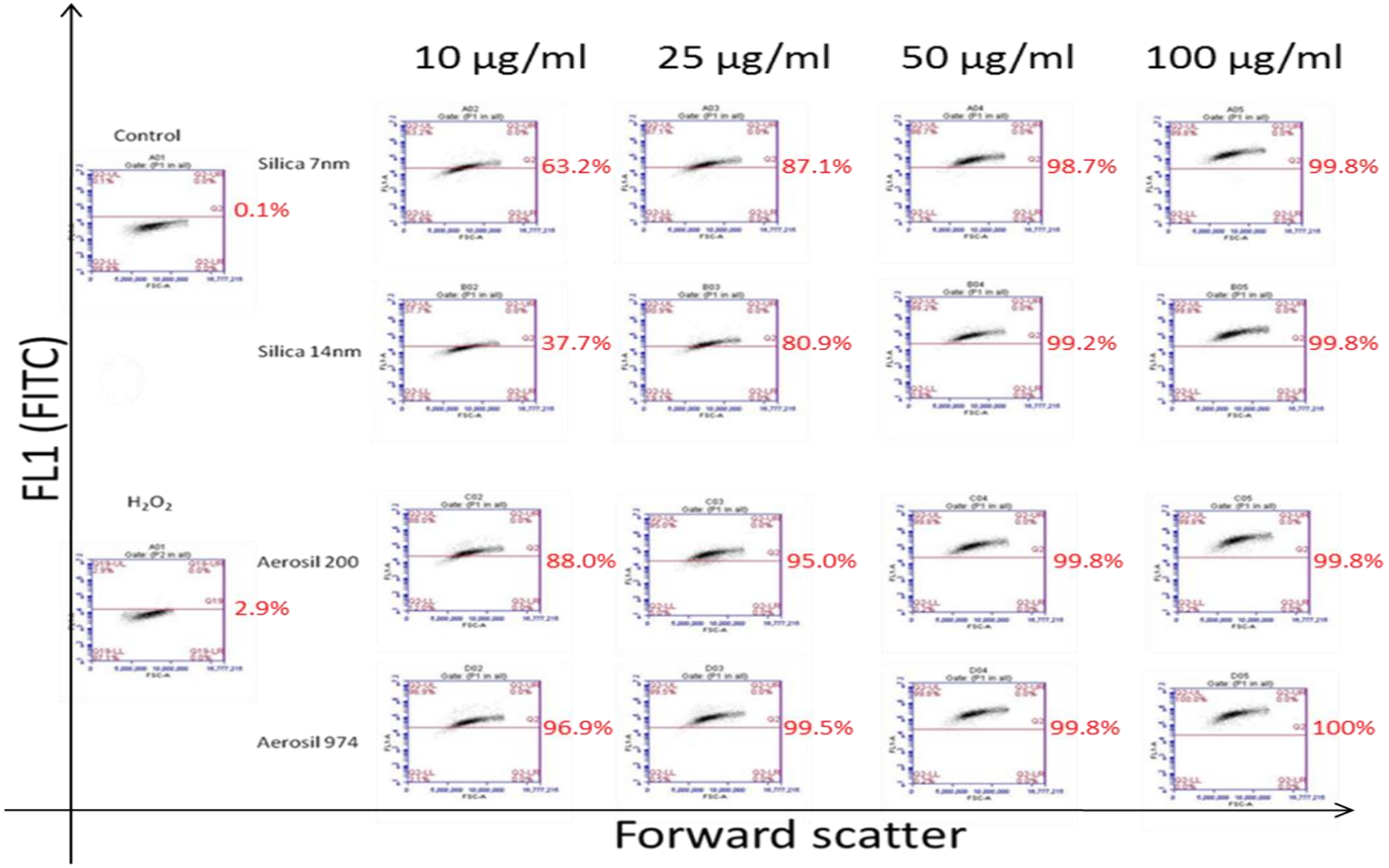

Figure 4.12 Pattern of A549 cells distribution as displayed as forward scatter vs. FL1 (FITC). Threshold was manually set based on the distribution of negative control cells. Cell uptake of NP was indicated by shift of cell distribution upwards beyond threshold.

A concentration dependent uptake of SiNP was also detected in HaCaT cells. However the uptake of all SiNP at low concentrations (10-50 µg/ml) was lower by HaCAT cells than the uptake by A549 cells at the same concentrations (compared figures 4.10 and 4.11 with figure 4.12 and 4.13). There appeared no apparent change in forward scatter, suggesting that the HaCaT cells were relatively healthy at this time point after treatment with these SiNP at the concentration range applied.

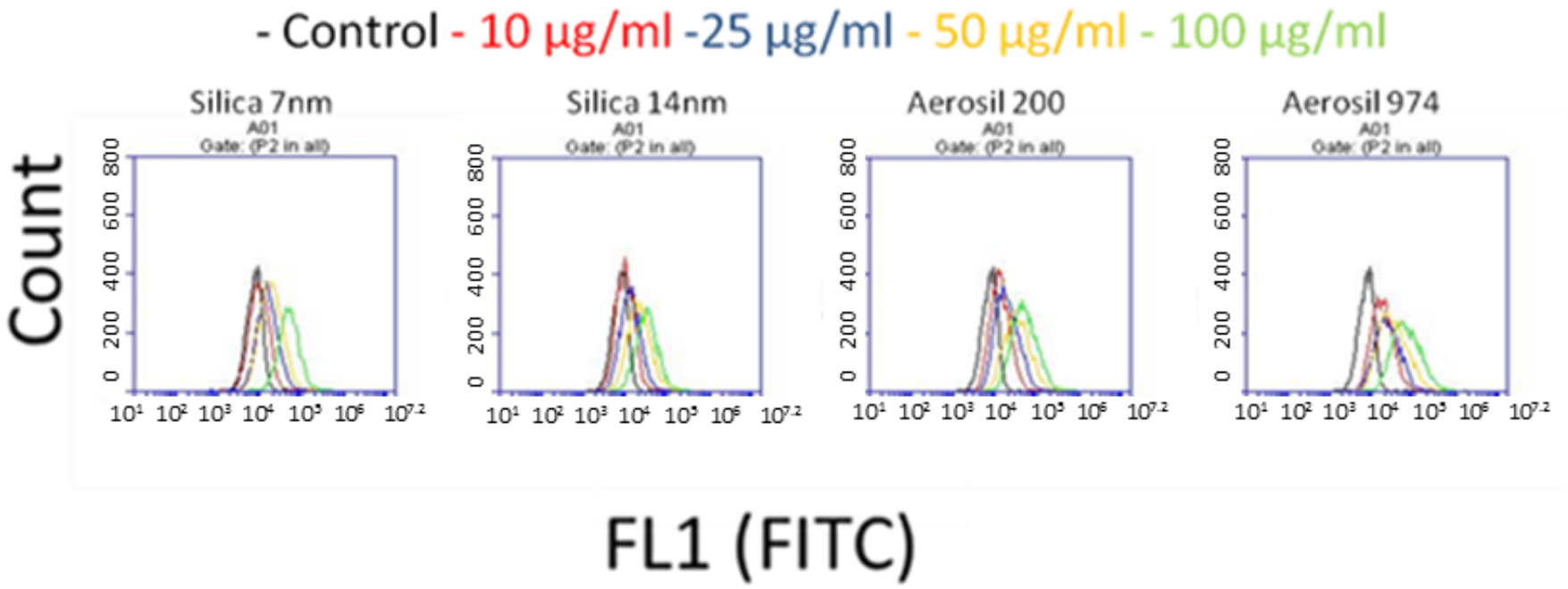

Figure 4.13 Flow cytometry NP uptake analysis in HaCaT cells. Results were displayed as cell count vs fluorescence intensity. FL1 represents the flourscent channel for FITC; any increase in FITC will lead to increased FL1 reading.

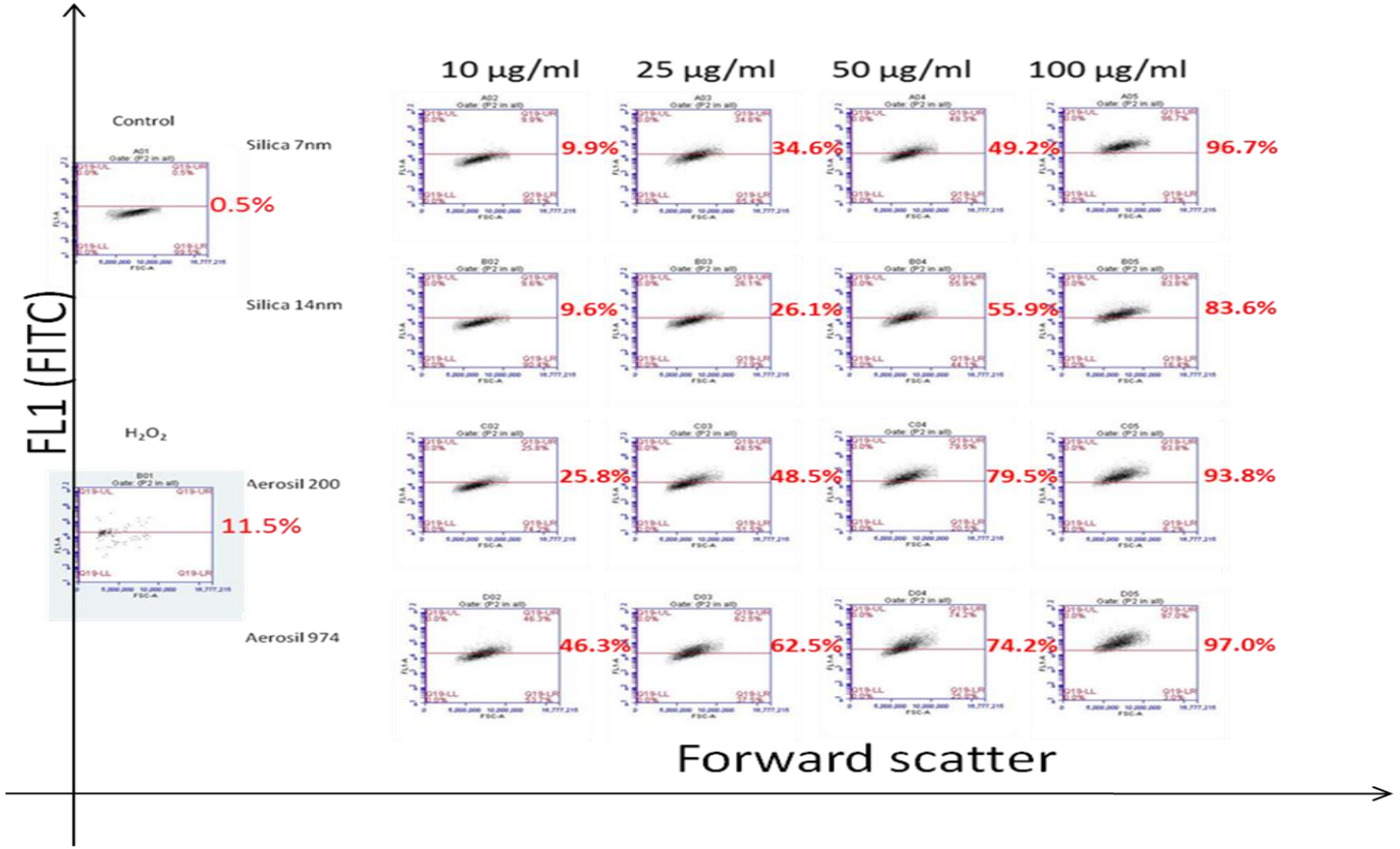

Figure 4.14 Pattern of HaCaT cells distribution as displayed by forward scatter vs. FL1 (FITC). Threshold was manually set based on the distribution of negative control cells. Cell uptake of NP was indicated by shift of cell distribution upwards beyond threshold.

As shown in figure 4.15 and 4.16, the uptake of SiNP also occurred in MRC-5 cells in a similar fashion to A549 and HaCaT cells. There was a distinct shift in accordance to the increasing concentrations. The cell counts remained high until the highest concentration. This may be that the some cells were lost during the sample preparation as the cell treated with NP at the highest concentration could be too fragile to withstand the process.

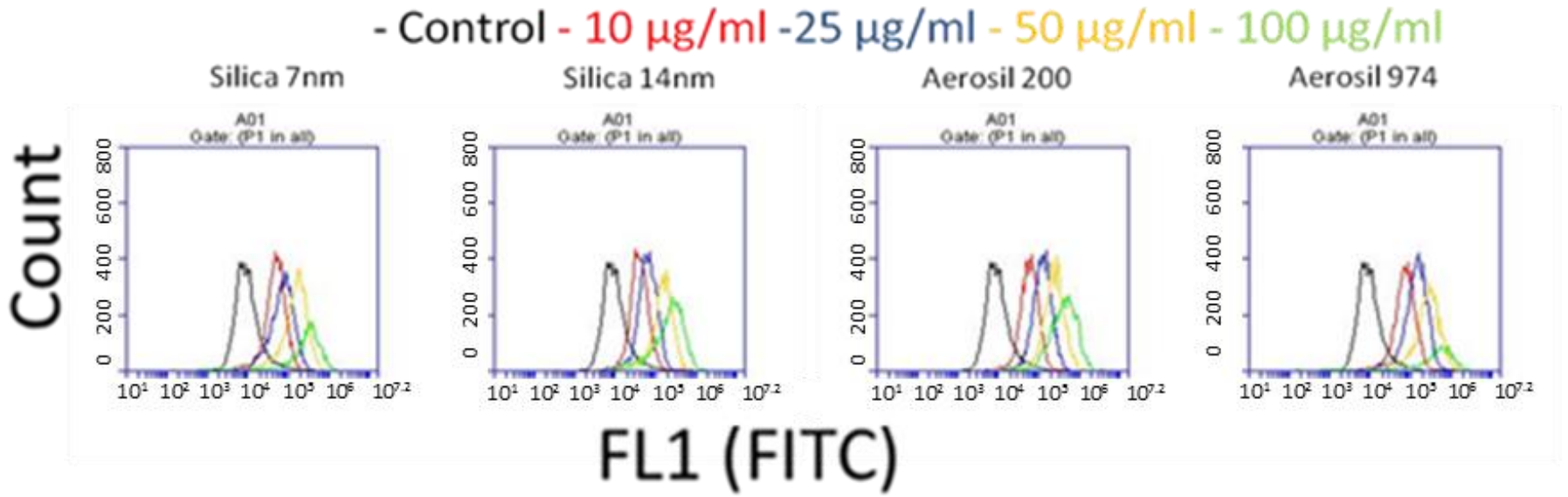

Figure 4.15 Flow cytometry NP uptake analysis in HaCaT cells. Results were display using cell count vs fluorescence intensity.FL1 represents the flourscent channel for FITC and any increase in FITC will lead to increased FL1 reading.

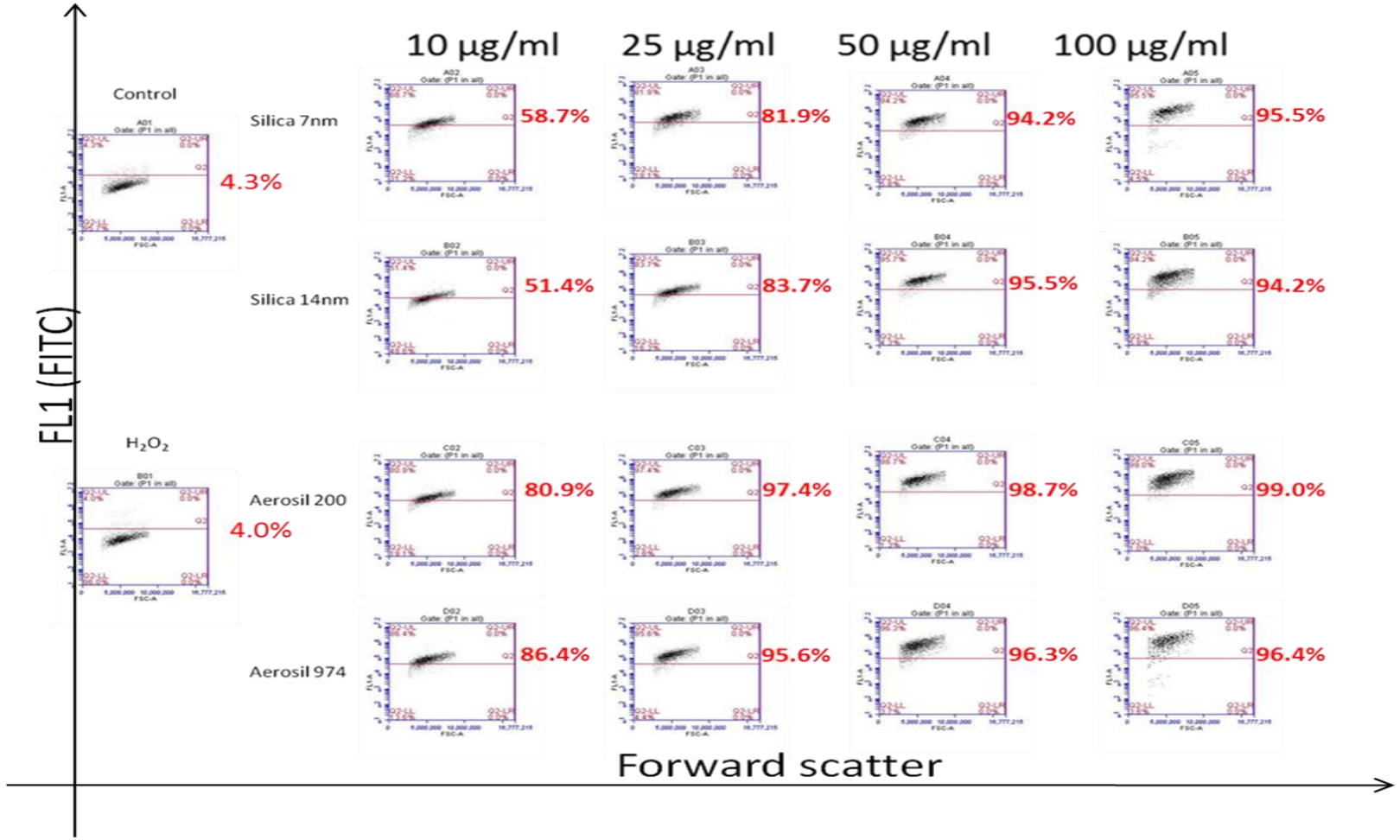

Figure 4.16 Pattern of MRC-5 cells distribution as displayed by forward scatter vs. FL1 (FITC). Threshold was manually set based on the distribution of negative control cells. Cell uptake of NP was indicated by shift of cell distribution upwards beyond threshold.

The detection of NP in samples treated with SiNP by flow cytometry suggests that cell uptake of SiNP occurred in a NP concentration dependent manner in all 3 cell lines. Further to this, the degree of NP uptake in the 3 cell lines was in the order of A549 cells> MRC-5 cells> HaCAT cells, which was particularly evident at the lowest concentration of SiNP. In addition, cell uptake of the hydrophobic SiNP was more than hydrophilic SiNP.

4.2.5 Confocal images of uptake

Confocal imaging studies were conducted in conjunction with the flow cytometry to back up the findings and to define the cellular location of the NP. It can be seen in figure 4.17, a single slice image taken by confocal microscopy, the uptake of SiNP occurred in A549 cells at 24 h of NP treatment at10 µg/ml. This was in agreement with the results from the flow cytometry assay.

As seen in figure 4.17, control A549 cells showed fluorescence staining of nucleus and very faint staining of lysosomes (A). In contrast, after treatment with SiNP for 24 h, the lysosome staining was enhanced (B-E). From these images it is apparent the presence of lysosomes is increased upon treatment with NPs, this suggests uptake may be utilising lysosome related uptake pathways. However, some NPs appear to be present within the cell without association with any lysosomal staining. The smaller aggregates of NP were generally associated with lysosome (stained with Lysotracker red). Whereas the larger NP aggregates were not associated with Lysotracker red staining. This pattern of staining may be an indication of different NP uptake mechanisms. The larger particles may not be suitable for uptake via lysosomes, but they could be taken up through a different pathway. Importantly, both set particles were seen near the nucleus but not inside the nucleus, suggesting that SiNP may not interact with genetic materials directly.

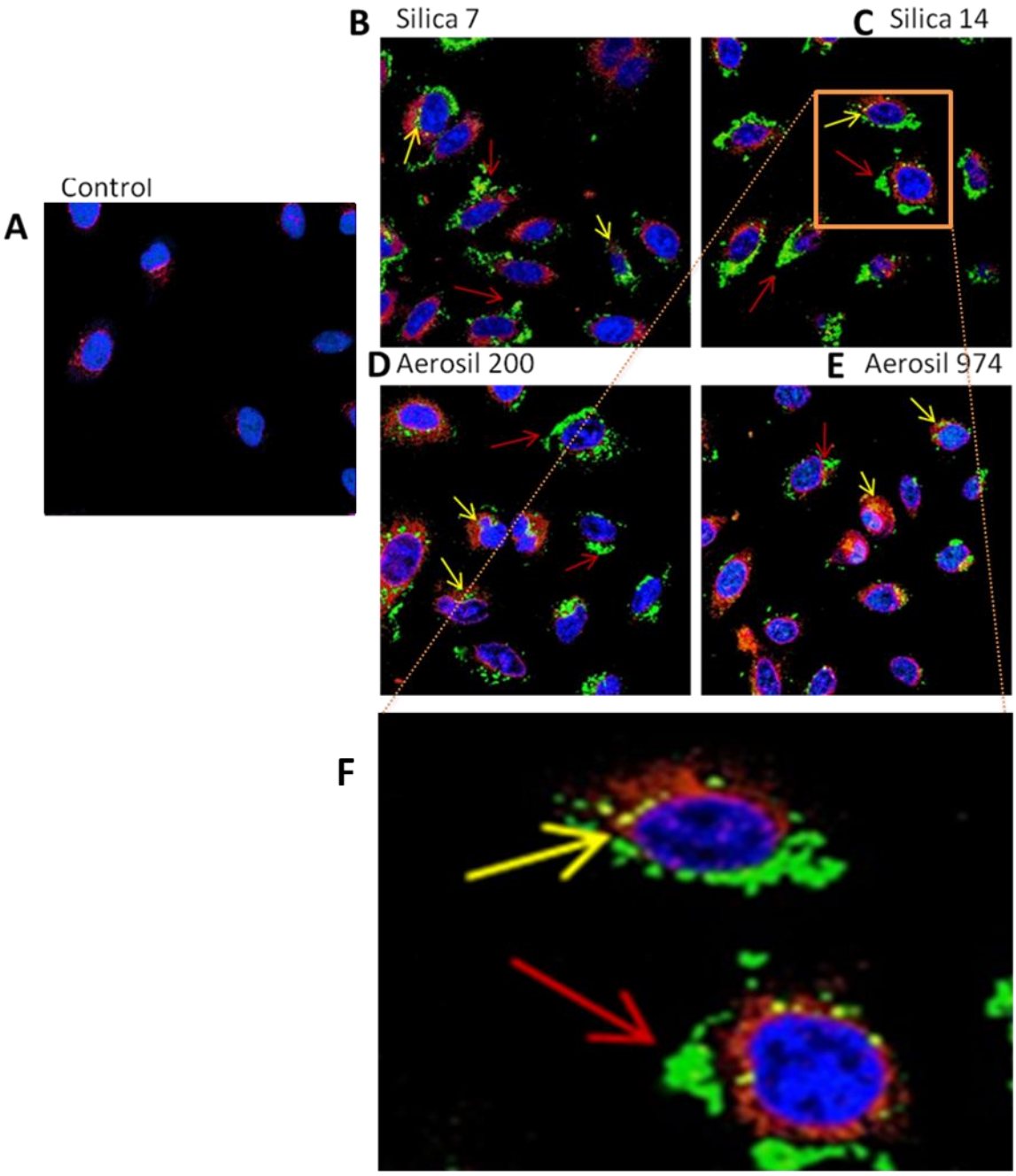

Figure 4.17 Confocal microscopy of SiNP uptake in A549 cells. Cells were labelled with DRAQ5 (1 µg/ml) and Lysotracker (75 nM). Cells were treated with FITC labelled SiNPs for 24 hours. A. control cells without treatment; B. cells treated with SiNP-FITC 7 at 10 µg/ml; C. cells treated with SiNP-FITC 14 at 10 µg/ml; D. cells treated with Aerosil-FITC 200 at 10 µg/ml; E. cells treated with Aerosil 974-FITC at 10 µg/ml; F. Inset magnified from SiNP-FITC 14 to illustrate the staining pattern of Lysotracker with smaller NPs (yellow arrows), whereas larger NPs are without Lysotracker staining (red arrows).

There seems to be a distinct difference in the uptake of hydrophobic Aerosil 974 as compared with other SiNP. For cells treated with Aerosil 974 (figure 4.17 E), an enhanced lysosome staining was evident. Also the colour appeared to be orange rather than red as seen in cells treated with other SiNP (figure 4.17 B-D), which could be the result of costaining of the lysosome with lysotracker (red) and SiNP-FITC (green). This pattern of staining suggests that more hydrophobic SiNP were uptaken into lysosome as compared with other SiNP.

4.2.6 ^{1}H-NMR assay of SiNPs effect on cellular metabolic pathways

In order to assess the effect of SiNP on cellular metabolism, ^{1}H-NMR metabonomic profiling of culture medium from cells with and without SiNP treatment was performed. For this study, A549 cells were treated with SiNP 7 nm for up to 24 h. Cell culture medium was collected for the ^{1}H-NMR assay at 6 h, 12 h and 24 h. Principal components analysis (PCA) revealed a clear distinction between the samples acquired at different time points after treatment (Figure 4.18A). Further PCA at each time point revealed a clear separation across PC2 of the higher concentrations 50 and 100 µg/ml from controls and samples treated with lower concentration of SiNP at 24 h of treatment (Figure 4.19B).

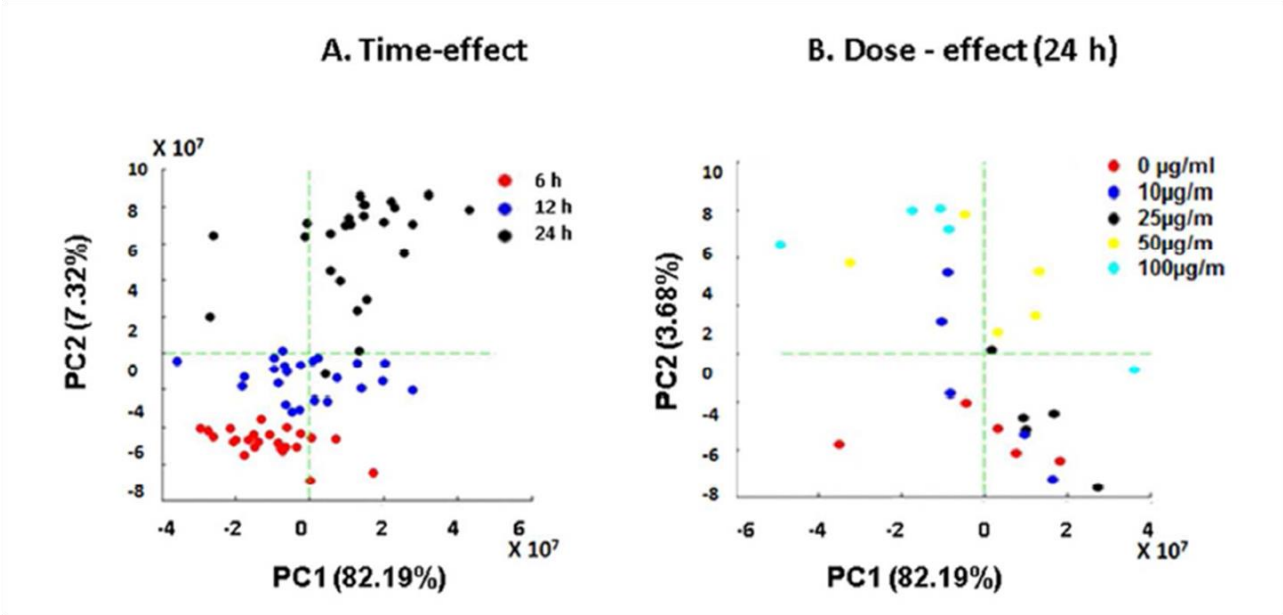

Figure 4.18 PCA plots of ^{1}H-NMR metabolites with respect to time and dosage of SiNP 7 treatment. A: a clear distinction can be seen between samples acquired at different time point of treatment. B: a clear discrimination was achieved between doses 50 and 100 µg/ml with untreated samples and samples treated with lower concentrations of SiNP 7 at 24 h.

Table 4.3 presents the PLS-DA (partial least squares discriminant analysis) of the treatments of SiNP 7. After individual scaling of the data by the most suitable methods LVs (latent variables) were derived. SiNP 7 of 50 µg/ml retained the highest overall score for specificity and sensitivity at all the time points assessed. SiNP 7 at 100 µg/ml scored

the same as SiNP 7 50 µg/ml at 12 and 24 h, whilst 10 and 25 µg/ml scored relatively low in comparison to 50 and 100 µg/ml at all the time points tested, suggesting that the effects of SiNP treatment is concentration dependent at all the time points tested.

Table 4.3 Summary of the 2-way classification using PLS-DA of the NMR profiles of all doses at different time points.

Time (h)	Dose (µg/ml)	Scale	LV	Overall %	Specificity %	Sensitivity %
4	10	RS1	2	66.7	80.0	50.0
4	25	RS1	6	80.0	80.0	80.0
4	**50**	**Norm**	**3**	**100.0**	**100.0**	**100.0**
4	100	PS	3	90.0	100.0	80.0
12	10	PS	2	80.0	80.0	80.0
12	25	AS	4	80.0	100.0	60.0
12	**50**	**RS1**	**3**	**100.0**	**100.0**	**100.0**
12	100	NS	2	100.0	100.0	100.0
24	10	NS	2	70.0	80.0	60.0
24	25	MC	4	80.0	80.0	80.0
24	**50**	**PS**	**2**	**100.0**	**100.0**	**100.0**
24	100	PS	2	100.0	100.0	100.0
ALL	10	PS	3	79.3	86.7	71.4
ALL	25	RS1	5	93.3	93.3	93.3
ALL	**50**	**Norm**	**6**	**100.0**	**100.0**	**100.0**
ALL	100	RS1	9	100.0	100.0	100.0

The latent variable (LV) numbers in Table 4.3 give indications of the dimensions of dose and effect relationship; the higher the number, the more complex the dose-effect relationship becomes. At 4 h the LVs ranged from 2 to 6 across all concentrations of SiNP, indicating distinctive cellular responses to different concentrations at this time point, which may reflect the initial polydispersion pattern of SiNP-associated effect. At 12 and 24 hours, however, the LVs range narrowed, from 2 to 4 across all concentrations of SiNP, indicating that the dose-effect relationship became less complex at these time points, which may suggest the reduction of polydispersity of SiNP at these time points. Interestingly, when all time points were taken into consideration together, the LVs increased in a SiNP concentration-dependent manner, indicating that the polydispersity of SiNP is concentration dependent.

In order to determine the metabolite identities, both the aliphatic and aromatic regions in the ^{1}H-NMR spectra were analysed. As shown in figure 4.19, a number of metabolites were affected by SiNP 7 treatment. The most affected metabolites include glucose, lactate and ethanol in the aliphatic region (fig 4.19), and histidine, phenylalanine, and tyrosine in the aromatic region (fig 4.20). The effects were most pronounced for the treatment of 50 µg/ml at 4 h and both 50 and100 µg/ml at 12 and 24 h. Some other metabolites also responded to the treatment but their identities have yet to be determined. For example, the peaks at 3 ppm of detected frequency could be acetate-methylene protons of EDTA. The singlet peak at around 3.4ppm could well be oxidised nicotinamide, derived from cellular excretion of nicotinamide N-oxide. The peaks just below 4ppm are likely to be amino acid or potentially sugar protons. According to the experimental metabonomic spectra data in the human metabolome database, the possibility of these peaks being folic acid, riboflavin, N-methylnicotinamide or niacin could be excluded (Human Metabolome Database Version 3.0 a-c).

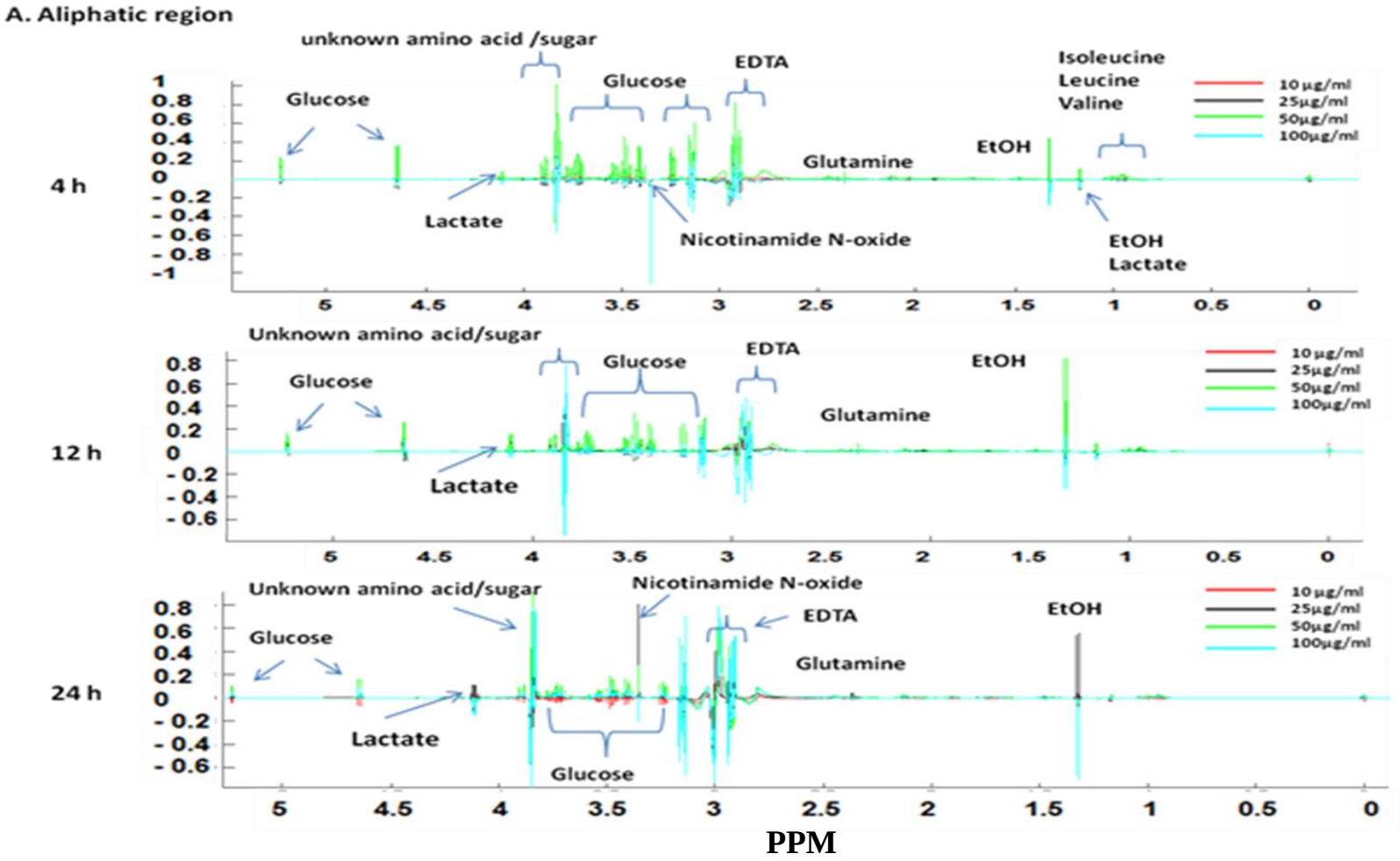

Figure 4.19 NMR profiles normalised against the TSP internal standard and subtracted from control. A: SiNP 7 induced changes of metabolites at the aliphatic region.

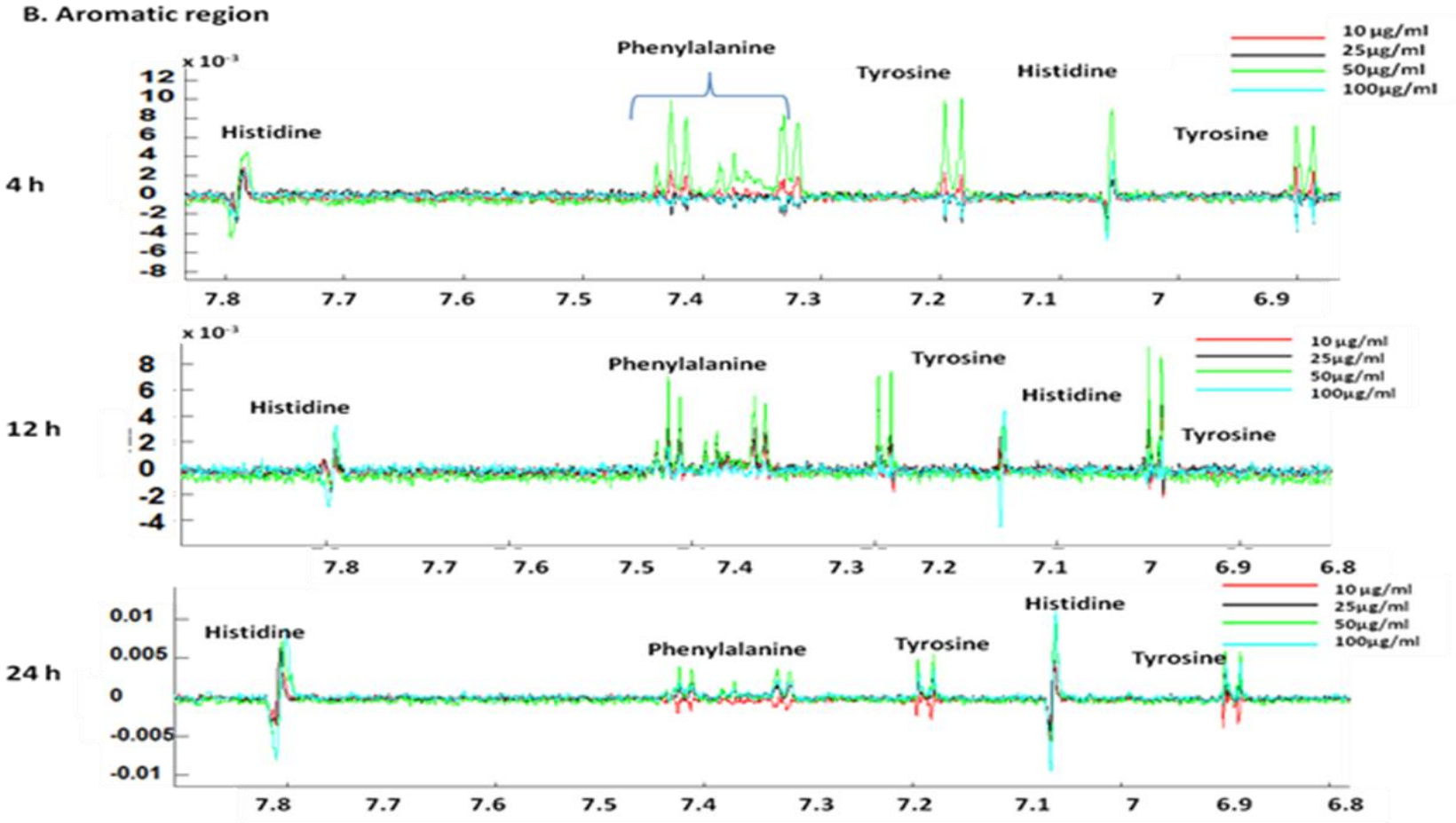

Figure 4.20 NMR profiles normalised against the TSP internal standard and subtracted from control. SiNP 7 induced changes of metabolites at the aromatic region.

The ^{1}H-NMR metabonomic assay revealed that in A549 cells, SiNP 7 induced pronounced effects on some metabolites at early time points when cell viability was not impaired. The effects induced by SiNP 7 at 50 and 100 µg/ml were detected at 4 h and 12 h. Importantly, some effects were also detected at 24 h in cells treated with the two lower concentrations of the SiNP.

4.2.7 miRNA targets for toxicity pathway detection

For miRNA assay, A549 cells were treated with SiNP 7 for 24 h. Before assessing the miRNA gene expression by RT-PCR it is important to assess the quality of the miRNA and the presence of any contaminations, which may alter or have major effects on any outcomes. For this Bio-rad Experion was used. As shown in figure 4.20, each sample produced a thick and a thin band with size of ~1600 and ~4000 respectively, the consistency of these bands suggest a high integrity of these miRNA samples. This was also reflected by high RQI scores (maximum possible 10). The results also suggest that no damage or degradation occurred to miRNA during the process of extraction, freeze storing (-80°C) and thawing.

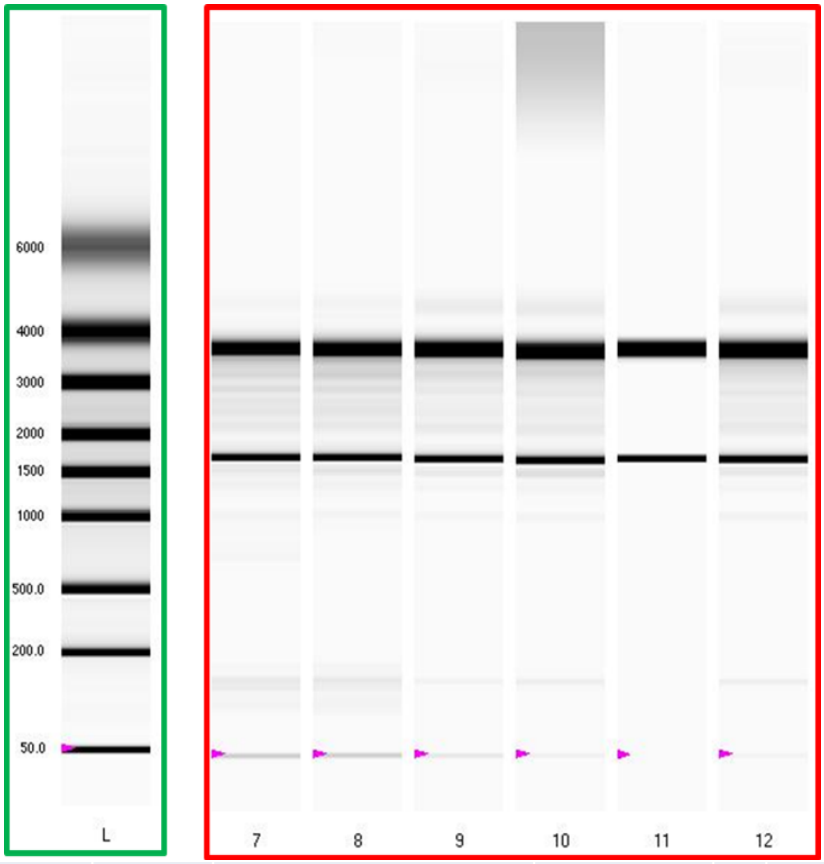

Well ID	Sample Name	RNA Area	RNA Concentration (ng/µl)	Ratio [28S:18S]	RQI	RQI Classification	Alert
7	Control_1	540.38	119.1	1.64	9.8	Green	-
8	Control_2	494.53	109	1.67	9.9	Green	-
9	Control_3	935.55	206.2	1.71	9.9	Green	-
10	Silica7_1	780.96	172.12	1.76	9.8	Green	-
11	Silica7_2	846.72	186.62	1.7	9.4	Green	-
12	Silica7_3	1,176.46	259.29	1.74	8.7	Green	-

Figure 4.21 miRNA integrity assay. The molecular standard (green) and miRNA from controls and cells treated with SiNP (red) were separated by electrophoresis in Bio-Rad Experion chambers the miRNAs with acceptable quality are classified as green.

The results obtained from the miRNA array assay could not be easily deciphered. Figure 4.22 is the volcano plot with data of pre normalisation. It was noted that the majority of miRNAs were significantly downregulated. After contacting the data analyst at Qaigen UK, it was advised that these results required to be normalised. Although the internal controls and the housekeeping genes had worked in a stable manner, it was suggested that normalisation should be based on better internal controls from each ring.

The ratio of the required PCR cycle for miRNA to be used as internal controls vs those in SiNP treated samples should be <1.5. The miRNA analysis software (Qaigen© web based analysis software) would select a miRNA set internal controls within each ring. If such a miRNA set was identified, they were then used to normalise the whole set mRNA within each miRNA array.

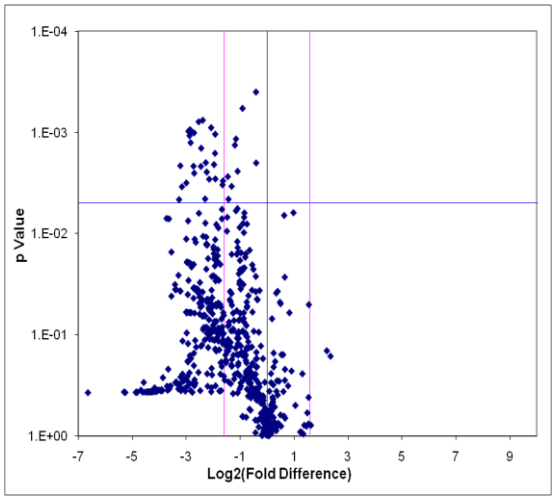

Figure 4.22 Total miRNA array volcano plot. A549 cells were treated for 24 hours with SiNP 7 at 10 µg/ml. The x-axis represents the fold difference in miRNA expression between control cells and those treated with SiNP 7. The red lines denote the significance level (*p<0.05*).

Among the 12 sets of miRNA arrays, only array 2, 4, and 8 could be successfully normalised. The remaining sets did not contain a miRNA(s) which met the requirement for being used for normalization. Upon explaining this circumstance to the experts at Qaigen they advised that this is an acceptable situation due to the magnitude of the experiment using unspecific targets. Therefore the results from only 3 rings were further analysed. A volcano plot was generated for each of the ring as displayed in figure 4.23. From these results 6 miRNA sequences (other than the house keeping genes as shown in figure 4.23 as HK) were highlighted as upregulated after 24 hour treatment with SiNP. The sequences of the 6 miRNA and the known information about these miRNA and their target genes were collected and researched using online database program, TarBase 6.0. These results are presented in table 4.4.

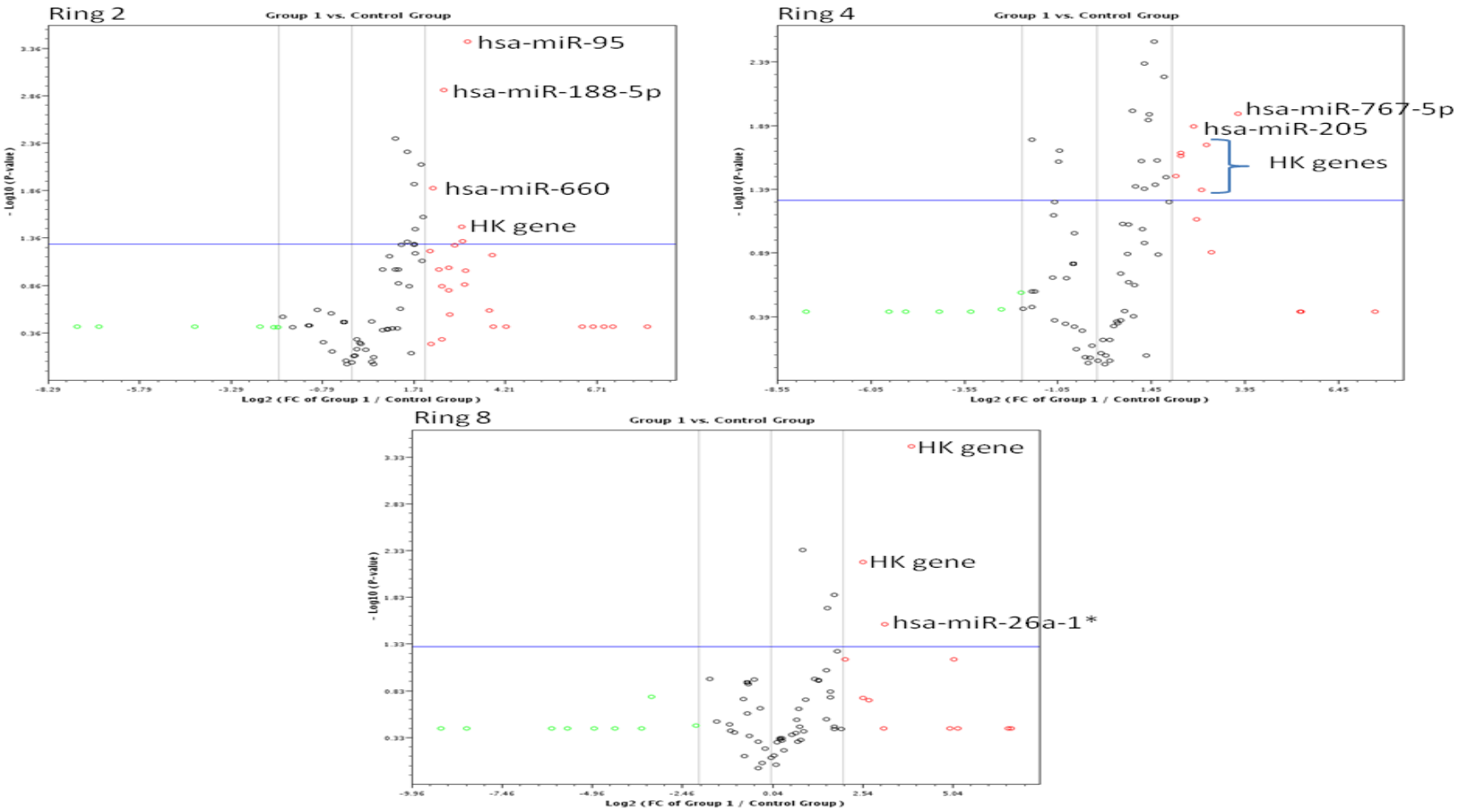

Figure 4.23 Volcano plots of miRNA data from succesfully normalised miRNA rings (Ring 2, 4 and 8). Red markers denote upregulated miRNA; green markers represent downregulated genes. The blue horizontal line is *p<0.05* marker above which miRNA expression was either signifiacntly up or downregulated.

The information presented in table 4.4 highlights the novel nature of miRNA regulation studies. Little is understood how miRNAs specifically effect gene expression and how they behave in cell signalling pathways. Although the work has been successfully conducted on a number of miRNAs, there is no enough evidence to link the highlighted miRNA from our study to a specific cellular effect. However several target genes of the SiNP responsive miRNAs appear to have roles in tumour suppression.

It is important to note that this study of miRNA response to SiNP was very preliminary. Only miRNA response at 24 h to a single low concentration (10 µg/ml) of SiNP was studied. However, it was evident that alteration of miRNA expression was a relatively early event. In order to understand whether/what miRNAs were involved in SiNP induced toxicity, further study will be needed to identify the time course and concentration-effect relationship of the miRNA response to SiNP.

The sequences identified have been associated with target genes related to cell proliferation and regulation of tumour suppressor genes. Hsa-miR-95 is responsible for silencing SNX1 to promote cell proliferation (Huang et al., 2011). Wu et al., (2009b) identified an association between hsa-miR-188-5p and SUMO-conjugate-enzyme-UBC9, it has been shown to be integral in the posttranslational modification of sumoylation (transfer of SUMO protein to other proteins). It is further linked to a number of cellular processes through the control of sumoylation (Jackson, 2001). From all of the identified sequences the most frequently studied is hsa-miR-205, from these studies a number of targets have been identified for it. The majority of targets are related to tumour suppression and cell proliferation (Gregory at al., 2008 ; Dar et al., 2011).

Table 4.4 Upregulated miRNA identities and known information are shown for fold change and p-value (Wu et al., 2009b; Wu et al., 2009a; Huang et al., 2011; Gregory et al., 2008; Dar et al., 2011).

miRNA identity	Sequence	Fold change	p-value	Target gene(s)	Action of sequence	Reference
hsa-miR-95	UUCAACGGGUAUUUAUUGAGCA	9.00	0.00037	SNX1 chromosome 15	Promotes cell proliferation by silencing SNX1	Huang 2011
hsa-miR-188-5p	CAUCCCUUGCAUGGUGGAGGG	5.82	0.00119	SUMO-conjugate enzyme UBC9 chromosome 16	Regulation of Ubc9	Wu 2009
hsa-miR-660	UACCCAUUGCAUAUCGGAGUUG	4.72	0.01295	No experimentally identified targets	unknown action	-
hsa-miR-767-5p	UGCACCAUGGUUGUCUGAGCAUG	13.64	0.01043	No experimentally identified targets	unknown action	-
hsa-miR-205	UCCUUCAUUCCACCGGAGUCUG	4.70	0.02109	- ERBB3 (Homo sapiens) chromosome 12 - E2F1 (Homo sapiens) chromosome 20 - E2F5 (Homo sapiens) chromosome 8 - LYN (Homo sapiens) chromosome 8 - SRC (Homo sapiens) chromosome 20 - ZEB1 (Homo sapiens) chromosome 10 - LRP1 (Homo sapiens) chromosome 12 - ZEB2 (Homo sapiens) chromosome 2 - SIGMAR1 (Homo sapiens) chromosome 9 - INPPL1 (Homo sapiens) chromosome 11 - IL24 (Homo sapiens) chromosome 1 - PRKCE (Homo sapiens) chromosome 2 - IL32 (Homo sapiens) chromosome 16 - DDX5 (Homo sapiens) chromosome 17 - SIP1 (Homo sapiens) chromosome 14 - ERBB3 (Homo sapiens) chromosome 12 - E2F1 (Homo sapiens) chromosome 20 - E2F5 (Homo sapiens) chromosome 8 - LYN (Homo sapiens) chromosome 8 - SRC (Homo sapiens) chromosome 20 - ZEB1 (Homo sapiens) chromosome 10 - LRP1 (Homo sapiens) chromosome 12 - ZEB2 (Homo sapiens) chromosome 2 - SIGMAR1 (Homo sapiens) chromosome 9 - INPPL1 (Homo sapiens) chromosome 11 - IL24 (Homo sapiens) chromosome 1 - PRKCE (Homo sapiens) chromosome 2 - IL32 (Homo sapiens) chromosome 16 - DDX5 (Homo sapiens) chromosome 17 - SIP1 (Homo sapiens) chromosome 14	It is associated with multiple targets regulation. ERBB3 identified as a tumour suppressor in breast cancer. ZEB1 and SIP1 function in transforming epithelial cells to mesenchymal cells. It has also been linked with suppression of melanoma cell proliferation and the induction of senesense via E2F1 regulation.	Gregory 2008, Wu 2009, Dar 2011
hsa-miR-26a-1*	CCUAUUCUUGGUUACUUGCACG	8.90	0.02874	No experimentally identified targets	unknown action	-

4.3 Discussion

SiNPs are representatives of nanoparticles that are manufactured in large quantity for different applications, therefore likely to interact with humans in many ways. Although it has been well documented that some smaller particles are more toxic than their larger counterparts, it is extremely challenging to study the toxicity potential of small MNP, such as SiNP <20 nm that have a very strong tendency to aggregate or agglomerate in the air, in biological media, and inside cells. This nature of behaviour could govern their toxicity potential.

The cytotoxicity of SiNP was studied in the *in vitro* models of A549, HaCaT and MRC-5 cell lines. In A549 cells, all the SiNP induced an increase in intracellular ROS and LDH release at 12 h, and a reduction of cell viability after 48 h of treatment at 10-100 µg/ml. These effects were also detected in both HaCaT and MRC-5 cell lines. SiNP also induced a dose-dependent IL8 production in A549 cells at 24 hours, although the effect was not tested in other 2 cell lines. The induction of ROS generation has been widely reported to be associated with cytotoxicity of different NP. Choi et al., (2009) reported a similar scenario, oxidative stress occurring at an earlier time point preceding to cell death in A549 and L-132 cells. Han et al., (2010) conducted *in vitro* tests with MWCNTs in A549 cells and suggested a link between the oxidative and inflammatory stress based on the increase production of IL-8.

Identification of early cellular and molecular changes using relevant *in vitro* models is an important approach for toxicity prediction, as early changes may lead to cell death if the cell cannot sufficiently deal with the stress. The production of ROS which leads to an increased production of IL-8 is itself a response to deal with the problem, this has been described as a co-mediated response both *iv vitro* and *in vivo* (Øvrevik et al., 2006; Donaldson et al., 2008; Donaldson et al., 2008; Samberg et al., 2010). The example of this mediation is presented by Han et al., (2010) who concluded that the production of ROS in A549 cells triggers the production of NF-κB, a protein complex which controls the transcription of DNA. NF- κB has been shown to be a precursor to the production of many pro-inflammatory factors. Although NP toxicity have been detected in many cell types, the associated mechanisms were not well

characterized. However it was suggested that NP can induce toxicity either internally and externally. Øvrevik et al., (2006) reported that NP uptake is not necessary for IL8 induction.

To understand the relationship of SiNP induced cytotoxicity with their internalization by cells, cell uptake of SiNP was studied by flow cytometry and confocal microscopy. From the flow cytometry experiments, it is clear that there is an association of SiNP with cells, although it was not conclusive whether the SiNP were taken up into the cells or associated with the cell membrane. When coupling these results with confocal images it was established that the SiNPs were taken up into the cell structure. Lysosomal dye and nuclear dye were used to assess whether the SiNP were taken up into lysosomes after endocytosis and or the SiNP were located inside nucleus. The results seemed to suggest the SiNP were uptaken by A549 cell via endocytosis and located mainly in the lysosome. As suggested by Unfried et al., (2007) there are many uptake mechanisms but a majority of mechanisms are dependent on NPs being encapsulated by lysosome and transported to final location within the cell.

From this work it is very interesting to note that the same cell and the same particles may induce various uptake mechanisms depending on aggregate size. However, this did not necessarily effect the final location of the SiNPs within the cell. All nanoparticles were located near the nuclear membrane, but did not breach it and enter the nucleus, indicating that SiNP do not interact directly with the nuclear DNA. Mu et al., (2012) suggested that 14 nm SiNPs enter cells through passive transport mechanisms at low concentrations (0.1 µg/ml) in both HaCaT and A549 cell lines, however there is no evidence of SiNP entry to nucleus, as observed under confocal microscope. Using TEM imaging technique, they suggested a similar subcellular location. However, they found DNA damage occurrence s without nuclear entry of NPs, this occurs through generation of oxidative stress by ROS leading to oxidation product 8-oxo-dG. They confirmed uptake by TEM imaging finding that NPs are located in similar areas as this study showed by confocal.

Metabonomics, combined with multivariate data analysis, is a powerful tool to study complex dose-effect relationships and biomarkers of toxic agents, and can also

generate models for toxicity prediction. ^{1}H-NMR-based assay on extracellular metabolites requires minimal sample preparation, thus minimizing artefacts and allowing better correlation with in vivo study (Dekker et al., 2012; MacIntyre et al., 2011). The ^{1}H-NMR metabonomic assay revealed that SiNP 7 induced pronounced effects on glucose, lactate, histidine, phenylalanine, and tyrosine at early time points when cell viability was not impaired. The effects were detected at 4 h of SiNP 7 treatment at 50 µg/ml and 12 h treatment at 50 and100 µg/ml. Importantly, some effects were also detected at later time points (24 h) in cells treated with the two lower concentrations (10 and 25 µg/ml).

Although the mechanisms for SiNP induced metabolite changes were not further investigated, the increase in some metabolites could in turn cause cytotoxicity or could serve as indications of cell damage. For instance, high concentration of glucose could result in oxidative stress and cell damage (Li et al., 2011a). As lactate is produced from glucose through glycoslysis in the cytosol then entering mitochondria to be oxidized via mL-LDH to pyruvate (Luo et al., 2012; Passarella et al., 2008), the increase of lactate could cause damage to mitochondria. It has also been reported that lactate can activate macrophages (Samuvel et al., 2009; Nareika et al., 2005). A recent study showed that in rat, zinc oxide NP induced an increase in lactate and glucose in urine, which is associated with kidney toxicity (Yan et al., 2012). It was shown that SiNP at doses 25 µg/ml and above induced both lactate increase and membrane damage in A549 cells. Taking all these together, lactate production could be a sensitive and global marker for cell damage and toxicity. In addition, SiNP 7 could also induce an increase of nicotinamide N-oxide, a potential biomarker of CYP2E1 activity that can be induced by ethanol and play a critical role in ethanol induced oxidative stress and toxicity (Cederbaum, 2009). The increase of nicotinamide-N-oxide coincided with the increase of ethanol suggests that CYP2E1 pathway could be involved in SiNP 7 induced toxicity. The increase in extracellular amino acids also suggests that SiNP may impair the mechanism of amino acids catabolism, preventing cells from utilizing phenylalanine, tyrosine and histidine. The dose range of SiNP causing metabonomic alteration is consistent with that causing cytotoxicity as assessed by multiparametric toxicity

assessment, suggesting that metabonomic modelling could be a useful tool for prediction of toxicity.

To further explore the mechanisms of SiNP cytotoxicity, the newly developed miRNA array technique was utilized. The dysregulation of any miRNA caused by SiNP could pinpoint to a specific pathway and may elucidate further intricacies of toxicity mechanisms for SiNPs. The miRNA data was difficult to analyse and interpret. Assistance was acquired from the Qaigen technical staff. It was advised that the web based software should be used for data analysis. This software allows automatic normalisation using the existing data. One or a set of miRNA that are well conserved between control and treatment (ratio <1.5 cycles) samples were chosen for data normalization.

After normalisation 6 miRNA was positively identified as being significantly up-regulated. Three of the 6 miRNA have unknown gene targets, highlighting the novelty the work. The miRNA arrays used include a total of 1008 miRNAs, covering all the miRNAs that have been identified so far, although majority of them have unknown mRNA targets. The 3 miRNAs upregulated by SiNP treatment may be critical in the translation of SiNP toxicity. It is noted from the identified targets of the sequences that they are heavily related to cancer regulation, by controlling the expression of a tumour suppressor gene. Until now most of the focus with miRNA is towards cancer diagnosis and treatment (Dar et al., 2011; Huang et al., 2011; Wu et al., 2009a; Wu et al., 2009b; Witten et al., 2010).

Little work has been done on the involvement of miRNA in toxicity regulation. However, from what is established, the translation of NP toxicity is most likely via oxidative and inflammatory stresses. Oxidative stress triggers signalling pathways leading to NF-κB activation, which leads to transcription of inflammatory cytokines and chemokines (Tripathi and Aggarwal, 2006). The miRNAs that have been identified in this study are not directly known to interact with this pathway. However, a study conducted by Ma et al., (2011) observed that a large number of miRNA interact with NF-κB pathway, directly or indirectly. They propose that miRNAs may play a fundamental role in negative/positive feedback loops which control many functions

within the cell, including cellular pathways such as NF-κB. Detection of both ROS and pro-inflammatory cytokines may be an indication that all 3 miRNA in some way are involved. Further study into the specific role of theses 3 miRNA in SiNP toxicity could be useful for understanding the exact mechanism of NP toxicity and miRNA involvement.

The work conducted on SiNP has shown toxic effects to occur as early as 4 hours (LDH) and 12 hours (ROS). The ROS assay conducted at 12 hours detected elevated levels of ROS, this was indicative of oxidative stress. The theory that oxidative stress triggers signalling pathways to increase the transcription of cytokines is also supported by the increased production of IL-8 as detected by ELISA. It is plausible to assume the uptake of NP leads to ROS generation, which also indicates that toxicity of NP may be sequential, from uptake to ROS generation then initiation of pathways leading to NF-κB activation and finally transcription of pro-inflammatory cytokines.

CHAPTER FIVE

5 Assessment of physiochemical property and toxicity of NP released from nanocomposites

5.1 Introduction

During the life of polymer products there are many applications involving some level of physical processing, such as drilling, cutting and impact crushing. These processes could all lead to the release of NPs. Studies on airborne particles have produced strong evidence that some NPs can be more toxic than larger particles both *in vitro* and *in vivo* (Oberdörster et al., 2005; Donaldson et al., 2000; Sayes et al., 2007). Therefore it is important to consider the possible particle release while developing new polymer products including micron and nanocomposites.

The possible release and increased toxicity potential of NPs cause potential health hazards. To address the concerns about potential release of NPs from novel products and associated effect on human health, scenario specific approach through all life stages of a given product is necessary (Hischier, and Walser, 2012). A comprehensive LCA allows identification of any points in the life of the product that NPs or NMs may be released, and therefore if a risk is posed. This study investigated the possibility of NP release from polyamide (PA6)-, polypropylene (PP)- and polyurethane (PU) silicon composites during mechanical processing.

Polyamide (PA6) is an engineered polymer that exhibits excellent thermal and mechanical properties. These properties make PA6 attractive for use in many areas. For example, polyamide has been used to develop strong flexible materials such as Nylon and Kevlar. More recently, PA6 has been explored for developing high performance materials ranging from automotive industry (Teixeira, et al., 2013) to sportswear (De Schrijver et al., 2009). Polypropylene (PP) is a semi-crystalline thermoplastic resin with commercial importance as an engineering polymer. With extremely versatile properties, PP has long been used to develop plastics for applications from food container plastics to

plastic chairs. The high mechanical, thermal and chemical properties make PP desirable as a matrix for nanocomposite products with possible use in automotive industries (Zokaei, et al., 2012). Polyurethane (PU), the third polymer used in this study can be both thermosetting and thermoplastic. Like PA6 and PP, PU also has a wide range of advantageous properties and applications. PU is used extensively as car seat foams (Obi, et al., 2012).

These 3 polymers were used to synthesize polymer-silicon composites. Based on the potential applications of these materials, different mechanical processing techniques were applied. PA6- and PP-group materials were subjected to drilling while PU-group materials were processed under crushing. The mechanical tests were conducted through collaborator with Dr James Njuguna at the school of applied sciences (SAS) of Cranfield University. The characteristics of the dust NP released from the testing materials were characterized both in the collaborator's laboratory and at Cranfield Health laboratory. The toxicity potential of the released NPs was studied *in vitro* using the human lung A549 cells. To our knowledge, this is the first comparative study of both the possible release and associated toxicity potential of NP from PA6-, PP- and PU-based polymers and polymer-silicon composites.

5.2 Results

5.2.1 Size and characteristics of particles provided by colleagues

Some results and details regarding the dry size and shape of particles generated during mechanical testing were provided by our colleagues who collected the samples. SEM images presented in figure 5.1 shows that airborne NP generated from all the PA6 group materials apart from PA6-MMT formed aggregates with sizes much larger than 100 nm. The aggregation of the particles made the determination of individual particle size and shape difficult. Nevertheless, it was evident that both the reinforcement NM (nanosilica and MMT) and the microsized fillers (GF and FGC) used in the polymer-silicon composites were not released freely. It is observed from the SEM images that

they were released as hybrid with matrix materials. NP released from PP-based and PU-based composites were not examined by SEM due to the low amount of airborne NP collected.

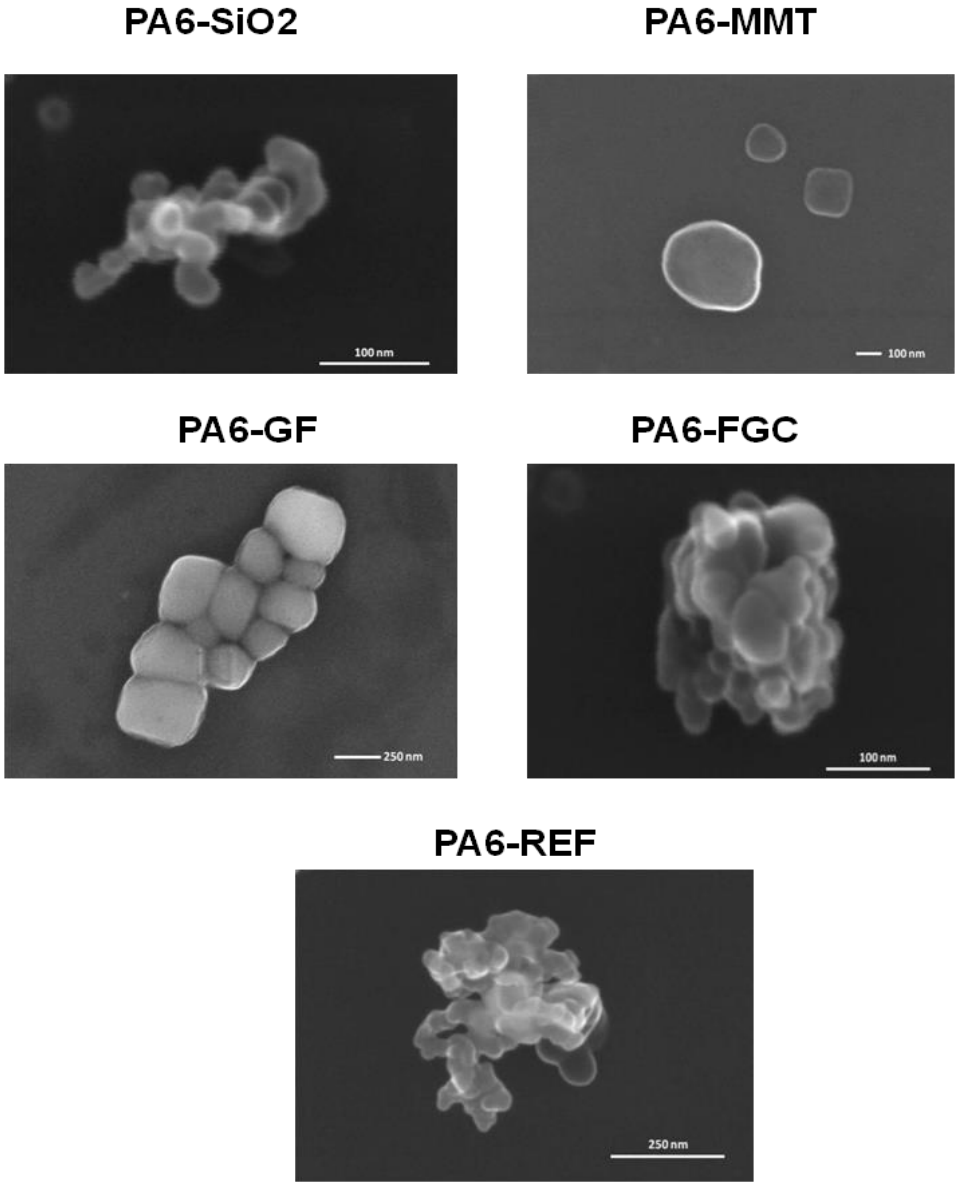

Figure 5.1 SEM images of NPs produced due to mechanical processing of polymer-silicon composites. Scale bars shown on images.

As shown in figure 5.2, during drilling more than 10 times more airborne NPs were generated from PA6 group materials than from PP group materials. The increase of air NP in the first 14 minutes and subsequent decrease in the second 14 minutes were detected while drilling all of the PA6 group materials apart from PA6-MMT composite. PA6-MMT had already been shown to generate larger particles from SEM images (figure 5.1). However, an increase of air NP of PA6-MMT was detected after 14 minutes of drilling (figure 5.2A).

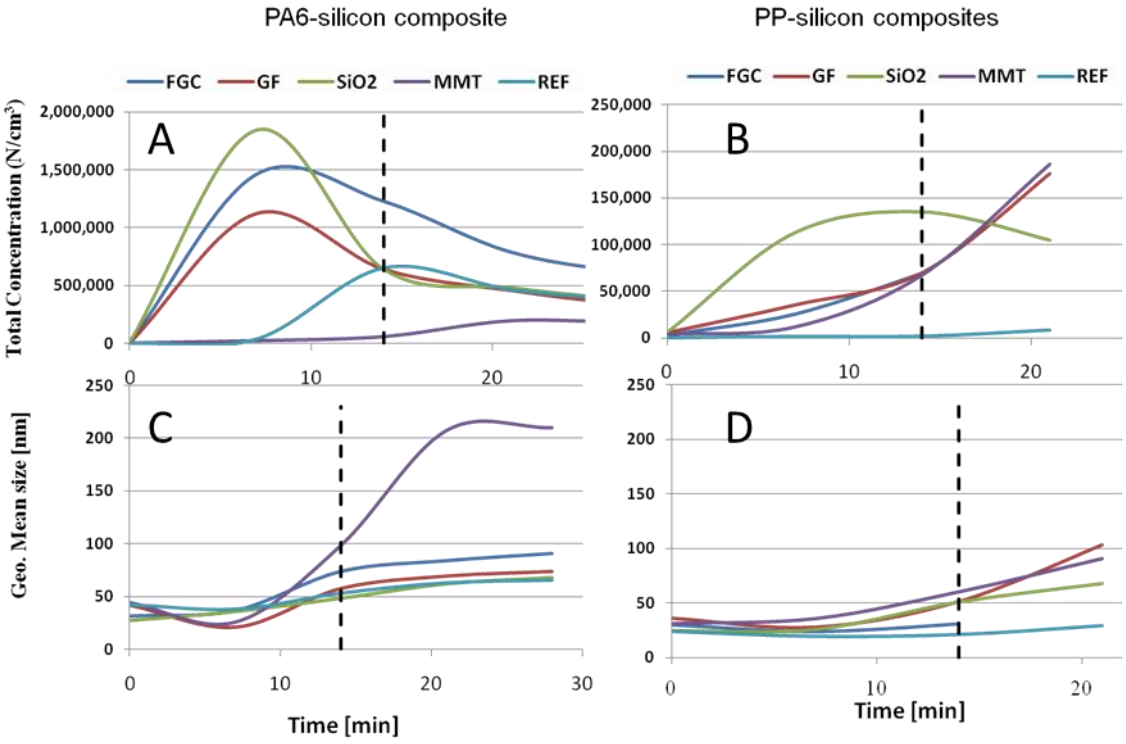

Figure 5.2 SPMS-C recording of NP release during drilling of PA6- and PP-composites. A) Total concentration of PA6 release measured over 28 minutes. B) Total concentration of PP released over 28 minutes. C) Geometric mean size of released PA6 particles detected over 28 minutes. D) Geometric mean size of PP particles detected over 28 minutes. The number of NPs released from PA6 group materials is 10-fold higher than PP group materials.

The level of airborne NP generated from PA6-based specimens in the first 14 min was in the order of PA6-SiO2>PA6-FGC>PA6-GF>PA6-REF>PA6-MMT. Interestingly, the low level of NP released from the PA6-MMT composite was coincided with larger NP size (~100 nm in the first 14 min and ~200 nm in the second 14 min, figure 5.2C) in comparison with the NP released from other PA6 group materials (<50 nm). In contrast, the airborne NP generated from all the PP group materials apart from PP-SiO_2 composite continuously increased over both 14 minute measurement cycles (figure 5.2B). The size of the airborne NP also increased with time (figure 5.2D). In both groups the neat polymers (reference specimens) released relatively low level of airborne NP whilst polymer-SiO_2 composites released the highest level of airborne NP. Thus it is seen that PA6 released higher concentration of NPs than PU, and with time the size of NPs increased while concentration of airborne NPs decreased.

5.2.2 Hydrodynamic size distribution of dust nanoparticles in water and in culture medium

As the nanodusts have been characterized for shape, morphology, and chemical composition at SAS, the only characterization carried out at Cranfield Health laboratory was their dispersity in water and in cell culture medium. As a reference the DLS profile of blank culture medium (figure 5.3A) was analysed. This profile showed 2 peaks with intensity in the regions of ~10 nm and ~100 nm, respectively. This indicates the presence of nanosized objects and their agglomerates as showed previously (van Gal et al., 2010). As the raw silica nanoparticles (SiNP 7) was used as a positive control in toxicity study of dust NP, the DLS profile of SiNP 7 in water and in culture medium at at100 µg/ml were also analyzed (figure 5.3B and C). in water , SiNP 7 exhibited one peak which was measured at 100-300 nm by the DLS assay. In culture medium SiNP 7 exhibited 3 major peaks (figure 5.3B), of which two have size greater than the given size 7 nm, suggesting the formation of agglomerates between silica NPs or between

silica NP and components of culture medium. When dispersed in water (figure 5.3C), SiNP 7 exhibited one peak which was measured at 100-300 nm by the DLS assay.

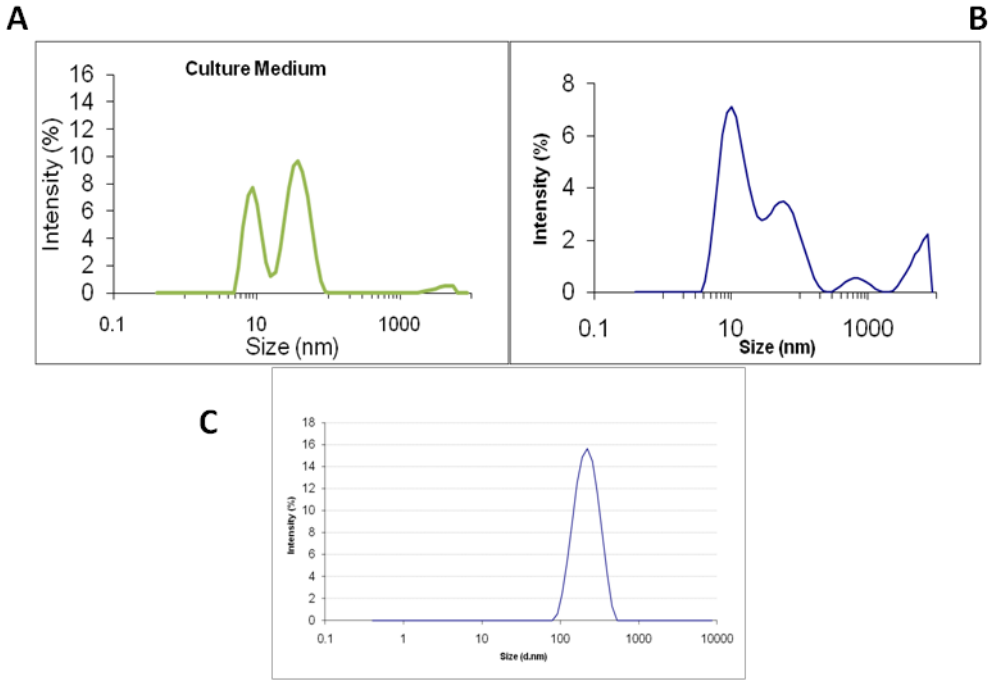

Figure 5.3 DLS spectrum of culture medium (A), Silica 7nm DLS spectra in culture medium at 100 µg/ml (B) and SiNP 7 dispersed in water at 100 µg/ml (C). Culture media has 2 distinctive peaks present ~10-25 nm. Silica 7 nm dispersed in culture medium is polydisperse, and in water is monodisperse.

Figure 5.4 shows the DLS spectra of the dust NPs suspended in water and in culture medium at 100 µg/ml. The DLS profile of the PU group dust samples in water suggests the presence of large monodispersed aggregates ranging from 150-500 nm (figure 5.4A). The PU-GF sample contained the smallest particles and the PU-FGC and PU-SiO2 sample contained the largest particle aggregates. When dispersed in culture medium the nanodusts become polydispersed (figure 5.4B). The average size of the dust particles was between 25-35 nm, with the PU-GF sample containing the largest dust particles and PU-SiO_2 sample containing the smallest dust particles. However the particle size differences between different samples were not statistically different (figure 5.4C).

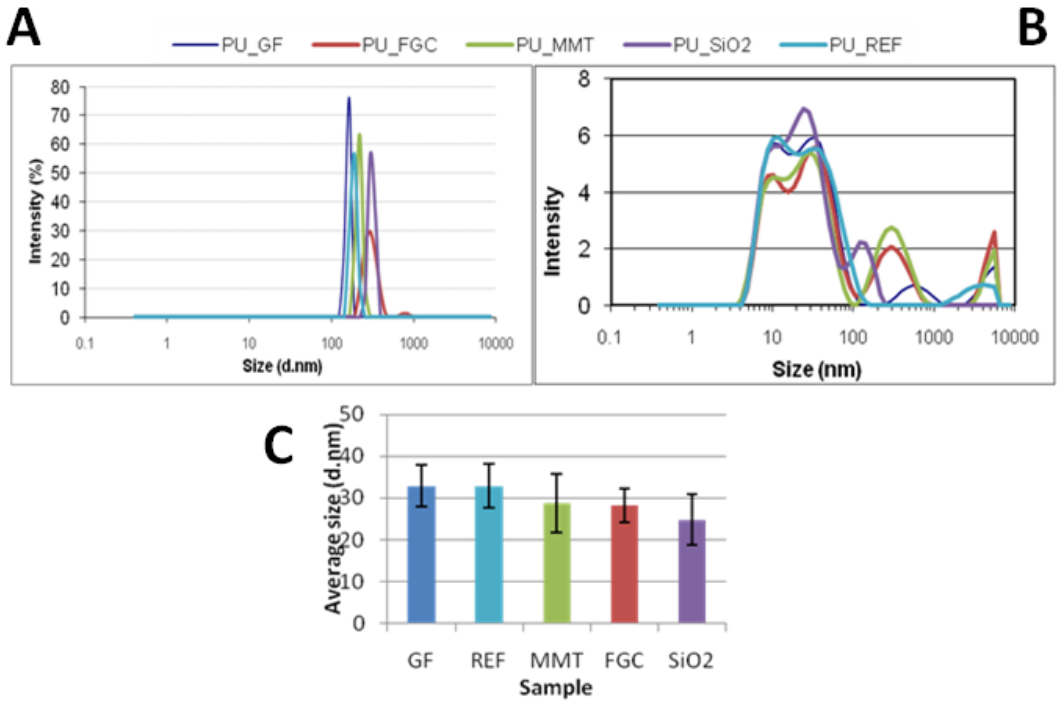

Figure 5.4 DLS profiles of PU group dust nanoparticles in; A) Water, suspended at 100 µg/ml; B) Culture medium at 100 µg/ml; C) Presents the average size of dust nanoparticles in culture media. Peaks in water are largely representative of monodisperse pattern, culture media leads to a much more polydisperse suspension, however, the average size of particles is smaller than in water.

The DLS spectra of PA6 group dust samples in water (figure 5.5A) suggest that they are similar in dispersion to PU group dust samples, both having large monodispersed aggregates present (>200 nm). The PA6-SiO_2 dust sample contained the smallest particle aggregates, whilst the PA6-REF dust sample contained the largest particle aggregates. When dispersed in culture medium the nanodusts became polydispersed and generally smaller in size (figure 5.5B). The average sizes of the dust particles in culture medium were between 35-60 nm, with the PA6-GF sample containing the largest particles and the PA6-REF sample containing the smallest particles (figure 5.5C).

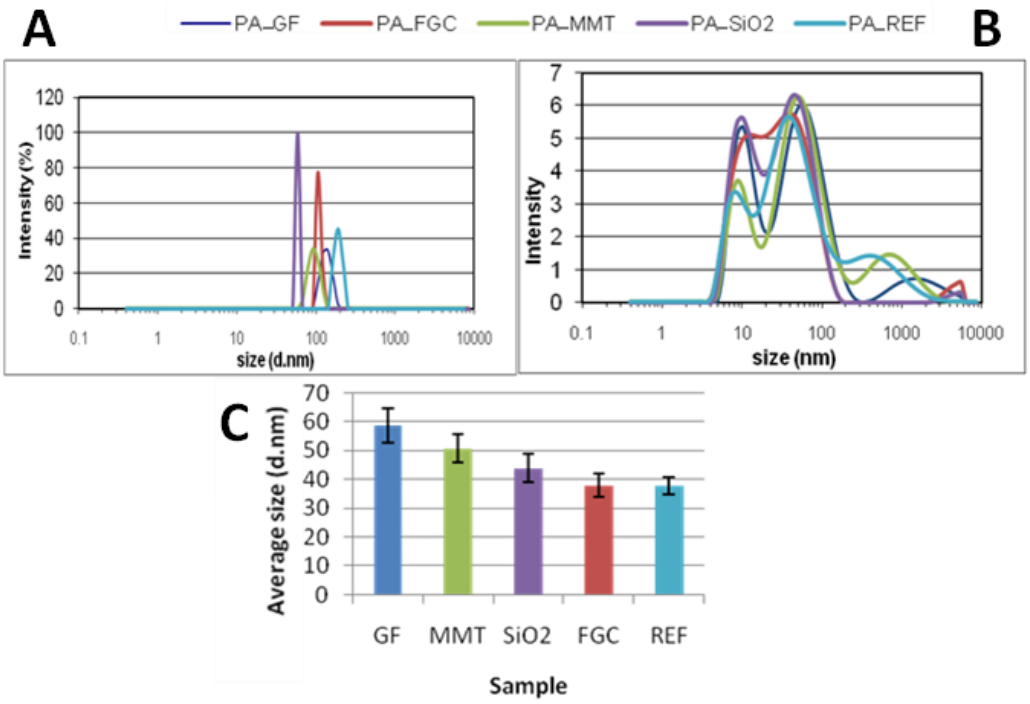

Figure 5.5 DLS profiles of PA group dust nanoparticles in; A) Water, suspended at 100 µg/ml; B) Culture medium at 100 µg/ml; C) Presents the average size of dust nanoparticles in culture media. Peaks in water are largely representative of monodisperse pattern, culture media leads to a much more polydisperse suspension, however, the average size of particles is smaller than in water.

DLS profiles of the PP dust samples suggest that like PA6 and PU dust samples, they were monodispersed in water and polydispersed in culture medium. The size distribution of particle aggregates was ~150 nm (figure 5.6A) in water, with the largest particles detected in the PP-FGC and PP-MMT samples. The size distribution of PP particles in culture medium was 35-50 nm (figure 5.6C).

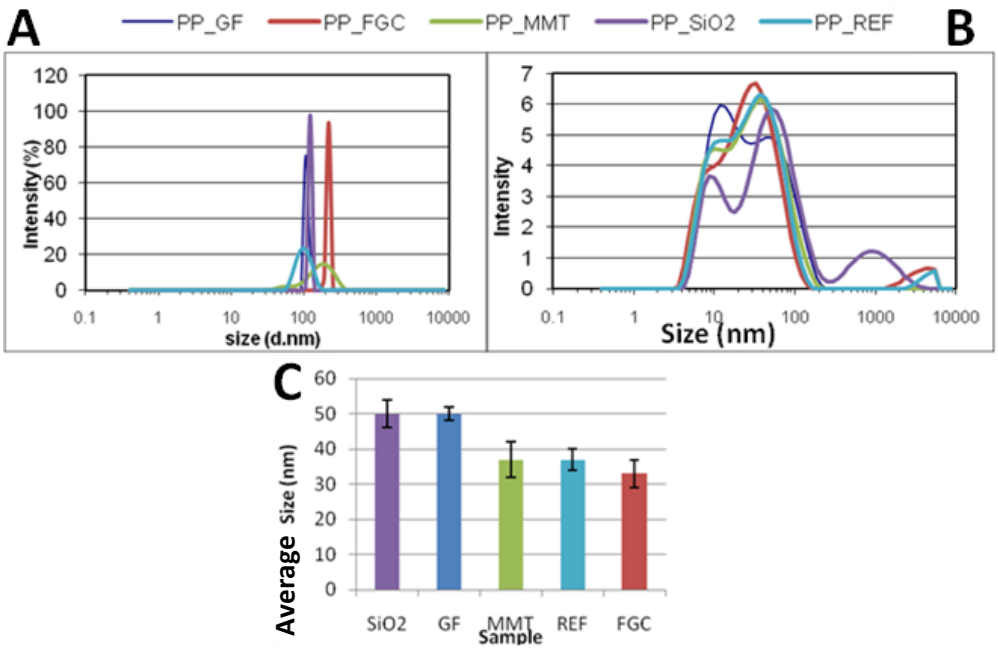

Figure 5.6 DLS profiles of PP group dust nanoparticles in; A) Water, suspended at 100 µg/ml; B) Culture medium at 100 µg/ml; C) Presents the average size of dust nanoparticles in culture media. Peaks in water are largely representative of monodisperse pattern, culture media leads to a much more polydisperse suspension, however, the average size of particles is smaller than in water.

Based on the results from DLS analysis and SEM results provided by Dr Sophia Sachse at SAS, it is clear that the dust NP from all samples exhibited a monodispersion pattern in water but polydispersion pattern in culture medium, and they formed different sized aggregates in different solutions.

5.2.3 Toxicity assay of dust NPs from different polymer-silicon composites in A549 cells

The effects of dust NP on cell viability was assessed by the MTT assay at treatment of 24, 48 and 72 h (Figure 5.7). Both SiNP 7 (10-100 µg/ml) and H_2O_2 (200 µM), included as positive controls, induced a time dependent reduction of cell viability.

All the PA6-based NP also induced a time dependent reduction of cell viability with the difference becoming significant only at 72 h ($p<0.05$), although no significant differences between NP from different polymer materials were detected. The effect appeared to be dose dependent as showed at the latest time point. In comparison, the PP-based and PU-based NP appeared to have no significant effect on cell viability (figure 5.7).

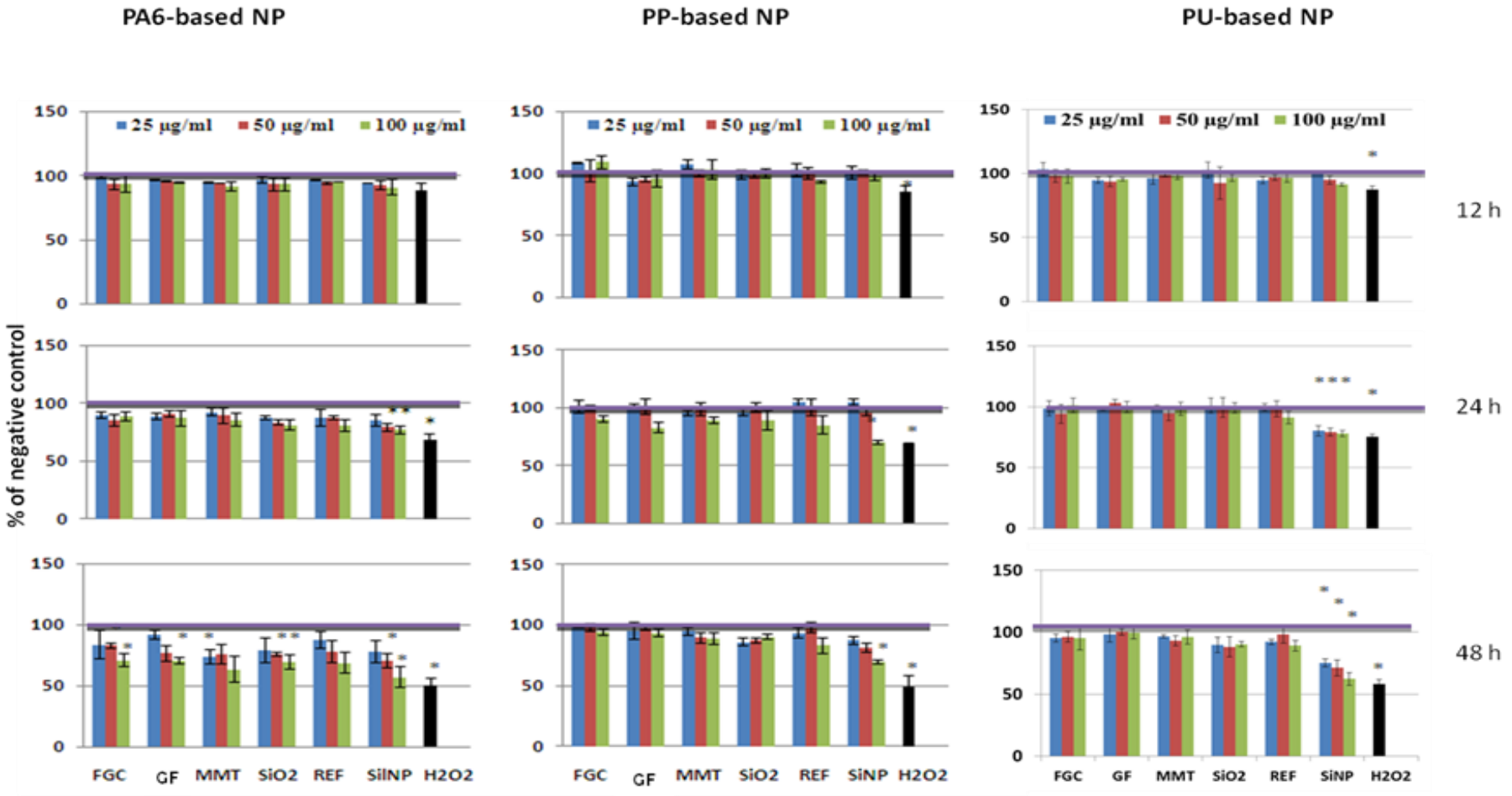

Figure 5.7 Effect of dust NP on cell viability in A549 cells detected by MTT assay. The viability of cells after treatment with dust NP were presented as % of negative control ± standard deviation (significance = p<0.05*).**

The effect of dust NP on intracellular level of ROS was assessed at 12 h, 24 h, 48 h and 72 h of treatment alongside positive controls. As shown in figure 5.8, the positive control H_2O_2 (200 µM) and SiNP 7 induced a consistent ROS increase before the time point of 48 h. The low level of intracellular ROS in the positive control samples at 72 h of treatment was due to the significant loss of cell viability. The NP derived from the PA6 reference material appeared to have an early time effect (figure 5.8), whilst all the rest showed no significant effect on the level of intracellular ROS.

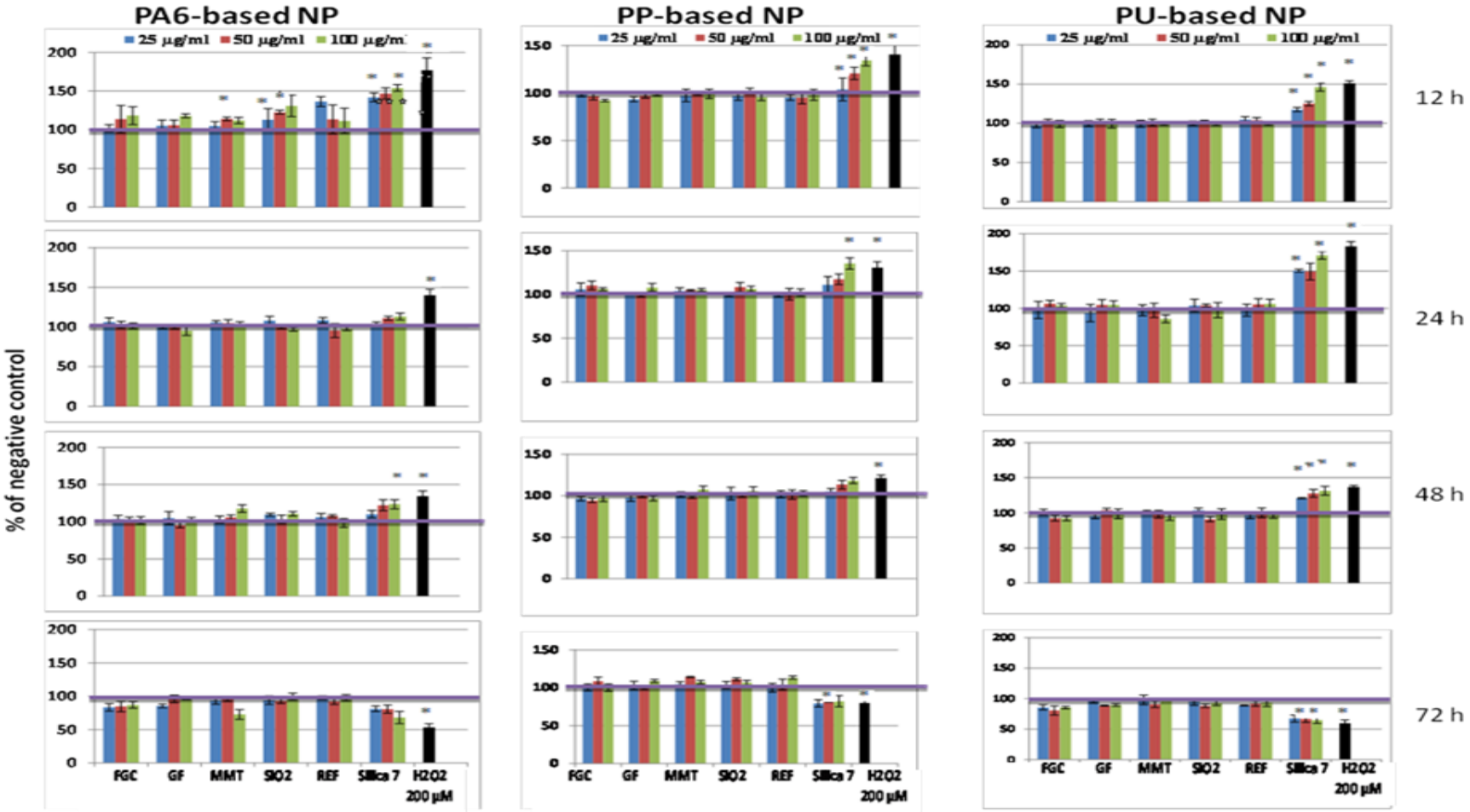

Figure 5.8 Effect of dust NP on intracellular ROS generation. The levels of intra cellular ROS after NP treatment were presented as % of negative control ± standard deviation (significance = $p<0.05$*).**

LDH release was assessed on both PA6 and PP based NPs. The PU based NPs were not tested. There was no detection of increased LDH in the culture medium after dust NP treatment (figure 5.9), suggesting that no membrane damage occurred. A time dependent induction in LDH release was detected in samples treated with SiNP 7 and H_2O_2 at 24, 48 and 72 h (figure 5.9).

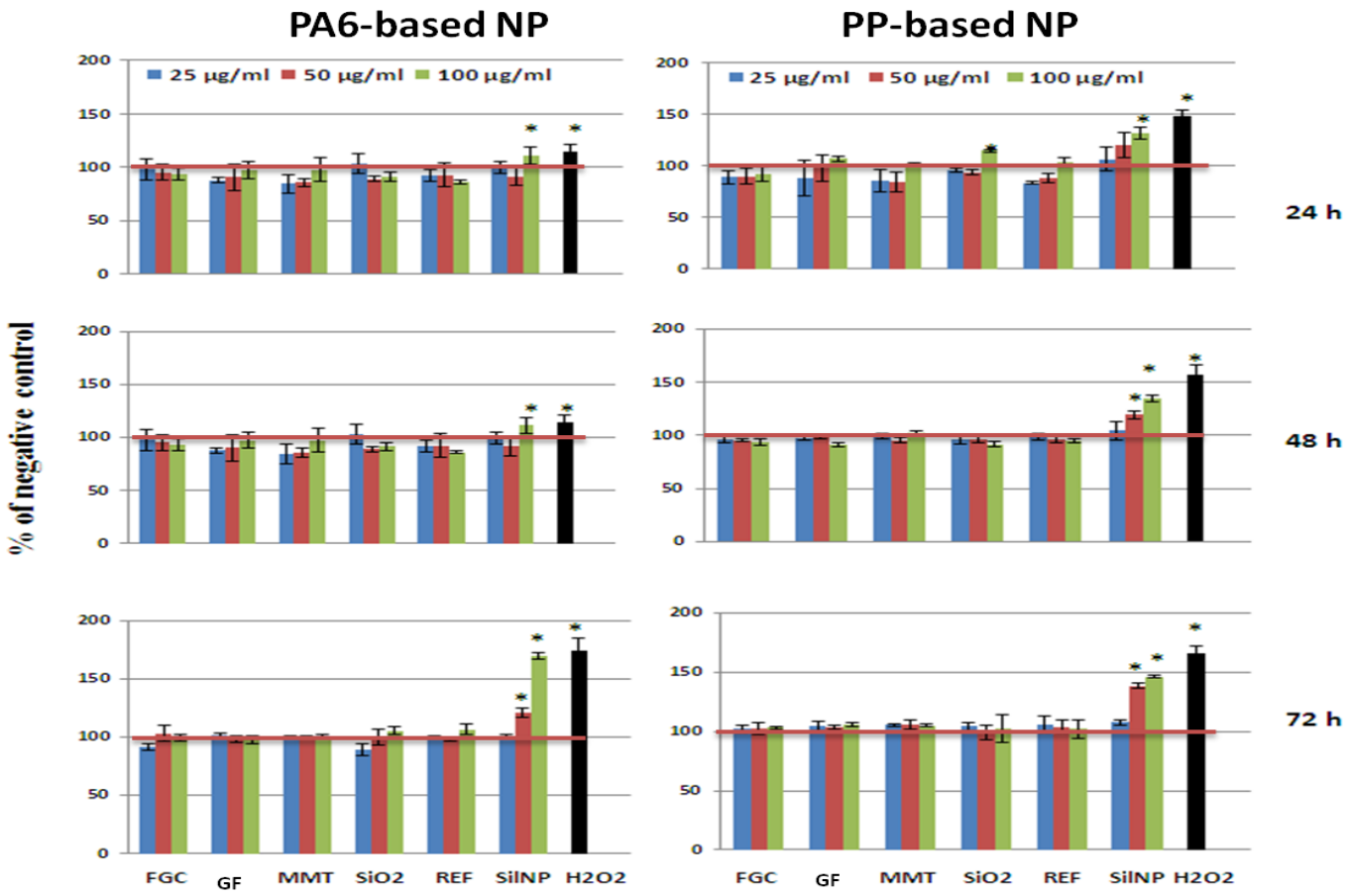

Figure 5.9 Effect of dust NP on cell membrane detected by LDH assay of cell culture medium. The LDH activity in A549 cells treated with different dust NP were presented as % of negative control ± standard deviation (significance = $p<0.05$*).**

5.3 Discussion

Data from the SEM study on airborne particles by our colleagues, Sachse et al., (2011) in SAS suggests that the NP released from PA6 materials were in clusters with size larger than 100 nm. However in the DLS assay, NP with the hydrodynamic sizes < 100 nm were detected, as indicated by the increase of intensity of NP in the size range of 10-100 nm in culture medium when the dust NP were added. These data suggest that some components in the culture medium prevented the formation of NP aggregates as suggested previously, indicating that NPs were present in the testing system.

Different tests were performed to determine the toxicity potential of the NP released from the PA6, PP and PU polymer composites with different silicon fillers. It was observed that all PA6-based NP reduced cell viability in a time dependent manner as measured by the MTT assay by 72 hours of exposure. The effect was only significant at 72 h and appeared to be concentration dependent. The reduction in cell viability was not associated with the cell membrane damage or with intracellular ROS increase. The data suggests that the loss of cell viability was not due to oxidative stress and cell membrane damage but could be the impairment of cell metabolism, which however could not be further investigated due to shortage of dust samples.

Due to the gravity, NP aggregates would gradually settle down on top of cells, which could affect cellular metabolism and growth as suggested previously (Allouni et al., 2009). The DLS data suggest that increased number of larger aggregates formed in dust NP samples from PA6 materials than that from the PP and PU materials in culture medium, which could be attributable to the higher toxicity caused by the PA6-based NP as compared with the PP and PU-based NP. There may be a secondary explanation to the toxicity of PA6-based NPs, which is based on the toxicity of caprolactam monomers. It has been shown that the monomeric form of polyacrylamide (PA6), caprolactam, is a toxic substance. Therefore, a production method using monomeric acrylic substances to produce PA6 may not be 100% efficient and leave traces of the monomer, which in turn could lead to toxicity (Autian, 1975).

The lack of variation in the toxicity potential amongst the dust NPs from PA6, PP and PU polymers with different filler materials could be due to the minimal difference in their hydrodynamic size distribution in the culture medium. Another aspect to consider is the very similar chemical composition within a given polymer materials group. As the low amount (5 wt %) of filler agent has little effect on the surface chemistry of the released NPs. According to the SEM images the fillers were not released freely but as hybrids within the polymeric matrices, therefore the filler materials will have little effect on dust NP toxicity property.

CHAPTER SIX

6 General Discussion

6.1 SiNPs toxicity *in vitro*

6.1.1 Influence of NP size, shape and chemistry in toxicity

The SiNP tested in this project are very similar in size range (7-14 nm), which does not allow the results to be interpreted in direct relation to size specific effect of the primary particle sizes. However the concentration dependent increase in their hydrodynamic size in culture medium could give some justification for any effects to be related to size. The DLS, SEM and TEM data all suggest that SiNP form aggregates when suspended in water and in culture medium. However TEM imaging study revealed that the NPs are clustered with adjacent NPs, which may not make their surface area inaccessible for reactions. In essence it creates a larger structure while maintaining a massive surface area to volume ratio. Based on the work with mesoporous SiNPs, Napierska et al., (2009) suggested that the surface area is the defining characteristic upon toxicity. Therefore, a larger aggregate may cause higher induction of ROS generation and thus causing greater toxicity.

As the surface chemistry of NP is an important determinant of NP toxicity, study of the difference of SiNPs chemical property in water and in culture medium would provide some insights into their reactivity with biomolecules and cells in the testing systems. As assessed by FTIR assay, suspension of SiNP in culture medium caused slight changes in the IR spectrum of SiNP, suggesting the adsorption of protein on the surface of NP and change in protein conformation. The changes were more pronounced in hydrophilic SiNP than in hydrophobic SiNP.

SiNP induced a concentration dependent cytotoxicity as detected by the MTT assay at 48 h and 72 h after SiNP treatment in A549 cells, HaCaT cells and MRC-5 cells. These results are consistent with the studies of Hussain et al., (2005) and Yu et al., (2009) who also found NP induced concentration-dependent toxicity. However Yu et

al., (2009) reported a significant toxicity in mouse keratinocytes after just 24 hours treatment with SiNP of 30 nm and 48 nm at 100 µg/ml. This difference may be attributable to a cell type specific response. Although SiNP induced an increase in LDH leakage as early as 4 hours, this does not seem to correspond to any concentration-dependant response. A concentration-dependent effect on LDH leakage was detected only after 12 hours of SiNP treatment. The induction of intracellular ROS generation by SiNP was detected after 12 h treatment with SiNP. Taking all of the multi parametric endpoint cytotoxicity/stress test results into account it appeared that the intracellular ROS and cell membrane damage are the mechanisms of SiNP cytotoxicity. The membrane damage may lead to increased internalization of NP as seen in confocal images and detected by flow cytometry. However the lysosomal cellular location also suggests the cellular transport of SiNP via endocytosis. The exact mechanisms of SiNP internalization need to be further investigated.

Interestingly there was no significant variation of cellular response to the hydrophilic SiNPs. As compared to the hydrophobic Aerosil 974, the cellular response differs as indicated by the MTT and ROS assays. Due to the poor solubility in culture medium, the actual particle number of Aerosil 974 despersed in suspension was much less than the same concentration of hydrophilic SiNP, which could explain the low level of cytotoxicity elicited by Aerosil 974. However the level of cellular internalization was higher for Aerosil 974 than for hydrophilic SiNP, as indicated by the flow cytometry and confocal microscopy assays. Collectively, these results suggest that the hydrophobic Aerosil 974 is less toxic than the 3 hydrophilic SiNP. Fubini et al., (1999) and Cedervall, (2007b) suggested that hydrophobicity is a major influence on the translation of toxicity from physical properties, which appeared to be in a disagreement with the results from this current study. The different results between these studies may be due to other variations such NP chemistry, size and cell types.

There appeared no significant variations between cell types in responses to SiNPs, as assessed by multiple end point toxicity assays, suggesting that a common toxicity mechanism(s) is shared among these cell lines.

6.1.2 Novel approaches to toxicity assessment

A concentration-effect relationship of SiNP toxicity was detected and modelled by the ^{1}H-NMRassay of extracellular metabolites combined with multivariation analysis of the attained data. A clear concentration-dependent relationship was detected in samples treated with SiNP 7 , suggesting that the concentration may be as important as size of aggregates in the determination of toxicity. Until now very little research has been conducted on NP toxicity using the ^{1}H-NMR analysis of cellular metabolites. ^{1}H-NMR-based metabonomic assay allows high throughput and quantitative measure of samples for toxicology evaluation (Liu, et al., 2011). With these methods toxicity pathways and mechanisms can be mapped and compared with comprehensive information database. ^{1}H-NMR metabonomics proved to be an excellent non-invasion technique for toxicity study in *vitro* and there is no reason that it cannot be translated to work *in vivo*.

Further to ^{1}H-NMR-metabonomics assay, miRNA assay that is relatively new to the field of toxicology was also employed to study the mechanisms of NP toxicity. Total miRNA analysis of SiNP effect provided some interesting insight into the cellular response to SiNP treatment at miRNA level. The identification of miRNAs that are upregulated due to SiNP when considered with the multiple end point assays suggest that the identified miRNA may influence the activation of signalling pathways to combat oxidative stress and lead to the transcription of pro-inflammatory factors, in the case of A549 the transcription of cytokine, IL-8.

The use of the metabonomic and miRNA techniques allows for the study of early cellular and molecular events before any lethal effects were detected. Very few groups have focused on changes in miRNA expression as an indicator for toxicity. Koufaris and Gooderham, (2013), Yokoi and Nakajima, (2013) and Li et al., (2011b) are some of the first groups to take steps forward in this field. However, one of the restrictions of these studies is the identification of miRNA targets for toxicity interpretation. Thankfully the development of tools such as TarBase 6.0 (Vergoulis et al., 2012) allows researchers to upload findings and identify total miRNA sequence

targets. Using these tools researchers can identify the miRNA which are regulated by external stimuli and the molecular pathways these miRNA may be influencing.

The results obtained so far provide some new insights about toxicity assessment of NP with tendency to aggregate in the testing system. ^{1}H-NMR has proved to be a potentially invaluable tool in analysing early effects *in vitro*. Potentially the use of miRNA arrays can specify and reveal in depth information about molecular mechanism of toxicity. Schrattenholz et al., (2012) emphasised the importance of proteomics in *in vitro* toxicology particularly the value of techniques such as mass spectrometry. Some studies are being conducted in the field of toxicology using such technique (Pedersen et al., 2012). These forms of studies have the potential to identify long term health effects that may occur due to exposures to NPs.

6.2 Nanoparticles released from composite materials

6.2.1 PA6 group materials generate more airborne NP than PP group materials during drilling process

During the drilling test, PA6 group materials released more NP than the PP group materials. The difference in the release of NP could be due to their distinct physical properties. It is known that the melting points are ~165 °C and ~223 °C for PP and PA6 respectively (Sachse et al., 2011). The melting temperatures could affect how the materials behave when subjected to physical process which involves heat generation. Under the heat generated during high speed drilling, PA6 materials could be more brittle than PP materials, therefore more likely to generate NP. The concentration of NP in the air in the drilling chamber was first increased and then gradually returned to low level. The reduction of air NP while drilling was still ongoing (second 14 min) could be that when reached a certain concentration, these airborne NP formed aggregates with size beyond the recorder's cut-off size. Moreover, due to the gravity the aggregates could move out of the air and settle down in the dust. The formation of aggregates was confirmed by the NP size increase with time as

determined by the SMPS+C and also by the SEM measurements. Notably the polymer-SiO2 nanocomposites generated the most airborne NP among all others in both PA6 and PP group materials during the first 14 min of drilling. In contrast, among the PA6 materials PA6-MMT produced the lowest level of airborne NP, suggesting that the use of MMT as filler agent could reduce the brittleness of PA6 polymer products.

The observation that the PA6 materials released a higher level of NP than the PP materials is interesting as both are among the most applied polymeric materials. Although many previous studies have focused on the thermo-mechanical property of polymeric materials, few have paid attention to their ability to release NP. This study indicates that from the ability of NP generation point of view, PP group materials and PA6-MMT composite could be considered as environment and consumer friendly polymeric materials for applications involving drilling. For the rest of the PA6 materials, improvement in product design is desirable in order to prevent or reduce the possible release of NP from the final products that are deemed to undergo physical process. Wearing masks may reduce the exposure of workers to particles, however not all masks have been tested for penetration of nanoparticles of different varieties. This is the first report on the comparative study of two groups of polymeric materials for both the release and toxicity of nanoparticles.

This study only simulated one scenario that is likely to occur during the product life cycle. For overall safety assessment, more relevant scenarios throughout the whole life stages of a given novel material need to be simulated (Roubicek et al., 2008) to fulfil the development of safe products.

6.2.2 Dust NP from PA6 group materials showed higher cytotoxicity than that from PP and PU group materials

SEM images showed that airborne NPs released from PA6-, PP- and PU polymeric products were in clusters with size larger than 100 nm. However in the DLS assays of dust samples dispersed in culture medium, NP with the hydrodynamic sizes <

100 nm were detected. These data suggest that some components in the culture medium prevented the formation of NP aggregates as suggested previously, indicating that nanoparticles were bioavailable in the testing system.

Different tests were performed to determine the toxicity potential of the NP released from the PA6, PP and PU groups of materials. The entire PA6 group NP reduced cell viability in a time dependent manner as measured by the MTT assay. The effect only became significant at the latest time point (72 h). The reduction in cell viability was not associated with the cell membrane damage and intracellular ROS increase. The slow reduction in cell viability while retaining cell membrane integrity suggests that the cells could undergo slowing down in metabolism but not cell death. Due to the gravity, NP could gradually settle down on top of cells, which could affect cellular metabolism and growth as suggested by (Allouni et al., 2009; Wittmaack, 2011).

The lack of differences in the toxicity property among the NP from different polymer materials groups could be due to (1) the insignificant difference in their hydrodynamic size distribution in the culture medium; (2) NP have very similar chemical compositions; (3) the addition of a low amount (5 wt %) reinforcement materials had little effect on the surface chemistry of polymer NP as the reinforce materials were not released freely but as hybrid within the polymeric matrix.

6.2.3 Life cycle analysis

This study demonstrated the importance of life cycle analysis as opposed to single stage analysis of novel materials. The raw SiNPs exhibited cytotoxic potency, whereas the dust NPs generated from the mechanically tested polymer-silicon composites were generally low in toxicity potency, although PA6 induced a slight reduction in cell viability by 72 hours that could be related to the PA6 matrix itself as this was also seen by PA6-REF sample. As was argued by Kloepffer, (2008), the toxicity assessment of materials from the starting material (raw materials) to the final products is a requirement. LCA of toxicity highlights stages where concerns about the

safety of the products need to be addressed, and safe measure to be introduced in handling of the different forms of the material from production to application.

This study suggests that a raw NP which is toxic can be ‘neutralised’ and used safely by embedded in an organic polymer matrix at a low wt (NP) /wt (polymer) ratio. This idea of reduction of NP toxicity by the modification has been widely implemented in biomedical applications. such as drug delivery or molecular imaging (Jevprasesphant et al., 2003; Hoshino et al., 2004). However, it is possible that a modification may lead to a non-toxic material becoming toxic, or the modification agent itself may be toxic.

The results of this study support the resolutions of ISO 14040 (ISO, 2006), which set out a framework and provided guidelines of LCA, testing of the manufactured materials in a fashion which mimics the scenarios of real life exposures.

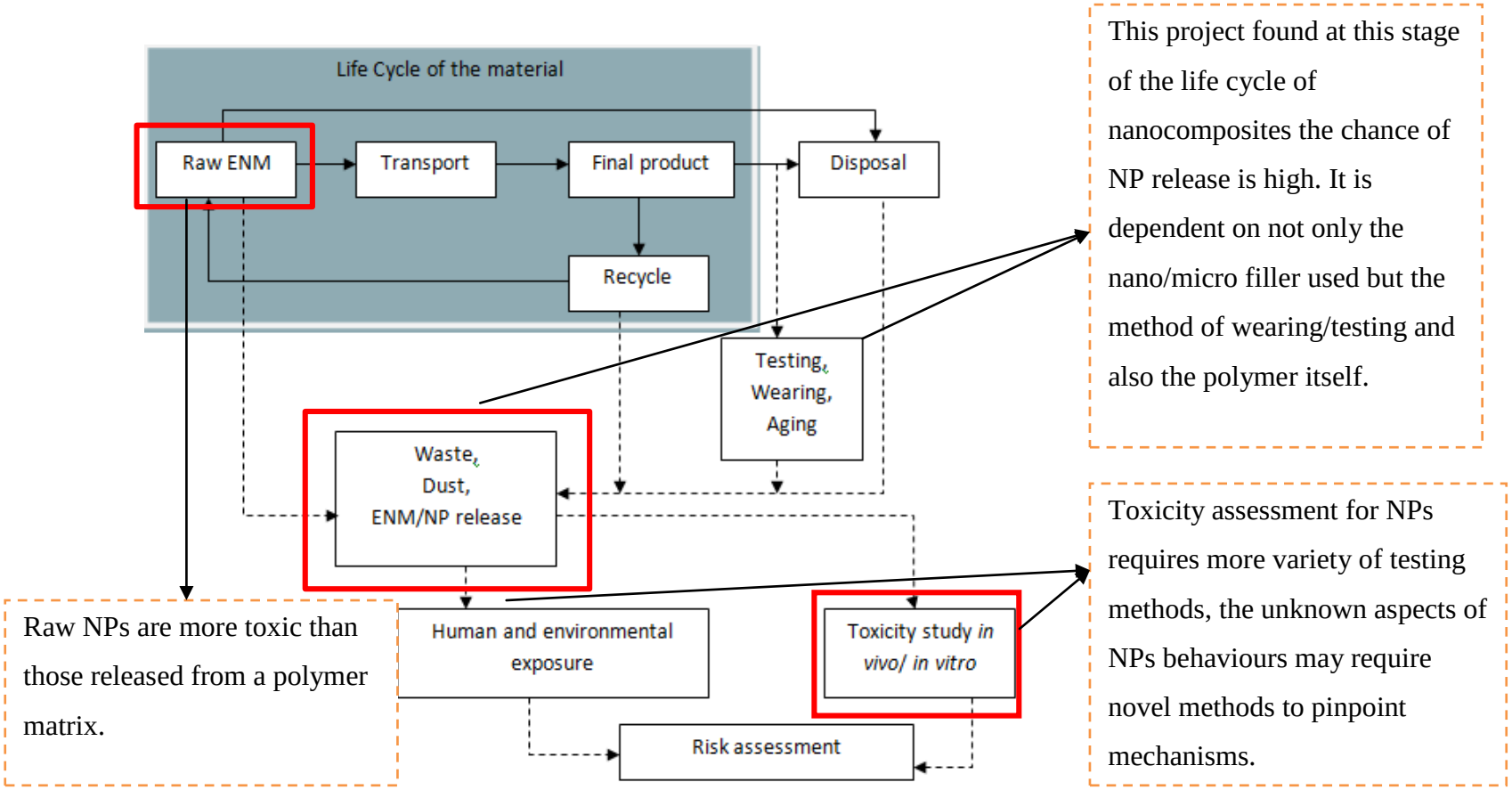

Figure 6.1 Schematic diagram of LCA: Exposure and risk assessment prediction, the findings of this study are incorporated into the diagram.

6.2.4 Development of approaches for risk assessment of nanoproduct on human health

So far little work has been done on evaluation of the release of NP from different polymeric materials. This present study has developed integrated methods and protocols for monitoring and collecting airborne NP, separation of NP from the dust generated during mechanical test, and NP toxicity assessment using human *in vitro* cell models. The results from this study are consistent with the report by Tardif et al., (2009) that polymeric products even without any nanofiller can generate NP when submitted to mechanical process. This present study also suggested that the addition of reinforcement agents can either increase or decrease the release of NP from polymer products. For overall risk assessment of a novel product to human health, the toxicity data needs to be evaluated in connection with the ability of a given product to release NP.

An integrated approach for monitoring, sampling and toxicity testing of NP was developed in the current study. The approach developed based on one scenario can be adopted for assessing the level of NP release from different products under different scenarios and the associated health effect.

6.3 Conclusion

This project aimed to investigate the *in vitro* toxicity of raw silica SiNP and dust NP released from silicon-based polymer composites and mechanisms of SiNP toxicity. The results achieved so far suggest 1) both small and larger aggregates of SiNP were taken up into the cells and caused cytotoxicity via mechanisms involving intracellular ROS elevation and membrane damage; 2) conventional cytotoxicity assays combined with miRNA array and ^{1}H-NMR metabonomic assay could provide insights into molecular mechanisms of NP toxicity; 3) metabonomics and miRNA assays can serve as robust tools for recognising sub toxic dose-effect relationships; 4) the toxicity of dust NP from polymer composites depends on polymer types but not reinforcement materials.

Importantly, this study explored new avenues to study the mechanisms of NP cytotoxicity. The miRNA assay allows the identification of factors that regulate the cellular response to NP at transcription level. The non-invasive ^{1}H-NMR metabonomic profiling proved robust in identifying metabolic biomarkers of toxicity *in vitro*.

This study also highlights the importance of LCA in assessment of health effect of new materials. Clearly the toxicity of a given material will not necessarily remain the same throughout its lifecycle. Alterations to the physic-chemical properties of materials during their lifecycle will inevitably alter their toxicity potency. Therefore, this study provides evidence supporting the concept that toxicity testing should be conducted on all stages of materials' whole life.

Some aspects of the original objectives were not achieved, such as identification of specific uptake pathways and the mechanism of toxicity. Although SiNP uptake and toxicity have been detected, the mechanisms for each are still unknown. To understand which pathway is triggered by the NP toxicity studies should be conducted based on the template highlighted in this study. They must also maintain a focus on LCA of NP, the toxicity mechanisms of NP combined with LCA studies will lead to a complete risk assessment. Such risk assessments are necessary for safe applications of new technologies such as NPs.

6.3.1 Outlook and further study

The outlook for nanotechnology is bright and there are many exciting possibilities. For industry there are little constraints, due to the lack of identified health hazard at present. This is where research must keep pace with a profit driven market. The standardisation of NP toxicity testing and characterisation is a major step to bridging the gap. Alongside the development of methods such as miRNA assays and metabonomics cellular changes caused by toxic NP can be potentially detected earlier. From these assays detecting cellular and metabolic changes the overall long term effect of NP can be predicted effectively.

With ever-increasing novel nanoproducts being developed, LCA of nanotoxicity will play an important role in safe implementation of advanced materials in modern society without compromising environment and human health.

Specifically from this project the next step must be to build upon the novel methods. The early results gave hope that these methods may be useful and lead to a better understanding of toxicity mechanisms and pathways, possible better than conventional methods could alone. The way to build upon these results is through validation. The miRNA sequences that have been identified must be validated using specific primers, once validated the function of these miRNAs must be established from further assays of the predicted targets of the sequences. Metabonomics has also given interesting results, which may provide a non-invasive diagnostic tool, not only *in vitro*, but possible all the way to clinical examinations. It is important to optimise the method for easier, quicker and more reproducible detection.

In summary, the future plans for NP toxicity evaluation must include standardization of protocals for NP characterisation and testing, and validation of data gathered from novel techniques. Work should be continued in a multidisciplinary manner, as this is the only way that the unknown questions about NPs safety and can be addressed, through sharing the knowledge between material engineers, biologists, toxicologists and ecotoxicologists to understand how NP characteristics will translate into potential health hazards.

REFERENCES

Allouni, Z. E., Cimpan, M. R., Høl, P. J., Skodvin, T. and Gjerdet, N. R. (2009), "Agglomeration and sedimentation of TiO2 nanoparticles in cell culture medium", *Colloids and Surfaces B: Biointerfaces*, vol. 68, no. 1, pp. 83-87.

Auten, R. L. and Davis, J. M. (2009), "Oxygen toxicity and reactive oxygen species: The devil is in the details", *Pediatric research*, vol. 66, no. 2, pp. 121-127.

Autian, J. (1975), "Structure toxicity relationships of acrylic monomers", *Environmental health perspectives*, vol. vol. 11, pp. 141-152.

Baek, M., Lee, J. -. and Choi, S. -. (2012), "Toxicological effects of a cationic clay, montmorillonite in vitro and in vivo", *Molecular and Cellular Toxicology*, vol. 8, no. 1, pp. 95-101.

Baker, G. L., Gupta, A., Clark, M. L., Valenzuela, B. R., Staska, L. M., HarboS.J., S. J., Pierce, J. T. and Dill, J. A. (2008), "Inhalation Toxicity and Lung Toxicokinetics of C60 Fullerene Nanoparticles and Microparticles", *Toxicological Sciences*, vol. 101, no. 1, pp. 122-131.

Barker, M. and Rayens, W. (2003), "Partial least squares for discrimination", *Journal of Chemometrics*, vol. 17, no. 3, pp. 166-173.

Bauer, C., Buchgeister, J., Hischier, R., Poganietz, W.R., Schebek, L. and Warsen, J., (2008), *Towards a framework for life cycle thinking in the assessment of nanotechnology*.

Bottini, M., Bruckner, S., Nika, K., Bottini, N., Bellucci, S., Magrini, A., Bergamaschi, A. and Mustelin, T. (2006), "Multi-walled carbon nanotubes induce T lymphocyte apoptosis", *Toxicology letters*, vol. 160, no. 2, pp. 121-126.

Bourdon, J.A., Saber, A.T., Jacobsen, N.R., Jensen, K.A., Madsen, A.M., Lamson, J.S., Wallin, H., Møller, P., Loft, S., Yauk, C.L. and Vogel, U.B., (2012), *Carbon black nanoparticle instillation induces sustained inflammation and genotoxicity in mouse lung and liver*.

Boutonnet, M., Kizling, J., Stenius, P. and Maire, G. (1982), "The preparation of monodisperse colloidal metal particles from microemulsions", *Colloids and Surfaces*, vol. 5, no. 3, pp. 209-225.

Brereton, R. (2003), *Chemometrics: Data Analysis for the Laboratory and Chemical Plant* , 1st ed, John Wiley & Sons, UK.

Bruchez Jr., M., Moronne, M., Gin, P., Weiss, S. and Alivisatos, A. P. (1998), "Semiconductor nanocrystals as fluorescent biological labels", *Science,* vol. 281, no. 5385, pp. 2013-2016.

Cai, X., Hao, J., Zhang, X., Yu, B., Ren, J., Luo, C., Li, Q., Huang, Q., Shi, X., Li, W. and Liu, J. (2010), "The polyhydroxylated fullerene derivative C60(OH)24 protects mice from ionizing-radiation-induced immune and mitochondrial dysfunction", *Toxicology and applied pharmacology,* vol. 243, no. 1, pp. 27-34.

Calvert, G. M., Rice, F. L., Boiano, J. M., Sheehy, J. W. and Sanderson, W. T. (2003), "Occupational silica exposure and risk of various diseases: An analysis using death certificates from 27 states of the United States", *Occupational and environmental medicine,* vol. 60, no. 2, pp. 122-129.

Cederbaum, A. (2009), "Nrf2 and antioxidant defense against CYP2E1 toxicity", *Expert Opinion on Drug Metabolism and Toxicology,* vol. 5, no. 10, pp. 1223-1244.

Cedervall, T., Lynch, I., Foy, M., Berggård, T., Donnelly, S. C., Cagney, G., Linse, S. and Dawson, K. A. (2007a), "Detailed identification of plasma proteins adsorbed on copolymer nanoparticles", *Angewandte Chemie - International Edition,* vol. 46, no. 30, pp. 5754-5756.

Cedervall, T., Lynch, I., Lindman, S., Berggård, T., Thulin, E., Nilsson, H., Dawson, K. A. and Linse, S. (2007b), "Understanding the nanoparticle-protein corona using methods to quntify exchange rates and affinities of proteins for nanoparticles", *Proceedings of the National Academy of Sciences of the United States of America,* vol. 104, no. 7, pp. 2050-2055.

Chan, I. H., Westervelt, R. M., Maranowski, K. D. and Gossard, A. C. (2002), "Strongly capacitively coupled quantum dots", *Applied Physics Letters,* vol. 80, no. 10, pp. 1818-1820.

Chang, J. -., Chang, K. L. B., Hwang, D. -. and Kong, Z. -. (2007), "In vitro cytotoxicitiy of silica nanoparticles at high concentrations strongly depends on the metabolic activity type of the cell line", *Environmental Science and Technology,* vol. 41, no. 6, pp. 2064-2068.

Chen, C., Justice, R. S., Schaefer, D. W. and Baur, J. W. (2008), "Highly dispersed nanosilica-epoxy resins with enhanced mechanical properties", *Polymer,* vol. 49, no. 17, pp. 3805-3815.

Chen, H. -., Neerman, M. F., Parrish, A. R. and Simanek, E. E. (2004), "Cytotoxicity, hemolysis, and acute in vivo toxicity of dendrimers based on melamine, candidate vehicles for drug delivery", *Journal of the American Chemical Society,* vol. 126, no. 32, pp. 10044-10048.

Chhabra, V., Pillai, V., Mishra, B. K., Morrone, A. and Shah, D. O. (1995), "Synthesis, characterization, and properties of microemulsion-mediated nanophase TiO_2 particles", *Langmuir*, vol. 11, no. 9, pp. 3307-3311.

Cho, J. W., Logsdon, J., Omachinski, S., Qian, G., Lan, T., Womer, T. W. and Smith, S. W. (2002), "Nanocomposites: A Single Screw Mixing Study of Nanoclay-filled Polypropylene", 2002, ANTEC 2002, Society of Plastics Engineers Inc, .

Cho, M., Cho, W. -., Choi, M., Kim, S. J., Han, B. S., Kim, S. H., Kim, H. O., Sheen, Y. Y. and Jeong, J. (2009), "The impact of size on tissue distribution and elimination by single intravenous injection of silica nanoparticles", *Toxicology letters*, vol. 189, no. 3, pp. 177-183.

Cho, N. -., Cheong, T. -., Min, J. H., Wu, J. H., Lee, S. J., Kim, D., Yang, J. -., Kim, S., Kim, Y. K. and Seong, S. -. (2011), "A multifunctional core-shell nanoparticle for dendritic cell-based cancer immunotherapy", *Nature Nanotechnology*, .

Cho, W. -., Choi, M., Han, B. S., Cho, M., Oh, J., Park, K., Kim, S. J., Kim, S. H. and Jeong, J. (2007), "Inflammatory mediators induced by intratracheal instillation of ultrafine amorphous silica particles", *Toxicology letters*, vol. 175, no. 1-3, pp. 24-33.

Cho, W. -., Duffin, R., Thielbeer, F., Bradley, M., Megson, I. L., MacNee, W., Poland, C. A., Tran, C. L. and Donaldson, K. (2012), "Zeta potential and solubility to toxic ions as mechanisms of lung inflammation caused by metal/metal oxide nanoparticles", *Toxicological Sciences*, vol. 126, no. 2, pp. 469-477.

Choi, S. -., Oh, J. -. and Choy, J. -. (2009), "Toxicological effects of inorganic nanoparticles on human lung cancer A549 cells", *Journal of inorganic biochemistry*, vol. 103, no. 3, pp. 463-471.

Christensen, F. M. and Olsen, S. I. (2004), "The potential role of life cycle assessment in regulation of chemicals in the European union", *International Journal of Life Cycle Assessment*, vol. 9, no. 5, pp. 327-332.

Clemedson, C., Barile, F. A., Ekwall, B., Gómez-Lechón, M. J., Hall, T., Imai, K., Kahru, A., Logemann, P., Monaco, F., Ohno, T., Segner, H., Sjöström, M., Valentino, M., Walum, E., Wang, X. and Ekwall, B. (1998), "MEIC Evaluation of Acute Systemic Toxicity: Part III. In Vitro Results from 16 Additional Methods Used to Test the First 30 Reference Chemicals and a Comparative Cytotoxicity Analysis", *ATLA Alternatives to Laboratory Animals*, vol. 26 SUPPL. 1, pp. 93-129.

Conner, G. E., Salathe, M. and Forteza, R. (2002), "Lactoperoxidase and hydrogen peroxide metabolism in the airway", *American Journal of Respiratory and Critical Care Medicine*, vol. 166, no. 12 II, pp. S57-S61.

Connor, E. E., Mwamuka, J., Gole, A., Murphy, C. J. and Wyatt, M. D. (2005), "Gold nanoparticles are taken up by human cells but do not cause acute cytotoxicity", *Small*, vol. 1, no. 3, pp. 325-327.

Dar, A. A., Majid, S., De Semir, D., Nosrati, M., Bezrookove, V. and Kashani-Sabet, M. (2011), "miRNA-205 suppresses melanoma cell proliferation and induces senescence via regulation of E2F1 protein", *Journal of Biological Chemistry*, vol. 286, no. 19, pp. 16606-16614.

De Jong, S. (1993), "SIMPLS: An alternative approach to partial least squares regression", *Chemometrics and Intelligent Laboratory Systems*, vol. 18, no. 3, pp. 251-253.

De Schrijver, I., Eufinger, K., Heyse, P., Vanneste, M. and Ruys, L. (2009), "Textiles of the future? Incorporation of nanotechnology in textile applications", *Unitex*, , no. 2, pp. 4-6.

Dekker, P., Meissner, A., Dirks, R. W., Eline Slagboom, P., Van Heemst, D., Deelder, A. M., Tanke, H. J., Westendorp, R. G. J. and Maier, A. B. (2012), "Human in vivo longevity is reflected in vitro by differential metabolism as measured by 1H-NMR profiling of cell culture supernatants", *Molecular BioSystems*, vol. 8, no. 3, pp. 783-789.

Deng, X., Xiong, D., Wang, Y., Chen, W., Luan, Q., Zhang, H., Jiao, Z. and Wu, M., (2010), *Water soluble multi-walled carbon nanotubes enhance peritoneal macrophage activity in vivo*.

Donaldson, K., Aitken, R., Tran, L., Stone, V., Duffin, R., Forrest, G. and Alexander, A. (2006), "Carbon nanotubes: A review of their properties in relation to pulmonary toxicology and workplace safety", *Toxicological Sciences*, vol. 92, no. 1, pp. 5-22.

Donaldson, K. and Borm, P. J. A. (1998), "The quartz hazard: A variable entity", *Annals of Occupational Hygiene*, vol. 42, no. 5, pp. 287-294.

Donaldson, K., Borm, P. J. A., Oberdorster, G., Pinkerton, K. E., Stone, V. and Tran, C. L. (2008), "Concordance between in vitro and in vivo dosimetry in the proinflammatory effects of low-toxicity, low-solubility particles: The key role of the proximal alveolar region", *Inhalation toxicology*, vol. 20, no. 1, pp. 53-62.

Donaldson, K., Li, X. Y. and MacNee, W. (1998), "Ultrafine (nanometre) particle mediated lung injury", *Journal of Aerosol Science*, vol. 29, no. 5-6, pp. 553-560.

Donaldson, K., Stone, V., Gilmour, P. S., Brown, D. M. and Macnee, W. (2000), "Ultrafine particles: Mechanisms of lung injury", *Philosophical Transactions of the Royal Society A: Mathematical, Physical and Engineering Sciences*, vol. 358, no. 1775, pp. 2741-2749.

Donaldson, K., Stone, V., Tran, C. L., Kreyling, W. and Borm, P. J. A. (2004), "Nanotoxicology", *Occupational and environmental medicine*, vol. 61, no. 9, pp. 727-728.

Doymuş, K. (2007), "The effect of ionic electrolytes and pH on the zeta potential of fine coal particles", *Turkish Journal of Chemistry*, vol. 31, no. 6, pp. 589-597.

Duarte, I. (2011), " Following dynamic biological processes through NMR-based metabonomics: A new tool in nanomedicine?", *Journal of Controlled Release*, vol. 153, no. 1, pp. 34-39.

EL- Sharkawy, I. N., Hamza, M. S. and Abou-Zeid, H. E. (2010), "Toxic Impact of Titanium Dioxide (TiO2) In Male Albino Rats with Special Reference to its Effect on Reproductive System", *Journal of American Science*, vol. 11, no. 6, pp. 865-872.

El-Sayed, M., Ginski, M., Rhodes, C. and Ghandehari, H. (2002), "Transepithelial transport of poly(amidoamine) dendrimers across Caco-2 cell monolayers", *Journal of Controlled Release*, vol. 81, no. 3, pp. 355-365.

ENCO Engineering GmbH Switzerland (2004), *Foamed Glass Technology*, available at: http://www.enco.ch/glass.htm (accessed 11/2010).

Eom, H. -. and Choi, J. (2009a), "Oxidative stress of CeO2 nanoparticles via p38-Nrf-2 signaling pathway in human bronchial epithelial cell, Beas-2B", *Toxicology letters*, vol. 187, no. 2, pp. 77-83.

Eom, H. -. and Choi, J. (2009b), "Oxidative stress of silica nanoparticles in human bronchial epithelial cell, Beas-2B", *Toxicology in Vitro*, vol. 23, no. 7, pp. 1326-1332.

Erber, B., Governa, M. and Mollo, F. (1961), "In culture behavior of macrophages after the phagocytosis of particles of crystalline silica or inert dusts.", *La Medicina del lavoro*, vol. 52, pp. 744-755.

Fadeel, B., Kagan, V., Krug, H., Shvedova, A., Svartengren, M., Tran, L. and Wiklund, L. (2007), "There's plenty of room at the forum: Potential risks and safety assessment of engineered nanomaterials", Nanotoxicology, vol. 1, no. 2, pp. 73-84.

Fenoglio, I., Martra, G., Coluccia, S. and Fubini, B. (2000), "Possible role of ascorbic acid in the oxidative damage induced by inhaled crystalline silica particles", *Chemical research in toxicology*, vol. 13, no. 10, pp. 971-975.

Firoze Khan, M., Boor, P. J., Gu, Y., Alcock, N. W. and Ansari, A. G. A. S. (1997), "Oxidative stress in the splenotoxicity of aniline", *Toxicological Sciences*, vol. 35, no. 1, pp. 22-30.

Fruijtier-Pölloth, C. (2012), "The toxicological mode of action and the safety of synthetic amorphous silica-A nanostructured material", *Toxicology*, vol. 294, no. 2-3, pp. 61-79.

Fubini, B., Ghiazza, M. and Fenoglio, I. (2010), "Physico-chemical features of engineered nanoparticles relevant to their toxicity", *Nanotoxicology*, vol. 4, no. 4, pp. 347-363.

Fubini, B., Zanetti, G., Altilia, S., Tiozzo, R., Lison, D. and Saffiotti, U. (1999), "Relationship between surface properties and cellular responses to crystalline silica: Studies with heat-treated cristobalite", *Chemical research in toxicology*, vol. 12, no. 8, pp. 737-745.

Gable, K. (2000), *FTIR instrumentation and theory*, available at: http://www.chemistry.oregonstate.edu/courses/ch361-464/ch362/irinstrs.htm (accessed June 2012).

Geys, J., Nemery, B. and Hoet, P. H. M. (2010), "Assay conditions can influence the outcome of cytotoxicity tests of nanomaterials: Better assay characterization is needed to compare studies", *Toxicology in Vitro*, vol. 24, no. 2, pp. 620-629.

Gregory, P. A., Bert, A. G., Paterson, E. L., Barry, S. C., Tsykin, A., Farshid, G., Vadas, M. A., Khew-Goodall, Y. and Goodall, G. J. (2008), "The miR-200 family and miR-205 regulate epithelial to mesenchymal transition by targeting ZEB1 and SIP1", *Nature cell biology*, vol. 10, no. 5, pp. 593-601.

Grim, R. E. (1962), "Clay mineralogy", *Science*, vol. 135, no. 3507, pp. 890-898.

Gupta, A. K. and Gupta, M. (2005), "Synthesis and surface engineering of iron oxide nanoparticles for biomedical applications", *Biomaterials*, vol. 26, no. 18, pp. 3995-4021.

Gutteridge, J. M. C., Richmond, R. and Halliwell, B. (1980), "Oxygen free-radicals and lipid peroxidation: inhibition by the protein caeruloplasmin", *FEBS letters*, vol. 112, no. 2, pp. 269-272.

Han, G., Ghosh, P. and Rotello, V. M. (2007), "Functionalized gold nanoparticles for drug delivery", *Nanomedicine*, vol. 2, no. 1, pp. 113-123.

Han, M., Ye, S., Wen, W. and Zhang, Q. (2010), "Oxidative stress-mediated pro-inflammatory responses in lung epithelial cells exposed to multiwalled carbon nanotubes", .

Hardman, R. (2006), "A toxicologic review of quantum dots: Toxicity depends on physicochemical and environmental factors", *Environmental health perspectives*, vol. 114, no. 2, pp. 165-172.

Herzog, E., Casey, A., Lyng, F. M., Chambers, G., Byrne, H. J. and Davoren, M. (2007), "A new approach to the toxicity testing of carbon-based nanomaterials-The clonogenic assay", *Toxicology letters*, vol. 174, no. 1-3, pp. 49-60.

Hessel, P. A. and Sluis-Cremer, G. K. (1987), "Silica, silicosis, and lung cancer among ceramic workers: a case-referent study.", *American Journal of Industrial Medicine*, vol. 12, no. 2, pp. 219-222.

Hischier, R. and Walser, T., (2012), "Life cycle assessment of engineered nanomaterials: State of the art and strategies to overcome existing gaps.", *Science of the Total Environment*, vol. 425, pp. 291-282.

HM Government, (2010), *UK Nanotechnologies Strategy Small Technologies, Great Opportunities*.

Hoshino, A., Fujioka, K., Oku, T., Suga, M., Sasaki, Y. F., Ohta, T., Yasuhara, M., Suzuki, K. and Yamamoto, K. (2004), "Physicochemical properties and cellular toxicity of nanocrystal quantum dots depend on their surface modification", *Nano Letters*, vol. 4, no. 11, pp. 2163-2169.

Huang, X., Teng, X., Chen, D., Tang, F. and He, J. (2010), "The effect of the shape of mesoporous silica nanoparticles on cellular uptake and cell function", *Biomaterials*, vol. 31, no. 3, pp. 438-448.

Huang, Z., Huang, S., Wang, Q., Liang, L., Ni, S., Wang, L., Sheng, W., He, X. and Du, X. (2011), "MicroRNA-95 promotes cell proliferation and targets sorting nexin 1 in human colorectal carcinoma", *Cancer research*, vol. 71, no. 7, pp. 2582-2589.

Huaux, F. (2007), "New developments in the understanding of immunology in silicosis", *Current Opinion in Allergy and Clinical Immunology*, vol. 7, no. 2, pp. 168-173.

Hussain, S. M., Hess, K. L., Gearhart, J. M., Geiss, K. T. and Schlager, J. J. (2005), "In vitro toxicity of nanoparticles in BRL 3A rat liver cells", *Toxicology in Vitro*, vol. 19, no. 7, pp. 975-983.

IARC, (1987), *IARC Monographs on the Evaluation of Carcinogenic Risks to Humans Supplement 7*.

IARC, (1997), *IARC Monographs on the Evaluation of Carcinogenic Risks to Humans*.

Immunologie et Chimie Therapeutiques (2004), *Functionalised carbon nanotubes as therapeutic vectors*, available at: http://www-ibmc.u-strasbg.fr/ict/vectorisation/nanotubes_eng.shtml (accessed July).

Irfan, A., Sachse, S., Njuguna, J., Pielichowski, K., Silva, K. and Zhu, H. (2013), "Assessment of Nanoparticle Release from Polyamide 6- and Polypropylene-

Silicon Composites and Cytotoxicity in Human Lung A549 Cells", *Journal of Inorganic and Organometallic Polymers and Materials*, vol. 23.

Irfan, A., Sachse, S., Njuguna, J. and Zhu, H., (2010a), *Assessment of nanoparticle release from nanoproducts and their toxicity potential in human lung A549 cells*, 1st ed., Cranfield, Gloucester.

Irfan, A., Sachse, S., Njuguna, J. and Zhu, H., (2010b), *In vitro hazard identification and characterization of manufactured nanoparticles throughout products life cycle* , 1st ed., Air pollution conference by Institute of Environmental Health, Cranfield, UK.

Irfan, A., Sachse, S., Njuguna, J. and Zhu, H., (2010c), *In vitro Nanoparticle toxicity study- focusing on development of testing protocols*, 1st ed., NEPHH, Milan.

Irfan, A., Sachse, S., Njuguna, J. and Zhu, H., (2010d), *Investigation of silica nanoparticle toxicity-toward standardization of NP toxicity test in vitro* , 1st ed., NEPHH, Milan.

Irfan, A., Sachse, S., Njuguna, J. and Zhu, H., (2011a), *In vitro analysis of nanoparticles and nanodust released, from polymer/nanostructured-material composite, during drilling process.*, 1st ed., Nano roadshow, Cranfield,UK.

Irfan, A., Sachse, S., Njuguna, J. and Zhu, H., (2011b), *In vitro hazard identification and characterization of manufactured nanomaterials throughout products life cycle*, 1st ed., Air pollution conference by Institute of Environmental Health, Cranfield, UK.

Irfan, A., Sachse, S., Njuguna, J. and Zhu, H. (2012), "Assessment of release and toxicity of nanoparticles from polymer-silicon composites in a life cycle perspective", pp. 315.

ISO, (2006), *Environmental management -- Life cycle assessment -- Requirements and guidelines.*

ISO, (2008), *International Organization for Standardization. Technical Specification ISO/TS 27687:2008(E): Nanotechnologies – Terminology and Definitions for Nano-objects – Nanoparticle, Nanofibre and Nanoplate.*

Jackson, P. K. (2001), "A new RING for SUMO: Wrestling transcriptional responses into nuclear bodies with PIAS family E3 SUMO ligases", Genes and Development, vol. 15, no. 23, pp. 3053-3058.

Jaszczyszyn, A. and Gasiorowski, K. (2008), "Limitations of the MTT assay in cell viability testing", *Advances in Clinical and Experimental Medicine*, vol. 17, no. 5, pp. 525-529.

Jevprasesphant, R., Penny, J., Jalal, R., Attwood, D., McKeown, N. B. and D'Emanuele, A. (2003), "The influence of surface modification on the cytotoxicity of PAMAM dendrimers", *International journal of pharmaceutics,* vol. 252, no. 1-2, pp. 263-266.

Jia, G., Wang, H., Yan, L., Wang, X., Pei, R., Yan, T., Zhao, Y. and Guo, X. (2005), "Cytotoxicity of carbon nanomaterials: Single-wall nanotube, multi-wall nanotube, and fullerene", *Environmental Science and Technology,* vol. 39, no. 5, pp. 1378-1383.

Jiang, J., Oberdörster, G. and Biswas, P. (2009), "Characterization of size, surface charge, and agglomeration state of nanoparticle dispersions for toxicological studies", *Journal of Nanoparticle Research,* vol. 11, no. 1, pp. 77-89.

Johnston, C. J., Driscoll, K. E., Finkelstein, J. N., Baggs, R., O'Reilly, M. A., Carter, J., Gelein, R. and Oberdörster, G. (2000), "Pulmonary chemokine and mutagenic responses in rats after subchronic inhalation of amorphous and crystalline silica", *Toxicological Sciences,* vol. 56, no. 2, pp. 405-413.

Kaewamatawong, T., Shimada, A., Okajima, M., Inoue, H., Morita, T., Inoue, K. and Takano, H. (2006), "Acute and subacute pulmonary toxicity of low dose of ultrafine colloidal silica particles in mice after intratracheal instillation", *Toxicologic pathology,* vol. 34, no. 7, pp. 958-965.

Karakoti, A. S., Hench, L. L. and Seal, S. (2006), "The potential toxicity of nanomaterials - The role of surfaces", *JOM,* vol. 58, no. 7, pp. 77-82.

Kelly, S. A., Havrilla, C. M., Brady, T. C., Abramo, K. H. and Levin, E. D. (1998), "Oxidative stress in toxicology: Established mammalian and emerging piscine model systems", *Environmental health perspectives,* vol. 106, no. 7, pp. 375-384.

Khandelia, R., Jaiswal, A., Ghosh, S. S. and Chattopadhyay, A. (2013), "Gold Nanoparticle?Protein Agglomerates as Versatile Nanocarriers for Drug Delivery", *Small,* , pp. n/a-n/a.

Kim, H. J. and Vaziri, N. D. (2010), "Contribution of impaired Nrf2-Keap1 pathway to oxidative stress and inflammation in chronic renal failure", *American Journal of Physiology - Renal Physiology,* vol. 298, no. 3, pp. F662-F671.

Kloepffer, W. (2008), "Life cycle sustainability assessment of products (with Comments by Helias A. Udo de Haes, p. 95)", *International Journal of Life Cycle Assessment,* vol. 13, no. 2, pp. 89-94.

Kolb, M., Margetts, P. J., Anthony, D. C., Pitossi, F. and Gauldie, J. (2001), "Transient expression of IL-1β induces acute lung injury and chronic repair leading to pulmonary fibrosis", *Journal of Clinical Investigation,* vol. 107, no. 12, pp. 1529-1536.

Koufaris, C. and Gooderham, N. J. (2013), "Are differences in microRNA regulation implicated in species-dependent response to toxicological exposures?", *Toxicological Sciences,* vol. 131, no. 2, pp. 337-342.

Kumar, R., Roy, I., Ohulchanskky, T. Y., Vathy, L. A., Bergey, E. J., Sajjad, M. and Prasad, P. N. (2010), "In vivo biodistribution and clearance studies using multimodal organically modified silica nanoparticles", *ACS Nano,* vol. 4, no. 2, pp. 699-708.

Lacerda, L., Ali-Boucetta, H., Herrero, M.A., Pastorin, G., Bianco, A., Prato, M. and Kostarelos, K., (2008), *Tissue histology and physiology following intravenous administration of different types of functionalized multiwalled carbon nanotubes.*

Lam, C. -., James, J. T., McCluskey, R. and Hunter, R. L. (2004), "Pulmonary toxicity of single-wall carbon nanotubes in mice 7 and 90 days after intractracheal instillation", *Toxicological Sciences,* vol. 77, no. 1, pp. 126-134.

Lee, R. C., Feinbaum, R. L. and Ambros, V. (1993), "The C. elegans heterochronic gene lin-4 encodes small RNAs with antisense complementarity to lin-14", *Cell,* vol. 75, no. 5, pp. 843-854.

Lesniak, A., Fenaroli, F., Monopoli, M. P., Åberg, C., Dawson, K. A. and Salvati, A. (2012), "Effects of the presence or absence of a protein corona on silica nanoparticle uptake and impact on cells", *ACS Nano,* vol. 6, no. 7, pp. 5845-5857.

Lesniak, W., Blelinska, A. U., Sun, K., Janczak, K. W., Shi, X., Baker Jr., J. R. and Balogh, L. P. (2005), "Silver/dendrimer nanocomposites as biomarkers: Fabrication, characterization, in vitro toxicity, and intracellular detection", *Nano Letters,* vol. 5, no. 11, pp. 2123-2130.

Li, H., Cao, Y. -., Zhang, L. -., Chen, W., Wang, H. -., Zhang, J. -. and Duan, H. -. (2011a), "tBHQ attenuates high glucose induced oxidative stress injury in mouse mesangial cells", *Chinese Pharmacological Bulletin,* vol. 27, no. 4, pp. 528-533.

Li, S., Wang, H., Qi, Y., Tu, J., Bai, Y., Tian, T., Huang, N., Wang, Y., Xiong, F., Lu, Z. and Xiao, Z. (2011b), "Assessment of nanomaterial cytotoxicity with SOLiD sequencing-based microRNA expression profiling", *Biomaterials,* vol. 32, no. 34, pp. 9021-9030.

Limbach, L. K., Wick, P., Manser, P., Grass, R. N., Bruinink, A. and Stark, W. J. (2007), "Exposure of engineered nanoparticles to human lung epithelial cells: Influence of chemical composition and catalytic activity on oxidative stress", *Environmental Science and Technology,* vol. 41, no. 11, pp. 4158-4163.

Links, J. M., Schwartz, B. S., Simon, D., Bandeen-Roche, K. and Stewart, W. F. (2001), "Characterization of toxicokinetics and toxicodynamics with linear systems theory:

Application to lead-associated cognitive decline", *Environmental health perspectives,* vol. 109, no. 4, pp. 361-368.

Liu, J., Litt, L., Segal, M. R., Kelly, M. J. S., Pelton, J. G., and Kim, M. (2011), " Metabolomics of Oxidative Stress in Recent Studies of Endogenous and Exogenously Administered Intermediate Metabolites" *International Journal of Molecular Science,* vol. 12, no. 10, pp. 6469-6501.

Liu, Z., Fan, A. C., Rakhra, K., Sherlock, S., Goodwin, A., Chen, X., Yang, Q., Felsher, D. W. and Dai, H. (2009), "Supramolecular stacking of doxorubicin on carbon nanotubes for in vivo cancer therapy", *Angewandte Chemie - International Edition,* vol. 48, no. 41, pp. 7668-7672.

Lovrić, J., Bazzi, H. S., Cuie, Y., Fortin, G. R. A., Winnik, F. M. and Maysinger, D. (2005a), "Differences in subcellular distribution and toxicity of green and red emitting CdTe quantum dots", *Journal of Molecular Medicine,* vol. 83, no. 5, pp. 377-385.

Lovrić, J., Cho, S. J., Winnik, F. M. and Maysinger, D. (2005b), "Unmodified cadmium telluride quantum dots induce reactive oxygen species formation leading to multiple organelle damage and cell death", *Chemistry and Biology,* vol. 12, no. 11, pp. 1227-1234.

Luo, J., Vijayasankaran, N., Autsen, J., Santuray, R., Hudson, T., Amanullah, A. and Li, F. (2012), "Comparative metabolite analysis to understand lactate metabolism shift in Chinese hamster ovary cell culture process", *Biotechnology and bioengineering,* vol. 109, no. 1, pp. 146-156.

Lynn, A. D., Kyriakides, T. R. and Bryant, S. J. (2010), "Characterization of the in vitro macrophage response and in vivo host response to poly(ethylene glycol)-based hydrogels", *Journal of Biomedical Materials Research - Part A,* vol. 93, no. 3, pp. 941-953.

Ma, J. Y., Zhao, H., Mercer, R. R., Barger, M., Rao, M., Meighan, T., Schwegler-Berry, D., Castranova, V. and Ma, J. K. (2011), "Cerium oxide nanoparticle-induced pulmonary inflammation and alveolar macrophage functional change in rats", *Nanotoxicology,* vol. 5, no. 3, pp. 312-325.

MacCormack, T. J., Clark, R. J., Dang, M. K. M., Ma, G., Kelly, J. A., Veinot, J. G. C. and Goss, G. G. (2012), "Inhibition of enzyme activity by nanomaterials: Potential mechanisms and implications for nanotoxicity testing", *Nanotoxicology,* vol. 6, no. 5, pp. 514-525.

MacIntyre, D. A., Sanchís, D. M., Jiménez, B., Moreno, R., Stojkovic, M. and Pineda-Lucena, A. (2011), "Characterisation of human embryonic stem cells conditioning media by 1H-nuclear magnetic resonance spectroscopy", *PLoS ONE,* vol. 6, no. 2.

MATBASE (2009), *Material Properties of E-Glass Fibre, Fiberglass | Fibers Data Sheet*
, available at: http://www.matbase.com/material/fibres/glass/e-glass-fibre/properties (accessed 11/2010).

Maynard, A. D. (2006), *Nanotechnology: a Reasearch Strategy for Addressing Risk*, , Woodrow Wilson International Center for Scholars.

McCord, J. M. and Fridovich, I. (1969), "Superoxide dismutase. An enzymic function for erythrocuprein (hemocuprein).", *Journal of Biological Chemistry*, vol. 244, no. 22, pp. 6049-6055.

Meiner, T., Potthoff, A. and Richter, V. (2009), "Suspension characterization as important key for toxicological investigations", *Journal of Physics: Conference Series*, vol. 170.

Miyazaki, Y., Araki, K., Vesin, C., Garcia, I., Kapanci, Y., Whitsett, J. A., Piguet, P. -. and Vassalli, P. (1995), "Expression of a tumor necrosis factor-α transgene in murine lung causes lymphocytic and fibrosing alveolitis. A mouse model of progressive pulmonary fibrosis", *Journal of Clinical Investigation*, vol. 96, no. 1, pp. 250-259.

Monteiro-Riviere, N. A., Inman, A. O. and Zhang, L. W. (2009), "Limitations and relative utility of screening assays to assess engineered nanoparticle toxicity in a human cell line", *Toxicology and applied pharmacology*, vol. 234, no. 2, pp. 222-235.

Montes-Burgos, I., Walczyk, D., Hole, P., Smith, J., Lynch, I. and Dawson, K. (2010), "Characterisation of nanoparticle size and state prior to nanotoxicological studies", *Journal of Nanoparticle Research*, vol. 12, no. 1, pp. 47-53.

Mornet, S., Vasseur, S., Grasset, F. and Duguet, E. (2004), "Magnetic nanoparticle design for medical diagnosis and therapy", *Journal of Materials Chemistry*, vol. 14, no. 14, pp. 2161-2175.

Mu, Q., Hondow, N. S., Krzemiński, T., Brown, A. P., Jeuken, L. J. C. and Routledge, M. N. (2012), "Mechanism of cellular uptake of genotoxic silica nanoparticles", *Particle and Fibre Toxicology*, vol. 9.

Mühlfeld, C., Gehr, P. and Rothen-Rutishauser, B. (2008), "Translocation and cellular entering mechanisms of nanoparticles in the respiratory tract", *Swiss Medical Weekly*, vol. 138, no. 27-28, pp. 387-391.

Murashov, V., Harper, M. and Demchuk, E. (2006), "Impact of silanol surface density on the toxicity of silica aerosols measured by erythrocyte haemolysis.", *Journal of occupational and environmental hygiene*, vol. 3, no. 12, pp. 718-723.

Naha, P. C., Davoren, M., Lyng, F. M. and Byrne, H. J. (2010), "Reactive oxygen species (ROS) induced cytokine production and cytotoxicity of PAMAM dendrimers in J774A.1 cells", *Toxicology and applied pharmacology*, vol. 246, no. 1-2, pp. 91-99.

Napierska, D., Thomassen, L. C. J., Rabolli, V., Lison, D., Gonzalez, L., Kirsch-Volders, M., Martens, J. A. and Hoet, P. H. (2009), "Size-dependent cytotoxicity of monodisperse silica nanoparticles in human endothelial cells", *Small*, vol. 5, no. 7, pp. 846-853.

Naqvi, S., Samim, M., Abdin, M. Z., Ahmed, F. J., Maitra, A. N., Prashant, C. K. and Dinda, A. K. (2010), "Concentration-dependent toxicity of iron oxide nanoparticles mediated by increased oxidative stress", *International Journal of Nanomedicine*, vol. 5, no. 1, pp. 983-989.

Nareika, A., He, L., Game, B. A., Slate, E. H., Sanders, J. J., London, S. D., Lopes-Virella, M. F. and Huang, Y. (2005), "Sodium lactate increases LPS-stimulated MMP and cytokine expression in U937 histiocytes by enhancing AP-1 and NF-κB transcriptional activities", *American Journal of Physiology - Endocrinology and Metabolism*, vol. 289, no. 4 52-4, pp. E534-E542.

Nature (2011), *The history of the journal Nature*, available at: http://www.nature.com/nature/history/timeline_1980s.html (accessed July).

Oberdörster, G., Ferin, J., Finkelstein, G., Wade, P. and Corson, N. (1990), "Increased pulmonary toxicity of ultrafine particles? II. Lung lavage studies", *Journal of Aerosol Science*, vol. 21, no. 3, pp. 384-387.

Oberdorster, G., Ferin, J., Gelein, R., Soderholm, S. C. and Finkelstein, J. (1992), "Role of the alveolar macrophage in lung injury: Studies with ultrafine particles", *Environmental health perspectives*, vol. 97, pp. 193-199.

Oberdörster, G., Oberdörster, E. and Oberdörster, J. (2005), "Nanotoxicology: An emerging discipline evolving from studies of ultrafine particles", *Environmental health perspectives*, vol. 113, no. 7, pp. 823-839.

Oberdörster, G., Sharp, Z., Atudorei, V., Elder, A., Gelein, R., Kreyling, W. and Cox, C. (2004), "Translocation of inhaled ultrafine particles to the brain", *Inhalation toxicology*, vol. 16, no. 6-7, pp. 437-445.

Obi, B. E., Leyva, E., Miyazaki, Y., Walia, P. and Minnikanti, V. (2012), "Model validation for predicting comfort in automotive seating polyurethane foams", Vol. 1, pp. 110.

Øvrevik, J., Refsnes, M., Namork, E., Becher, R., Sandnes, D., Schwarze, P. E. and Låg, M. (2006), "Mechanisms of silica-induced IL-8 release from A549 cells:

Initial kinase-activation does not require EGFR activation or particle uptake", *Toxicology*, vol. 227, no. 1-2, pp. 105-116.

Park, E. -. and Park, K. (2009), "Oxidative stress and pro-inflammatory responses induced by silica nanoparticles in vivo and in vitro", *Toxicology letters*, vol. 184, no. 1, pp. 18-25.

Park, M. V. D. Z., Annema, W., Salvati, A., Lesniak, A., Elsaesser, A., Barnes, C., McKerr, G., Howard, C. V., Lynch, I., Dawson, K. A., Piersma, A. H. and de Jong, W. H. (2009), "In vitro developmental toxicity test detects inhibition of stem cell differentiation by silica nanoparticles", *Toxicology and applied pharmacology*, vol. 240, no. 1, pp. 108-116.

Park, Y. -., Kim, J. N., Jeong, S. H., Choi, J. E., Lee, S. -., Choi, B. H., Lee, J. P., Sohn, K. H., Park, K. L., Kim, M. -. and Son, S. W. (2010), "Assessment of dermal toxicity of nanosilica using cultured keratinocytes, a human skin equivalent model and an in vivo model", *Toxicology*, vol. 267, no. 1-3, pp. 178-181.

Passarella, S., de Bari, L., Valenti, D., Pizzuto, R., Paventi, G. and Atlante, A. (2008), "Mitochondria and l-lactate metabolism", *FEBS letters*, vol. 582, no. 25-26, pp. 3569-3576.

Pedersen, A. J., Reitzel, L. A., Johansen, S. S. and Linnet, K. (2012), "In vitro metabolism studies on mephedrone and analysis of forensic cases", *Drug Testing and Analysis*, .

Pervaiz, S., Taneja, R. and Ghaffari, S. (2009), "Oxidative stress regulation of stem and progenitor cells", *Antioxidants and Redox Signaling*, vol. 11, no. 11, pp. 2777-2789.

Pratsinis, S. E. (1998), "Flame aerosol synthesis of ceramic powders", *Progress in Energy and Combustion Science*, vol. 24, no. 3, pp. 197-219.

Rahman, I., Gilmour, P. S., Jimenez, L. A. and MacNee, W. (2002), "Oxidative stress an TNF-α induce histone acetylation and NF-κB/AP-1 activation in alveolar epithelial cells: Potential mechanism in gene transcription in lung inflammation", *Molecular and cellular biochemistry*, vol. 234-235, pp. 239-248.

Rayavarapu, R. G., Petersen, W., Hartsuiker, L., Chin, P., Janssen, H., Van Leeuwen, F. W. B., Otto, C., Manohar, S. and Van Leeuwen, T. G. (2010), "In vitro toxicity studies of polymer-coated gold nanorods", *Nanotechnology*, vol. 21, no. 14.

Rivera Gil, P., Hühn, D., del Mercato, L. L., Sasse, D. and Parak, W. J. (2010), "Nanopharmacy: Inorganic nanoscale devices as vectors and active compounds", *Pharmacological Research*, vol. 62, no. 2, pp. 115-125.

Roberts, R. A., Laskin, D. L., Smith, C. V., Robertson, F. M., Allen, E. M. G., Doorn, J. A. and Slikker, W. (2009), "Nitrative and oxidative stress in toxicology and disease", *Toxicological Sciences*, vol. 112, no. 1, pp. 4-16.

Rockwood specialities (2006), *Key Properties of Montmorillonite*, available at: http://www.nanoclay.com/keyproperties.asp (accessed 11/2010).

Roth, V. (2006), *Doubling Time*, available at: http://www.doubling-time.com/compute.php (accessed January 2013).

Roubicek, V., Raclavska, H., Juchelkova, D. and Filip, P. (2008), "Wear and environmental aspects of composite materials for automotive braking industry", *Wear*, vol. 265, no. 1-2, pp. 167-175.

Sachse, S., Irfan, A., Zhu, H. and Njuguna, J. (2011), "Morphology studies of nanodust generated from polyurethane/nanoclay nanofoams following mechanical fracture", *Journal of Nanostructured Polymers and Nanocomposites*, vol. 7, no. 1, pp. 5-9.

Sachse, S., Silva, F., Zhu, H., Irfan, A., Leszczyńska, A., Pielichowski, K., Ermini, V., Blazquez, M., Kuzmenko, O. and Njuguna, J. (2012), "The effect of nanoclay on dust generation during drilling of PA6 nanocomposites", *Journal of Nanomaterials*, vol. 2012.

Salcedo, I., Aguzzi, C., Sandri, G., Bonferoni, M. C., Mori, M., Cerezo, P., Sánchez, R., Viseras, C. and Caramella, C. (2012), "In vitro biocompatibility and mucoadhesion of montmorillonite chitosan nanocomposite: A new drug delivery", *Applied Clay Science*, vol. 55, pp. 131-137.

Samberg, M. E., Oldenburg, S. J. and Monteiro-Riviere, N. A. (2010), "Evaluation of silver nanoparticle toxicity in skin in vivo and keratinocytes in vitro", *Environmental health perspectives*, vol. 118, no. 3, pp. 407-413.

Samuvel, D. J., Sundararaj, K. P., Nareika, A., Lopes-Virella, M. F. and Huang, Y. (2009), "Lactate boosts TLR4 signaling and NF-κB pathway-mediated gene transcription in macrophages via monocarboxylate transporters and MD-2 up-regulation", *Journal of Immunology*, vol. 182, no. 4, pp. 2476-2484.

Sayes, C. M., Fortner, J. D., Guo, W., Lyon, D., Boyd, A. M., Ausman, K. D., Tao, Y. J., Sitharaman, B., Wilson, L. J., Hughes, J. B., West, J. L. and Colvin, V. L. (2004), "The differential cytotoxicity of water-soluble fullerenes", *Nano Letters*, vol. 4, no. 10, pp. 1881-1887.

Sayes, C. M., Gobin, A. M., Ausman, K. D., Mendez, J., West, J. L. and Colvin, V. L. (2005), "Nano-C60 cytotoxicity is due to lipid peroxidation", *Biomaterials*, vol. 26, no. 36, pp. 7587-7595.

Sayes, C. M., Marchione, A. A., Reed, K. L. and Warheit, D. B. (2007), "Comparative pulmonary toxicity assessments of C60 water suspensions in rats: Few differences in fullerene toxicity in Vivo in contrast to in Vitro profiles", *Nano Letters*, vol. 7, no. 8, pp. 2399-2406.

Schrattenholz, A., Šoškić, V., Schöpf, R., Poznanović, S., Klemm-Manns, M. and Groebe, K. (2012), "Protein biomarkers for in vitro testing of toxicology", *Mutation Research - Genetic Toxicology and Environmental Mutagenesis*, vol. 746, no. 2, pp. 113-123.

Seager, T. P. and Linkov, I. (2008), "Coupling multicriteria decision analysis and life cycle assessment for nanomaterials", *Journal of Industrial Ecology*, vol. 12, no. 3, pp. 282-285.

Shah, Y. M., Morimura, K., Yang, Q., Tanabe, T., Takagi, M. and Gonzalez, F. J. (2007), "Peroxisome proliferator-activated receptor α regulates a microRNA-mediated signaling cascade responsible for hepatocellular proliferation", *Molecular and cellular biology*, vol. 27, no. 12, pp. 4238-4247.

Sharma, J. N., Al-Omran, A. and Parvathy, S. S. (2007), "Role of nitric oxide in inflammatory diseases", *Inflammopharmacology*, vol. 15, no. 6, pp. 252-259.

Sheppard, C. J. R. and Wilson, T. (1981), "The theory of the direct-view confocal microscope", *Journal of microscopy*, vol. 124, no. 2, pp. 107-117.

Sime, P. J., Marr, R. A., Gauldie, D., Xing, Z., Hewlett, B. R., Graham, F. L. and Gauldie, J. (1998), "Transfer of tumor necrosis factor-alpha to rat lung induces severe pulmonary inflammation and patchy interstitial fibrogenesis with induction of transforming growth factor- beta1 and myofibroblasts.", *Amrican Journal of Pathology*, vol. 153, pp. 825-832.

Som, C., Berges, M., Chaudhry, Q., Dusinska, M., Fernandes, T. F., Olsen, S. I. and Nowack, B. (2010), "The importance of life cycle concepts for the development of safe nanoproducts", *Toxicology*, .

Soto, K., Garza, K. M. and Murr, L. E. (2007), "Cytotoxic effects of aggregated nanomaterials", *Acta Biomaterialia*, vol. 3, no. 3 SPEC. ISS., pp. 351-358.

Stayton, I., Winiarz, J., Shannon, K. and Ma, Y. (2009), "Study of uptake and loss of silica nanoparticles in living human lung epithelial cells at single cell level", *Analytical and Bioanalytical Chemistry*, vol. 394, no. 6, pp. 1595-1608.

Styan, K. E., Martin, D. J. and Poole-Warren, L. A. (2008), "In vitro fibroblast response to polyurethane organosilicate nanocomposites", *Journal of Biomedical Materials Research - Part A*, vol. 86, no. 3, pp. 571-582.

Szeto, S. S. W., Reinke, S. N., Sykes, B. D. and Lemire, B. D. (2010), "Mutations in the saccharomyces cerevisiae succinate dehydrogenase result in distinct metabolic phenotypes revealed through 1H NMR-based metabolic footprinting", *Journal of Proteome Research*, vol. 9, no. 12, pp. 6729-6739.

Tardif, F., Guiot, A. and Golanski, L. (2009), "Measurement of nanofiller removal by abrasion", Vol. 1, pp. 98.

Teixeira, D., Giovanela, M., Gonella, L. B. and Crespo, J. S. (2013), "Influence of flow restriction on the microstructure and mechanical properties of long glass fiber-reinforced polyamide 6.6 composites for automotive applications", *Materials and Design*, vol. 47, pp. 287-294.

Trewyn, B. G., Nieweg, J. A., Zhao, Y. and Lin, V. S. -. (2008), "Biocompatible mesoporous silica nanoparticles with different morphologies for animal cell membrane penetration", *Chemical Engineering Journal*, vol. 137, no. 1, pp. 23-29.

Tripathi, P. and Aggarwal, A. (2006), "NF-kB transcription factor: A key player in the generation of immune response", *Current science*, vol. 90, no. 4, pp. 519-531

Unfried, K., Albrecht, C., Klotz, L. -., Von Mikecz, A., Grether-Beck, S. and Schins, R. P. F. (2007), "Cellular responses to nanoparticles: Target structures and mechanisms", *Nanotoxicology*, vol. 1, no. 1, pp. 52-71.

van den Berg, R. A., Hoefsloot, H. C. J., Westerhuis, J. A., Smilde, A. K. and van der Werf, M. J. (2006), "Centering, scaling, and transformations: Improving the biological information content of metabolomics data", *BMC Genomics*, vol. 7.

van Gaal, E. V. B., Spierenburg, G., Hennink, W. E., Crommelin, D. J. A. and Mastrobattista, E. (2010), "Flow cytometry for rapid size determination and sorting of nucleic acid containing nanoparticles in biological fluids", *Journal of Controlled Release*, vol. 141, no. 3, pp. 328-338.

van Meerloo, J., Kaspers, G. J. and Cloos, J. (2011), "Cell sensitivity assays: the MTT assay.", *Methods in molecular biology (Clifton, N.J.)*, vol. 731, pp. 237-245.

Vergoulis, T., Vlachos, I. S., Alexiou, P., Georgakilas, G., Maragkakis, M., Reczko, M., Gerangelos, S., Koziris, N., Theodore, D. and Hatzigeorgiou, A. G. (2012), "TarBase 6.0: Capturing the exponential growth of miRNA targets with experimental support", *Nucleic acids research*, vol. 40, no. D1, pp. D222-D229.

Volokitin, Y., Sinzig, J., De Jongh, L. J., Schmidt, G., Vargaftik, M. N. and Moiseev, I. I. (1996), "Quantum-size effects in the thermodynamic properties of metallic nanoparticles", *Nature*, vol. 384, no. 6610, pp. 621-623.

Wacharawichanant, S., Thongyai, S., Phutthaphan, A. and Eiamsam-ang, C. (2008), "Effect of particle sizes of zinc oxide on mechanical, thermal and morphological

properties of polyoxymethylene/zinc oxide nanocomposites", *Polymer Testing*, vol. 27, no. 8, pp. 971-976.

Wallace, W. E., Keane, M. J., Murray, D. K., Chisholm, W. P., Maynard, A. D. and Ong, T. -. (2007), "Phospholipid lung surfactant and nanoparticle surface toxicity: Lessons from diesel soots and silicate dusts", *Journal of Nanoparticle Research*, vol. 9, no. 1, pp. 23-38.

Wang, F., Gao, F., Lan, M., Yuan, H., Huang, Y. and Liu, J. (2009), "Oxidative stress contributes to silica nanoparticle-induced cytotoxicity in human embryonic kidney cells", *Toxicology in Vitro*, vol. 23, no. 5, pp. 808-815.

Wang, L., Wang, L., Ding, W. and Zhang, F. (2010), "Acute toxicity of ferric oxide and zinc oxide nanoparticles in rats", *Journal of Nanoscience and Nanotechnology*, vol. 10, no. 12, pp. 8617-8624.

Wang, X., Li, Q., Xie, J., Jin, Z., Wang, J., Li, Y., Jiang, K. and Fan, S. (2009), "Fabrication of ultralong and electrically uniform single-walled carbon nanotubes on clean substrates", *Nano Letters*, vol. 9, no. 9, pp. 3137-3141.

Warheit, D. B. (2001), "Inhaled amorphous silica particulates: What do we know about their toxicological profiles?", *Journal of Environmental Pathology, Toxicology and Oncology*, vol. 20, no. SUPPL. 1, pp. 133-141.

Witten, D., Tibshirani, R., Gu, S. G., Fire, A. and Lui, W. (2010), "Ultra-high throughput sequencing-based small RNA discovery and discrete statistical biomarker analysis in a collection of cervical tumours and matched controls", *BMC Biology*, vol. 8.

Wittmaack, K. (2011), "Novel dose metric for apparent cytotoxicity effects generated by in vitro cell exposure to silica nanoparticles", *Chemical research in toxicology*, vol. 24, no. 2, pp. 150-158.

Wold, S., Esbensen, K. and Geladi, P. (1987), "Principal component analysis", *Chemometrics and Intelligent Laboratory Systems*, vol. 2, no. 1-3, pp. 37-52.

Woodrow Wilson International Centre for Scholars (2010), *The Nanotechnology Consumer Inventory*, available at: http://www.nanotechproject.org/inventories/consumer/ (accessed 2/23).

Wottrich, R., Diabaté, S. and Krug, H. F. (2004), "Biological effects of ultrafine model particles in human macrophages and epithelial cells in mono- and co-culture", *International journal of hygiene and environmental health*, vol. 207, no. 4, pp. 353-361.

Wu, F., Zhu, S., Ding, Y., Beck, W. T. and Mo, Y. -. (2009a), "MicroRNA-mediated regulation of Ubc9 expression in cancer cells", *Clinical Cancer Research,* vol. 15, no. 5, pp. 1550-1557.

Wu, H., Zhu, S. and Mo, Y. -. (2009b), "Suppression of cell growth and invasion by miR-205 in breast cancer", *Cell research,* vol. 19, no. 4, pp. 439-448.

Xie, G., Sun, J., ZhonG., G., Shi, L. and ZhanG., D. (2010), "Biodistribution and toxicity of intravenously administered silica nanoparticles in mice", *Archives of Toxicology,* vol. 84, no. 3, pp. 183-190.

Yamawaki, H. and Iwai, N. (2006), "Cytotoxicity of water-soluble fullerene in vascular endothelial cells", *American Journal of Physiology - Cell Physiology,* vol. 290, no. 6, pp. C1495-C1502.

Yan, G., Huang, Y., Bu, Q., Lv, L., Deng, P., Zhou, J., Wang, Y., Yang, Y., Liu, Q., Cen, X. and Zhao, Y. (2012), "Zinc oxide nanoparticles cause nephrotoxicity and kidney metabolism alterations in rats", *Journal of Environmental Science and Health - Part A Toxic/Hazardous Substances and Environmental Engineering,* vol. 47, no. 4, pp. 577-588.

Yang, A., Cardona, D. L. and Barile, F. A. (2002), "In vitro cytotoxicity testing with fluorescence-based assays in cultured human lung and dermal cells", *Cell biology and toxicology,* vol. 18, no. 2, pp. 97-108.

Yokel, R. A., Lasley, S. M. and Dorman, D. C. (2006), "The speciation of metals in mammals influences their toxicokinetics and toxicodynamics and therefore human health risk assessment", *Journal of Toxicology and Environmental Health - Part B: Critical Reviews,* vol. 9, no. 1, pp. 63-85.

Yokoi, T. and Nakajima, M., (2013), *MicroRNAs as mediators of drug toxicity*.

Yu, K. O., Grabinski, C. M., Schrand, A. M., Murdock, R. C., Wang, W., Gu, B., Schlager, J. J. and Hussain, S. M. (2009), "Toxicity of amorphous silica nanoparticles in mouse keratinocytes", *Journal of Nanoparticle Research,* vol. 11, no. 1, pp. 15-24.

Zhang, H., Kong, X., Kang, J., Su, J., Li, Y., Zhong, J. and Sun, L. (2009), "Oxidative stress induces parallel autophagy and mitochondria dysfunction in human glioma U251 cells", *Toxicological Sciences,* vol. 110, no. 2, pp. 376-388.

Zhang, S., Zhou, J., Zhang, Z., Du, Z., Vorontsov, A. V. and Jin, Z. (2000), "Morphological structure and physicochemical properties of nanotube TiO_2", *Chinese Science Bulletin,* vol. 45, no. 16, pp. 1533-1536.

Zheng, J. P., Wang, C. Z., Wang, X. X., Wang, H. Y., Zhuang, H. and Yao, K. D. (2007), "Preparation of biomimetic three-dimensional gelatin/montmorillonite-

chitosan scaffold for tissue engineering", *Reactive and Functional Polymers*, vol. 67, no. 9, pp. 780-788.

Zhu, H., Irfan, A., Sachse, S. and Njuguna, J., (2012), *Assessment of nanoparticle release and associated health effect of polymer-silicon composites*.

Zhuang, H., Zheng, J. P., Gao, H. and De Yao, K. (2007), "In vitro biodegradation and biocompatibility of gelatin/montmorillonite- chitosan intercalated nanocomposite", *Journal of Materials Science: Materials in Medicine*, vol. 18, no. 5, pp. 951-957.

Zokaei, S., Motamedi, P. and Bagheri, R. (2012), "A new polypropylene/clay nanocomposite for replacement of engineering plastics in automotive application", Vol. 1, pp. 102.

DISSEMINATION

Journal articles

Irfan, A., Sachse, S., Njuguna, J., Pielichowski, K., Silva, K. and Zhu, H. (2013), "Assessment of Nanoparticle Release from Polyamide 6- and Polypropylene-Silicon Composites and Cytotoxicity in Human Lung A549 Cells", *Journal of Inorganic and Organometallic Polymers and Materials*, vol. 23.

Sachse, S., Irfan, A., Zhu, H. and Njuguna, J. (2011), "Morphology studies of nanodust generated from polyurethane/nanoclay nanofoams following mechanical fracture", *Journal of Nanostructured Polymers and Nanocomposites*, vol. 7, no. 1, pp. 5-9.

Sachse, S., Silva, F., Zhu, H., Irfan, A., Leszczyńska, A., Pielichowski, K., Ermini, V., Blazquez, M., Kuzmenko, O. and Njuguna, J. (2012), "The effect of nanoclay on dust generation during drilling of PA6 nanocomposites", *Journal of Nanomaterials*, vol. 2012.

Oral presentations

Irfan, A., Sachse, S., Njuguna, J. and Zhu, H., (2010a), *Assessment of nanoparticle release from nanoproducts and their toxicity potential in human lung A549 cells*, 1st ed., Cranfield, Gloucester.

Irfan, A., Sachse, S., Njuguna, J. and Zhu, H., (2011c), *In vitro toxicological evaluation of engineered nanoparticles*, 1st ed., Cranfield, Gloucester

Irfan, A., Sachse, S., Njuguna, J. and Zhu, H. (2012), "Assessment of release and toxicity of nanoparticles from polymer-silicon composites in a life cycle perspective", pp. 315.

Abstracts and posters

Irfan, A., Sachse, S., Njuguna, J. and Zhu, H., (2010b), *In vitro hazard identification and characterization of manufactured nanoparticles throughout products life cycle* , 1st ed., Air pollution conference by Institute of Environmental Health, Cranfield, UK.

Irfan, A., Sachse, S., Njuguna, J. and Zhu, H., (2010c), *In vitro Nanoparticle toxicity study-focusing on development of testing protocols*, 1st ed., NEPHH, Milan.

Irfan, A., Sachse, S., Njuguna, J. and Zhu, H., (2011d*) Assessment of nanoparticle release from nanoproducts and their toxicity potential in human lung A549 cells*, 1st ed., Royal Society, London.

Irfan, A., Sachse, S., Njuguna, J. and Zhu, H., (2010d), *Investigation of silica nanoparticle toxicity-toward standardization of NP toxicity test in vitro* , 1st ed., NEPHH, Milan.

Irfan, A., Sachse, S., Njuguna, J. and Zhu, H., (2011a), *In vitro analysis of nanoparticles and nanodust released, from polymer/nanostructured-material composite, during drilling process.*, 1st ed., Nano roadshow, Cranfield,UK.

Irfan, A., Sachse, S., Njuguna, J. and Zhu, H., (2011b), *In vitro hazard identification and characterization of manufactured nanomaterials throughout products life cycle*, 1st ed., Air pollution conference by Institute of Environmental Health, Cranfield, UK.

Zhu, H., Irfan, A., Sachse, S. and Njuguna, J., (2012), *Assessment of nanoparticle release and associated health effect of polymer-silicon composites*.

Appendix A

Human IL8 ELISA Kit for IL8 Human ELISA Kit (1 x 96 Well Plate)

Materials Required

- Distilled water.
- Pipettes : 5µl, 10 µl, 50 µl, 100 µl, 200 µl and 1000 µl.
- Vortex mixer and magnetic stirrer.

Procedural Notes/Lab, Quality Control:

1. When not in use, kit components should be stored refrigerated or frozen as indicated on the vials or bottles labels. All the reagents should be warmed to room temperature before use. Lyophilised standards should be discarded after use.
2. Once the desired number of strips have been removed, immediately reseal the bag to protect the remaining strips from degradation.
3. Cover or cap all reagents when not in use.
4. Do not mix or interchange reagents between different lots.
5. Do not use reagents beyond the expiration date of the kit.
6. Use a clean disposable plastic pipette tip for each reagent, standard, or specimen addition in order to avoid cross-contamination; for the dispensing of H_2SO_4 and substrate solution, avoid pipettes with metal parts.
7. Use a clean plastic container to prepare the washing solution.
8. Thoroughly mix the reagents and samples before use by agitation or swirling.
9. All residual washing liquid must be drained from the wells by efficient aspiration or by decantation followed by tapping the plate forcefully on absorbent paper. Never insert absorbent paper directly into the wells.
10. The TMB solution is light sensitive. Avoid prolonged exposure to light. Also, avoid contact of the TMB solution with metal to prevent colour development. Warning TMB is toxic avoid direct contact with hands. Dispose off properly.
11. If a dark blue colour develops within a few minutes after preparation, this indicates that the TMB solution has been contaminated and must be discarded. Read absorbances within 1 hour after completion of the assay.
12. When pipetting reagents, maintain a consistent order of addition from well-to-well. This will ensure equal incubation times for all wells.
13. Respect incubation times described in the assay procedure.
14. Dispense the TMB solution within 15 min. following the washing of the microtiter plate.
15. Exposure to acids will inactivate the conjugate.
16. Substrate solutions must be at room temperature prior to use.

Specimen Collection, Processing and Storage:

- **Cell culture supernatants**
  Remove particulates and aggregates by spinning at approximately 1000 x g for 10 min.

- **Serum**
  Avoid any unintentional stimulation of the cells by the procedure. Use pyrogen/endotoxin free collecting tubes. Serum should be removed rapidly and carefully from the red cells after clotting. For that, after clotting, centrifuge at approximately 1000 x g for 10 min and remove serum.

- **Plasma**
  EDTA, citrate and heparin plasma can be assayed. Spin samples at 1000 x g for 30 min to remove particulates. Harvest plasma.

- **Storage**
  If not analyzed shortly after collection, samples should be aliquoted (250-500µl) to avoid freeze-thaw cycles and stored frozen at –70°C. Avoid multiple freeze-thaw cycles of frozen specimens.
  When possible, avoid use of badly hemolyzed or lipemic sera. If large amounts of particles are present, this should be removed prior to assay by centrifugation or filtration.

- **Recommendation** Do not thaw by heating at 37°C or 56°C. Thaw at room temperature and make sure that sample is completely thawed and homogeneous before assaying.

Reagent Preparation:

- **Standard Buffer Diluent**
  Add the content of the vial (X10) to 225 ml distilled water before use.

- **Standards**
  Depending on the type of samples you are assaying, the kit includes two standard diluents. Because biological fluids might contain proteases or cytokine-

binding proteins that could modify the recognition of the cytokine you want to measure, you should reconstitute standard vials with the most appropriate standard diluent.
For serum and plasma samples use **Standard Diluent: Human Serum** and for cell culture supernatants use **Standard Diluent Buffer**. Reconstitute IL8 Standard by addition of appropriate diluent. Reconstitute volume is stated on the label of the standard vial. This reconstitution produces a stock solution of 2000 pg/ml IL8. Allow standard to stand for 5 minutes with gentle swirling prior to making dilutions. Serial dilutions of standard must be made before each assay and cannot be stored.

- **Controls**
  Freeze-dried control vials should also be reconstituted with the most appropriate standard diluent to your samples. For serum and plasma samples use **Standard Diluent: Human Serum** and for cell culture supernatants use **Standard Diluent Buffer**. Controls have to be reconstituted with the volume of standard buffer diluent indicated on the vial. Reconstitution of the freeze-dried material with the indicated volume, will give a solution for which the IL8 concentration is stated on the vial. Allow control to stand for 5 minutes with gentle swirling prior to distribution to control wells. Do not store after use.

- **Dilution of biotinylated anti-IL8**
  Preparation immediately before use is recommended. Dilute the biotinylated anti-IL8 with the biotinylated antibody diluent in a clean glass vial according to the number of wells to be used. See the next table for volumes to pipette.

Number of Strips	Biotinylated Antibody (µl)	Biotinylated Antibody Diluent (µl)
2	40	1060
3	60	1590
4	80	2120
6	120	3180

12	240	6360

- **Dilution of Streptavidin-HRP**
  Add 0.5 ml of HRP diluent to a 5 µl vial of Streptavidin-HRP. DO NOT KEEP THIS DILUTION FOR FURTHER EXPERIMENTS. Dilute immediately before use. Make further dilutions with HRP-Diluent in a clean glass vial as needed according to the following table:

Number of Strips	Streptavidin-HRP (µl)	Strep-HRP Diluent (ml)
2	30	2
3	45	3
4	60	4
6	75	5
12	150	10

- **Washing Buffer 200x Concentrate**
  Dilute 200 times in distilled water.
  Pour entire contents (10 ml) of the Washing Buffer Concentrate into a clean 2,000 ml graduated cylinder. Bring final volume to 2,000 ml with glass-distilled or deionized water. Mix gently to avoid foaming. Transfer to a clean wash bottle and store at 2° to 25°C. Washing Buffer may be prepared as needed according to the following table:

Number of Strips	Washing Buffer Concentrate (ml)	Distilled Water (ml)

1-6	5	995
1-12	10	1,990

Assay Protocol:

1. Before use, mix all reagents thoroughly without making any foam.

2. Determine the number of microwell strips required to test the desired number of samples, plus appropriate number of wells needed for running blanks and standards.
   Please note: Each sample, standard, blank and optional control samples should be assayed in duplicate. Remove sufficient microwell strips from the pouch.

3. Add 100 µl of appropriate standard diluent (see preparation of reagents) to standard wells B1, B2, C1, C2, D1, D2, E1, E2, F1, F2. Reconstitute standard vial with the appropriate volume as described under reagents preparation. Pipette 200 µl of standard into wells A1 and A2. Transfer 100 µl from A1 and A2 to B1 and B2 wells. Mix the contents by repeated aspirations and ejections. Take care not to scratch the inner surface of microwells. Repeat this procedure from the wells B1, B2 to wells C1, C2 and from wells C1, C2 to D1, D2 and so on creating two parallel rows of IL8 standard dilutions ranging from 2000 to 31.25 pg/ml. Discard 100 µl from the content of the last microwells used (F1, F2).

   Note: Alternatively these dilutions can be done in separate tube and diluted standard pipetted directly into wells.

4. Add 100 µl of appropriate standard diluent to the blank wells (G1-G2).

5. Add 100 µl of sample to sample wells and 100 µl of the reconstituted control vial to the control wells (H1,H2).

6. Preparation of biotinylated anti-IL8 : (see preparation of reagents).

7. Add 50 µl of diluted biotinylated anti-IL8 to all wells.

8. Cover with a plate cover and incubate for 1 hour at room temperature (18°C - 25°C).

9. Remove the cover and wash the plate as follows:
    a. aspirate the liquid from each well
    b. dispense 0.3 ml of washing solution into each well
    c. aspirate again the content of each well
    d. Repeat steps-b and c two times.

10. Prepare Streptavidin-HRP solution just before use: (see preparation of reagents).

11. Dispense 100 µl of Streptavidin-HRP solution into all wells, including the blank wells. Put back the cover.

12. Incubate the microwell strips at room temperature for 30 minutes.

13. Remove plate cover and empty wells. Wash microwell strips according to Step-9. Proceed immediately to the next step.

14. Pipette 100 µl of ready-to-use TMB substrate solution into all wells, including the blank wells and incubate in the dark for 12-15 minutes at room temperature. Avoid direct exposure to light by wrapping the plate in aluminium foil.

15. Incubation time of the substrate solution is usually determined by the ELISA reader performances: many ELISA readers record absorbance only up to 2.0 O.D. The O.D. values of the plate should be monitored and the substrate reaction stopped before positive wells are no longer properly readable (maximum 20 minutes).

16. The enzyme-substrate reaction is stopped by quickly pipetting 100 µl of H_2SO_4 : stop reagent into each well, including the blank wells, to completely and uniformly inactivate the enzyme. Results must be read immediately after the addition of H_2SO_4 : stop reagent.

17. Read absorbance of each well on a spectrophotometer using 450 nm as the primary wavelength and optionally 620 nm (610 nm to 650 nm is acceptable) as the reference wavelength.

Suggested Plate Scheme:

Standard Concentrations pg/ml	**Sample Wells**

	1	**2**	**3**	**4**	**5**	**6**	**7**	**8**	**9**	**10**	**11**	**12**
A	2000	2000										
B	1000	1000										
C	500	500										
D	250	250										
E	125	125										
F	62.5	62.5										

G	Blank	Blank										
H	CTRL	CTRL										

Limitations:

- Do not extrapolate the standard curve beyond the 2000 pg/ml standard curve point. The dose-response is non-linear in this region and good accuracy is difficult to obtain. Concentrated samples (> 2000 pg/ml) have to be diluted with standard diluent or with your own sample buffer. During analysis, multiply results by the appropriate dilution factor.

- The influence of various drugs, aberrant sera (hemolyzed, hyperlipidemic, jaundiced...) has not been investigated.

- The rate of degradation of native IL8 in various matrices has not been investigated.

Sensitivity:

- The minimum detectable dose of IL8 is less than 29 pg/ml

  This has been determined by adding 3 standard deviations to the mean optical density when the zero standard was assayed 34 times.

Intra-Assay					**Inter-Assay**				
Sample	**n**	**Mean(pg/mL)**	**SD**	**CV%**	**Sample**	**n**	**Mean(pg/mL)**	**SD**	**CV%**
A	8	1934	11.71	0.60	A	40	1977	39.21	1.96
B	8	267.3	5.35	2.0	B	40	249.9	15.34	6.13

Linearity of dilution

- A human serum pool containing 1000 pg/ml of measured IL8 was serially diluted in standard buffer diluent over the range of the assay. Linear regression of samples versus the expected concentration yielded a correlation coefficient of 0.99.

Normal Serum Values:

- On a panel of 32 human sera, 9 are below the detection level. 21 are ranged between 25 and 76 pg/ml with a mean level of 44 pg/ml.

Recovery:

- Recovery of IL8 added to pooled normal serum was 100% (84% to 114%) for IL8 concentration ranging from 2000 to 62.5 pg/ml.

Total procedure length: 1hr 45 min

Protocol revised: 24/02/09

Appendix B

May 2012

miScript® miRNA PCR Array Handbook

miScript II RT Kit
miScript SYBR® Green PCR Kit
miScript miRNA PCR Arrays
miScript miRNA QC PCR Array

For SYBR Green-based, real-time PCR profiling of microRNAs using pathway-focused arrays, HC arrays, and miRNome arrays

QIAGEN®

Sample & Assay Technologies

QIAGEN Sample and Assay Technologies

QIAGEN is the leading provider of innovative sample and assay technologies, enabling the isolation and detection of contents of any biological sample. Our advanced, high-quality products and services ensure success from sample to result.

QIAGEN sets standards in:

- Purification of DNA, RNA, and proteins
- Nucleic acid and protein assays
- microRNA research and RNAi
- Automation of sample and assay technologies

Our mission is to enable you to achieve outstanding success and breakthroughs. For more information, visit www.qiagen.com.

Contents

Kit Contents

miScript II RT Kit	**(12)**	**(50)**
Catalog no.	**218160**	**218161**
Number of standard reactions*	**12**	**50**
miScript Reverse Transcriptase Mix	24 µl	100 µl
10x miScript Nucleics Mix	50 µl	200 µl
5x miScript HiSpec Buffer	100 µl	400 µl
5x miScript HiFlex Buffer	100 µl	400 µl
RNase-Free Water	1.9 ml	1.9 ml
Quick-Start Protocol	1	1

* A standard reaction is 20 µl in volume with up to 2 µg total RNA (when using miScript HiSpec Buffer).

miScript SYBR Green PCR Kit	**(200)**	**(1000)**
Catalog no.	**218073**	**218075**
Number of 50 µl reactions	**200†**	**1000‡**
2x QuantiTect® SYBR Green PCR Master Mix, containing:	3 x 1.7 ml	25 ml
■ HotStarTaq® DNA Polymerase		
■ QuantiTect SYBR Green PCR Buffer		
■ dNTP mix, including dUTP		
■ SYBR Green I		
■ ROX™ passive reference dye		
■ 5 mM $MgCl_2$		
10x miScript Universal Primer	1 ml	5 x 1 ml
RNase-Free Water	2 x 2 ml	20 ml
Quick-Start Protocol	2	2

† Provides sufficient reagents for 4 x 96-well arrays (110 µl residual), 2 x 384-well pathway-focused arrays (1210 µl residual), 2 x 384-well HC/miRNome arrays (1510 µl residual), or 5 Rotor-Disc 100 arrays (110 µl residual). ‡ Provides sufficient reagents for 20 x 96-well arrays (0 µl residual), 12 x 384-well pathway-focused arrays (1100 µl residual), 13 x 384-well HC/miRNome arrays (850 µl residual), or 25 Rotor-Disc 100 arrays (0 µl residual).

Pathway-Focused miScript miRNA PCR Array							
Catalog no.	**Varies**						
Format	**A**	**C**	**D**	**E**	**F**	**G**	**R**
96-well plate containing dried assays	2, 12, or 24	2, 12, or 24	2, 12, or 24	–	2, 12, or 24	–	–
384-well plate containing dried assays	–	–	–	4	–	4	–
Rotor-Disc® 100 containing dried assays	–	–	–	–	–	–	2, 12, or 24
Optical Thin-Wall 8-Cap Strips (12 per plate)	24, 144, or 288	–	24, 144, or 288	–	–	–	–
Optical Adhesive Film (1 per plate)	–	2, 12, or 24	–	4	2, 12, or 24	4	–
384EZLoad Covers (1 set of 4 per plate)	–	–	–	4 sets	–	4 sets	–
Rotor-Disc Heat Sealing Film (1 per Rotor-Disc)	–	–	–	–	–	–	2, 12, or 24

miScript miRNA HC PCR Array		
Catalog no.	**Varies**	
Format	**E**	**G**
384-well plate containing dried assays	2, 12, or 24	2, 12, or 24
Optical Adhesive Film (1 per plate)	2, 12, or 24	2, 12, or 24

miRNome miScript miRNA PCR Array

Catalog no.	Varies						
Format	**A**	**C**	**D**	**E**	**F**	**G**	**R**
96-well plate containing dried assays	Varies	Varies	Varies	–	Varies	–	–
384-well plate containing dried assays	–	–	–	Varies	–	Varies	–
Rotor-Disc 100 containing dried assays	–	–	–	–	–	–	Varies
Optical Thin-Wall 8-Cap Strips (12 per plate)	Varies	–	Varies	–	–	–	–
Optical Adhesive Film (1 per plate)	–	Varies	–	Varies	Varies	Varies	–
Rotor-Disc Heat Sealing Film (1 per Rotor-Disc)	–	–	–	–	–	–	Varies

miScript miRNA QC PCR Array

Catalog no.	Varies						
Format	**A**	**C**	**D**	**E**	**F**	**G**	**R**
96-well plate containing dried assays	1	1	1	–	1	–	–
384-well plate containing dried assays	–	–	–	1	–	1	–
Rotor-Disc 100 containing dried assays	–	–	–	–	–	–	1
Optical Thin-Wall 8-Cap Strips	12	–	12	–	–	–	–
Optical Adhesive Film	–	1	–	1	1	1	–
Rotor-Disc Heat Sealing Film (1 per Rotor-Disc)	–	–	–	–	–	–	1

Cyclers for use with array formats

Format	Suitable real-time cyclers	Plate
A	Applied Biosystems® models 5700, 7000, 7300, 7500, 7700, 7900HT, ViiA™ 7 (96-well block); Bio-Rad® models iCycler®, iQ™5, MyiQ™, MyiQ2; Bio-Rad/MJ Research Chromo4™; Eppendorf® Mastercycler® ep realplex models 2, 2S, 4, 4S; Stratagene® models Mx3005P®, Mx3000P®; Takara TP-800	96-well
C	Applied Biosystems models 7500 (Fast block), 7900HT (Fast block), StepOnePlus™, ViiA 7 (Fast block)	96-well
D	Bio-Rad CFX96™; Bio-Rad/MJ Research models DNA Engine Opticon®, DNA Engine Opticon 2; Stratagene Mx4000®	96-well
E	Applied Biosystems models 7900HT (384-well block), ViiA 7 (384-well block); Bio-Rad CFX384™	384-well
F	Roche® LightCycler® 480 (96-well block)	96-well
G	Roche LightCycler 480 (384-well block)	384-well
R	Rotor-Gene® Q; Rotor-Gene 6000; other Rotor-Gene cyclers	Rotor-Disc 100

Shipping and Storage

The miScript II RT Kit and miScript SYBR Green PCR Kit are shipped on dry ice. The kits, including all reagents and buffers, should be stored immediately upon receipt at –20°C in a constant-temperature freezer.

miScript miRNA PCR Arrays and miScript miRNA QC PCR Arrays are shipped at ambient temperature, on ice, or on dry ice depending on the destination and accompanying products. Upon receipt, store at –20 °C. If stored under these conditions, miScript miRNA PCR Arrays and miScript miRNA QC PCR Arrays are stable for 6 months after receipt.

Intended Use

The miScript II RT Kit, miScript SYBR Green PCR Kit, miScript miRNA PCR Arrays and miScript miRNA QC PCR Array are intended for molecular biology applications. These products are not intended for the diagnosis, prevention, or treatment of a disease.

All due care and attention should be exercised in the handling of the products. We recommend all users of QIAGEN® products to adhere to the NIH guidelines that have been developed for recombinant DNA experiments, or to other applicable guidelines.

Safety Information

When working with chemicals, always wear a suitable lab coat, disposable gloves, and protective goggles. For more information, please consult the appropriate material safety data sheets (MSDSs). These are available online in convenient and compact PDF format at www.qiagen.com/Support/MSDS.aspx where you can find, view, and print the MSDS for each QIAGEN kit and kit component.

24-hour emergency information

Emergency medical information in English, French, and German can be obtained 24 hours a day from:

Poison Information Center Mainz, Germany

Tel: +49-6131-19240

Quality Control

In accordance with QIAGEN's ISO-certified Quality Management System, each lot of miScript II RT Kit and miScript SYBR Green PCR Kit is tested against predetermined specifications to ensure consistent product quality.

Introduction

The miScript PCR System consists of the miScript II RT Kit, miScript PreAMP PCR Kit, miScript miRNA PCR Array, miScript Primer Assay, miScript SYBR Green PCR Kit, and miScript miRNA PCR Array data analysis tool. The miScript PCR System allows sensitive and specific detection and quantification of microRNA (miRNA). The miScript PCR System uses total RNA that contains miRNA as the starting material for cDNA synthesis, and separate enrichment of small RNA is not needed. A single cDNA preparation can be used with a miScript miRNA PCR Array to rapidly profile the expression of mature miRNAs.

miScript miRNA PCR Arrays are mature miRNA-specific forward primers (miScript Primer Assays) that have been arrayed in biologically relevant pathway-focused and whole miRNome panels. These PCR arrays are provided in ready-to-use 384-well plate, 96-well plate, and 100-well Rotor-Disc formats. miScript miRNA PCR Arrays, which are available for several species, provide guaranteed high performance and are fully customizable. Each assay in a miScript miRNA PCR Array has been verified to ensure sensitive and specific detection of mature miRNA by real-time PCR. A free, Web-based miScript miRNA PCR Array data analysis tool simplifies the analysis of real-time PCR data. Once raw threshold cycle (C_T) data has been uploaded, the tool automatically performs all fold-change calculations using the $\Delta\Delta C_T$ method of relative quantification, and presents the results in several formats. Mature miRNome expression profiling is now within reach of every laboratory because of the ease, convenience, and consistent performance of miScript miRNA PCR Arrays. miScript miRNA PCR Arrays are at the forefront of real-time PCR-based mature miRNA profiling tools.

miScript miRNA PCR Array workflow

Prepare reverse-transcription reaction

Incubate at 37°C for 60 min, then at 95°C for 5 min

Prepare PCR mix

Add PCR mix to miScript miRNA PCR Array

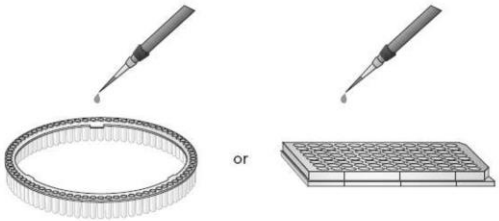

Perform real-time PCR

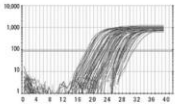

Analyze results using miScript miRNA PCR Array data analysis tool

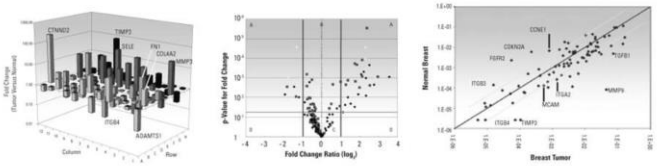

miScript II RT Kit

The expanded miScript II RT Kit includes miScript Reverse Transcriptase Mix, 10x miScript Nucleics Mix, 5x miScript HiSpec Buffer, and 5x miScript HiFlex Buffer. miScript Reverse Transcriptase Mix is an optimized blend of poly(A) polymerase and reverse transcriptase. 10x miScript Nucleics Mix contains dNTPs, rATP, oligo-dT primers, and an internal synthetic RNA control (miRNA reverse transcription control [miRTC]) that is used to assess reverse transcription performance during profiling experiments with miScript miRNA PCR Arrays. Two buffers, 5x miScript HiSpec Buffer and 5x miScript HiFlex Buffer, are provided in the miScript II RT Kit to meet the distinctive needs of miRNA quantification studies using real-time PCR (Figure 1). The unique, patent-pending formulation of 5x miScript HiSpec Buffer facilitates the selective conversion of mature miRNAs into cDNA, which can then be used for miRNA quantification with either miScript miRNA PCR Arrays or miScript Primer Assays. Using miScript HiSpec Buffer, the conversion of long RNAs, such as mRNAs, is suppressed. As a result, background signals potentially contributed by long RNAs are nonexistent, making a reverse-transcription reaction buffered using miScript HiSpec Buffer highly suitable for profiling the expression of mature miRNAs. **Only 5x miScript HiSpec Buffer should be used to prepare cDNA for real-time PCR with miScript miRNA PCR Arrays.** For protocols using miScript Primer Assays, refer to the ***miScript PCR System Handbook***. If working with samples that contain low amounts of RNA, 5x miScript HiSpec Buffer should also be used to prepare cDNA for preamplification with the miScript PreAMP PCR Kit. For protocols using the miScript PreAMP PCR Kit, refer to the ***miScript PreAMP Handbook***.

5x miScript HiFlex Buffer promotes conversion of all RNA species (mature miRNA, precursor miRNA, other noncoding RNA, and mRNA) into cDNA, and this cDNA can then be used to quantify each RNA species (using appropriate primer assays). **Do not use 5x miScript HiFlex Buffer to prepare cDNA for real-time PCR with miScript miRNA PCR Arrays.** For protocols using miScript HiFlex Buffer, refer to the ***miScript PCR System Handbook***.

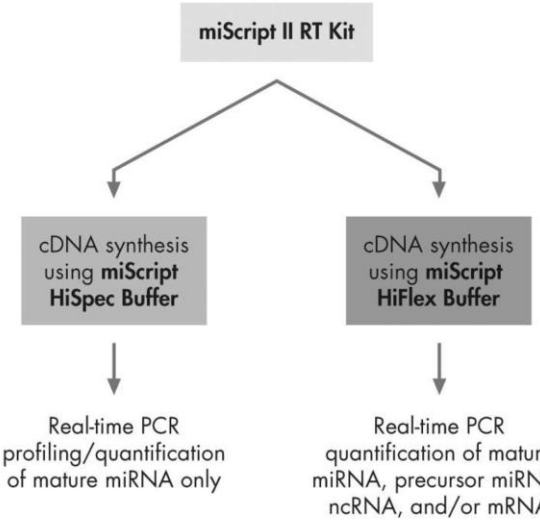

Figure 1. Mature miRNA, precursor miRNA, other noncoding RNA, and mRNA detection. Two buffers are provided with the miScript II RT Kit. Use miScript HiSpec Buffer for cDNA synthesis to enable either mature miRNA profiling (using miScript miRNA PCR Arrays) or mature miRNA quantification (using individual miScript Primer Assays). For protocols using miScript HiSpec Buffer in combination with miScript Primer Assays, refer to the *miScript PCR System Handbook*. If samples being assessed have low RNA content, miScript HiSpec Buffer should be used to prepare cDNA for preamplification with the miScript PreAMP PCR Kit. For protocols using the miScript PreAMP PCR Kit, refer to the *miScript PreAMP Handbook*. Use miScript HiFlex Buffer for cDNA synthesis to enable quantification of mature miRNA, precursor miRNA, other noncoding RNA (ncRNA), and/or mRNA from the same cDNA (using appropriate primer assays). For protocols using miScript HiFlex Buffer, refer to the *miScript PCR System Handbook*. Only 5x miScript HiSpec Buffer should be used to prepare cDNA for real-time PCR with miScript miRNA PCR Arrays.

Principle and procedure

Mature miRNAs are naturally occurring, 22-nucleotide, noncoding RNAs that mediate posttranscriptional gene regulation. Unlike mRNAs, miRNAs are not polyadenylated in nature.

Reverse transcription using miScript HiSpec Buffer

When reverse-transcription reactions are performed in miScript HiSpec Buffer, mature miRNAs and certain small nucleolar RNAs and small nuclear RNAs (snoRNAs and snRNAs, see "Controls in miScript miRNA PCR Arrays and miScript miRNA QC PCR Arrays", page 21) are selectively converted into cDNA. The conversion of long RNAs, such as mRNAs, is suppressed. Mature miRNAs

are polyadenylated by poly(A) polymerase and reverse transcribed into cDNA using oligo-dT primers (Figure 2). Polyadenylation and reverse transcription are performed in parallel in the same tube. The oligo-dT primers have a 3' degenerate anchor and a universal tag sequence on the 5' end, allowing amplification of mature miRNA in the real-time PCR step. miScript miRNA PCR Arrays, used in combination with the miScript SYBR Green PCR Kit, enable quantification of mature miRNA by real-time PCR. The combination of polyadenylation and the universal tag addition ensures that miScript miRNA PCR Arrays do not detect genomic DNA.

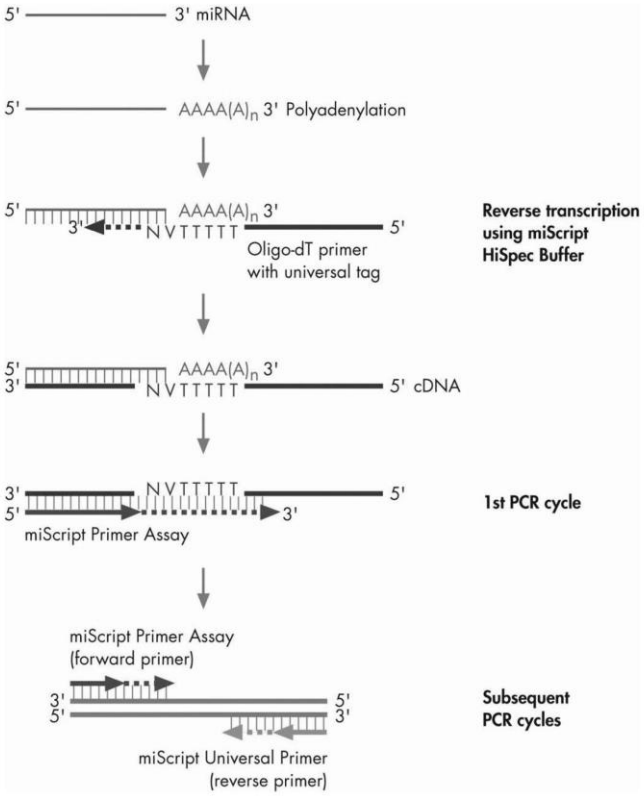

Figure 2. Conversion of mature miRNAs into cDNA and subsequent detection. In a reverse-transcription reaction using miScript HiSpec Buffer, mature miRNAs are polyadenylated by poly(A) polymerase and subsequently converted into cDNA by reverse transcriptase with oligo-dT priming. The cDNA is then used for real-time PCR profiling of mature miRNA expression (using a miScript miRNA PCR Array and the miScript Universal Primer).

Optional cDNA preamplification using miScript PreAMP PCR Kit

The miScript PreAMP PCR Kit enables researchers to perform miRNA profiling experiments using very limited amounts of starting RNA. This is particularly important when working with samples such as body fluids, formalin-fixed, paraffin-embedded (FFPE) samples, and small cell number samples such as laser capture microdissection (LCM) samples, flow-sorted cells, circulating tumor cells, and fine needle biopsies, where the low RNA yields obtained are often insufficient for reliable miRNA profiling experiments.

The miScript PreAMP PCR Kit, in combination with miScript PreAMP Primer Mixes, uses highly multiplex, PCR-based preamplification of up to 400 miRNA-specific cDNA targets in one reaction. This breakthrough technology enables accurate and comprehensive miRNome-wide expression analysis with as little as 10 ng total RNA. For more information, refer to the *miScript PreAMP Handbook* or visit www.qiagen.com/miRNA.

Mature miRNA expression profiling using miScript miRNA PCR Arrays

cDNA prepared in a reverse-transcription reaction using miScript HiSpec Buffer serves as the template for real-time PCR analysis using a miScript miRNA PCR Array (which contains miRNA-specific miScript Primer Assays) and the miScript SYBR Green Kit, which contains the miScript Universal Primer (reverse primer) and QuantiTect SYBR Green PCR Master Mix. To profile mature miRNA expression, a premix of cDNA, miScript Universal Primer, QuantiTect SYBR Green PCR Master Mix, and RNase-free water is added to a miScript miRNA PCR Array.

miScript miRNA PCR Array plate layout

miScript miRNA PCR Arrays are available in 96-well, 384-well, and Rotor-Disc 100 formats (Figures 3–6). Each array contains several control assays. The purpose of each control is described on page 21.

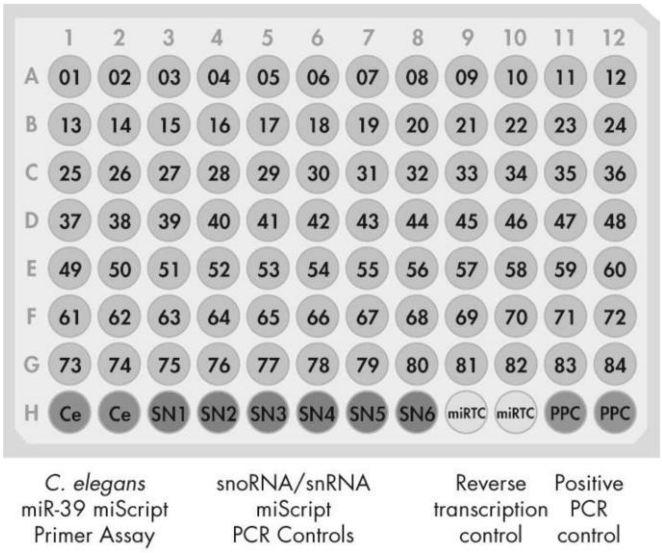

Figure 3. Pathway-Focused or miRNome miScript miRNA PCR Array layout for plate formats A, C, D, F. Wells A1 to G12 (**1–84**) each contain a miScript Primer Assay for a pathway/disease/functionally related mature miRNA. Wells H1 and H2 contain replicate *C. elegans* miR-39 miScript Primer Assays that can be used as an alternative normalizer for array data (**Ce**). Wells H3 to H8 each contain an assay for a different snoRNA/snRNA that can be used as a normalization control for the array data (**SN1**=SNORD61 assay, **SN2**=SNORD68 assay, **SN3**=SNORD72 assay, **SN4**=SNORD95 assay, **SN5**=SNORD96A assay, **SN6**=RNU6B/RNU6-2 assay). Wells H9 and H10 contain replicate miRTC miScript Primer Assays (**miRTC**). Wells H11 and H12 contain replicate positive PCR controls (**PPC**).

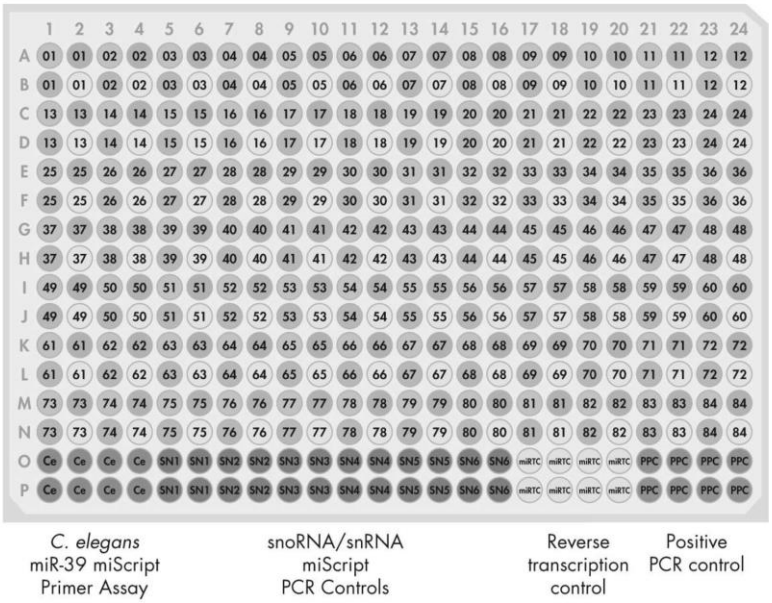

Figure 4. Pathway-Focused miScript miRNA PCR Array layout for plate formats E, G. Pathway-Focused miScript miRNA PCR Arrays in formats E and G include 4 replicates of the same assays as provided in the 96-well format shown in Figure 3.

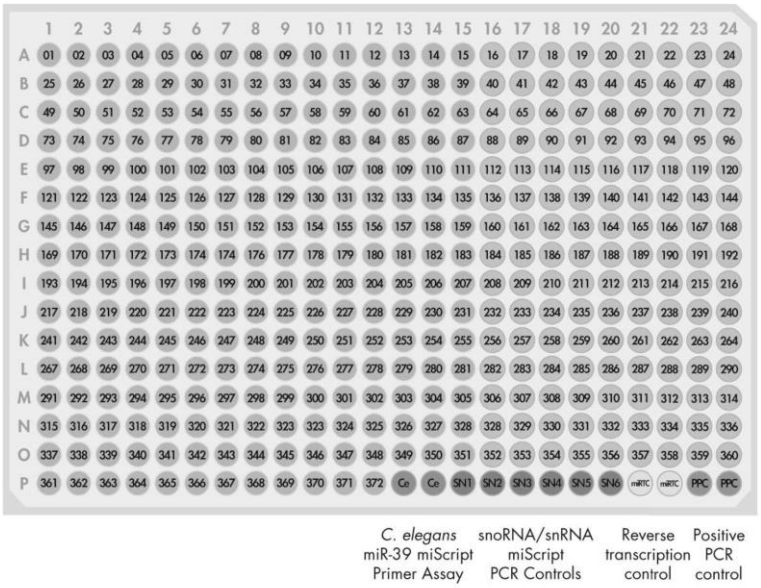

Figure 5. miRNome miScript miRNA PCR Array and miScript miRNA HC PCR Array layout for plate formats E, G. Wells A1 to P12 (**1–372**) each contain a miScript Primer Assay for a miRNome or pathway/disease/ functionally related mature miRNA. Wells P13 and P14 contain replicate *C. elegans* miR-39 miScript Primer Assays that can be used as an alternative normalizer for array data (**Ce**). Wells P15 to P20 each contain an assay for a different snoRNA/snRNA that can be used as a normalization control for the array data (**SN1** = SNORD61 assay, **SN2** = SNORD68 assay, **SN3** = SNORD72 assay, **SN4** = SNORD95 assay, **SN5** = SNORD96A assay, **SN6** = RNU6B/RNU6-2 assay). Wells P21 and P22 contain replicate miRTC miScript Primer Assays (**miRTC**). Wells P23 and P24 contain replicate positive PCR controls (**PPC**).

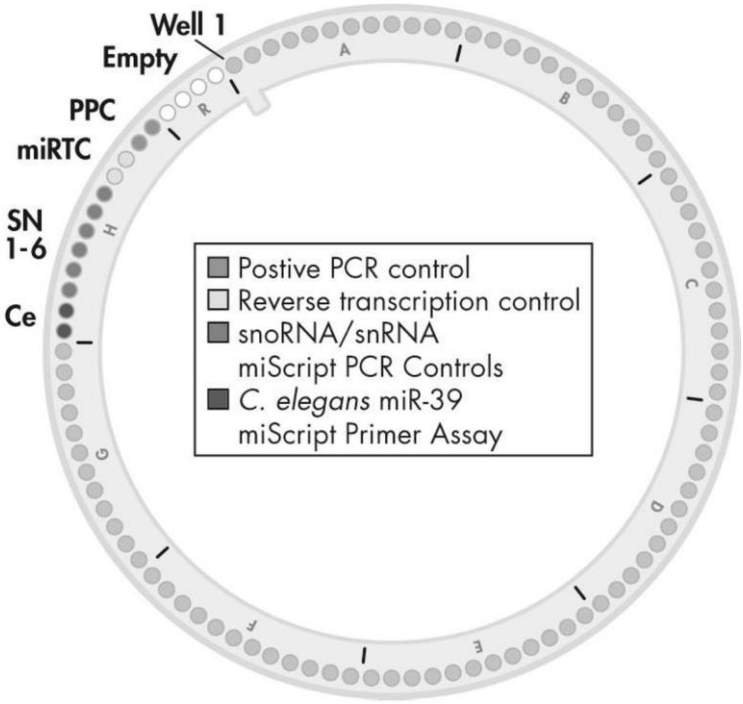

Figure 6. miScript miRNA PCR Array layout for Rotor-Disc format R. Wells 1 to 84 each contain a miScript Primer Assay for a pathway/disease/functionally related gene. Wells 85 and 86 contain replicate *C. elegans* miR-39 miScript Primer Assays that can be used as an alternative normalizer for array data (**Ce**). Wells 87 to 92 each contain an assay for a different snoRNA/snRNA that can be used as a normalization control for the array data (**SN1**=SNORD61 assay, **SN2**=SNORD68 assay, **SN3**=SNORD72 assay, **SN4**=SNORD95 assay, **SN5**=SNORD96A assay, **SN6**=RNU6B/RNU6-2 assay). Wells 93 and 94 contain replicate miRTC miScript Primer Assays (**miRTC**). Wells 95 and 96 contain replicate positive PCR controls (**PPC**). Wells 97–100 are empty.

miScript miRNA QC PCR Array plate layout

miScript miRNA QC PCR Arrays enable assessment of the quality of multiple cDNA samples using real-time PCR. miScript miRNA QC PCR Arrays are available in 96-well, 384-well, and Rotor-Disc 100 formats (Figures 7–9). The purpose of each control is described on page 21. The 96-well plate and Rotor-Disc 100 formats allow quality control of up to 8 cDNA samples. The 384-well format allows quality control of up to 32 cDNA samples.

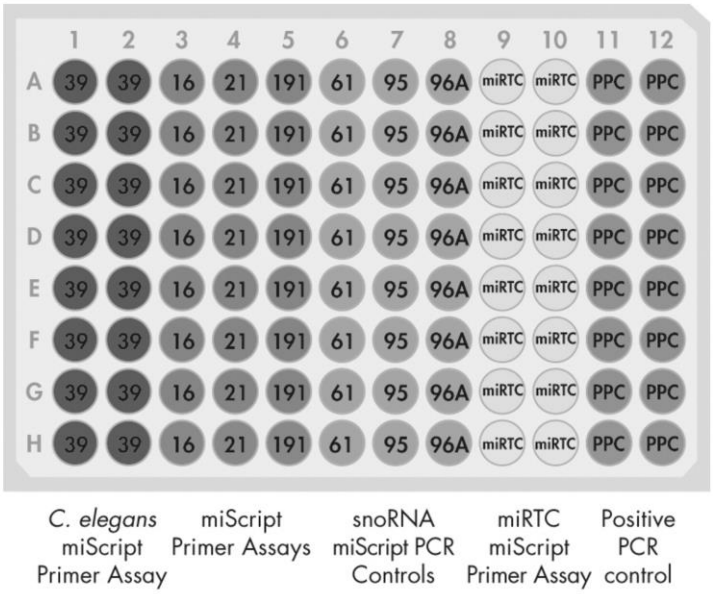

Figure 7. miScript miRNA QC PCR Array layout for plate formats A, C, D, F. Wells 1 and 2 of each row contain replicate *C. elegans* miR-39 miScript Primer Assays (**39**). Well 3 of each row contains a miR-16 miScript Primer Assay (**16**). Well 4 of each row contains a miR-21 miScript Primer Assay (**21**). Well 5 of each row contains a miR-191 miScript Primer Assay (**191**). Wells 6 to 8 of each row each contain an assay for a different snoRNA (**61** = SNORD61 assay, **95** = SNORD95 assay, **96A** = SNORD96A assay). Wells 9 and 10 of each row contain replicate miRTC miScript Primer Assays (**miRTC**). Wells 11 and 12 of each row contain replicate positive PCR controls (**PPC**). These formats enable the quality assessment of up to 8 cDNA samples.

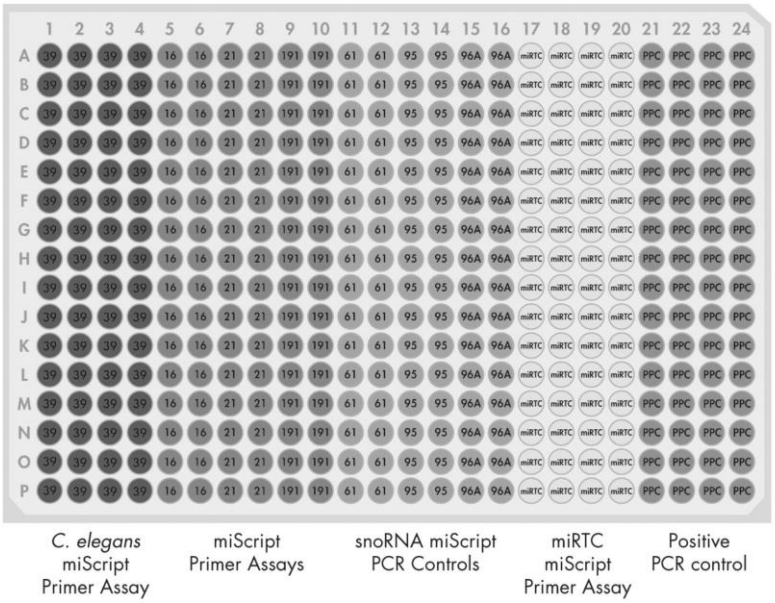

Figure 8. miScript miRNA QC PCR Array layout for plate formats E and G. Wells 1 to 4 of each row contain replicate *C. elegans* miR-39 miScript Primer Assays (**39**). Wells 5 and 6 of each row contain replicate miR-16 miScript Primer Assays (**16**). Wells 7 and 8 of each row contain replicate miR-21 miScript Primer Assays (**21**). Wells 9 and 10 of each row contain replicate miR-191 miScript Primer Assays (**191**). Wells 11 to 16 of each row contain assays for different snoRNAs (**61** = SNORD61 assay, **95** = SNORD95 assay, **96A** = SNORD96A assay). Wells 17 to 20 of each row contain replicate miRTC miScript Primer Assays (**miRTC**). Wells 21 to 24 of each row contain replicate positive PCR controls (**PPC**). These formats enable the quality assessment of up to 32 cDNA samples.

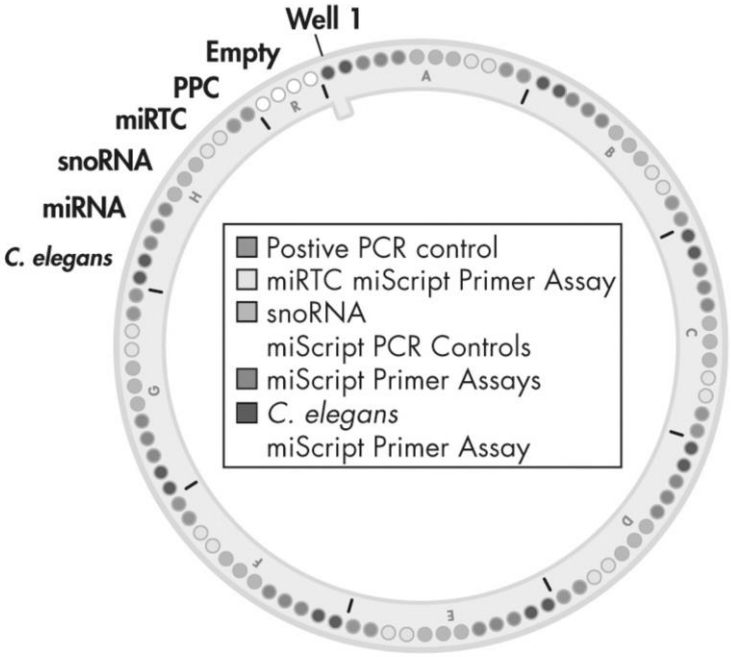

Figure 9. miScript miRNA QC PCR Array layout for Rotor-Disc format R. Wells 1 and 2 contain replicate *C. elegans* miR-39 miScript Primer Assays. Well 3 contains a miR-16 miScript Primer Assay. Well 4 contains a miR-21 miScript Primer Assay. Well 5 contains a miR-191 miScript Primer Assay. Wells 6 to 8 each contain an assay for a different snoRNA (Well 6 = SNORD61 assay, Well 7 = SNORD95 assay, Well 8 = SNORD96A assay). Wells 9 and 10 contain replicate miRTC miScript Primer Assays (**miRTC**). Wells 11 and 12 contain replicate positive PCR controls (**PPC**). This pattern is repeated 7 additional times from wells 13 to 96. Wells 97 to 100 are empty. This format enables the quality assessment of up to 8 cDNA samples.

Controls in miScript miRNA PCR Arrays and miScript miRNA QC PCR Arrays

The final 12 wells of each miScript miRNA PCR Array contain controls. The purpose of the controls in miScript miRNA PCR Arrays and the miScript miRNA QC PCR Array is detailed below and in Table 1.

Table 1. Controls in each miScript miRNA PCR Array

Control	Purpose
C. elegans miR-39 miScript Primer Assay	Alternative data normalization using exogenously spiked Syn-cel-miR-39 miScript miRNA Mimic
3 mature miRNA miScript Primer Assays (miR-16, miR-21, miR-191)*	Ubiquitously expressed mature miRNAs
6 snoRNA/snRNA miScript PCR Controls: SNORD61 assay SNORD95 assay SNORD96A assay SNORD68 assay† SNORD72 assay† RNU6B/RNU6-2 assay†	Data normalization using the $\Delta\Delta C_T$ method of relative quantification
miRNA reverse transcription control (miRTC miScript Primer Assay)	Assessment of reverse transcription performance
Positive PCR control (PPC)	Assessment of PCR performance

* Only included on miScript miRNA QC PCR Array.

† Only included on Pathway-Focused miScript miRNA PCR Array, miRNome miScript miRNA PCR Array, and miScript miRNA HC PCR Array.

The miScript Primer Assay for *C. elegans* miR-39 detects the miRNeasy Serum/Plasma Spike-In Control (cat. no. 219610), (also called Syn-cel-miR-39 miScript miRNA Mimic [cat. no. MSY0000010]), which is a *C. elegans* miR-39 mimic. This mimic can be added to samples, particularly serum or plasma samples, to control for variations during the preparation of total RNA and subsequent steps. After purification, real-time RT-PCR detection of the miRNeasy Serum/Plasma Spike-In Control can be performed and these results can then be used for normalization of real-time RT-PCR results for endogenous miRNAs in the sample. For more information on the use of the miRNeasy Serum/Plasma Spike-In Control, see the *miRNeasy Serum/Plasma Handbook*.

The miScript Primer Assays for miR-16, miR-21, and miR-191 are included in the miScript miRNA QC PCR Array since their targeted miRNAs are ubiquitously expressed in a wide range of cells, tissues, and body fluid samples (including whole blood, serum, and plasma). This is in contrast to the snoRNA/snRNA miScript PCR Controls whose intended targets are typically only expressed in

cells, tissues, and whole blood samples. In addition, the sequences for these mature miRNAs are conserved across a wide range of species, including all species currently supported by miScript miRNA PCR Arrays. These benefits make the miScript Primer Assays for miR-16, miR-21, and miR-191 ideal for sample quality assessment.

For accurate and reproducible results in miRNA quantification by real-time PCR, it is necessary to normalize the amount of target miRNA by using a suitable endogenous reference RNA. This approach is known as relative quantification. Normalization corrects for factors that could otherwise lead to inaccurate quantification. These factors include variation in quantity of input RNA, possible RNA degradation or presence of inhibitors in the RNA samples, and differences in sample handling. Normalization also allows results from different experiments and samples to be compared directly. miScript PCR Controls are primers designed to quantify a panel of 5 snoRNAs (SNORD61, SNORD68, SNORD72, SNORD95, and SNORD96A) and the snRNA RNU6B (RNU6-2). These controls take into consideration sequence homologies in human, mouse, rat, dog, and rhesus macaque so that the same controls can be used for all 4 species. In addition, these small RNAs have been verified to have relatively stable expression levels across tissues and cell types. As a result, miScript PCR Controls serve as normalization controls for relative quantification using the miScript PCR System. All the controls have amplification efficiencies close to 100%. For more information and to view data, visit www.qiagen.com/miRNAControls.

The miRTC miScript Primer Assay is an assay that assesses the performance of a reverse-transcription reaction using the miScript II RT Kit by detecting template synthesized from the kit's built-in miRNA reverse transcription control RNA (miRTC). This control monitors for any variables that may inhibit the reverse transcription reaction.

The positive PCR control (PPC) wells contain a predispensed artificial DNA sequence and the assay that detects it. This control monitors for any variables that may inhibit the PCR reaction.

Data analysis

Free data analysis software for each miScript miRNA PCR Array is available at http://pcrdataanalysis.sabiosciences.com/mirna. At this Web page, both the miScript miRNA PCR Array Web-based software and the miScript miRNA PCR Array Data Analysis Excel® Template can be accessed. Both tools will automatically perform quantification using the $\Delta\Delta C_T$ method of relative quantification and interpretation of the control assays (for more details, see page 35). Results are presented in a tabular format, a scatter plot, a three-dimensional profile, and a volcano plot (when replicates are included).

Template RNA requirements

Total RNA containing miRNA is the required starting material for miScript miRNA PCR Arrays. It is not necessary to enrich for small RNA. QIAGEN provides a range of solutions for purification of total RNA including miRNA (Table 2).

Table 2. Kits for purification of RNA including miRNA

Kit	Cat. no.	Starting material
miRNeasy Micro Kit	217084	Small amounts of cells and tissues
miRNeasy Mini Kit	217004	Animal/human tissues and cells
miRNeasy 96 Kit	217061	Animal/human tissues and cells
miRNeasy Serum/Plasma Kit	217184	Animal and human plasma and serum
miRNeasy FFPE Kit	217504	FFPE tissue samples
PAXgene® Tissue miRNA Kit	766134	Animal/human tissues that have been fixed and stabilized in PAXgene Tissue Containers
PAXgene Blood miRNA Kit	763134	Human blood that has been stabilized in PAXgene Blood RNA Tubes

Equipment and Reagents to Be Supplied by User

When working with chemicals, always wear a suitable lab coat, disposable gloves, and protective goggles. For more information, consult the appropriate material safety data sheets (MSDSs), available from the product supplier.

For reverse transcription

- Thin-walled, DNase-free, RNase-free PCR tubes (for 20 µl reactions)
- Ice
- Thermal cycler, heating blocks, or water baths (capable of reaching 95°C)
- Microcentrifuge

For quantitative, real-time PCR

- Real-time PCR cycler; the table on page 7 shows the appropriate real-time cycler for each array format
- Multichannel pipettor
- Nuclease-free pipet tips and tubes

Protocol: Reverse Transcription for Quantitative, Real-Time PCR

Important points before starting

- The miScript II RT Kit includes 2 buffers: 5x miScript HiSpec Buffer and 5x miScript HiFlex Buffer. Only 5x miScript HiSpec Buffer should be used to prepare cDNA for mature miRNA profiling using Pathway-Focused or miRNome miScript miRNA PCR Arrays or miScript miRNA HC PCR Arrays.
- **IMPORTANT**: **Only miScript HiSpec Buffer should be used to prepare cDNA for real-time PCR with miScript miRNA PCR Arrays.**
- **IMPORTANT**: **Do not use miScript HiFlex Buffer to prepare cDNA for real-time PCR with miScript miRNA PCR Arrays.**
- **IMPORTANT**: **If performing a reverse-transcription reaction for use with the miScript PreAMP PCR Kit, refer to the reverse-transcription protocol in the *miScript PreAMP Handbook*.**
- Total RNA containing miRNA should be used as starting material. For RNA purification recommendations, see page 24. This protocol is for use with up to 2 µg quantifiable RNA or up to 9 µl RNA prepared from 100–200 µl serum or plasma using the *miRNeasy Serum/Plasma Kit*. If using higher RNA amounts, scale up the reaction linearly. Recommended starting amounts are shown in Table 3. If working with RNA for the first time, read Appendix B (page 52).
- If an miRNA-enriched fraction has been prepared separate from larger RNAs (e.g., using the miRNeasy Mini Kit), use one-tenth the recommended RNA input for total RNA. For example, if 125–250 ng total RNA is recommended for use with a Pathway-Focused miScript miRNA PCR Array, use 12.5–25 ng miRNA-enriched fraction.
- Set up all reactions on ice to minimize the risk of RNA degradation.
- Do not vortex template RNA or any of the components of the miScript II RT Kit.

Table 3. Recommended RNA starting amounts and buffers for reverse-transcription reactions

PCR application	Assay	Buffer	Recommended RNA input*
Pathway profiling of mature miRNA	Pathway-Focused miScript miRNA PCR Arrays	5x miScript HiSpec Buffer	125–250 ng per RNA sample†
High-content pathway profiling of mature miRNA	miScript miRNA HC PCR Arrays	5x miScript HiSpec Buffer	250–500 ng per RNA sample†
Whole miRNome profiling of mature miRNA	miRNome miScript miRNA PCR Arrays	5x miScript HiSpec Buffer	250–500 ng per 384-well plate or per 4 x 96-well plates/ Rotor-Discs (the number of plates provided in a miRNome miScript miRNA PCR Array varies depending on the species of interest)‡§

* If the RNA sample is not limiting, use the upper amount of the recommended range.

† If RNA was prepared from 100–200 µl serum or plasma using the miRNeasy Serum/Plasma Kit, we recommend using 1.5 µl RNA prep (approximately one-tenth final eluate) per miScript miRNA PCR Array.

‡ If RNA was prepared from 100–200 µl serum or plasma using the miRNeasy Serum/Plasma Kit, we recommend using 1.5 µl RNA prep (approximately one-tenth final eluate) per 384-well plate or per 4 x 96-well plates/Rotor-Discs.

§ Depending on the RNA starting amount, a single reverse-transcription reaction can provide sufficient cDNA for 8 x 384-well plates or 32 x 96-well plates/Rotor-Discs.

Procedure

1. **Thaw template RNA on ice. Thaw RNase-free water, 10x miScript Nucleics Mix and 5x miScript HiSpec Buffer at room temperature (15–25°C).**

   Mix each solution by flicking the tubes. Centrifuge briefly to collect residual liquid from the sides of the tubes and then store on ice.

2. **Prepare the reverse-transcription reaction on ice according to Table 4.**

Gently mix and then store on ice. The reverse-transcription master mix contains all components required for first-strand cDNA synthesis except template RNA.

Note: miScript Reverse Transcriptase Mix should be removed from the –20°C freezer just before preparation of the master mix, gently mixed, and placed on ice. It should be returned to the freezer immediately after use.

Note: If setting up more than one reaction, prepare a volume of master mix 10% greater than that required for the total number of reactions to be performed.

Table 4. Reverse-transcription reaction components

Component	Volume/reaction
5x miScript HiSpec Buffer	4 µl
10x miScript Nucleics Mix	2 µl
RNase-free water	Variable
miScript Reverse Transcriptase Mix	2 µl
Template RNA (added in step 3)	Variable (see Table 3 for recommendations)*
Total volume	**20 µl**

* If RNA was prepared from 100–200 µl serum or plasma using the miRNeasy Serum/Plasma Kit, up to 9 µl RNA prep can be added to the reverse-transcription reaction (sufficient for 6 x 384-well plates or 24 x 96-well plates/Rotor-Discs).

3. **Add template RNA to each tube containing reverse-transcription master mix. Gently mix, briefly centrifuge, and then store on ice.**
4. **Incubate for 60 min at 37°C.**
5. **Incubate for 5 min at 95°C to inactivate miScript Reverse Transcriptase Mix and place on ice.**
6. **Dilute the cDNA in RNase-free water according to Table 5, and proceed with real-time PCR immediately.**

   If you wish to store the reverse-transcription reactions prior to real-time PCR, transfer the undiluted cDNA to a –20°C freezer, or dispense the diluted cDNA into 110 µl aliquots and transfer them to a –20°C freezer.

Table 5. cDNA dilution prior to PCR

PCR application	Array	Reaction dilution
Pathway profiling	Pathway-Focused miScript miRNA PCR Arrays	Add 200 µl RNase-free water to each 20 µl reverse-transcription reaction
High-content pathway profiling	miScript miRNA HC PCR Arrays	Add 90 µl RNase-free water to each 20 µl reverse-transcription reaction
Whole miRNome profiling	miRNome miScript miRNA PCR Arrays	Dilution depends on the number of plates/Rotor-Discs in the miRNome miScript miRNA PCR Array: For 1 x 384-well plate or 4 x 96-well plates/Rotor-Discs: add 90 µl RNase-free water to the 20 µl reverse-transcription reaction For 2 x 384-well plate or 8 x 96-well plates/Rotor-Discs: add 200 µl RNase-free water to the 20 µl reverse-transcription reaction For 3 x 384-well plate or 12 x 96-well plates/Rotor-Discs: add 310 µl RNase-free water to the 20 µl reverse-transcription reaction For 4 x 384-well plate or 16 x 96-well plates/Rotor-Discs: add 420 µl RNase-free water to the 20 µl reverse-transcription reaction

Protocol: Real-Time PCR for Mature miRNA Expression Profiling

cDNA prepared using the miScript II RT Kit with miScript HiSpec Buffer (with optional preamplification, if required, using the miScript PreAMP PCR Kit) is the appropriate starting material for this protocol. This protocol enables real-time PCR profiling of mature miRNA using miScript miRNA PCR Arrays in combination with the miScript SYBR Green PCR Kit, which contains the miScript Universal Primer (reverse primer) and QuantiTect SYBR Green PCR Master Mix.

Important points before starting

- The PCR must start with an **initial incubation step of 15 minutes at 95°C** to activate HotStarTaq DNA Polymerase (included in 2x QuantiTect SYBR Green PCR Master Mix).
- **IMPORTANT**: **Only miScript HiSpec Buffer should be used to prepare cDNA for real-time PCR with miScript miRNA PCR Arrays.**
- **IMPORTANT**: **Do not use miScript HiFlex Buffer to prepare cDNA for real-time PCR with miScript miRNA PCR Arrays.**
- Ensure that the 20 µl cDNA synthesis reaction has been diluted appropriately. See Table 5 for recommendations. If cDNA has been preamplified using the miScript PreAMP PCR Kit with a miScript PreAMP Primer Mix, see the *miScript PreAMP Handbook* for dilution recommendations.
- Do not vortex template cDNA or any of the components of the miScript SYBR Green PCR Kit.
- The standard miScript miRNA PCR Array reaction volumes are 10 µl per well for a 384-well plate, 25 µl per well for a 96-well plate, and 20 µl per well for a 100-well Rotor-Disc.
- The miScript SYBR Green PCR Kit (200) provides sufficient reagents for 4 x 96-well arrays (110 µl residual), 2 x 384-well pathway arrays (1210 µl residual), 2 x 384-well HC/miRNome arrays (1510 µl residual), or 5 Rotor-Disc 100 arrays (110 µl residual). The miScript SYBR Green PCR Kit (1000) provides sufficient reagents for 20 x 96-well arrays (0 µl residual), 12 x 384-well pathway arrays (1100 µl residual), 13 x 384-well HC/miRNome arrays (850 µl residual), or 25 Rotor-Disc 100 arrays (0 µl residual).
- If using the iCycler iQ, iQ5, or MyiQ, well factors must be collected at the beginning of each experiment. Well factors are used to compensate for any system or pipetting nonuniformity. For details, refer to the user manual supplied with the instrument or *Technical Information: Using QuantiTect SYBR Green Kits on Bio-Rad cyclers* available at www.qiagen.com.

- The miScript miRNA QC PCR Array can be used to assess the quality of cDNA samples prior to running a miScript miRNA PCR Array (see protocol, page 39).

Procedure

1. **Thaw 2x QuantiTect SYBR Green PCR Master Mix, 10x miScript Universal Primer, template cDNA, and RNase-free water at room temperature (15–25°C). Mix the individual solutions.**
2. **Prepare a reaction mix according to either Table 6 (for a Pathway-Focused miScript miRNA PCR Array) or Table 7 (for a miRNome miScript miRNA PCR Array). Mix thoroughly but gently.**

   Due to the hot start, it is not necessary to keep samples on ice during reaction setup or while programming the real-time cycler.

Table 6. Reaction mix for Pathway-Focused miScript miRNA PCR Arrays

Array format: Component	384-well (4 x 96) Formats E, G*	96-well Formats A, C, D, F	Rotor-Disc 100 Format R
2x QuantiTect SYBR Green PCR Master Mix†	550 µl	1375 µl	1100 µl
10x miScript Universal Primer	110 µl	275 µl	220 µl
RNase-free water	340 µl	1000 µl	780 µl
Template cDNA‡	100 µl	100 µl	100 µl
Total volume	**1100 µl**	**2750 µl**	**2200 µl**

* Volumes shown are sufficient for one cDNA template. In total, 4 cDNA templates can be analyzed on one 384-well Pathway-Focused miScript miRNA PCR Array because assays are arrayed in quadruplicate (see Figure 4, page 16).

† No optimization of the Mg^{2+} concentration is required. The final Mg^{2+} concentration provided by 2x QuantiTect SYBR Green PCR Master Mix gives optimal results.

‡ Provides 0.5–1 ng cDNA per well.

Table 7. Reaction mix for miRNome miScript miRNA PCR Arrays* and miScript miRNA HC PCR Arrays†

Array format: Component	384-well Formats E, G	96-well Formats A, C, D, F	Rotor-Disc 100 Format R
2x QuantiTect SYBR Green PCR Master Mix‡	2050 µl	1375 µl	1100 µl
10x miScript Universal Primer	410 µl	275 µl	220 µl
RNase-free water	1540 µl	1075 µl	855 µl
Template cDNA§	100 µl	25 µl	25 µl
Total volume	**4100 µl**	**2750 µl**	**2200 µl**

* Volumes are for a single plate or Rotor-Disc associated with a miRNome set. The number of plates in a miRNome set vary depending on the species. Scale up volumes according to the number of plates/Rotor-Discs to be run. If the miRNome set contains a plate/Rotor-Disc that is less than half full, scale down volumes accordingly.

† For miScript miRNA HC PCR Arrays, use the volumes shown for 384-well, Formats E, G.

‡ No optimization of the Mg^{2+} concentration is required. The final Mg^{2+} concentration provided by 2x QuantiTect SYBR Green PCR Master Mix gives optimal results.

§ Provides 0.5–1 ng cDNA per well.

3. **Carefully remove the miScript miRNA PCR Array from its sealed bag.**
   Optional for 96-well and 384-well array formats: If the reaction mix is in a tube, transfer to a loading reservoir, such as the RT² PCR Array Loading Reservoir (cat. no. 338162).

4. **Add reaction mix to each well of the miScript miRNA PCR Array as follows.**
   Note: For 384-well and 96-well array formats, a multichannel pipettor can be used to add reaction mix to the array. For the Rotor-Disc 100 format, a repeater pipettor or a QIAgility® can be used to load the array.

   For 384-well miScript miRNA PCR Array: add 10 µl per well.
   For 96-well miScript miRNA PCR Array: add 25 µl per well.
   For Rotor-Disc miScript miRNA PCR Array: add 20 µl per well.

   Loading 384-well (4 x 96) Pathway-Focused miScript miRNA PCR Arrays:

   Note: Each Pathway-Focused miScript miRNA PCR Array contains 4 replicates of 96 assays that can be used for analysis of 4 samples. The

spacing between the tips of standard multichannel pipettors allows rows or columns to be skipped when adding each sample. Be sure to load each sample into the correct set of wells using a multichannel pipettor and the 384EZLoad Covers (provided). Use Figure 10 as a guide. Do not reuse 384EZLoad Covers.

- Place 384EZLoad Cover 1 (white) on the plate. Add 10 µl reaction mix for sample 1 to the open wells (odd number wells of rows A, C, E, G, I, K, M, and O). Remove and discard 384EZLoad Cover 1.
- Place 384EZLoad Cover 2 (yellow) on the plate. Add 10 µl reaction mix for sample 2 to the open wells (even number wells of rows A, C, E, G, I, K, M, and O). Remove and discard 384EZLoad Cover 2.
- Place 384EZLoad Cover 3 (black) on the plate. Add 10 µl reaction mix for sample 3 to the open wells (odd number wells of rows B, D, F, H, J, L, N, and P). Remove and discard 384EZLoad Cover 3.
- Place 384EZLoad Cover 4 (red) on the plate. Add 10 µl reaction mix for sample 4 to the open wells (even number wells of rows B, D, F, H, J, L, N, and P). Remove and discard 384EZLoad Cover 4.

Cover 1 (white) for sample 1

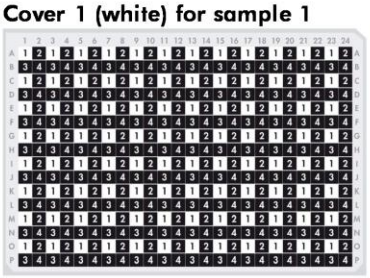

Cover 2 (yellow) for sample 2

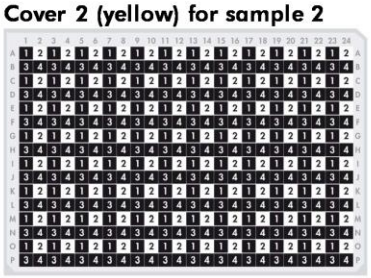

Cover 3 (black) for sample 3

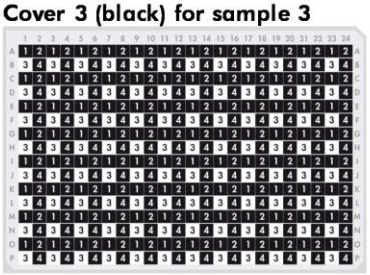

Cover 4 (red) for sample 4

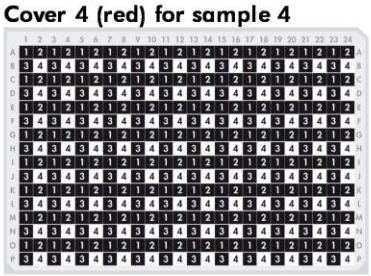

Figure 10. Loading Pathway-Focused miScript miRNA PCR Arrays, plate format E, G (384-well). Add 10 µl reaction mix for each of 4 samples into the staggered wells with the same number as indicated in the figure.

5. **Carefully, tightly seal the miScript miRNA PCR Array with Optical Thin-Wall 8-Cap Strips (Formats A and D), Optical Adhesive Film (Formats C, E, F, and G), or Rotor-Disc Heat-Sealing Film (Format R).**
6. **Centrifuge the PCR plate for 1 min at 1000 g at room temperature (15–25°C) to remove bubbles.**

   Note: This step is not necessary for reactions set up in Rotor-Discs.
7. **Program the real-time cycler according to Table 8.**

   Note: Perform dissociation curve analysis of the PCR product(s) to verify their specificity and identity. Dissociation curve analysis is an analysis step built into the software of real-time cyclers. Follow the instructions provided by the supplier.

Table 8. Cycling conditions for real-time PCR

Step	Time	Temperature	Additional comments
PCR Initial activation step	**15 min**	**95°C**	HotStarTaq DNA Polymerase is activated by this heating step.
3-step cycling:*†‡			
Denaturation	15 s	94°C	
Annealing	30 s	55°C	
Extension§	30 s	70°C	Perform fluorescence data collection.
Cycle number	40 cycles¶		Cycle number depends on the amount of template cDNA and abundance of the target.

* For Bio-Rad models CFX96 and CFX384: adjust the ramp rate to 1°C/s.

† For Eppendorf Mastercycler ep realplex models 2, 2S, 4, and 4S: for the Silver Thermoblock, adjust the ramp rate to 26%; for the Aluminum Thermoblock, adjust the ramp rate to 35%.

‡ If using a Roche LightCycler 480, adjust the ramp rate to 1°C/s.

§ Due to software requirements, the fluorescence detection step must be at least 30 s with the ABI PRISM® 7000 or 34 s with the Applied Biosystems 7300 and 7500.

¶ If using a Roche LightCycler 480, use 45 cycles.

8. **Place the plate/Rotor-Disc in the real-time cycler and start the cycling program.**
9. **Perform data analysis.**

Protocol: Data Analysis Using the $\Delta\Delta C_T$ Method of Relative Quantification for miScript miRNA PCR Arrays

This protocol describes the steps for analysis of data from miScript miRNA PCR Arrays. The first steps should be performed by the user. The later steps are performed by the free data analysis software. This data analysis software for miScript miRNA PCR Arrays is available at http://pcrdataanalysis.sabiosciences.com/mirna. Either the miScript miRNA PCR Array Web-based software or the miScript miRNA PCR Array Data Analysis Excel Template can be accessed. Both tools automatically perform quantification using the $\Delta\Delta C_T$ method of relative quantification and interpretation of the control wells. Results are presented in a tabular format, a scatter plot, a three-dimensional profile, and a volcano plot (when replicates are included).

If cDNA was preamplified using the miScript PreAMP PCR Kit with a miScript PreAMP Primer Mix, refer to the *miScript PreAMP Handbook* for a data analysis protocol.

Important point before starting

■ Text marked with a ■ denotes instructions for 96-well and 384-well plates (formats A, C, D, E, F, and G); text marked with a ▲ denotes instructions for 100-well Rotor-Discs (format R).

Procedure

Steps performed by the user

1. **Define the baseline.**

   The baseline is the noise level in early cycles, where there is no detectable increase in fluorescence due to PCR products.

   ■ Use the "Linear View" of the amplification plot to determine the earliest visible amplification. Set the baseline from cycle 2 to 2 cycles before the earliest visible amplification. Do not use greater than cycle 15. The number of cycles used to calculate the baseline can be changed and should be reduced if high template amounts are used. For more information regarding real-time PCR data output, refer to Appendix A, page 49.

   ▲ For the Rotor-Gene Q, we recommend using the "Dynamic Tube" setting along with the "Slope Correct" and/or "Ignore First" settings. For more information, refer to the *Rotor-Gene Q User Manual*.

   Note: Ensure that baseline settings are the same across all PCR runs associated with the same experiment to allow comparison of results.

2. **Define the threshold.**

   The threshold should be set using a logarithmic amplification plot so that the log-linear range of the curve can be easily identified. Using the "Log View" of the amplification plot, place the threshold above the background signal but within the lower half of the log-linear range of the amplification plot. The threshold should never be set in the plateau phase. The absolute position of the threshold is less critical than its consistent position across PCR runs.

   ■ Various PCR instruments (such as Applied Biosystems models 7500 and ViiA 7, and Stratagene models Mx3005P and Mx3000P) may require adjustment of the default "Manual C_T" threshold value of 0.2 to a lower value in order to analyze the data properly. Use a value of 0.02 as a starting point.

   ▲ For the Rotor-Gene Q, we recommend a C_T threshold value of approximately 0.02 in order to analyze the data properly.

   Note: Ensure that threshold settings are the same across all PCR runs in the same analysis to allow comparison of results.

3. **Export C_T values according to the manual supplied with the real-time PCR instrument.**
4. **Access the free data analysis tools at http://pcrdataanalysis.sabiosciences.com/mirna.**

   Choose either the Web-based software or the Excel template and follow the instructions provided.

Steps performed by data analysis software

5. **All C_T values reported ■ as greater than 35 or as N/A (not detected) are changed to 35 or ▲ as greater than 33 or as N/A (not detected) are changed to 33.**

   At this point, any C_T value equal to ■ 35 or ▲ 33 is considered a negative call.

6. **C_T values of the positive PCR control wells (PPC) are examined.**

   If the RNA sample is of high quality, the cycling program has been correctly run, and the thresholds have been correctly defined, the value of C_T^{PPC} should be ■ 19 ± 2 or ▲ 15 ± 2 across all arrays or samples.

7. **C_T values of the reverse transcription control (miRTC) are examined using the values for the positive PCR control (PPC) by calculating ΔC_T = AVG C_T^{miRTC} – AVG C_T^{PPC}.**

   If this value is less than 7, then no inhibition of the reverse-transcription reaction is apparent. No action is needed. If this value is greater than 7, there is evidence of impurities that may have inhibited the reverse transcription reaction. See the "Troubleshooting Guide", page 46.

Note: The ΔC_T = AVG C_T^{miRTC} – AVG C_T^{PPC} calculation is specific for Pathway-Focused miScript miRNA PCR Arrays. For miRNome miScript miRNA PCR Arrays, as the cDNA is divided among significantly more wells, a correction factor is introduced into the calculation according to the number of plates/Rotor-Discs that are being used. This corrects for the dilution of the miRTC. The calculation is performed as shown in Table 9.

Table 9. $\Delta C_T^{(miRTC-PPC)}$ calculation for miRNome miScript miRNA PCR Arrays and miScript miRNA HC PCR Arrays*

Number of plates/Rotor-Discs				
384-well	96-well	Rotor-Disc 100	Correction factor	$\Delta C_T^{(miRTC-PPC)}$ calculation
1	4	4	1.1	(AVG C_T^{miRTC} – 1.1) – (AVG C_T^{PPC})
2	8	8	2.1	(AVG C_T^{miRTC} – 2.1) – (AVG C_T^{PPC})
3	12	12	2.7	(AVG C_T^{miRTC} – 2.7) – (AVG C_T^{PPC})
4	16	16	3.1	(AVG C_T^{miRTC} – 3.1) – (AVG C_T^{PPC})

* For miScript miRNA HC PCR Arrays, use the calculation shown for 1 x 384-well plate.

8. **ΔC_T value for each mature miRNA profiled in the plate is calculated using the formula $\Delta C_T = C_T^{miRNA} - AVG\ C_T^{SN1/2/3/4/5/6}$.**
   Note: Choose an appropriate snoRNA/snRNA control for normalization. Six snoRNA/snRNA controls (SN1–6) are included on each array. Make sure that the selected controls are not influenced by the experimental conditions. If one or more snoRNA/snRNA have been previously independently identified and if the miScript miRNA PCR Array reproduces those results, use the average of their C_T values in the equation above. If an appropriate snoRNA/snRNA has not been previously identified, use the average C_T value of all the snoRNA/snRNA. When biological and/or technical replicates are performed, calculate the average ΔC_T value of each snoRNA/snRNA (each well) across those replicate arrays for each treatment group.
9. **$\Delta\Delta C_T$ for each miRNA across 2 miScript miRNA PCR Arrays or 2 samples is calculated using the formula: $\Delta\Delta C_T = \Delta C_T$ (sample 2) – ΔC_T (sample 1) where sample 1 is the control sample and sample 2 is the experimental sample.**
10. **Fold-change for each gene from sample 1 to sample 2 is calculated as $2^{(-\Delta\Delta CT)}$.**

Optional: If the fold-change is greater than 1, the result may be reported as a fold upregulation. If the fold-change is less than 1, the negative inverse of the result may be reported as a fold downregulation.

11. **Fold-changes are presented by the data analysis tool in a variety of formats, including a tabular format, a scatter plot, a three-dimensional profile, and a volcano plot (when replicates are included).**

Protocol: cDNA Quality Control Prior to Profiling Mature miRNA

Use of the miScript miRNA QC PCR Array enables testing of the quality of cDNA prepared using miScript HiSpec Buffer, saving time and reagents. Only 5 µl diluted cDNA sample is required for quality control using the miScript miRNA QC PCR Array. cDNA prepared using the miScript II RT Kit with miScript HiSpec Buffer is the appropriate starting material for this protocol. This protocol describes quality control of multiple cDNA samples using the miScript SYBR Green PCR Kit and miScript miRNA QC PCR Array prior to miRNA profiling using miScript miRNA PCR Arrays. In total, 32 cDNA samples can be analyzed on one 384-well miScript miRNA QC PCR Array, 8 cDNA samples can be analyzed on one 96-well miScript miRNA QC PCR Array, and 8 cDNA samples can be analyzed on one Rotor-Disc 100 miScript miRNA QC PCR Array.

If cDNA was preamplified using the miScript PreAMP PCR Kit with a miScript PreAMP Primer Mix, refer to the *miScript PreAMP Handbook* for a preamplification-specific, quality control protocol.

Important points before starting

- The PCR must start with an **initial incubation step of 15 minutes at 95°C** to activate HotStarTaq DNA Polymerase (included in 2x QuantiTect SYBR Green PCR Master Mix).
- Only cDNA template prepared using miScript HiSpec Buffer should be used with this protocol.
- Ensure cDNA samples were prepared according to the protocol on page 26, and that the 20 µl cDNA synthesis reaction has been diluted appropriately (see Table 5, page 29).
- Do not vortex template cDNA or any of the components of the miScript SYBR Green PCR Kit.
- The standard miScript miRNA PCR Array reaction volumes are 10 µl per well for a 384-well plate, 25 µl per well for a 96-well plate, and 20 µl per well for a 100-well Rotor-Disc.
- If using the iCycler iQ, iQ5, or MyiQ, well factors must be collected at the beginning of each experiment. Well factors are used to compensate for any system or pipetting nonuniformity. For details, refer to the user manual supplied with the instrument or *Technical Information: Using QuantiTect SYBR Green Kits on Bio-Rad cyclers* available at www.qiagen.com.

Procedure

1. **Thaw 2x QuantiTect SYBR Green PCR Master Mix, 10x miScript Universal Primer, template cDNA, and RNase-free water at room temperature (15–25°C). Mix the individual solutions.**
2. **Prepare a reaction mix according to Table 10. Mix gently and thoroughly.**

   Due to the hot start, it is not necessary to keep samples on ice during reaction setup or while programming the real-time cycler.

Table 10. Reaction mix for miScript miRNA QC PCR Arrays*

Array format: Component	384-well Formats E, G†	96-well Formats A, C, D, F†	Rotor-Disc 100 Format R†
2x QuantiTect SYBR Green PCR Master Mix‡	75 µl	175 µl	150 µl
10x miScript Universal Primer	15 µl	35 µl	30 µl
RNase-free water	55 µl	135 µl	115 µl
Template cDNA	5 µl	5 µl	5 µl
Total volume	**150 µl**	**350 µl**	**300 µl**

* These volumes provide a 10 µl per well reaction volume for a 384-well plate, 25 µl per well reaction volume for a 96-well plate, and 20 µl per well reaction volume for a 100-well Rotor-Disc.

† Volumes shown are sufficient for one cDNA template. In total, 8 cDNA samples can be analyzed on one 96-well miScript miRNA QC PCR Array, 8 cDNA samples can be analyzed on one Rotor-Disc 100 miScript miRNA QC PCR Array, and 32 cDNA samples can be analyzed on one 384-well miScript miRNA QC PCR Array.

‡ No optimization of the Mg^{2+} concentration is required. The final Mg^{2+} concentration provided by 2x QuantiTect SYBR Green PCR Master Mix gives optimal results.

3. **Carefully remove the miScript miRNA QC PCR Array from its sealed bag.**
4. **Add reaction mix to the wells of the miScript miRNA QC PCR Array as follows.**

   For 384-well miScript miRNA PCR Array: add 10 µl per well.
   For 96-well miScript miRNA PCR Array: add 25 µl per well.
   For Rotor-Disc 100 miScript miRNA PCR Array: add 20 µl per well.

5. **Carefully, tightly seal the miScript miRNA QC PCR Array with Optical Thin-Wall 8-Cap Strips (Formats A and D), Optical Adhesive Film (Formats C, E, F, and G), or Rotor-Disc Heat-Sealing Film (Format R).**
6. **Centrifuge the PCR plate for 1 min at 1000 *g* at room temperature (15–25°C) to remove bubbles.**

   Note: This step is not necessary for reactions set up in Rotor-Discs.
7. **Program the real-time cycler according to Table 11.**

   Note: Perform dissociation curve analysis of the PCR product(s) to verify their specificity and identity. Dissociation curve analysis is an analysis step built into the software of real-time cyclers. Follow the instructions provided by the supplier.

Table 11. Cycling conditions for real-time PCR

Step	Time	Temperature	Additional comments
PCR Initial activation step	**15 min**	**95°C**	HotStarTaq DNA Polymerase is activated by this heating step.
3-step cycling:*†‡			
Denaturation	15 s	94°C	
Annealing	30 s	55°C	
Extension§	30 s	70°C	Perform fluorescence data collection.
Cycle number	40 cycles¶		Cycle number depends on the amount of template cDNA and abundance of the target.

* For Bio-Rad models CFX96 and CFX384: adjust the ramp rate to 1°C/s.

† For Eppendorf Mastercycler ep realplex models 2, 2S, 4, and 4S: for the Silver Thermoblock, adjust the ramp rate to 26%; for the Aluminum Thermobock, adjust the ramp rate to 35%.

‡ If using a Roche LightCycler 480, adjust the ramp rate to 1°C/s.

§ Due to software requirements, the fluorescence detection step must be at least 30 s with the ABI PRISM 7000 or 34 s with the Applied Biosystems 7300 and 7500.

¶ If using a Roche LightCycler 480, use 45 cycles.

8. **Place the plate/Rotor-Disc in the real-time cycler and start the cycling program.**
9. **Perform data analysis.**

Protocol: Data Analysis for Quality Control Using miScript miRNA QC PCR Arrays

This protocol describes the steps for analysis of data from miScript miRNA QC PCR Arrays. The first steps should be performed by the user. The later steps are performed by the free data analysis software. A free miScript miRNA QC PCR Array Data Analysis Excel Template is available at http://pcrdataanalysis.sabiosciences.com/mirna. This tool provides a summary of the data from the miScript miRNA QC PCR Array and interprets the miRNA reverse transcription control and positive PCR control.

If cDNA was preamplified using the miScript PreAMP PCR Kit and a miScript PreAMP Primer Mix, refer to the *miScript PreAMP Handbook* for a data analysis protocol.

Important point before starting

- Text marked with a ■ denotes instructions for 96-well and 384-well plates (formats A, C, D, E, F, and G); text marked with a ▲ denotes instructions for 100-well Rotor-Discs (format R).

Procedure

Steps performed by the user

1. **Define the baseline.**

   The baseline is the noise level in early cycles, where there is no detectable increase in fluorescence due to PCR products.

   ■ Use the "Linear View" of the amplification plot to determine the earliest visible amplification. Set the baseline from cycle 2 to 2 cycles before the earliest visible amplification. Do not use greater than cycle 15. The number of cycles used to calculate the baseline can be changed and should be reduced if high template amounts are used. For more information regarding real-time PCR data output, refer to Appendix A, page 49.

   ▲ For the Rotor-Gene Q, we recommend using the "Dynamic Tube" setting along with the "Slope Correct" and/or "Ignore First" settings. For more information, refer to the *Rotor-Gene Q User Manual*.

   Note: Ensure that baseline settings are the same across all PCR runs in the same analysis to allow comparison of results.

2. **Define the threshold.**

   The threshold should be set using a logarithmic amplification plot so that the log-linear range of the curve can be easily identified. Using the "Log View" of the amplification plot, place the threshold above the background signal but within the lower half of the log-linear range of the amplification plot. The threshold should never be set in the plateau phase. The absolute

position of the threshold is less critical than its consistent position across PCR runs.

■ Various PCR instruments (such as Applied Biosystems models 7500 and ViiA 7, and Stratagene models Mx3005P and Mx3000P) may require adjustment of the default "Manual C_T" threshold value of 0.2 to a lower value in order to analyze the data properly. Use a value of 0.02 as a starting point.

▲ For the Rotor-Gene Q, we recommend a C_T threshold value of approximately 0.02 in order to analyze the data properly.

Note: Ensure that threshold settings are the same across all PCR runs in the same analysis to allow comparison of results.

3. **Export C_T values according to the manual supplied with the real-time PCR instrument.**
4. **Access the free data analysis tools at http://pcrdataanalysis.sabiosciences.com/mirna.**
   Follow the instructions provided in the Excel template.

Steps performed by data analysis Excel template

5. **All C_T values reported ■ as greater than 35 or as N/A (not detected) are changed to 35 or ▲ as greater than 33 or as N/A (not detected) are changed to 33.**
   At this point, any C_T value equal to ■ 35 or ▲ 33 is considered a negative call.
6. **C_T values of the positive PCR control wells (PPC) are examined.**
   If the RNA sample is of high quality, the cycling program has been correctly run, and the thresholds have been correctly defined, the value of C_T^{PPC} should be ■ 19 ± 2 or ▲ 15 ± 2 across all arrays or samples.
7. **C_T values of the reverse transcription control (miRTC) are examined using the values for the positive PCR control (PPC) by calculating ΔC_T = AVG C_T^{miRTC} – AVG C_T^{PPC} – correction factor.**
   If this value is less than 7, then no inhibition of the reverse-transcription reaction is apparent. No action is needed. If this value is greater than 7, there is evidence of impurities that may have inhibited the reverse transcription reaction. See the "Troubleshooting Guide", page 46.

   Note: As the cDNA will be divided among different numbers of wells in the downstream experiment, a correction factor is introduced into the calculation according to the number of plates/Rotor-Discs that will used. This corrects for the dilution of the miRTC. The calculation is performed as shown in Table 12.

Table 12. $\Delta C_T^{(miRTC\ -PPC)}$ calculations for miScript miRNA QC PCR Arrays

Intended use of cDNA	Correction factor	$\Delta C_T^{(miRTC\ -PPC)}$ calculation
Pathway-Focused miScript miRNA PCR Array	1.5	(AVG C_T^{miRTC} – 1.5) – (AVG C_T^{PPC})
miScript miRNA HC PCR Array	0.5	(AVG C_T^{miRTC} – 0.5) – (AVG C_T^{PPC})
Whole miRNome: 1 x 384-well plate or 4 x 96-well plates/Rotor-Discs	0.5	(AVG C_T^{miRTC} – 0.5) – (AVG C_T^{PPC})
Whole miRNome: 2 x 384-well plate or 8 x 96-well plates/Rotor-Discs	1.5	(AVG C_T^{miRTC} – 1.5) – (AVG C_T^{PPC})
Whole miRNome: 3 x 384-well plate or 12 x 96-well plates/Rotor-Discs	2.0	(AVG C_T^{miRTC} – 2.0) – (AVG C_T^{PPC})
Whole miRNome: 4 x 384-well plate or 16 x 96-well plates/Rotor-Discs	2.5	(AVG C_T^{miRTC} – 2.5) – (AVG C_T^{PPC})

8. **C_T values of the miScript Primer Assays for miR-16, miR-21, and miR-191 are examined.**

   Note: Mature miRNAs miR-16, miR-21, and miR-191 are ubiquitously expressed in a wide range of cells, tissues, and body fluid samples (including whole blood, serum, and plasma).

9. **C_T values of the miScript PCR Controls for SNORD61, SNORD95, and SNORD96A are examined.**

   Note: These small RNAs have been verified to have relatively stable expression levels across tissues and cell types. Nevertheless, snoRNA/snRNA control C_T values remain sample dependent and should be checked to determine whether their expression is consistent across the samples that are being analyzed. In particular, snoRNAs and long noncoding RNAs are usually not present in serum, plasma, urine, and other body fluids. If the expression of a particular control is not consistent across experimental

samples, that control should not be used for data normalization. For examples of C_T values associated with various tissue types, refer to the miScript PCR Controls application data at www.qiagen.com/miRNAControls.

10. **C. *elegans* miR-39 miScript Primer Assay C_T values (Ce) are examined.**
    The C. *elegans* miR-39 miScript Primer Assay should only result in C_T values above the threshold if the miRNeasy Serum/Plasma Spike-In Control (Syn-cel-miR-39 miScript miRNA Mimic) has been spiked in to the sample prior to RNA purification. For more information, see the *miRNeasy Serum/Plasma Handbook*.
11. **If all criteria described above are met, cDNA samples are of sufficient quality for analysis. Proceed with miScript miRNA PCR Array experiments.**

Troubleshooting Guide

This troubleshooting guide may be helpful in solving any problems that may arise. For more information, see also the Frequently Asked Questions page at our Technical Support Center: www.qiagen.com/FAQ/FAQList.aspx. The scientists in QIAGEN Technical Services are always happy to answer any questions you may have about either the information and protocols in this handbook or sample and assay technologies (for contact information, see back cover or visit www.qiagen.com).

	Comments and suggestions
Evidence of poor reverse transcription efficiency (value of AVG C_T^{miRTC} – AVG C_T^{PPC} > 7)	
a) Poor quality RNA	Check the A_{260}:A_{280} and A_{260}:A_{230} ratios of the RNA samples. Be sure to perform the dilutions for spectrophotometry in RNase-free 10 mM Tris·Cl, pH 7.5. If necessary, repurify RNA with a spin-column based clean up method, such as the miRNeasy Mini Kit (cat. no. 217004).
b) Calculation did not include correction factor	If using miRNome miScript miRNA PCR Arrays, miScript miRNA HC PCR Arrays, or miScript miRNA QC PCR Arrays, be sure to include the correction factors detailed in Table 9, page 37 or Table 12, page 44.
Evidence of poor, overall PCR amplification efficiency (AVG C_T^{PPC} varies by more than 2 across arrays and/or is greater than 21 for 96-well and 384-well plates or 17 for 100-well Rotor-Discs)	
a) Variation in instrument sensitivity	Different instruments have different levels of sensitivity. If an average C_T^{PPC} value of 19 ± 2 for 96-well and 384-well plates or 15 ± 2 for 100-well Rotor-Discs is difficult to obtain for the instrument used, the observed average C_T^{PPC} value should be acceptable as long as it does not vary by more than 2 cycles between arrays being compared.
b) HotStarTaq DNA Polymerase not activated with a hot start	Be sure that the initial heat activation step at 95°C took place for 15 minutes, and that all other cycle parameters were performed according to the protocol.

	Comments and suggestions
c) Poor quality RNA that may contain PCR inhibitors	Check the A_{260}:A_{280} and A_{260}:A_{230} ratios of the RNA samples. Be sure to perform the dilutions for spectrophotometry in RNase-free 10 mM Tris·Cl, pH 7.5. If necessary, repurify RNA with a spin-column based clean up method, such as the miRNeasy Mini Kit (cat. no. 217004).

No product, or product detected late in real-time PCR (indicative of problems occurring during reverse transcription)

a) Pipetting error or missing reagent when setting up reverse-transcription reaction	Check the pipets used for experimental setup. Mix all reagents well after thawing and repeat the reverse-transcription reaction.
b) Incorrect setup of reverse-transcription reaction	Be sure to set up the reaction on ice.
c) Poor quality or incorrect amount of template RNA for reverse-transcription reaction	Check the concentration, integrity, and purity of the template RNA before starting the protocol. Mix well after thawing the template RNA. Even minute amounts of RNases can affect synthesis of cDNA and sensitivity in RT-PCR, particularly with small amounts of RNA.
d) RNA concentration too high or too low	See Table 3, page 27 for recommended RNA amounts.
e) RNA denatured	Denaturation of the template RNA is not necessary. If denaturation was performed, the integrity of the RNA may be affected.
f) Incubation temperature too high	Reverse transcription should be carried out at 37°C. Higher temperatures may reduce the length of cDNA products or the activity of miScript Reverse Transcriptase Mix. Check the temperature of your heating block or water bath.

	Comments and suggestions
No product, or product detected late in real-time PCR, or only primer–dimers detected (indicative of problems occurring during real-time PCR)	
a) PCR annealing time too short	Use the annealing time specified in the protocol.
b) PCR extension time too short	Use the extension time specified in the protocol.
c) Pipetting error or missing reagent when setting up PCR	Check the concentrations and storage conditions of reagents, including primers and cDNA.
d) HotStarTaq DNA Polymerase not activated with a hot start	Ensure that the cycling program includes the hot start activation step for HotStarTaq DNA polymerase; for details, check the protocol.
e) No detection activated	Check that fluorescence detection was activated in the cycling program.
f) Wrong detection step	Ensure that fluorescence detection takes place during the extension step of the PCR cycling program.
g) Wrong dye layer/filter chosen	Ensure that the appropriate layer/filter is activated.
h) Insufficient starting template	Increase the amount of template cDNA.
No linearity in ratio of C_T value/crossing point to log of the template amount	
a) Template amount too high	Do not exceed maximum recommended amounts of template cDNA. For details, see the protocol.
b) Template amount too low	Increase amount of template RNA.
Varying fluorescence intensity	
a) Real-time cycler contaminated	Decontaminate the real-time cycler according to the supplier's instructions.
b) Real-time cycler no longer calibrated	Recalibrate the real-time cycler according to the supplier's instructions.

Appendix A: Real-Time PCR Data Output and Dissociation Curve Analysis

In a typical amplification plot resulting from a real-time PCR reaction, fluorescence is plotted against the number of cycles, producing sigmoidal-shaped plots (when using a linear scale). The threshold cycle (C_T) serves as a tool for calculation of the starting template amount in each sample. This is the cycle in which there is the first detectable increase in fluorescence. There may be variation in how determination of C_T values is carried out depending on the real-time PCR cycler that is used.

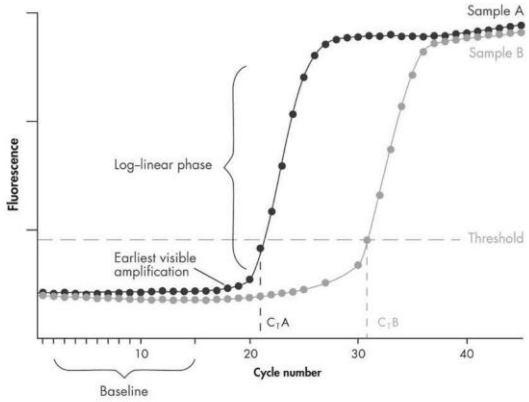

Figure 11. Amplification plot. Amplification plots showing increases in fluorescence from 2 samples (A and B). Sample A contains a higher amount of starting template than sample B.

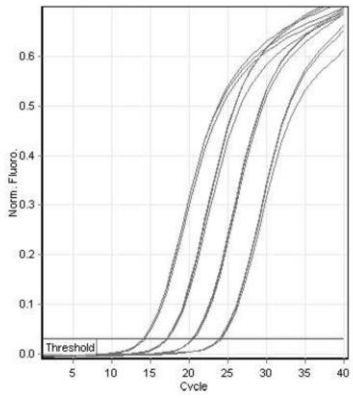

Figure 12. Typical amplification plot. Amplification plot after quantification of a range of amounts of miR-21. Real-time PCR was performed using the Rotor-Gene Q.

Dissociation curve analysis

A dissociation curve analysis of PCR product(s) may be optionally performed to aid in verifying their specificity and identity. Dissociation curve analysis is an analysis step built into the software of real-time cyclers. Follow instructions provided by the supplier.

To carry out dissociation curve analysis, the temperature is increased very slowly from a low temperature (e.g., 65°C) to a high temperature (e.g., 95°C). At low temperatures, PCR products are double stranded, so SYBR Green I dye binds to them and fluorescence is high. However at high temperatures, PCR products are denatured, resulting in rapid decreases in fluorescence.

The fluorescence is measured continuously as the temperature is increased and the fluorescence values are plotted against temperature. A curve is produced, because fluorescence decreases slightly through the lower end of the temperature range, but decreases much more rapidly at higher temperatures as the dissociation temperatures of nonspecific and specific PCR products are reached. The detection systems calculate the first derivatives of the curves, resulting in curves with peaks at the respective T_ms (Figures 13 and 14). Curves with peaks at a T_m lower than that of the specific PCR product indicate the formation of primer–dimers, while diverse peaks with different T_ms or plateaus indicate production of nonspecific products or a smear.

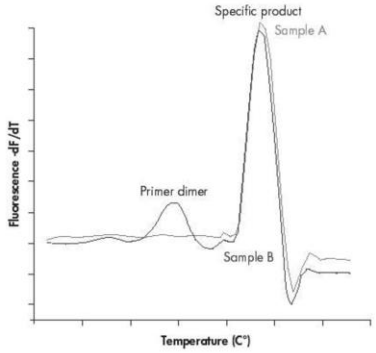

Figure 13. Dissociation curve analysis. Dissociation curve analysis of 2 samples (A and B). Sample A yields only 1 peak, resulting from the specific amplification product (primer–dimers not coamplified). Sample B shows a peak from the specific product and a peak at a lower temperature from amplification of primer–dimers.

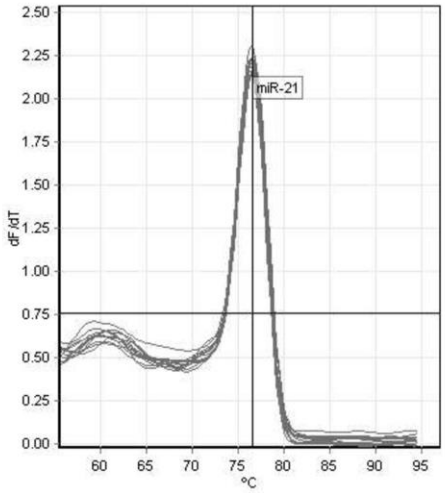

Figure 14. miRNA dissociation curve. Dissociation curve analysis of an miR-21 PCR produd showing a single peak from the specific amplification product. Dissociation curve analysis was performed using the Rotor-Gene Q.

Appendix B: General Remarks on Handling RNA

Handling RNA

Ribonucleases (RNases) are very stable and active enzymes that generally do not require cofactors to function. Since RNases are difficult to inactivate and even minute amounts are sufficient to degrade RNA, do not use any plasticware or glassware without first eliminating possible RNase contamination. Care should be taken to avoid inadvertently introducing RNases into the RNA sample during or after the purification procedure. In order to create and maintain an RNase-free environment, the following precautions must be taken during pretreatment and use of disposable and nondisposable vessels and solutions while working with RNA.

General handling

Proper microbiological, aseptic technique should always be used when working with RNA. Hands and dust particles may carry bacteria and molds and are the most common sources of RNase contamination. Always wear latex or vinyl gloves while handling reagents and RNA samples to prevent RNase contamination from the surface of the skin or from dusty laboratory equipment. Change gloves frequently and keep tubes closed whenever possible. Keep purified RNA on ice when aliquots are pipetted for downstream applications.

To remove RNase contamination from bench surfaces, nondisposable plasticware, and laboratory equipment (e.g., pipets and electrophoresis tanks), use of RNaseKiller (cat. no. 2500080) from 5 PRIME (www.5prime.com) is recommended. RNase contamination can alternatively be removed using general laboratory reagents. To decontaminate plasticware, rinse with 0.1 M NaOH, 1 mM EDTA* followed by RNase-free water (see "Solutions", page 53), or rinse with chloroform* if the plasticware is chloroform-resistant. To decontaminate electrophoresis tanks, clean with detergent (e.g., 0.5% SDS),* rinse with RNase-free water, rinse with ethanol (if the tanks are ethanol-resistant), and allow to dry.

Disposable plasticware

The use of sterile, disposable polypropylene tubes is recommended throughout the procedure. These tubes are generally RNase-free and do not require pretreatment to inactivate RNases.

* When working with chemicals, always wear a suitable lab coat, disposable gloves, and protective goggles. For more information, consult the appropriate material data sheets (MSDSs), available from the product supplier.

Glassware

Glassware should be treated before use to ensure that it is RNase-free. Glassware used for RNA work should be cleaned with a detergent,* thoroughly rinsed, and oven baked at 240°C for 4 hours or more (overnight, if more convenient) before use. Autoclaving alone will not fully inactivate many RNases. Alternatively, glassware can be treated with DEPC* (diethyl pyrocarbonate), as described in "Solutions" below.

Solutions

Note: QIAGEN solutions, such as miScript Nucleics Mix, miScript HiFlex Buffer, miScript HiSpec Buffer, and RNase-free water, are guaranteed RNase-free without using DEPC treatment and are therefore free of any DEPC contamination.

Solutions (water and other solutions) should be treated with 0.1% DEPC. DEPC is a strong, but not absolute, inhibitor of RNases. It is commonly used at a concentration of 0.1% to inactivate RNases on glass or plasticware or to create RNase-free solutions and water. DEPC inactivates RNases by covalent modification. Add 0.1 ml DEPC to 100 ml of the solution to be treated and shake vigorously to bring the DEPC into solution. Let the solution incubate for 12 hours at 37°C. Autoclave for 15 minutes to remove any trace of DEPC. DEPC will react with primary amines and cannot be used directly to treat Tris* buffers. DEPC is highly unstable in the presence of Tris buffers and decomposes rapidly into ethanol and CO_2. When preparing Tris buffers, treat water with DEPC first, and then dissolve Tris to make the appropriate buffer. Trace amounts of DEPC will modify purine residues in RNA by carbethoxylation. Carbethoxylated RNA is translated with very low efficiency in cell-free systems. However, its ability to form DNA:RNA or RNA:RNA hybrids is not seriously affected unless a large fraction of the purine residues have been modified. Residual DEPC must always be eliminated from solutions or vessels by autoclaving or heating to 100°C for 15 minutes.

* When working with chemicals, always wear a suitable lab coat, disposable gloves, and protective goggles. For more information, consult the appropriate material data sheets (MSDSs), available from the product supplier.

Appendix C: Preparation, Quantification, and Storage of RNA

RNA preparation and quality

Since PCR consists of multiple rounds of enzymatic reactions, it is more sensitive to impurities such as proteins, phenol/chloroform, salts, and EDTA than single-step enzyme-catalyzed reactions. Purity of nucleic acid templates is particularly important for real-time PCR, since contaminants can interfere with fluorescence detection. See Table 2, page 24 for kits recommended for the purification of total RNA that includes miRNA. For more information about kits for miRNA purification, visit www.qiagen.com/miRNA.

Determining concentration and purity of RNA

The concentration of RNA should be determined by measuring the absorbance at 260 nm (A_{260}) in a spectrophotometer. The sample should be diluted in water since the relationship between absorbance and concentration (A_{260} reading of 1 = 40 µg/ml RNA) is based on an extinction coefficient calculated for RNA in water. To ensure significance, readings should fall between 0.15 and 1.0.

Note that absorbance measurements cannot discriminate between DNA and RNA. Depending on the method used for RNA preparation, RNA may be contaminated with DNA, and this will result in misleadingly high A_{260} values.

The ratios between the absorbance values at 260 nm and 280 nm and at 260 nm and 230 nm give an estimate of RNA purity. To determine RNA purity, we recommend measuring absorbance in 10 mM Tris·Cl, pH 7.5.* Pure RNA has an A_{260}/A_{280} ratio of 1.9–2.1 and an A_{260}/A_{230} ratio of 2.0–2.2.† Lower ratios indicate the presence of contaminants such as proteins.

Storage of RNA

Purified RNA should be stored at –20°C or –70°C in RNase-free water. When purified using QIAGEN systems, no degradation is detectable for at least 1 year under these conditions. Diluted solutions of RNA (e.g., dilution series used as standards) should be stored in aliquots and thawed once only. We recommend storage of aliquots in siliconized tubes where possible. This avoids adsorption of the RNA to the tube walls, which would reduce the concentration of RNA in solution.

* When working with chemicals, always wear a suitable lab coat, disposable gloves, and protective goggles. For more information, consult the appropriate material safety data sheets (MSDSs), available from the product supplier.

† A_{260}:A_{280} values up to 2.3 are routinely obtained for pure RNA (in 10 mM Tris·Cl, pH 7.5) with some spectrophotometers.

DNA contamination in RNA samples purified from different tissues

Depending on the type of tissue used as starting material for RNA purification, a fluorescent signal may also be generated in "no RT" control reactions. When RNA is purified from tissues that contain large amounts of DNA, such as spleen or thymus, the level of DNase treatment required may be higher than for other tissues. For such tissues, we recommend performing a DNase digestion (using the QIAGEN RNase-Free DNase Set, cat. no. 79254) when using the miRNeasy Mini and miRNeasy 96 Kits for RNA purification.

Ordering Information

Product	Contents	Cat. no.
miScript II RT Kit (12)	For 12 cDNA synthesis reactions: miScript Reverse Transcriptase Mix, 10x miScript Nucleics Mix, 5x miScript HiSpec Buffer, 5x miScript HiFlex Buffer, RNase-Free Water	218160
miScript II RT Kit (50)	For 50 cDNA synthesis reactions: miScript Reverse Transcriptase Mix, 10x miScript Nucleics Mix, 5x miScript HiSpec Buffer, 5x miScript HiFlex Buffer, RNase-Free Water	218161
miScript SYBR Green PCR Kit (200)	For 200 reactions: QuantiTect SYBR Green PCR Master Mix, miScript Universal Primer	218073
miScript SYBR Green PCR Kit (1000)	For 1000 reactions: QuantiTect SYBR Green PCR Master Mix, miScript Universal Primer	218075
miScript Primer Assay (100)	10x miScript Primer Assay (contains one miRNA-specific primer)	Varies*
Pathway-Focused miScript miRNA PCR Array	Array of assays for a pathway, disease, or gene family for human, mouse, rat, dog, or rhesus macaque miRNAs; available in 96-well, 384-well, or Rotor-Disc 100 format	Varies
miScript miRNA HC PCR Array	High-content array of assays for a pathway, disease, or gene family miRNAs; available in 384-well format	Varies
miRNome miScript miRNA PCR Array	Array of assays for the complete human, mouse, rat, dog, or rhesus macaque miRNome; available in 96-well, 384-well, or Rotor-Disc 100 format	Varies

*Visit www.qiagen.com/GeneGlobe to search for and order these products.

Product	Contents	Cat. no.
miScript miRNA QC PCR Array	Array of quality control assays for human, mouse, rat, dog, or rhesus macaque miRNAs; available in 96-well, 384-well, or Rotor-Disc 100 format	Varies
RT^2 PCR Array Loading Reservoir	12 x 5 ml capacity, irradiation-sterilized loading reservoirs	338162
384EZLoad Covers	Pack of 4 color-coded covers for loading 384-well plates	338125
Related products		
miScript PreAMP PCR Kit (12)	For 12 preamplification reactions: 5x miScript PreAMP Buffer, HotStarTaq DNA Polymerase (2 U/µl), miScript PreAMP Universal Primer, 4 miScript Primer Assays, RNase-Free Water	331451
miScript PreAMP PCR Kit (60)	For 60 preamplification reactions: 5x miScript PreAMP Buffer, HotStarTaq DNA Polymerase (2 U/µl), miScript PreAMP Universal Primer, 4 miScript Primer Assays, RNase-Free Water	331452
miScript PreAMP Primer Mix	Primer mix for preamplification; for use with corresponding miScript miRNA PCR Array	Varies
miRNeasy Micro Kit (50)	For 50 total RNA preps: 50 RNeasy® MinElute® Spin Columns, Collection Tubes (1.5 ml and 2 ml), QIAzol® Lysis Reagent, RNase-Free Reagents and Buffers	217084
miRNeasy Mini Kit (50)	For 50 preps: 50 RNeasy Mini Spin Columns, Collection Tubes (1.5 ml and 2 ml), QIAzol Lysis Reagent, RNase-Free Reagents and Buffers	217004
miRNeasy 96 Kit (4)	For 4 x 96 preps: 4 RNeasy 96 plates, Collection Microtubes (racked), Elution Microtubes CL, Caps, S-Blocks, AirPore Tape Sheets, QIAzol Lysis Reagent, RNase-Free Reagents and Buffers	217061

Product	Contents	Cat. no.
miRNeasy Serum/Plasma Kit (50)	For 50 total RNA preps: 50 RNeasy MinElute Spin Columns, Collection Tubes (1.5 ml and 2 ml), QIAzol Lysis Reagent, Ce_miR-39_1 miScript Primer Assay, RNase-free Reagents and Buffers	217184
miRNeasy Serum/Plasma Spike-In Control	10 pmol lyophilized *C. elegans* miR-39 miRNA mimic	219610
miRNeasy FFPE Kit (50)	50 RNeasy MinElute Spin Columns, Collection Tubes, Proteinase K, RNase-Free DNase I, DNase Booster Buffer, RNase-Free Buffers, RNase-Free Water	217504
PAXgene Tissue miRNA Kit (50)	For 50 RNA preps: PAXgene RNA MinElute Spin Columns, PAXgene Shredder Spin Columns, Processing Tubes, Microcentrifuge Tubes, Carrier RNA, RNase-Free DNase, and RNase-Free Buffers; to be used with PAXgene Tissue Containers	766134
PAXgene Tissue Containers (10)	For collection, fixation, and stabilization of 10 samples: 10 Prefilled Reagent Containers, containing PAXgene Tissue Fix and PAXgene Tissue Stabilizer	765112
PAXgene Blood miRNA Kit (50)	For 50 RNA preps: PAXgene Spin Columns, PAXgene Shredder Spin Columns, Processing Tubes, Microcentrifuge Tubes, RNase-Free DNase, RNase-Free Reagents and Buffers; to be used with PAXgene Blood RNA Tubes (available from BD, cat. no. 762165)	763134

For up-to-date licensing information and product-specific disclaimers, see the respective QIAGEN kit handbook or user manual. QIAGEN kit handbooks and user manuals are available at www.qiagen.com or can be requested from QIAGEN Technical Services or your local distributor.

Trademarks: QIAGEN®, QIAzol®, QIAgility®, HotStarTaq®, miScript®, QuantiTect®, RNeasy®, Rotor-Gene®, Rotor-Disc®, MinElute® (QIAGEN Group); PAXgene® (PreAnalytiX GmbH); Roche®, LightCycler® (Roche Group); ABI PRISM®, Applied Biosystems®, StepOnePlus™, ViiA™, ROX™, SYBR® (Life Technologies Corporation); Eppendorf®, Mastercycler® (Eppendorf AG); Stratagene®, Mx3005P®, Mx3000P®, Mx4000® (Agilent Technologies); Bio-Rad®, iCycler®, Chromo4™, CFX96™, DNA Engine Opticon®, CFX384™, iQ™, MyiQ™ (Bio-Rad Laboratories, Inc.); Excel® (Microsoft, Inc.). Registered names, trademarks, etc. used in this document, even when not specifically marked as such, are not to be considered unprotected by law.

Use of this product (miScript SYBR Green PCR Kit) is covered by one or more of the following US patents and corresponding patent claims outside the US: 5,994,056 and 6,171,785. The purchase of this product includes a limited, nontransferable immunity from suit under the foregoing patent claims for using only this amount of product for the purchaser's own internal research. No right under any other patent claim and no right to perform commercial services of any kind, including without limitation reporting the results of purchaser's activities for a fee or other commercial consideration, is conveyed expressly, by implication, or by estoppel. This product is for research use only. Diagnostic uses under Roche patents require a separate license from Roche. Further information on purchasing licenses may be obtained by contacting the Director of Licensing, Applied Biosystems, 850 Lincoln Centre Drive, Foster City, California 94404, USA.

The purchase of this product (miScript SYBR Green PCR Kit) includes a limited, non-transferable license under U.S. Patent No. 5,871,908 and all continuations and divisionals, and corresponding claims in patents and patent applications outside the United States, owned by Roche Diagnostics GmbH, for internal research use or for non-in vitro diagnostics applications with authorized reagents with regard to Melting Curve Analysis. No right is conveyed, expressly, by implication or estoppel, under any other patent or patent claims owned by Roche Diagnostics GmbH, or by any other Party.

NOTICE TO PURCHASER: DISCLAIMER OF LICENSE
No license is conveyed with the purchase of this product (miScript Reverse Transcription Kit, miScript Primer Assay, miScript Precursor Assay) under any of US Patents Nos. 5,804,375, 5,994,056, 6,171,785, 5,538,848, 5,723,591, 5,876,930, 6,030,787, and 6,258,569, and corresponding patents outside the United States, or any other patents or patent applications, relating to the 5' Nuclease and dsDNA-Binding Dye Processes. For further information contact the Director of Licensing, Applied Biosystems, 850 Lincoln Centre Drive, Foster City, California 94404, USA.

NOTICE TO PURCHASER: LIMITED LICENSE.
The use of this product (miScript SYBR Green PCR Kit) is covered by at least one claim of U.S. Patent No. 7,687,247 owned by Life Technologies Corporation. The purchase of this product conveys to the buyer the non-transferable right to use the purchased amount of the product and components of the product in research conducted by the buyer (whether the buyer is an academic or for-profit entity). The buyer cannot sell or otherwise transfer (a) this product, (b) its components, or (c) materials made by the employment of this product or its components to a third party or otherwise use this product or its components or materials made by the employment of this product or its components for Commercial Purposes. Commercial Purposes means any activity for which a party receives or is due to receive consideration and may include, but is not limited to: (1) use of the product or its components in manufacturing; (2) use of the product or its components to provide a service, information, or data; (3) use of the product or its components for therapeutic, diagnostic or prophylactic purposes; or (4) resale of the product or its components, whether or not such product or its components are resold for use in research. The buyer cannot use this product or its components or materials made using this product or its components for therapeutic, diagnostic or prophylactic purposes. Further information on purchasing licenses under the above patents may be obtained by contacting the Licensing Department, Life Technologies Corporation, 5791 Van Allen Way, Carlsbad, CA 92008. Email: outlicensing@lifetech.com.

NOTICE TO PURCHASER: LIMITED LICENSE
The purchase of this product (miScript SYBR Green PCR Kit) includes a limited, non-transferable right to use the purchased amount of the product to perform Applied Biosystems' patented Passive Reference Method for the purchaser's own internal research. No right under any other patent claim and no right to perform commercial services of any kind, including without limitation reporting the results of purchaser's activities for a fee or other commercial consideration. is conveyed expressly, by implication, or by estoppel. This product is for research use only. For information on obtaining additional rights, please contact outlicensing@lifetech.com or Out Licensing. Life Technologies, 5791 Van Allen Way, Carlsbad, California 92008.

Limited License Agreement for the miScript PCR System

Use of this product signifies the agreement of any purchaser or user of the product to the following terms:

1. The product may be used solely in accordance with the protocols provided with the product and this handbook and for use with components contained in the kit only. QIAGEN grants no license under any of its intellectual property to use or incorporate the enclosed components of this kit with any components not included within this kit except as described in the protocols provided with the product, this handbook, and additional protocols available at www.qiagen.com. Some of these additional protocols have been provided by QIAGEN users for QIAGEN users. These protocols have not been thoroughly tested or optimized by QIAGEN. QIAGEN neither guarantees them nor warrants that they do not infringe the rights of third-parties.
2. Other than expressly stated licenses, QIAGEN makes no warranty that this kit and/or its use(s) do not infringe the rights of third-parties.
3. This kit and its components are licensed for one-time use and may not be reused, refurbished, or resold.
4. QIAGEN specifically disclaims any other licenses, expressed or implied other than those expressly stated.
5. The purchaser and user of the kit agree not to take or permit anyone else to take any steps that could lead to or facilitate any acts prohibited above. QIAGEN may enforce the prohibitions of this Limited License Agreement in any Court, and shall recover all its investigative and Court costs, including attorney fees, in any action to enforce this Limited License Agreement or any of its intellectual property rights relating to the kit and/or its components.

For updated license terms, see www.qiagen.com.

© 2011–2012 QIAGEN, all rights reserved.

www.qiagen.com

Australia ■ techservice-au@qiagen.com

Austria ■ techservice-at@qiagen.com

Belgium ■ techservice-bnl@qiagen.com

Brazil ■ suportetecnico.brasil@qiagen.com

Canada ■ techservice-ca@qiagen.com

China ■ techservice-cn@qiagen.com

Denmark ■ techservice-nordic@qiagen.com

Finland ■ techservice-nordic@qiagen.com

France ■ techservice-fr@qiagen.com

Germany ■ techservice-de@qiagen.com

Hong Kong ■ techservice-hk@qiagen.com

India ■ techservice-india@qiagen.com

Ireland ■ techservice-uk@qiagen.com

Italy ■ techservice-it@qiagen.com

Japan ■ techservice-jp@qiagen.com

Korea (South) ■ techservice-kr@qiagen.com

Luxembourg ■ techservice-bnl@qiagen.com

Mexico ■ techservice-mx@qiagen.com

The Netherlands ■ techservice-bnl@qiagen.com

Norway ■ techservice-nordic@qiagen.com

Singapore ■ techservice-sg@qiagen.com

Sweden ■ techservice-nordic@qiagen.com

Switzerland ■ techservice-ch@qiagen.com

UK ■ techservice-uk@qiagen.com

USA ■ techservice-us@qiagen.com

1072580 05/2012

Sample & Assay Technologies